UNIVERSITÀ DEGLI STUDI DI MILANO

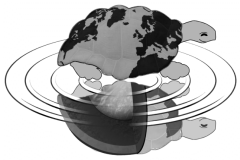

Dottorato di Ricerca in Scienze della Terra
Ciclo XXVII

Response of calcareous nannoplankton morphology to environmental perturbations: the latest Cenomanian Oceanic Anoxic Event 2 and lab simulations

Ph.D. Thesis

Giulia Faucher
Matricola R09572

Tutore	**Anno Accademico**	*Coordinatore*
Prof.ssa Elisabetta Erba	**2013-2014**	**Prof.ssa Elisabetta Erba**

“Chi vuole vedere bene la terra, deve tenersi alla distanza necessaria.”

I. Calvino

Index

Abstract

Anthropogenic emissions of carbon dioxide into the atmosphere has indirectly driven acidification and reduced carbonate saturation of the oceans. Among calcareous plankton, coccolithophore algae are the major producers of pelagic $CaCO_3$ in the modern ocean: they are direct contributors of the ocean biogeochemical cycles and climate system and, therefore, coccolithophore sensitivity to changes in surface water conditions is of major concern. Coccolithophores build around the cell an exoskeleton of calcite (coccosphere) that consists of single platelets called coccoliths and nannoliths. This phytoplanktonic group are affected by changes in surface water temperature, fertility, salinity, light and consequently are important instrument to A) predict the future state of the ocean, particularly its carbonate chemistry B) to reconstruct changes in past surface-water conditions. This PhD thesis is aimed to combine the geological and biological approaches, quantifying tempo and mode of coccolithophore response to specific combinations of stressing environmental conditions through investigation of a geological case history and laboratory experiments trying to simulate conditions of the past.

During the Aptian Oceanic Anoxic Event 1a (OAE 1a) an extreme global perturbation of the atmosphere-ocean system was documented, with evidence of geologically rapid warming associated to ocean fertility and acidification at global scale. Erba et al. (2010) demonstrated that calcareous nannoplankton was extremely sensitive to ocean acidification during OAE 1a, allowing separation of most-, intermediate-, and least-tolerant taxa. After a major calcification failure of heavily calcified forms, ephemeral coccolith dwarfism and malformation represent the most remarkable species-specific adjustments to survive surface water acidity.

The case history I focused on, is the latest Cenomanian Oceanic Anoxic Event 2 (OAE 2, ~ 94 Ma) which represents a profound perturbation of the ocean-atmosphere system caused by natural CO_2 emissions related to the emplacement of the Caribbean Plateau causing climate change, ocean fertilization and acidification. The study was performed on pelagic sediments from five localities: Eastbourne (Sussex, United Kingdom), Clot de Chevalier (France), Novara di Sicilia (Sicily, Italy) and two Western Interior sections (Pueblo, Colorado and Cuba, Kansas, USA). These five sections have been chosen based

on availability of integrated stratigraphy. In fact, they all have a good time control, especially C isotopic stratigraphy and biostratigraphy, that offers the opportunity to correlate data from the different localities, discriminating between local, regional and global changes. Moreover, the selected sections represent short and long-distance locations with respect to the Caribbean Plateau paleo-position.

Morphometric analyses were performed on selected calcareous nannofossil taxa namely *Biscutum constans, Zeugrhabdotus erectus, Discorhabdus rotatorius* and *Watznaueria barnesiae*. During OAE 2 calcareous nannoplankton responded to variations in surface-water fertility, temperature and CO_2-induced acidification with a calcification decline in the form of a general size reduction of coccoliths. Calcareous nannoplankton, also, was affected by dwarfism in a species-specific way: in all the five analyzed sections *B. constans* shows the amplest size fluctuations through the event. *D. rotatorius* shows a well express reduction in size while *Z. erectus* displays the minor size decrease. *W. barnesiae* doesn't show significant changes in mean coccolith size or in morphology (e.g. ellipticity).

Coccolith size fluctuations across OAE 2 are similar and synchronous in all the analyzed sections located at great distance in different oceans and settings. The nannofossil preservation was carefully assessed in order to avoid diagenetically altered material Accurate screening under light polarizing microscope ascertained that individual coccoliths considered for morphometry were complete, with a continuous outline and without evidence of crimping due to etching or overgrowth.

At the OAE 2 onset an increase in coccolith size leads to maximum dimension around the first $\delta^{13}C$ isotopic peak (peak A). Subsequently, *B. constans, Z. erectus* and *D. rotatorius* show a progressive decrease in the mean size, reaching the maximum reduction (dwarfism) at $\delta^{13}C$ isotopic peak B. Smaller specimens are still present till the end of the event and only after $\delta^{13}C$ isotopic peak C, in the upper part of the analyzed sections, a partial recovery in size is observed. High-resolution integrated stratigraphy allows to say that coccolith size fluctuations match paleoceanographic changes:

- the first decrease in coccolith size is coeval with a CO_2 pulse at the beginning of OAE 2;

- the increase in coccolith size at $\delta^{13}C$ isotopic peak A is well correlated with a significant CO_2 drawdown and a discrete cooling episode.
- the major decrease in coccolith size at $\delta^{13}C$ isotopic peak B correlates with a strong metal peak along with a new increase in sea surface temperature.

B. constans appears to be the most sensitive species to OAE 2 perturbations: the decrease in its coccolith size recorded in all the analyzed sections, is associated to some malformation (increased ellipticity).

Calcareous nannofossil morphometric and morphological data obtained for the latest OAE 2 were compared with those available for the early Aptian OAE 1a data in order to derive similarities and differences. Such a comparison suggests that species-specific coccolith dwarfism was experienced during both OAE 1a and OAE 2. Such calcification change is associated to:

- high pCO_2 (> 900 ppm);

- high temperature (ca. 35°C);

- trace metal enrichment.

Temperature and nutrient availability in surface waters do not seem to have been crucial for *B. constans* size, although warmer and more fertile oceans preconditioned the environmental perturbation. Available data, instead, suggest that ocean chemistry related to the amount of CO_2 concentrations, played a central role in coccolith secretion by *B. constans* with a repetitive reduction in size during OAE 1a and OAE 2. Massive submarine volcanism of Ontong Java Plateau during OAE 1a and the Caribbean Plateau during OAE 2 triggered a disruption in the oceanic carbonate system: excess CO_2 arguably induced ocean acidification associated that was detrimental to some marine calcifiers, with temporary failure of a few taxa and production of dwarf and malformed coccoliths in *B. constans*. Hydrothermal plumes during construction of large submarine plateaus introduced biolimiting metals that fertilized the global ocean. However, submarine hydrothermalism might have also pumped in some toxic metals that might have disturbed the functioning of some intolerant coccolithophorid species, thus affecting their biocalcification. Species-specific coccolith dwarfism seems to be the response of nannoplankton to ocean acidification during OAE 1a and OAE 2, and this resulted in a

reduction in total calcification under high pCO_2. Evidence of dwarfism and production of malformed coccoliths possibly represents species-specific adjustment to survive lower pH. Therefore, there is possibly a causal link between intervals of major submarine volcanism and changes in nannoplankton composition, abundance and biocalcification through OAE 1a and OAE 2.

The second part of this thesis focuses on laboratory experiments of coccolithophores performed at the GEOMAR Helmholtz Centre for Ocean Research Kiel (Kiel, Germany). Only preliminary results are here presented. The starting point was the idea that changes in some environmental factors directly affect the physiology of coccolithophorid algae, thereby directly causing a change in coccolith mean size and weight. Environmental factors known to modify coccolith size and/or weight are salinity (Green et al., 1998; Bollmann and Herrle, 2007; Fielding et al., 2009), temperature (Watabe and Wilbur, 1966), nutrient availability (Batvik et al., 1997; Paasche, 1998), growth stage (Young and Westbroek, 1991), seasonality (Triantaphyllou et al., 2010) and carbonate chemistry (Riebesell et al., 2000, Iglesias-Rodriguez et al., 2008; Halloran et al., 2008; Beaufort et al., 2011; Bach et a., 2012). In this thesis I consider the potential role of some of these environmental factors - specifically salinity, carbonate chemistry, light intensities, trace metal enrichment and nutrient depleted conditions) as triggers of changes in coccolith size and/or weight. Five species were investigated (*Emiliania huxleyi, Gephyrocapsa oceanica, Pleurochrysis carterae, Coccolithus pelagicus* ssp. *braarudii*) in five different experiments. Similarly to fossils data, a species-specific response to the different treatments has been observed. *E. huxleyi* evidences an increase in the coccosphere diameter associated to an increase in coccolith volume under nutrient-starved conditions and specifically with low phosphate content. On the other hand, major decrease in coccolith volume has been observed for *E. huxleyi* only with the highest CO_2 concentration (3000 ppm). However, with increased trace metal contents, a reduction in coccolith volume has been detected, too. *G. oceanica* appears to be very sensitive to carbonate chemistry variations and future more specific analyses should be done to figure out which parameter(s) of the carbonate system drive morphological modifications (e.g. carbon dioxide, bicarbonate, carbonate ion, protons). *P. carterae* instead shows very erratic patterns to the tested parameters. Furthermore, among experiments, different replicates resulted in different response suggesting unclear sensitivity to specific

environmental conditions. Finally, *Coccolithus pelagicus* ssp. *braarudii* calcification appears to be beneficial under low-nutrient conditions and, specifically, in the phosphate-limited treatment. On the contrary, increased CO_2 concentration appears to impart a negative feedback to coccolith volume, with an evident decrease hand in hand with increasing CO_2 content. As mentioned above, further analyses are planned in the near future and particularly SEM investigation of coccolith morphology and morphometry to quantify changes in coccolith size and malformation.

The results of my thesis emphasize that changes in environmental factors do affect coccolithophore growth: salinity, carbonate chemistry, nutrient content and trace metal can significantly impact coccolith calcification in present and past oceans. The OAE 2 paleoenvironmental perturbation indicates that there is a causal link between intervals of abnormal submarine volcanism and changes in nannoplankton biocalcification through OAE 2. Comparison with data available for OAE 1a and OAE 1d indicate that analogous causes (construction of large igneous provinces) have induced similar response at different times in the Cretaceous. Finally, the geological record indicates that at wide spatial scale calcareous nannoplankton can adapt to high pCO_2, but past changes occurred over tens of thousands of years, giving time for life to adjust or even take advantage. Laboratory experiments on modern coccolithophore species (evolutionary-linked to Cretaceous taxa) remain the only means to assess if and which role environmental parameters have on quantity, type and amount of coccolith secretion. Although conscious of the very different time scales of processes and resolution, the double biological and geological approach to coccolithophore calcification is aimed at integrating the daily-decadal datasets with medium to long-term (thousands to millions of years in duration) data. This has the potential for achieving an improved understanding of coccolith biomineralization mechanisms and providing some guidance as to the response of biota to abrupt massive CO_2 releases and how and at what rate pre-perturbation conditions are eventually restored.

The work developed for this doctoral thesis resulted in two submitted publications. For further information see Appendix I and II.

Chapter 1

Introduction

One of the most pressing issues for humankind is the understanding of the future state of the planet within the context of increasing carbon dioxide (CO_2) concentrations (Keeling & Whorf 2004). In the past 650,000 years atmCO_2 has varied between 180 to 300 parts per million (ppm) till the inception of the Industrial Revolution that marks a major turning point also for the global environment and biota evolution. Industrialization and new land use have caused accelerated rising of atmCO_2 at rates unprecedented in Earth history. The unfortunate consequence has been the emission of billions of tons of carbon dioxide (CO_2) and other greenhouse gases in the Earth's atmosphere (IPCC, 2013). About half of this man-made CO_2 has been already absorbed by the ocean (Sabine et al, 2004), slowing down/mitigating the climate change that these emissions would have instigated if the total CO_2 amount had remained in the atmosphere. However, relatively recent research has pointed out the so-called "other pCO_2 problem" (Doney et al., 2009): the massive amount of CO_2 into the sea is altering the water chemistry, inducing ocean acidification and affecting the life cycles of many marine organisms. Indeed, when CO_2 dissolves in seawater, it forms carbonic acid, which increases seawater acidity and decreases carbonate ion concentration and carbonate saturation: the price for restoring CO_2 is an ongoing decrease of seawater pH (Fig. 1.1).

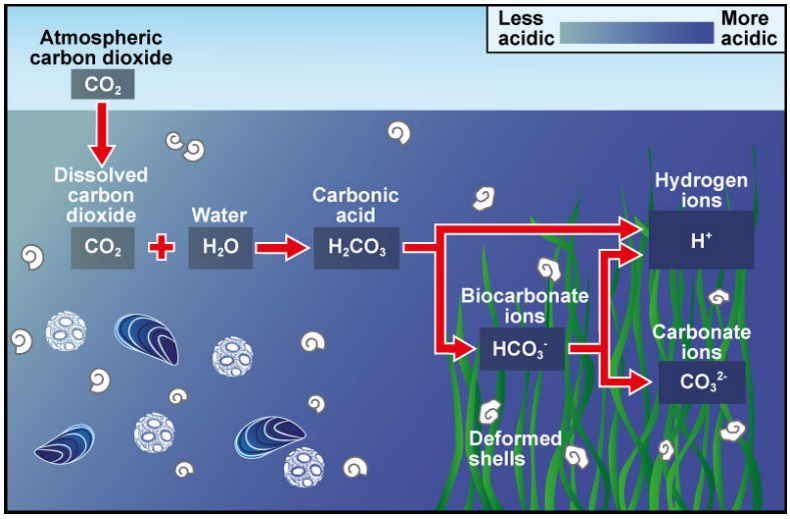

Fig. 1.1 Credits: http://www.oceanacidification.org.uk

The natural recovery from global ocean acidification implies A) accelerated dissolution of marine carbonates and removal of excess CO_2 via enhanced burial of organic matter and B) weathering of rocks exposed on land. All these processes, however, operate on long timescales, especially if ocean acidification occurs in conjunction with global warming, fertilization and pollution. Moreover the CO_2-driven pH lowering, is causing a reduction of $CaCO_3$ saturation state and shoaling of Calcite Compensation Depth (CCD), generating serious problems for calcifying organism, such as corals, foraminifera and coccolithophorid algae, becoming vulnerable and unable to produce their shells-skeletons. The ecological effects of such changes on calcareous plankton are largely unknown but need to be quantified. The impact of atmCO_2 concentrations on marine calcification rates emerged about 40 years ago (Broecker & Takahashi, 1966). Early calculations predicted that the surface ocean would become undersaturated with respect to calcite by the year 2000, but were biased by improper consideration of seawater C system equilibrium. Later laboratory-field experiments revealed the influence of the $CaCO_3$ saturation on calcification rates and controversial response on different species.

Among marine calcifiers, coccolithophores, golden-brown algae (phylum Haptophyta), have a very long evolutionary history (their appearance is dated as Late Triassic) and they stay at the base of the food chain in the oceans and are, therefore, expected to be seriously affected by the anthropogenic perturbation that we are experiencing. Coccolithophorid algae are most effective calcite producers on Earth: they build around the cell an exoskeleton of calcite (coccosphere) constituted by single platelets called coccoliths and nannoliths. Biocalcification made coccolithophores very important rock-forming organisms during the Jurassic and Cretaceous as well as through the Cenozoic (e.g. Erba, 2006). They are directly affected by changes in surface water temperature, fertility, salinity, light, and pH and, consequently, their remains (coccoliths and nannoliths) can be studied to reconstruct changes in past surface-water conditions. At present, coccolithophores are affected by increasing CO_2 emissions which are rapidly inducing climatic changes and altering surface-water carbonate saturation state causing ocean acidification (OA). Laboratory experiments of coccolithophores indicate a direct effect of OA on calcification rates, production of malformed coccoliths or incomplete coccospheres (Riebesell et al., 2000), although the CO_2 and pH sensitivity among species is different (Langer et al., 2006; Krug et al., 2011). Additional factors, such as

temperature and nutrients, have also an influence on coccolithophores. Recent studies provide evidence for different pCO_2 and pH sensitivities among species and strains (Langer et al 2006; Iglesias Rodriguez et al., 2008) with some species more tolerant (e.g. *C. pelagicus braarudii*, Krug at al 2011) than others. However, most of the experiments focus on a limited number of model species (specifically *E. huxleyi* and *G. oceanica*) and not many studies have focused on how changes in coccosphere/cell diameter influence the coccolith volume or size. In addition, the understanding of the effects of OA on living coccolithophores is limited, due to the presence of multiple factors (e.g. temperature, nutrients availability) concurring during climate changes, which can influence the coccolithophore response. As discussed by Herfort et al. (2004) coccolithophore morphology, rates of calcification and photosynthesis are also influenced by calcium and magnesium concentrations. Coccoliths are formed of low-Mgcalcite, and calcification rates in *E. huxleyi* are positively correlated with the Ca concentration of the medium, with significant undercalcification at low [Ca^{2+}] and malformation with incomplete grown elements and decreased width of the distal shield elements (Young & Westbroek 1991). Low [Mg^{2+}] also cause malformations, while high concentrations cause under-calcification and malformation. No variation in width was determined.

The geological record offers the opportunity to investigate case histories marked by profound changes in the ocean-atmosphere system, including volcanic injection of large amounts of CO_2, super-greenhouse conditions, ocean anoxia, increased surface-water fertility and introduction of bio-limiting metals (e.g. Larson & Erba, 1999; Erba, 2004; Jenkyns 2010; Erba et al., 2015). These intervals can be seen as “natural experiments” useful to decipher the ecosystem response to major perturbations. Under such extreme conditions, the oceans experienced prolonged global anoxia, known as Oceanic Anoxic Events (OAEs), when unusually large amounts of organic matter accumulated in marine sediments (Schlanger and Jenkyns, 1976).

This thesis is aimed at combining geological and biological approaches, quantifying tempo and mode of coccolithophore response to specific combination of stressing environmental conditions through investigation of a geological case history and laboratory experiments trying to simulate conditions of the past. Specifically, I focused on the latest Cenomanian Oceanic Anoxic Event 2 (OAE 2), in order to trace the effects of extreme environmental changes on calcareous nannoplankton. A comprehensive

background characterization of the latest Cenomanian OAE 2 is available based on integrated stratigraphy (bio-, chemo-, litho-, cyclo- stratigraphy) and sedimentological, paleontological and geochemical signatures (Leckie et al 2002; Erba 2004; Jenkyns 2010; fig. 1.2).

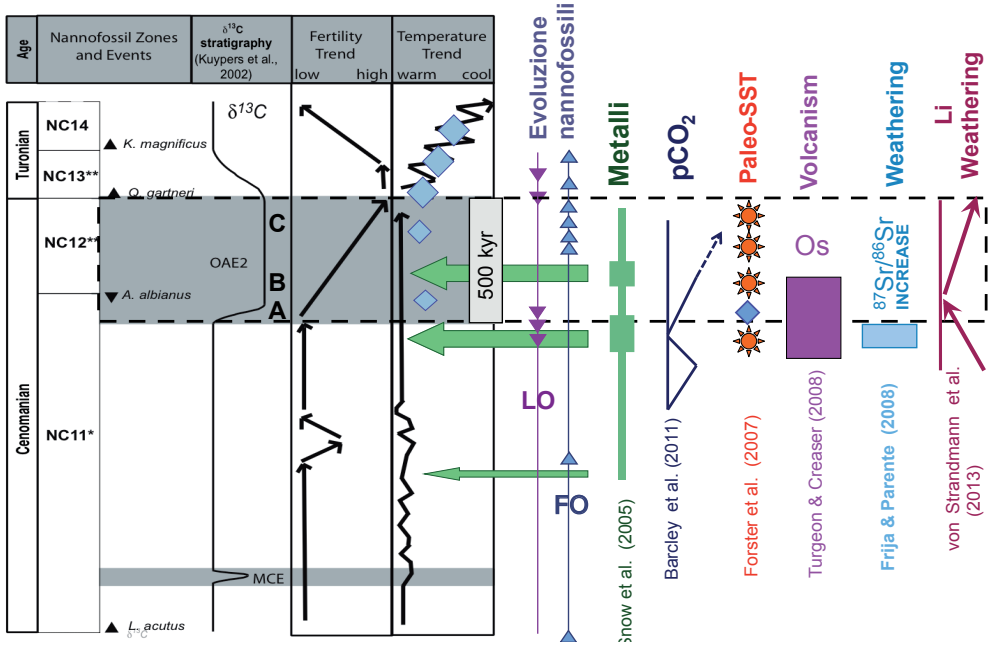

Fig. 1.2 Synthesis of major biotic and geological events during OAE 2

However, the transient or permanent response and/or adaptation of calcareous nannoplankton to excess CO_2 and climate change during OAE 2 are still poorly known. The investigation was conducted on five sections from different paleolatitudes and paleoceanographic contexts, in order to distinguish global and local responses of calcareous nannoplankton during OAE 2.

Data on calcareous nannoplankton response to OAE 2 perturbations will be compared with published data from another extreme case, namely the early Aptian Oceanic Anoxic Event 1a (OAE 1a; e.g. Erba et al, 2010).

The Cretaceous OAE 1a has been demonstrated to record a strong CO_2 perturbation of the atmosphere-ocean system (Larson & Erba 1999; Leckie et al 2002; Weissert & Erba 2004; Erba 2004; Mehay et al 2009; Erba et al 2010), with evidence of a geologically rapid warming (increase of 5-6°C) and decreased pH in surface and deep waters at global

scale. In an unprecedented high-resolution (Malinverno et al., 2010) study of organic matter compounds, Mehay et al., (2009) dated successive CO_2 emissions (total of ~9600Gt C) and one episode of methane hydrate dissociation (~270 Gt C). Os isotopes (Tajada et al 2009; Bottini et al. 2012) confirmed multiple volcanic phases before and during OAE 1a, plus one episode of accelerated weathering (Fig. 1.3).

Quantitative studies on nannoplankton changes across OAE 1a showed a decrease in calcification (Erba and Tremolada 2004) with production of dwarf/malformed coccoliths (Erba et al. 2010, 2015; Bottini et al., 2014, 2015). In particular, Erba et al. (2010) demonstrated that calcareous nannoplankton was extremely sensitive to OA associated to OAE 1a, allowing separation of most-, intermediate-, and least-tolerant taxa. After a major calcification failure of heavily calcified forms, ephemeral coccolith dwarfism and malformation represent the most remarkable species-specific adjustments to survive surface water acidity. Deep-water acidification started with a delay of 25-30kyr, with a 1-2 km CCD shoaling just prior to onset of global anoxia. Repetitive abundance peaks of peculiar heavily-calcified nannoliths trace intermittent alkalinity recovery alternating with OA peaks marked by coccolith dwarfism and malformation.

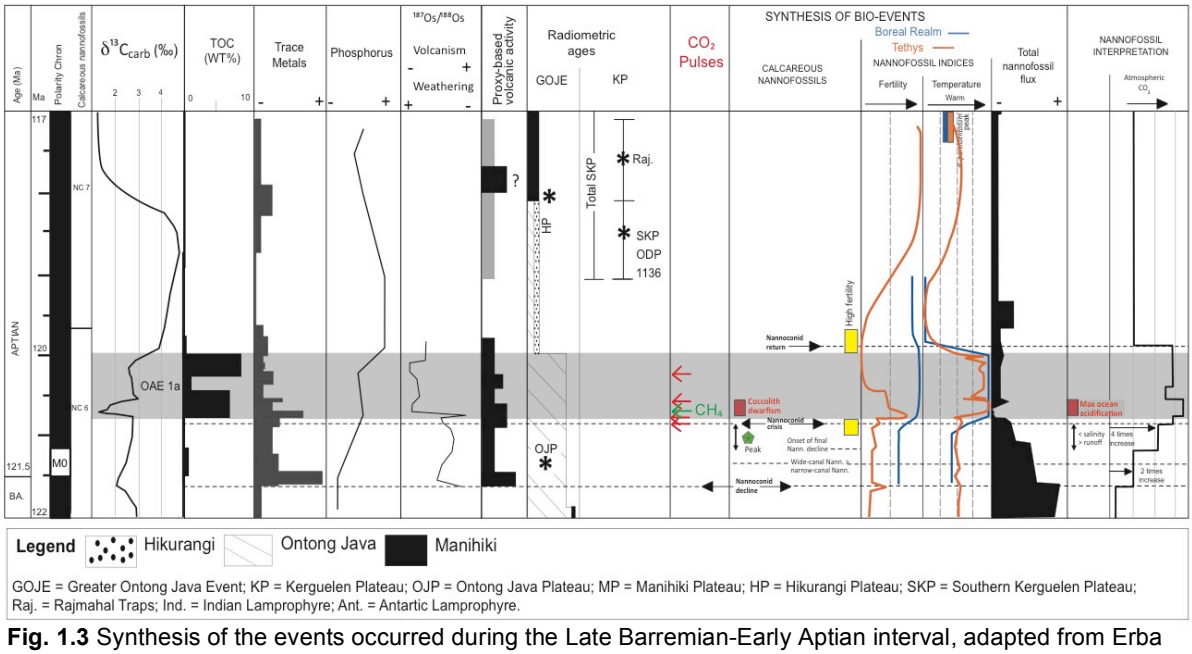

Fig. 1.3 Synthesis of the events occurred during the Late Barremian-Early Aptian interval, adapted from Erba et al., 2010, 2015; Bottini et al., 2014, 2015; Patruno et al., 2015.

The overarching goal of my thesis is the identification of the effects on coccolithophores calcification of the past episode of OA, excess CO_2, global warming and ocean fertilization associated to OAE 2.

In second part of the thesis, I tried to simulate environmental conditions associated to the latest Cenomanian OAE 2 and tested coccolithophore response through laboratory cultures. Five experiments have been performed at the GEOMAR (Helmholtz Centre for Ocean Research Kiel) in the Biological Oceanography unit in order to reproduce some of the "extreme" physical and chemical changes known for the onset of Cretaceous OAEs.

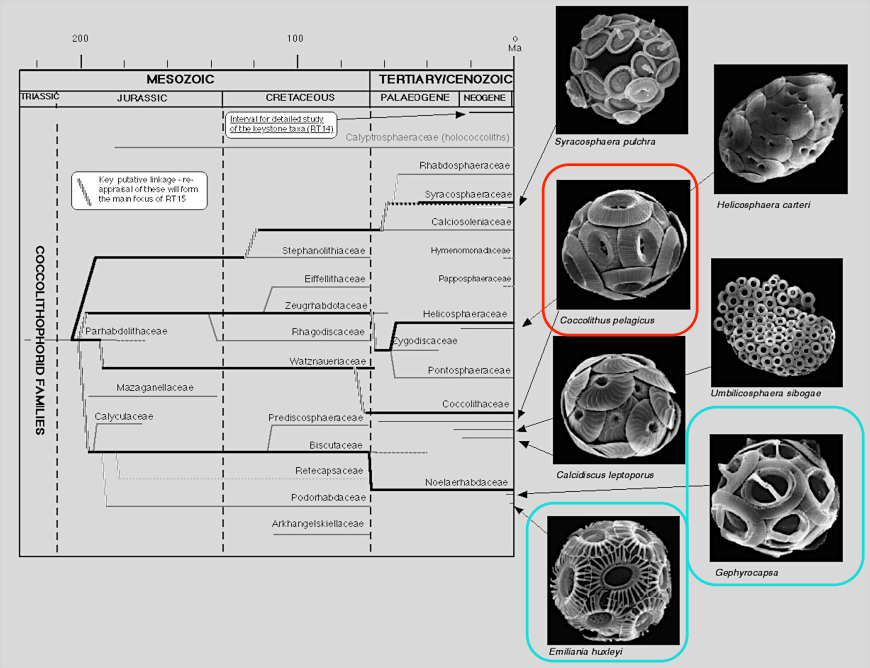

Fig. 1.4 Synthesis of coccolithophorid phylogeny and taxonomical position of investigated living coccolithophores [from Young and Bown, 1999, modified].

Every experiment tested a single abiotic parameter (e.g. temperature, carbonate chemistry, nutrient content, metal enrichment) on four coccolithophore species (*Emiliania huxleyi, Gephyrocapsa oceanica*, *Pleurochrysis carterae* and *Coccolithus pelagicus* ssp. *braarudii*) and focused on coccolith size (volume) and morphology. *Emiliania huxleyi* and *Gephyrocapsa oceanica* belong to the Noelaerhabdaceae family derived, from the extinct Prinsiaceae that, in turn, developed from the Mesozoic Biscutaceae (Liu et al., 2010; Fig. 1.4). *C. pelagicus*, belonging to the Coccolithacease, is a descendant of the Mesozoic Watznaueriaceae family. Therefore, *E. huxleyi* and *G. oceanica* are assimilated to *B. constans*, while *C pelagicus* might be a living analogue of *W. barnesiae*.

For the experiments on coccolithopores only preliminary results will be presented and discussed in this thesis. Quantification of calcification and characterization of coccolith ultrastructure will be achieved in the next few months under the supervision of Dr. Lennart Bach (GEOMAR, Helmholtz Centre for Ocean Research Kiel).

The main objectives of this thesis can be summarized as follows:

a) To reconstruct the response of calcareous nannofossil assemblages to ocean acidification and extreme climatic conditions associated to OAE 2.
b) To determine time relationships between nannoplankton changes, ocean acidification, fertilization, temperature and anoxia.
c) To compare variations in coccolith morphometry in different case histories (OAE 1a, OAE 1d, OAE 2) in order detect similarities and differences of calcareous nannoplankton response to chemical and physical extreme conditions through time.
d) To decipher which abiotic parameter mainly influenced coccolithophore calcification and specifically coccolith size.

During my PhD I spent one year at the GEOMAR Helmholtz Centre for Ocean Research Kiel (Kiel, Germany) where I learn how to culture and perform experiments on coccolithophores, under the supervision of Prof. Ulf Riebesell, Dr. Linn Hoffmann and Dr. Lennart Bach.

Some of the results obtained during this PhD project have been submitted for publication, and the papers are included as part of this thesis in Appendix I and II.

Chapter 2
The Marine Carbon Cycle

Since the beginning of the industrial era, the Earth is experiencing progressive increase in carbon dioxide (CO_2) concentration in the atmosphere: the never-ending use of fossil fuels and intensive use of land for agriculture are responsible of an increase in CO_2 of almost 40%. Anthropogenic CO_2 emissions has increased from ~ 280 parts per million (ppm) in the mid of the 18^{th} century to around 398 ppm in 2014 (Mauna Loa Observatory, Scripps Institution of Oceanography) with an annual rate of increase of about 2.07 ppm. As indicated from analysis on bubbles trapped in Antarctic ice, such levels are the higher level ever recorded in the last 800,000 years (and likely much more than what has occurred in several ten of millions years; Kump et al., 2009). Many studies are focusing on the impacts of anthropogenic CO_2 on climate: one primal consequence of this extraordinary atmospheric CO_2 input, in fact, is the intensification of the greenhouse effects. But in the recent years, much of the scientific debate takes into account a second major impact of CO_2 emissions, namely ocean acidification. This is also called "the other CO_2 problem" and refers to the ongoing decrease in oceanic pH owing to ocean capability to uptake CO_2 (Royal Society, 2005). In the past 150 years surface ocean pH significantly dropped from 8.0-8.3 (before the Industrial Revolution) to present 7.9-8.1 units. The phenomenon of ocean acidification requires a brief introduction to seawater carbonate chemistry to be properly understood.

2.1 Seawater carbonate chemistry

Dissolved carbon dioxide (CO_2) is present in the ocean water in three inorganic forms: free aqueous carbon dioxide ($CO_2(aq)$), bicarbonate ion (HCO^{3-}) and carbonate ion (CO_3^{-2}). There's a fourth form that is H_2CO_3 that occurs in a very small concentration ($\leq 3\%$) and is chemically indistinguishable from CO_2. Therefore, the sum of $[CO_2(aq)]$ and $[H_2CO_3]$ is denoted as $[CO_2]$. There's a constant equilibrium and exchange of inorganic

carbon between the atmosphere and the ocean that is ruled by the Henry's law:

$$[CO_2] = K_0\,[CO_2]$$

where K_0 is the temperature and salinity-dependent solubility coefficient of CO_2 in seawater (Weiss, 1974). CO_2 rapidly reacts with the seawater to form H_2CO_3 that rapidly dissociates into (HCO^{3-}), (CO_3^{2-}) and protons (H^+) following the reactions:

$$CO_2 + H_2O \overset{K_1^*}{\Leftrightarrow} HCO_3^- + H^+ \overset{K_2^*}{\Leftrightarrow} CO_3^{2-} + H^+$$

where K_1 and K_2 are temperature, salinity and pressure dependent and usually expressed in terms of concentrations and has been analytically determined. This equation represents the marine carbonate system (Fig. 2.1): for eg. in sea surface, temperature of 15°C, salinity of 35 ‰, surface pressure P= 1 atm, at a typical surface seawater pH of 8.2, the speciation between dissolved inorganic carbon is 0.5% [CO_2], 89% [HCO_3^2], 10.5% [CO_3^{2-}] (Zeebe, 2012).

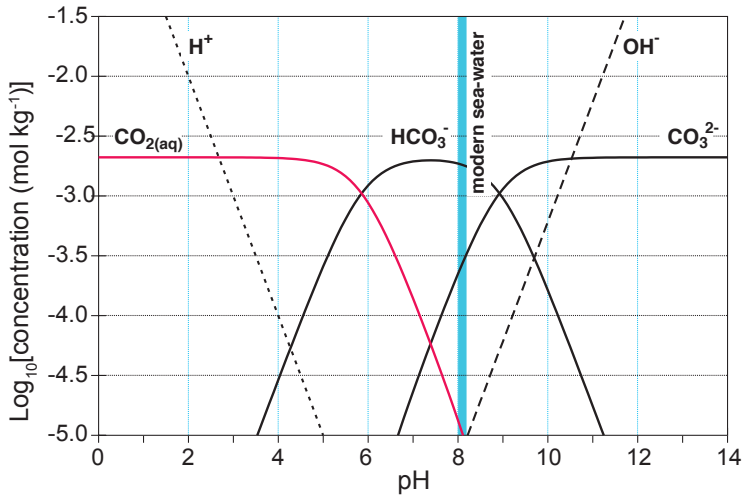

Fig. 2.1 Concentration of the dissolved carbon species as a function of pH [from Ridgwell and Zeebe, 2005].

The second fundamental chemical concept is the DIC that is the sum of all dissolved inorganic carbon species and is defined as

$$DIC = [CO_2] + [HCO_3^-] + [CO_3^{2-}]$$

The last fundamental chemical concept is total alkalinity (TA), which is a measure of charge balance in seawater

$$TA=[HCO_3^-] + 2[CO_3^{2-}] + [B(OH)_4^-] + [OH^-] - [H^+] + \text{minor component}$$

TA can also be described as the amount of negative charge that is able to accept the H^+ released in the dissociation reactions of carbonic acid (or on the other way round, the number of moles of H^+ equivalent to the excess of the proton acceptors); it's analytically determined from tritation of seawater with a strong acid (Dickson, 1981). As the equations indicate, DIC and TA are unaffected by changes in pressure or temperature (conservatives quantities) and along with pCO_2 and pH, can be determined analytically (Dickson et al., 2007). Furthermore for given temperature, salinity and pressure, two parameters are needed to calculate all the other parameters (pCO_2, $[CO_2]$, $[HCO^{3-}]$, $[CO_3^{2-}]$, pH, DIC and TA).

The last parameter that is important to take in consideration is the calcium carbonate saturation state of seawater (Ω) that is expressed as

$$\Omega=\frac{[Ca^{2+}]_{sw} \times [CO_3^{2-}]_{sw}}{k^*_{sp}}$$

where sw refers to the ion concentration in seawater and k^*_{sp} is the solubility product of calcite or aragonite at the in situ temperature, salinity and pressure conditions. When Ω >1 it means supersaturation ($CaCO_3$ doesn't dissolved) while on the contrary when Ω <1, the seawater is undersaturated (dissolution is favored). The calcite saturation horizon occurs at depth where Ω=1. Dissolution proceeds slowly below this depth reaching the lysocline where the dissolution impact becomes noticeable. Finally, the calcite compensation depth (CCD) is the depth at which the dissolution flux balances the rain flux of calcite. Nowadays saturation states of surface water for $CaCO_3$ ranges between 4.8 - 3.2 (Ridgwell and Zeebe, 2005).

2.2 The Marine Carbon Cycle

The Carbon Cycle can be represented as a series of major reservoirs of carbon in the Earth system, connected by exchange fluxes of carbon. These four reservoirs are the atmosphere, the hydrosphere, the lithosphere and the biosphere. The reservoir turnover time (carbon cycling within or between reservoir), significantly vary among them,

ranging from a few years for the atmosphere to million of years for the geological processes (Fig. 2.2). Conceptually, in the global carbon cycle, two domains can be distinguished: a ***fast domain*** with large and rapid reservoir turnover, which consists of carbon in the atmosphere, fresh water and surface ocean sediments and on land soils. And a ***slow domain*** where the huge carbon stores in rocks and sediments, exchange carbon with the fast domain through volcanic emission, chemical weathering and sediment formation on the sea floor (IPCC 2013). The ocean contain almost 50 times more carbon than either the atmosphere or the world's terrestrial vegetation, but even if shifts in the abundance of carbon among the major reservoirs will have a much greater significance for the terrestrial biota and for the atmosphere than for the ocean, the strong exchange of considerable amounts of carbon from the atmosphere to the ocean, will strongly influence the marine carbon cycle too.

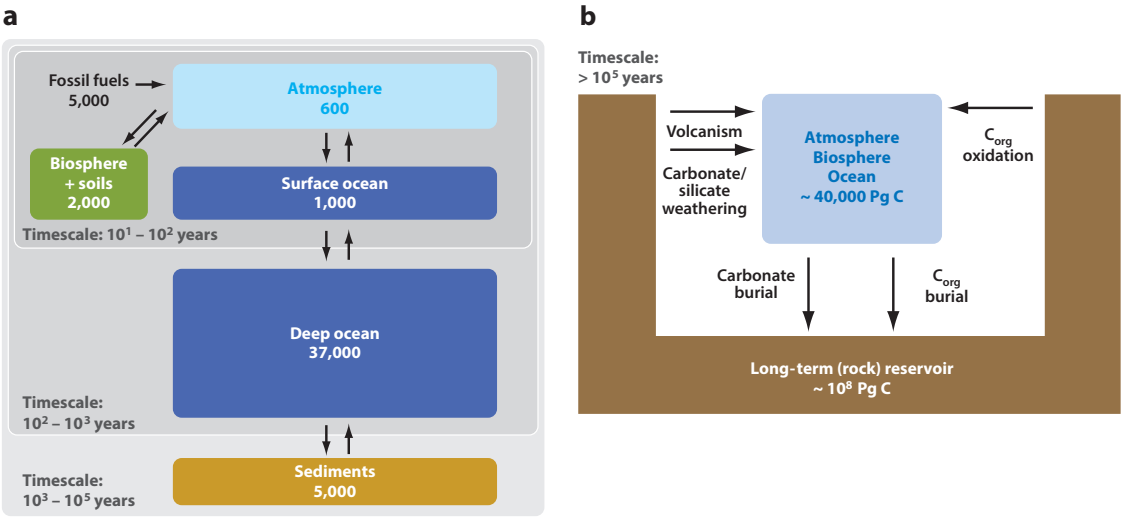

Fig. 2.2 a) Surface carbon cycle: reservoir sizes are in unit of petagrams of carbon, PgC ($1Pg=10^{15}g$). Grey boxes demarcate the reservoirs involved in carbon exchange on the respective timescales. **b)** Long-term carbon cycle [From Zeebe 2012].

Two processes are ruling the marine carbon cycle: the 'solubility pump' and the 'biological carbon pump'. The solubility pump determines about one third of the surface-to-deep gradient of dissolved inorganic carbon; it's a physical process driven by latitudinal solubility gradient of CO_2: as the solubility of gases increases with decreasing seawater temperature, the cold waters, sinking to depths during deep water formations at high latitudes, are CO_2-rich (DIC increased) relative to average surface waters. In one

thousand years flowing towards lower latitudes, they spread CO_2 throughout the deep ocean and finally upwell to the surface ocean releasing back the excess CO_2 to the atmosphere.

The remaining two thirds of the surface-to-depth DIC gradient is caused by the biological carbon pump that can be furthermore subdivided in two different processes: the 'organic carbon pump' and the 'carbonate pump (or 'carbonate counter pump'). The organic carbon pump is related to the phytoplanktonic photosynthesis that fixes DIC in the organic particles. Particulate organic matter usually aggregates and sinks into deep ocean where they oxidize through heterotrophic respiration, releasing DIC back in the water column. In the carbonate pump on the other hand, calcifying organisms, like foraminifera, coccolithophores and pteropods, band together the DIC with $CaCO_3$. When shell material sinks in the water column, it dissolves in undersaturated water in respect to $CaCO_3$. These two pumps have an opposite effect on the atmospheric pCO_2 budget: the photosynthetic carbon fixation lowers CO_2 partial pressure in the euphotic zone with a net reduction flux of CO_2 from the atmosphere to the ocean. On the contrary, in the counter carbonate pump, calcification cause an increase in CO_2 partial pressure (about 0.6 mole of CO_2 for every mole of $CaCO_3$), which is eventually released in the atmosphere. In equilibrium sinking (biological carbon pump) and upwelling (carbonate counter pump) reinforce each other maintaining a vertical DIC gradient.

2.3 Sensitivities of marine carbon fluxes and perturbations of the marine carbon cycle

Anthropogenic carbon dioxide emission is forcing rapid ocean chemistry alterations in the ocean. The ocean global carbon cycle will be directly affected by increase in $[CO_2]$ that will decrease the pH and indirectly by ocean warming and consequently change in the circulation and mixing regime (Fig. 2.3). Both solubility and biological carbon pump will be affected.

The solubility of CO_2 increases with decreasing temperature and is therefore higher at high latitudes where deep-water formation takes place: this resulted in a downward

transport of CO_2-enriched waters. The strength of the ocean sink for CO_2 is going to decrease in the future: in the last 50 years the ocean has uptaken 20 times more heat than the atmosphere and climate models project a mean temperature increase of the sea-surface water between 1 and 4°C by the end of the 21st century. Climate change will decrease the ocean buffer capacity in two ways: first of all decreasing the CO_2 solubility in seawater due to an inverse relationship between temperature and CO_2 solubility. And secondly, the solubility pump buffer capacity will be affected by the increase in seawater stratification and slowdown of the surface to deep exchange of carbon (Gattuso and Hansson, 2011). As for the biological carbon pump, the excess atmospheric CO_2 will cause both carbonification and acidification; the resulting changes in seawater chemistry, will in fact expose marine organism to conditions that they may not have experienced during their recent evolutionary history. Both carbonification and acidification are expected to result in winner and losers potentially leading to loss of biodiversity and restructuring of ecosystem (Riebesell et al., 2009). The consequences of carbonification on marine life are still uncertain but it is expected that the increase in CO_2 concentration will be likely beneficial to some phytoplanktonic organism: carbon fixation and primary production may increase in organism with inefficient DIC uptake and CO_2 production (Riebesell et al., 2007). On the other hand the increase in [CO_2], [DIC] and [HCO^{3-}] will consequently decrease and [CO_3^{2-}] and pH ~ 0.25-0.45 in 2100 compared to the industrial values. Ocean acidification has been proved to have negative effects on calcifying organism (Riebesell et al., 2000; Fabry et al., 2009; Riebesell and Tortell, 2011): coccolithophore algae show decreased calcification with decreasing pH in both laboratory and field observations (Engel et al., 2005). However, an increase in calcification of a strain of *E. huxleyi* has been observed (Iglesias-Rodriguez et al., 2008); this unexpected result seems to be mainly due to a different laboratory methodology (Riebesell et al., 2008). Studies on different coccolithophores strains and species suggest an inter- and intra-specific variation in response to ocean acidification and particularly an optimum response curve has been proposed (Krug et al., 2011), with the optimum met at different levels for different strains and or species, resulting in variations in observed responses over the same pCO_2 range.

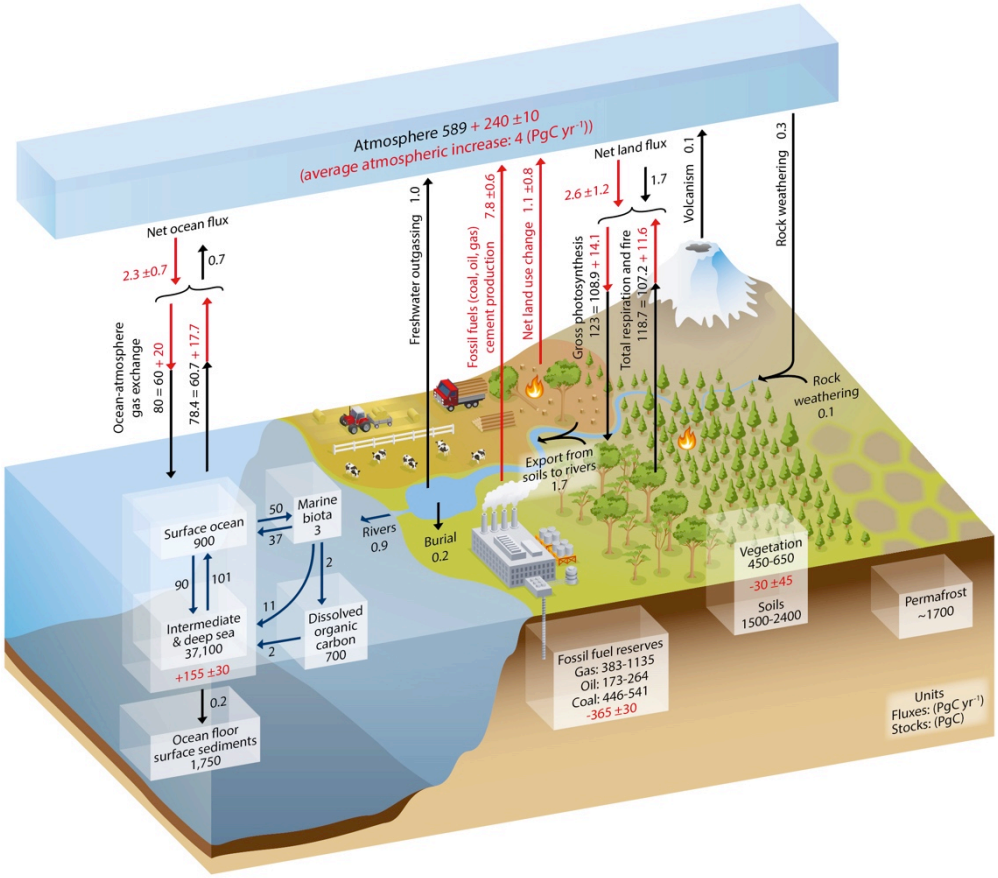

Fig. 2.3 Schematic representation of the global carbon cycle. Numbers represent reservoir mass (carbon stocks) expressed in PgC (1PgC=10^{15} gC) and annual carbon exchange fluxes (in Pg yr^{-1}). Black numbers and arrows are the reservoir mass and exchange fluxes estimated for the time prior to the Industrial era (prior to 1750). Red arrows and numbers indicate annual anthropogenic fluxes averaged over 2000-2009 time period. They represent the perturbation of the carbon cycle during the Industrial Era post 1750. These fluxes are: *Fossil fuel and cement emissions of CO_2*, *Net land use change* and the *Average atmospheric increase of CO_2*. The uptake of anthropogenic CO_2 (carbon sink) by the ocean and terrestrial ecosystem are represented by the red arrows of the *Net land use* and *Net ocean flux*. Red numbers in the reservoir highlight the cumulative changes of anthropogenic carbon over the Industrial period 1750-2011: positive cumulative changes mean that the reservoir has gained carbon since 1750. Fluxes of volcanic eruptions, rock weathering, export of carbon from soils to river, burial of carbon in freshwater lakes and reservoirs and transport of carbon by rivers to the ocean are assumed to be pre-industrial fluxes unchanged during 1750-2011 [from Jansen et al., In: Climate Change 2007: The Physical Science Basis. Contribution of Working Group I to the Fourth Assessment Report of the Intergovernmental Panel on Climate Change].

The expected decrease in calcification will have two different consequences on the global carbon cycle that will result in two opposite feedbacks:

1. Positive feedback: the calcite produced in surface waters acts as ballast and favors the downward flux of the biological pump. A decrease in $CaCO_3$
2. Production will determine a reduction in calcite ballast and therefore a reduction of the export of organic carbon into deep water (Armstrong et al., 2002). This will determine a reduction of the air-to-sea CO_2 flux.
3. Negative feedback: the decrease in calcification will reduce the carbonate counter pump, increasing the air-to-sea CO_2 flux (Riebesell et al., 2009).

It's not clear which of these two process will prevail and particularly which will be the response of coccolithophores over longer time-scales.

Chapter 3
Ocean acidification in the past

3.1 Introduction

Ocean acidification may have severe consequences for the marine ecosystem. The so-called "great geophysical experiment" (Revelle and Seuss, 1957) that we are experiencing has no precedents in the recent history of the Earth: reconstruction of pH evidences that the ocean surface has not been so acid (low pH) for the last 2 million years (Hönish et al., 2009). Laboratory simulations and computer models are currently insufficient to predict the future ocean scenario. However, the Earth has already experienced a huge numbers of natural perturbations of carbon cycling and climate change (Fig. 3.1). These global carbon cycle perturbation events share many of the characteristics of anthropogenic ocean acidification. Studies of the geological record can therefore provide valuable insights into ocean and marine ecosystem impact and recovery to natural perturbations, in order to understand and predict the consequences of the ocean acidification that we are nowadays experiencing. Particularly, studies of geological records may provide new information about the ability of marine species to adapt to extreme climatic conditions. Even if it is important to take in mind that there's not a perfect analogue for today in the Earth history, the strength of the geological record lies in revealing past coupled warming and ocean acidification events sharing with future events the same combination and sign of environmental changes.

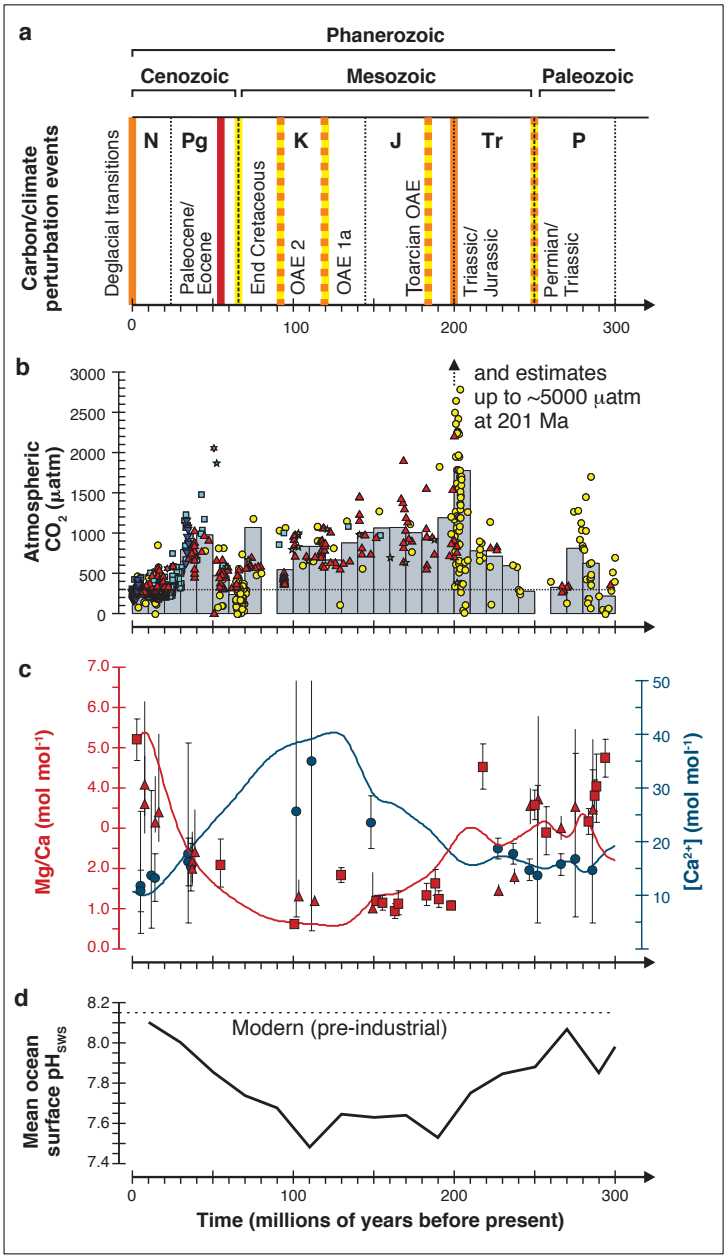

Fig.3.1 Models and reconstructions of past oceanic acidification events; **a)** past oceanic events and degree of similarity with modern ocean acidification. Red indicate most similar event; yellow less similar event. **b)** pCO_2 reconstruction with different proxy data (yellow circles: paleosol $\delta^{13}C$; light blue square: marine phytoplankton $\delta^{13}C$; red triangles: stomatal indices ratios; dark blue triangles planktic foraminiferal $\delta^{13}B$; purple stars: sodium carbonates. **c)** Ocean Mg/Ca ratio (red symbols) together with Phanerozoic seawater model (red line); $[Ca^{2+}]$ and models (blue line). **d)** Model reconstruction of pH variations [from Hönisch et al., 2012].

3.2 Oceanic Anoxic Events

In the early phases of ocean explorations (Deep Sea Drilling Project), blackish sediments exceptionally rich in organic carbon (C_{org}) were recovered from Cretaceous successions in a great variety of settings including rises and plateaus in the central Pacific Ocean and in the Atlantic ocean, in addition to the Tethyan continental margins and the shallow-shelf areas of northwest Europe. These coeval lithologies suggest widespread to global deposition of C_{org} -rich sediments (primarily black shales) during time intervals named

Oceanic Anoxic Event (OAE; Schlanger & Jenkyns, 1976) indicating dysoxic if not anoxic conditions at the seafloor. The general definition in early works was applied to two time intervals: Aptian-Albian (OAE 1) and Cenomanian-Turonian (OAE 2). Afterwards, the numbers of OAEs has multiplied over time and high-resolution stratigraphy modified the original lithostratigraphic concept of a long OAE 1 interval, by recognition of a number of discrete subevents. The most prominent OAEs have been identified within the Cretaceous; only another one is dated as early Toarcian (Jurassic), but a number of similar events are recognized also from the Palaeozoic Era. Nevertheless, of all OAEs only three are suggested to be of global significance: early Toarcian OAE (~183 Ma), early Aptian OAE 1a (~120 Ma) and latest Cenomanian-OAE 2 (~ 93 Ma). The definitions of these three truly global OAEs are "C_{org} rich black shales with extremely low or absent carbonate and locally abundant radiolarian layers " (Jenkyns, 1999). On the contrary, other OAEs (OAE 1b, OAE 1c, OAE 1d, OAE 3) seem to have a regional significance: OAE 1c and OAE 1d have been recognized particularly from the Tethyan domain (Arthur et al., 1990), while, although the Coniancian to Santonian OAE3 is essentially represented by extensive black shales in the Atlantic, equivalent outcrops in the Western Interior of United States are known (Fig. 3.2; Arthur et al., 1990; Wagner et al., 2004). Although global anoxia and enhanced organic matter burial are the most striking and intriguing paleoceanograhic phenomena, OAEs can be studied to decipher the oceanic ecosystem response to (sequence of) CO_2 pulses (e.g. Kemp et al. 2005; Turgeon & Creaser 2008; Mehay et al 2009), extreme warmth (Jenkyns, 2003), weathering changes (Cohen et al., 2004; Tejada et al 2009; Bottini et al. 2012), and ocean acidification (Erba 2004; Weissert & Erba 2004, Kump et al 2009; Erba et al. 2010). The main problem of using geological examples is the major difference in change rates, which are much faster today than for the long-term geological processes leaving fingerprints in sedimentary successions. I'm conscious of the limitations intrinsically imposed by the geological records, but believe that past episodes of excess CO_2, extreme warmth and ocean acidification should be analyzed to add the long-term and large-scale prospective to investigations on current, very-short-term and local responses.

For both the Toarcian and Cretaceous OAEs recent data suggest an abrupt rise in temperature, induced by rapid influx of CO_2 into the atmosphere from volcanogenic

and/or methanogenic sources, that set in train a concatenation of sedimentary, geochemical and biological events (e.g. changes in stratification and mixing, changes in marine productivity and/or turnover in the marine biota). Since OAEs are characterized by anomalously high burial rates of marine and organic matter, an increase in the $\delta^{13}C$ values of marine and atmospheric carbon is predicted. This is confirmed across the Cenomanian-Turonian boundary since 1980; instead, the Early Aptian and Early Toarcian OAE are more complex since carbonate and organic matter show both positive and negative excursions (Menegatti et al. 1998; Erba et al. 1999; Schouten et al., 2000; Jenkyns, 2003; Herrle et al., 2004; Jenkyns, 2010): early Aptian OAE 1a shows a negative excursion that coincides with the lowest stratigraphic levels of the organic-rich black shales; after it, isotopic values start to rise. A similar pattern is seen in the Torcian OAE: a positive excursion with an abrupt negative fall is registered in the central portion. The positive excursion may be attributed to massive global burial of marine organic matter on global scale (Jenkyns, 2010), while influx of isotopically light carbon into the ocean-atmosphere system may be responsible of the opposite negative excursion. Explanation for the input of isotopically light carbon might be large-scale venting of volcanogenic carbon dioxide, dissociation of methane gas hydrates and/or thermal metamorphism of coals. There's still a strong debate on the importance of these processes (Menegatti et al. 1998; Hesselbo et al. 2000; Jahren et al., 2001; McElwain et al., 2005; Kuroda et al., 2007; Jenkyns, 2003, 2010). The traditional model implies an accelerated hydrological cycle caused by global warming and consequently increased continental weathering (Weissert, 1989; 2000); this might have risen up nutrient content in oceans, intensified upwelling and increased production and preservation of organic matter. However, submarine igneous events per se probably have stimulated increases in organic productivity, with the introduction of biolimiting metals by hydrothermal plumes (Sinton and Duncan, 1997; Snow et al., 2005; Erba et al, 2015). Indeed the Mesozoic OAEs are interpreted as the related to submarine volcanism during the construction of large igneous provinces (LIPs). LIPs are massive emplacement of intrusive or extrusive rocks erupted over geologically short periods (1-3 My). The Early Aptian OAE 1a is correlated to the emplacement of the Ontong Java Plateau, while the Cenomanian-Turonian OAE 2 to the extrusion of the Caribbean Plateau and Madagascar traps. The osmium and strontium isotopic have the potential to reflect the balance among weathering and stream transport

and/or volcanism and hydrothermal activity (Tajada et al., 2009). During OAE 1a a 880 kyrs Os-isotope interval of unradiogenic values is unambiguously derived from a mantle source and most likely related to the Ontong Java Plateau eruption (Tajada et al., 2009; Bottini et al., 2012). Furthermore the unradiogenic Os isotopic excursion is accompanied by an increase in $\delta^{13}C_{org}$ suggesting a causative link between volcanism and enhanced organic deposition. However a short-lived (100 kyrs) radiogenic Os-isotope excursion during OAE 1a suggests a diminished Ontong Java Plateau volcanic activity and/or an increase in the total flux of radiogenic Os supplied to the ocean through continental weathering. The same pattern is observed in the strontium isotope signature where the general negative excursion, is interrupted by an increase in the $^{87}Sr/^{86}Sr$ (Jones & Jenkyns, 2001). With or without a temporary cessation in the Ontong Java Plateau volcanic activity, the documented increase in global temperature (e.g. Ando et al., 2008; Erba et al., 2010) during the first phase of OAE 1a is likely to have been responsible for accelerated weathering rates and subsequent Os- and Sr positive isotope excursion. Similarly, the isotopic data for the latest Cenomanian OAE 2 highlight a progressive trend to unradiogenic Os values and a decline of the $^{87}Sr/^{86}Sr$ ratio that slightly preceded the OAE 2 onset (Jones & Jenkyns, 2001; Du Vivier et al., 2014): the mafic volcanism of the Caribbean plateau is considered responsible of the unradiogenic values. This trend is synchronous in different sections from different paleoceanographic settings, suggesting that the magnitude of the Caribbean plateau volcanism was sufficient to influence the seawater chemistry at a global level. During OAE 2 a progressive return to more radiogenic values might indicate a more intense weathering. However it is plausible that the extent of weathering on seawater chemistry is masked by the Caribbean LIP and vice versa: quantifying the magnitude and isolating the extent of the two signals appears to be problematic (Du Vivier et al., 2014). On the contrary across the Toarcian OAE the $^{87}Sr/^{86}Sr$ curve increases, with no evidence of a negative shift (McArthur et al., 2000). This positive excursion of the $^{87}Sr/^{86}Sr$ data is explained by the formation of subaerial flood basalts in the Karoo-Ferrar province (Jenkyns, 2010). Termination of OAEs may have been forced by sequestration of CO_2 by both silicate weathering and photosynthetic fixation into sedimentary organic matter, causing final sowing of the hydrological cycle.

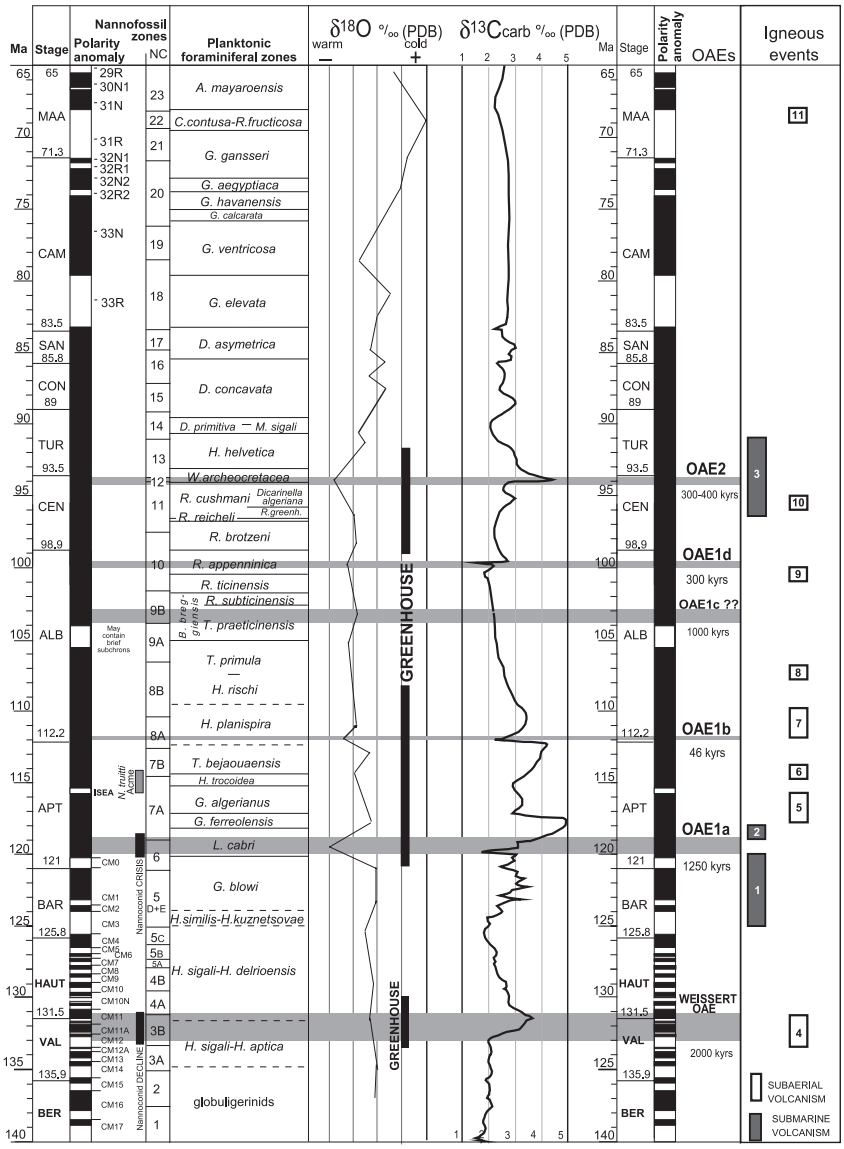

Fig.3.2 Cretaceous OAEs correlated with the Large Igneous Provinces (LIPs) and bio-, chrono-, magneto-, and chemo-stratigraphy [from Erba et al., 2004]

3.3 The latest Cenomanian

Oceanic Anoxic Event 2

The Cenomanian-Turonian Oceanic Anoxic Event 2 (OAE 2) is one of the best documented and most extensively studied oceanic anoxic events. It is dated at ~93 Ma (Fig. 3.3), close to the Cenomanian-Turonian boundary, and is associated with short-term changes in atmospheric pCO_2, extinction of a number of marine biota and ocean chemistry turnover. The sedimentary record of OAE 2 varies from place to place: the distribution of black shales during OAE 2 is clearly diachronous relative to the $\delta^{13}C$ anomaly and was therefore influenced by a variety of environmental factors peculiar to the basin (Tsikos et al., 2004; Meyers, 2007). This is in conflict with the original definition of an OAE that implies coeval deposition of organic-rich sediments at global scale. These organic-rich sediments, however, became globally significant: the increase of organic matter deposition led to enhanced burial of ^{13}C-depleted carbon, which resulted in a ^{13}C-enriched global carbon reservoir. This is registered as a positive excursion in the stable carbon isotopic composition, $\delta^{13}C$, of sedimentary components (including organic matter and carbonates) across the OAE 2 (Tsikos et al., 2004). This positive excursion is a major characteristic of OAE 2 and a fundamental tool to correlate different OAE 2 sections. Therefore, recent studies highlight that the total duration of OAE 2, from the first rise of the carbon isotope excursion to the termination of the plateau when values start to decrease (Fig 3.3; Kuypers et al., 2002), must range from 435 to 600kyr (Sageman et al., 2006; Joo & Sageman, 2014).

New high-resolution carbon- and oxygen-isotope records of OAE 2 were obtained for three Italian Tethyan sections: Cismon (Belluno Basin), and Furlo, and Monte Petrano (Umbria–Marche Basin) deposited in pelagic settings characterized by the alternation of nannofossil-planktonic foraminiferal oozes, radiolarian-rich intervals and shales (Fig. 3.4; Gambacorta et al., *submitted*). The $\delta^{13}C$ records a large positive anomaly (~2–3‰) in $\delta^{13}C_{org}$ of the Bonarelli Level corresponding with OAE 2. Detailed carbon-isotope stratigraphy, calibrated with nannofossil biostratigraphy, provided high-resolution dating and correlation, allowing the identification of hiatuses in the studied sections. In

particular, the high-resolution $\delta^{13}C$ profiles across the OAE 2 interval highlight the presence of hiatuses of variable extent that affect the middle to upper part of the characteristic carbon-isotope excursion and part of the following interval in all the studied sections. Locally, there is some evidence for a possible hiatus at the base of the Bonarelli Level. Correlations with complete carbon-isotope records available for widespread localities, allow an estimate of 400 to 700 kyrs missing time in the middle to late part of OAE 2 and the immediately following interval. The origin of such gaps can be attributed to physical and/or chemical processes operating at the seafloor. Complete recovery from the peculiar physico-chemical conditions that characterized the deeper parts of the Tethys Ocean during OAE 2 took at least 1 million years. For further details, the reader should consider Appendix I.

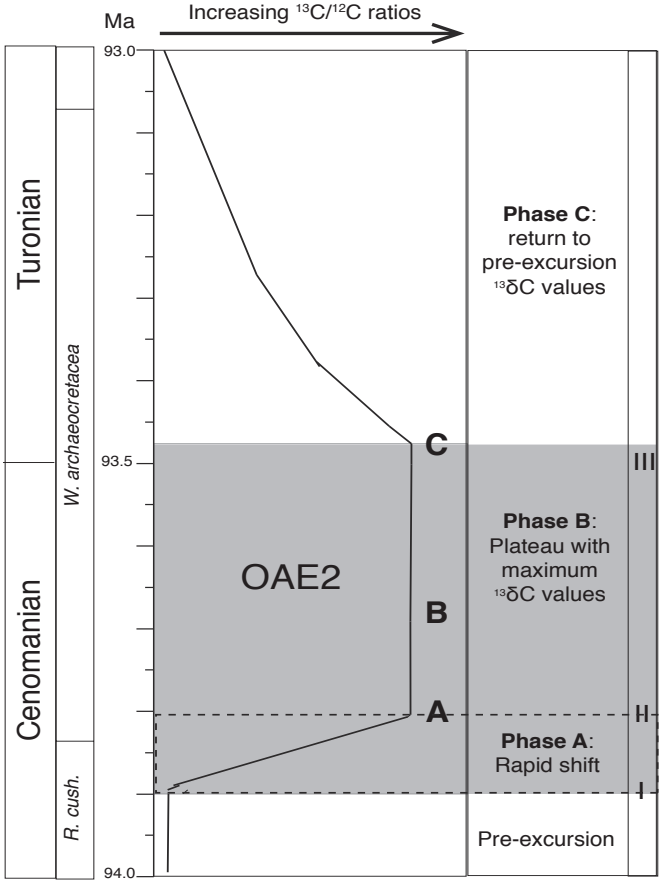

Fig.3.3 Schematic representation of OAE2 [modified from Kuypers et al., 2002].

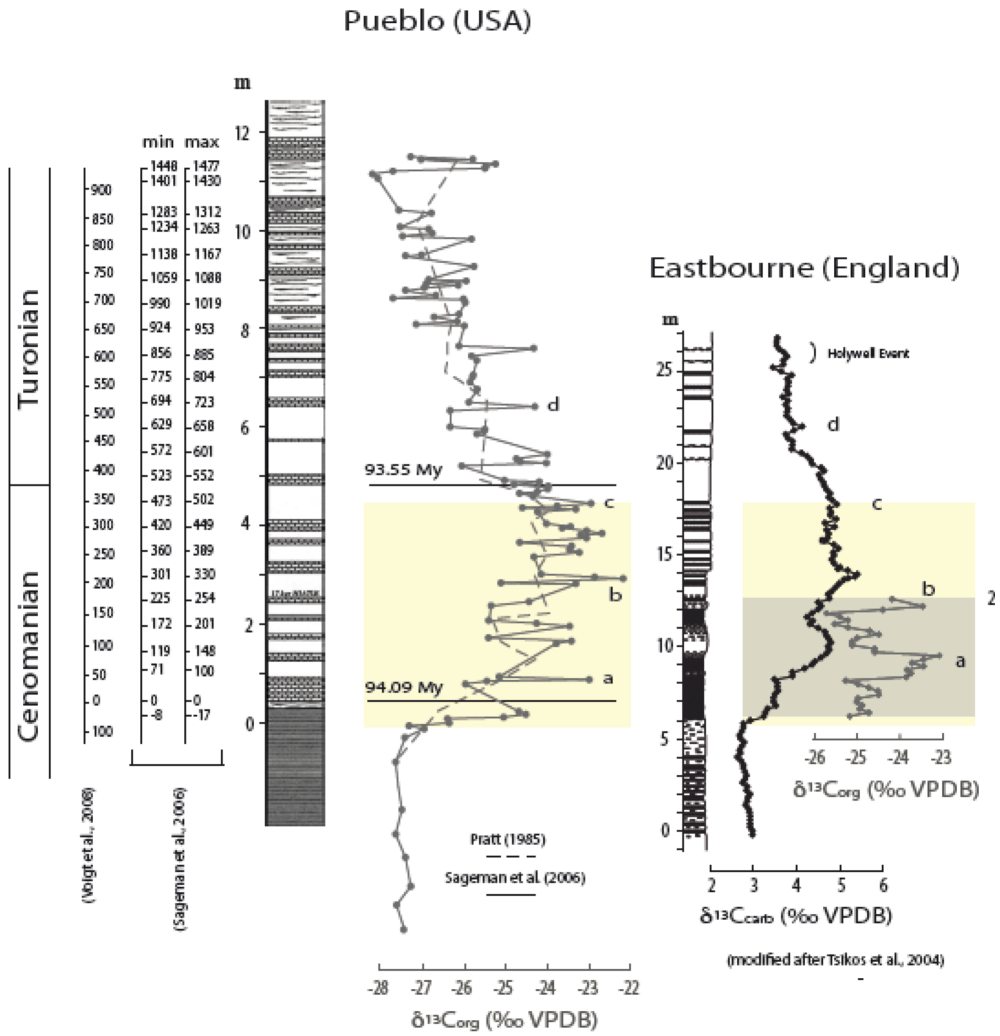

Fig. 3.4 Carbon-isotope profiles for the OAE 2 interval at the GSSP key-locality of Pueblo (Colorado) and the English section of Eastbourne. On the left the cyclostratigraphy is reported to show duration of OAE 2 [after Gambacorta et al., *submitted*]

Sea-waters during Cenomanian-Turonian OAE 2 were influenced by oxygen deficiency that set up frequent and prolonged suboxic conditions (Kuypers et al., 2002a; Kolonic et al., 2005; Scopelliti et al., 2006, 2008). Anoxic conditions can be triggered by different mechanism: restriction of the basin, intense upwelling and enhanced primary productivity with subsequent consumption of oxygen, or freshwater input promoting stratification of the water column. Restricted basin were favoured by the Cenomanian-Turonian paleogeography: the proto-North Atlantic was a semi-enclosed basin with steep continental slopes and relatively narrow connections to the Tethys in the East and Pacific Oceans in the West. Increased sea level during the mid-Cretaceous caused the formation of a vast epicontinental seaway (Western Interior Seaway) in the middle of North

America (Watkins, 1986; Eleson & Bralower, 2005; Corbett & Watkins, 2013) and an archipelago with extensive continental shelves in Europe (Hancock and Kauffmann, 1979). The restriction of the proto-North Atlantic Basin may have therefore favored the formation of oxygen-depleted water masses. Climatic conditions during OAE 2 were linked to very high carbon dioxide concentrations; reconstruction of sea surface temperature (SST) indicate strong warming within OAE 2, with SST increased of more than 5°C (Bice et al., 2006; Forster et al., 2007), possibly reaching 33-42°C in the mid and tropical latitudes and potentially more than 20°C in the Artic region (Jenkyns et al., 2004). However, the mid-Cretaceous temperature rise, at shorter timescales, displays temperature variations in relation to the global carbon cycle (Voigt et al., 2004): in the mid-Cenomanian, and late Turonian two cooling episodes of ~ 2-3°C are registered in the isotope signature; this is also testified by intrusion of boreal fauna, including belemnites and bivalves (Voigt et al., 2004; 2006). Cooling events are explained with two mechanisms: the decrease of CO_2 connected with excess carbon burial intervals (Kuypers et al., 1999, 2002a; Voigt et al., 2004; Gale et qal., 2005), or the increase in weathering of continental crust. Indeed OAE 2 models suggest that global warming, triggered from massive volcanism, caused an intensification of the hydrological cycle, promoting an increase in the basaltic weathering rate and intensity (Pogge von Strandmann et al., 2013). Weathering started to intensify almost 25-30 kyrs before the OAE 2 onset (Turgeon and Creaser, 2008; Pogge von Strandmann et al., 2013), and reached its peak around 300 kyrs after the start of volcanism. Intense weathering might have increased the flux of nutrient to the ocean and thus help to stimulate biological activity (Jones & Jenkyns, 2001). Subsequently, weathering began to decline to a more weathering-limited regime, reaching pre-excursion levels in 100-300 kyrs, allowing a gradual recovery of the ocean. Extensive volcanism was associated to the formation of the Caribbean, Madagascar and/or part of the Ontong Java Plateaus that acted as a natural source of CO_2. Geochemical data indicate that CO_2 started to increase (by ~600 ppm) prior to the major organic carbon burial and OAE 2 onset (Turgeon and Creaser, 2008; Du Vivier et al., 2014) reaching concentrations of about 900 – 1300 ppm (Damstè et al., 2008; Barclay et al., 2010).

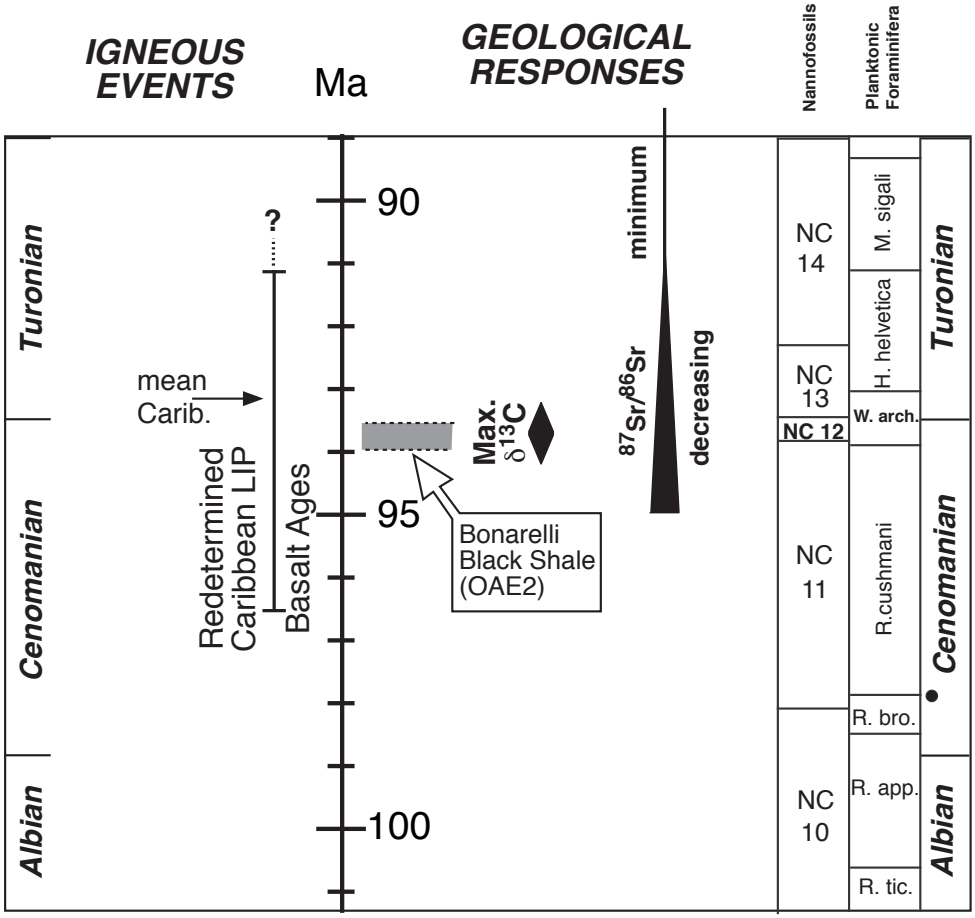

Fig. 3.5 Summary of the latest Cenomanian OAE2 [from Larson, Duncan, Erba 2002].

Recently, Du Vivier et al. (2014) documented high-resolution osmium isotope stratigraphy across the Cenomanian–Turonian Boundary Interval from sections from different basins. The $^{187}Os/^{188}Os$ profiles show a comparable trend with radiogenic values before OAE 2 and a synchronous abrupt unradiogenic interval at the onset of and through the first part of OAE2. At the end of the event, Os values return more radiogenic. The synchronicity of the unradiogenic Os pattern suggests that the Caribbean LIP volcanism was crucial in promoting global perturbation, perhaps with contributions by the High Arctic LIP. In the Western Interior Seaway, Du Vivier et al., (2004) noticed a radiogenic Os peak just before the onset of OAE 2, possibly indicating the onset of global warming promoting accelerated weathering and continental nutrient recycling into the ocean, thus pre-conditioning the environment to the major perturbation.

During OAE 2 a temporary CO_2 drawdown (decrease of circa 25%) is recorded reflecting the delicate balance between CO_2 input versus continental weathering and organic carbon burial, coherently with the previously quoted short-term temperature decrease. In particular, a marked pCO_2 minimum occurred with a SST minimum of the Plenus Cold Event showing >4°C of cooling in ~40kyr (Jarvis et al., 2011). This CO_2 minimum was also documented by terrestrial proxies (stomatal indices; Barclay et al., 2010). In the later phase of OAE 2, reduced negative feedbacks allow a further pCO_2 rise, indicating continued input of volcanic greenhouse gas emission. The end of OAE 2 points to several factors that might have synergically acted: decrease of volcanic activity (reduced CO_2 emissions), transgression and flooding of continental interiors (lower erosion rates), reduced weathering and subsequent reduction of terrestrial nutrient supply with a resulting drawdown of open-ocean productivity.

Changes in abundance and composition of calcareous nannoplankton precede the $\delta^{13}C$ anomaly and deposition of C_{org}-rich sediments (Erba, 1993, 2004). Therefore, nannoplankton responded to the early phases of paleoenvironmental variation and continued to trace the perturbation in the ocean/atmosphere system during OAE 2. Phytoplankton (and zooplankton) changes are interpreted as the response of the biosphere to increasing fertility, culminating in the high-productivity event coincident with OAE 2 (Erba, 2004): fertility could have become so high that only the most opportunistic nannoplankton taxa continued to thrive. Since enhanced primary productivity is the most accepted explanation for OAE 2 (Jenkyns, 1999), a mechanism capable of triggering eutrophism at a global scale must be found. Coastal nutrification due to increased continental weathering and run-off and/or local upwelling cannot explain the high productivity documented in remote parts of large oceans during the latest Cenomanian. High-resolution studies of sedimentary successions representing OAE 2 show trace-metal peaks coincident with major biotic changes reported before and during this event (Snow et al., 2005). Thus, increasing geological evidence suggests that OAE 2 was mainly an oceanic productivity event, largely controlled by submarine eruptions. Higher trophic levels were essentially induced and maintained by hydrothermal inputs of biolimiting metals (e.g. Fe, Zn) during the construction of the Caribbean Plateaus, which also affected ocean dynamics by warming deep - and intermediate - waters, causing more

efficient nutrient-cycling (warm upwelling; Erba, 2004). The Cenomanian-Turonian OAE 2 is characterized by a carbonate crisis, both in pelagic and neritic environments, during times of extreme greenhouse conditions. By analogy with extant communities, excess volcanogenic CO_2 most probably inhibited biocalcification in calcareous nannoplankton (Erba et al., 2006) and planktonic foraminifers, as well as in reef communities (Erba, 2004). Carbonate sedimentation resumed after excess CO_2 was drawdown by accelerated weathering and burial of organic matter and perhaps nutrient supply slowed down as well. The global carbonate decrease, expressed as deposition of large quantities of organic matter and temporarily biosiliceous sediments, was possibly caused by a combination of excess volcanogenic CO_2, preventing biocalcification in nannoplankton (and foraminifers), and eutrophic conditions favouring organic-walled and siliceous plankton. Extreme conditions during OAE 2 negatively affected nannofloras and a turnover characterizes nannofossil assemblages during OAE 2: several species disappeared, one after the other and then new species originated (Fig. 3.5, 3.6).

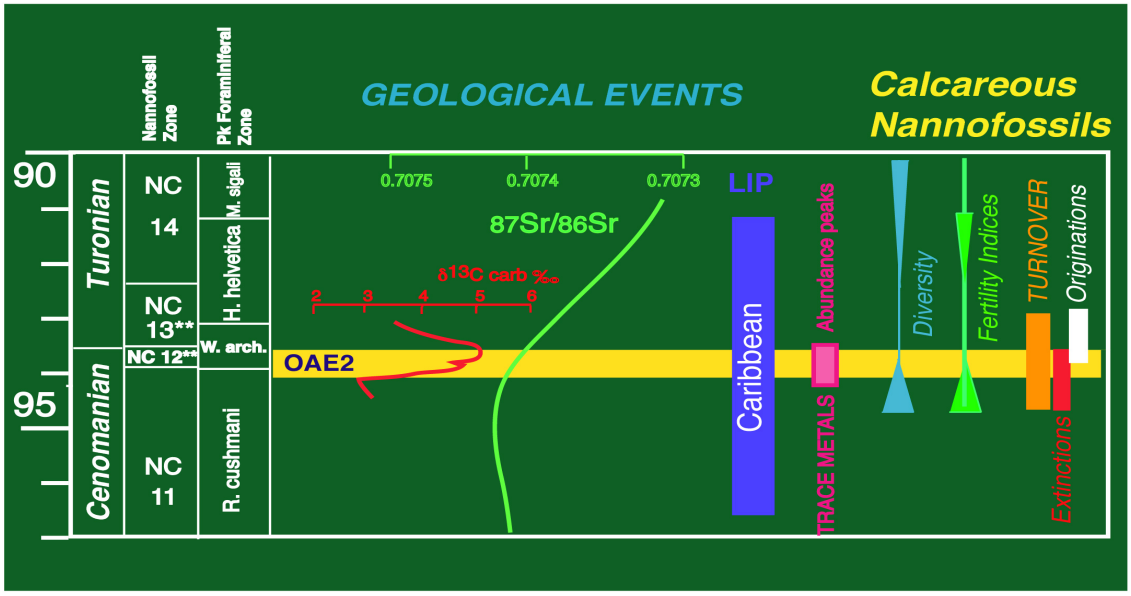

Fig. 3.6 Summary of the latest Cenomanian OAE 2 [from Erba et al., 2004].

Chapter 4

Calcareous nannoplankton

4.1 Coccolithophores algae

Coccolithophores include all haptophyte algae, which have evolved the ability to produce calcified scales (coccoliths) at some stage of their life. Coccolithophores first appearance is dated as Late Triassic, ca. 220 Ma (Bown et al., 1998) and their appearance and evolution can be considered a major revolution in the marine ecosystem. During the Carnian they were represented by 4 families (Fig. 4.1). They aren't convincingly documented in the Palaeozoic, although a few papers report coccolith-like structures (Deflandre, 1970; Pirini Radrizzani 1970; Noel, 1971). It can be hypothesized that nannoplankton already existed in the Paleozoic, but didn't produce mineralized scales at that time: the appearance of coccoliths corresponds to the emergence of calcite biomineralization within the haptophyte algal group, but the origin of haptophyte is considered far more ancient: molecular genetic analyses suggest that the divergence from other algal groups is as old as Neoproterozoic, almost 1200 Ma (Medlin et al., 2008). Observing the significant lag, that intercourse between haptophyte appearance and coccolith diversification (e.g. Falkoski et al., 2004) it can be speculated that coccolith biomineralization was evolutionary difficult to achieve, but once established, was fundamental for the diversification and prosperity of the group. Both Coccolithophore algae and Dinoflagellates appeared soon after the Permian/Triassic boundary mass extinction suggesting a major reorganization of the ocean plankton community at that time during a phase of complete collapse of the marine ecosystem. The oldest nannofossils had a very simple morphology: they were relatively large and heavily calcified nannoliths. But it was a little bit after, that real coccoliths, tiny and with simple morphology, appeared. After the Triassic/Jurassic boundary extinction, that affected calcareous nannofossils too, coccolithophores experienced an impressive diversification (Pliensbachian – early Toarcian; Roth, 1987, Erba 2006), becoming in the Jurassic and Cretaceous the most efficient rock-forming group. Together with planktonic foraminifera they still form the bulk of calcareous deep-sea deposits (Baumann et al., 2004), playing a

major role in oceanic biogeochemical cycle (Rost & Riebesell, 2004). Nowadays, of the approximately 300 haptophytes in the oceans, about 200 are in fact coccolithophores and so far these contribute significantly to the biodiversity of the group (Jordan & Chamberlain, 1997).

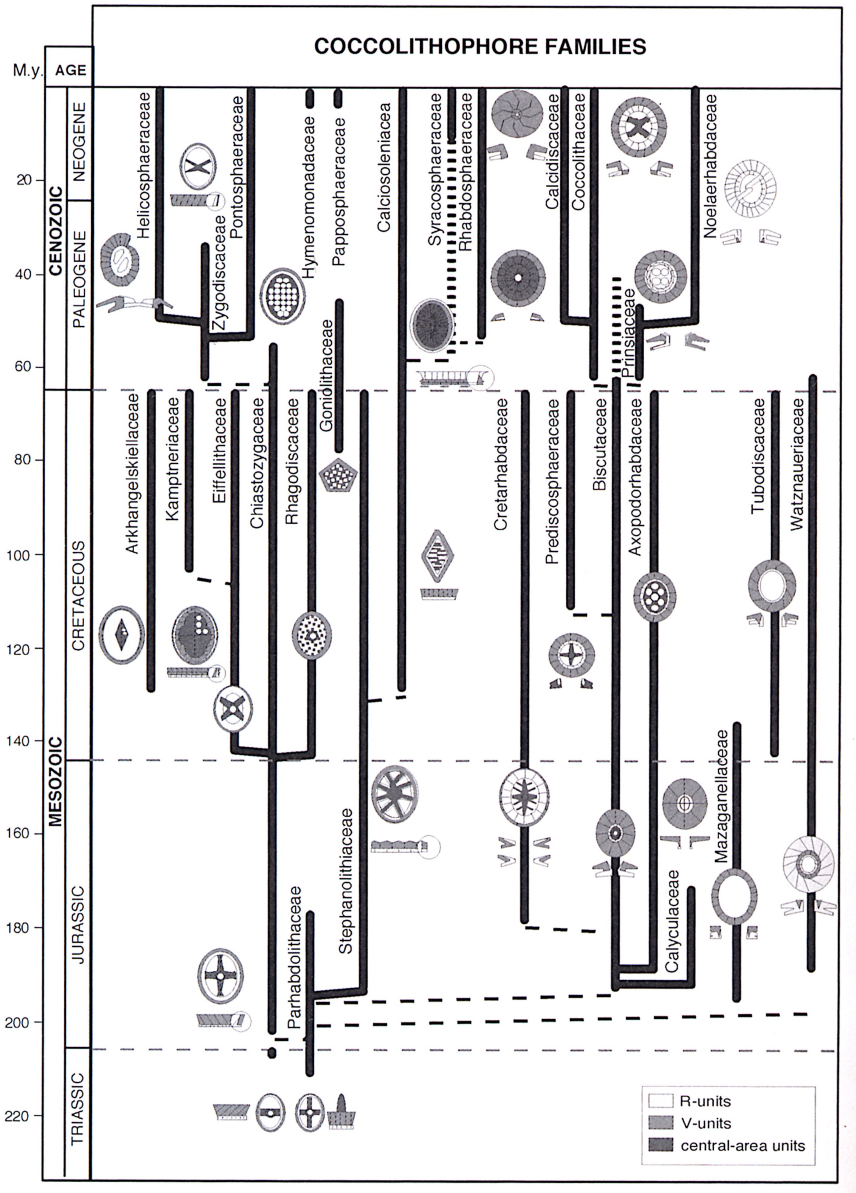

Fig. 4.1 Synthesis of coccolithophorid phylogeny [from Young et al., 1999].

They are a dominant phytoplanktonic group in all oceans except in the Artic seas and high latitudes of Southern Ocean and range from oligotrophic subtropical gyres to temperate and higher latitude eutrophic regimes. They are the most productive calcifiers

of our planet: with their shell they produce a continuous rain from the surface to the deep ocean, modifying upper-ocean alkalinity (reduction of the ocean's capacity to uptake CO_2), producing massive deposits of calcium carbonate at the sea floor and transferring organic matter to the deep ocean (contributing to the vertical CO_2 gradient in the ocean). As calcifying primary producers they contribute to both the organic carbon pump and carbonate counter pump: for instance the draw down of CO_2 due to organic carbon production is compensated by the release of CO_2 via calcification. Thus changes in the contribution of coccolithophores to ocean primary production, can deeply impact the global carbon cycle.

4.2 Coccolithophores biology and ultrastructure

Coccolithophores main cytological aspects have been extensively studied (Pienaar, 1994, Inouye, 1997, Billard and Inouye, 2004a). Briefly, the Coccolithophores consist of single cell composed of nucleus, and normally two golden brown chloroplasts, which contain chlorophylls a + c and capture available light. Chloroplasts are the centre of carbon dioxide fixation. The cell also contains mitochondria (production of enzymes which provide the energy for cell functions), vacuoles (deal with waste products), and the Golgi apparatus (Fig. 4.2). The Golgi body is involved both in the synthesis of organic scales and coccolithogenesis.

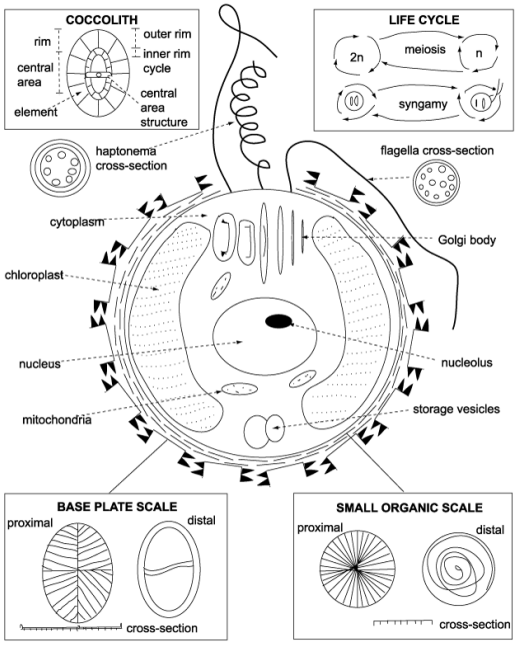

Fig. 4.2 Diagrammatic cross-section of a coccolithophore cell and cell wall coverings [from Bown et al., 1998].

Furthermore Coccolithophores have two flagella and one haptonema. The real function of the haptonema is not clear but it is considered a multi-functional organelle that might have a sensitive or adherence function or plays a role in food capture (Inouye, 1995; Billard and Inouye, 2004a). The flagellar-haptonema apparatus emerge from the cell wall: the periplast consists of various layers of organic scales; the distal scales of the periplast are the calcified coccoliths. Base plate scales are covered with polysaccharide that seems to have a role in attachment (Pienaar, 1994). Organic scales form a base for the precipitation of calcite heterococcolith, which are produced by the Golgi apparatus.

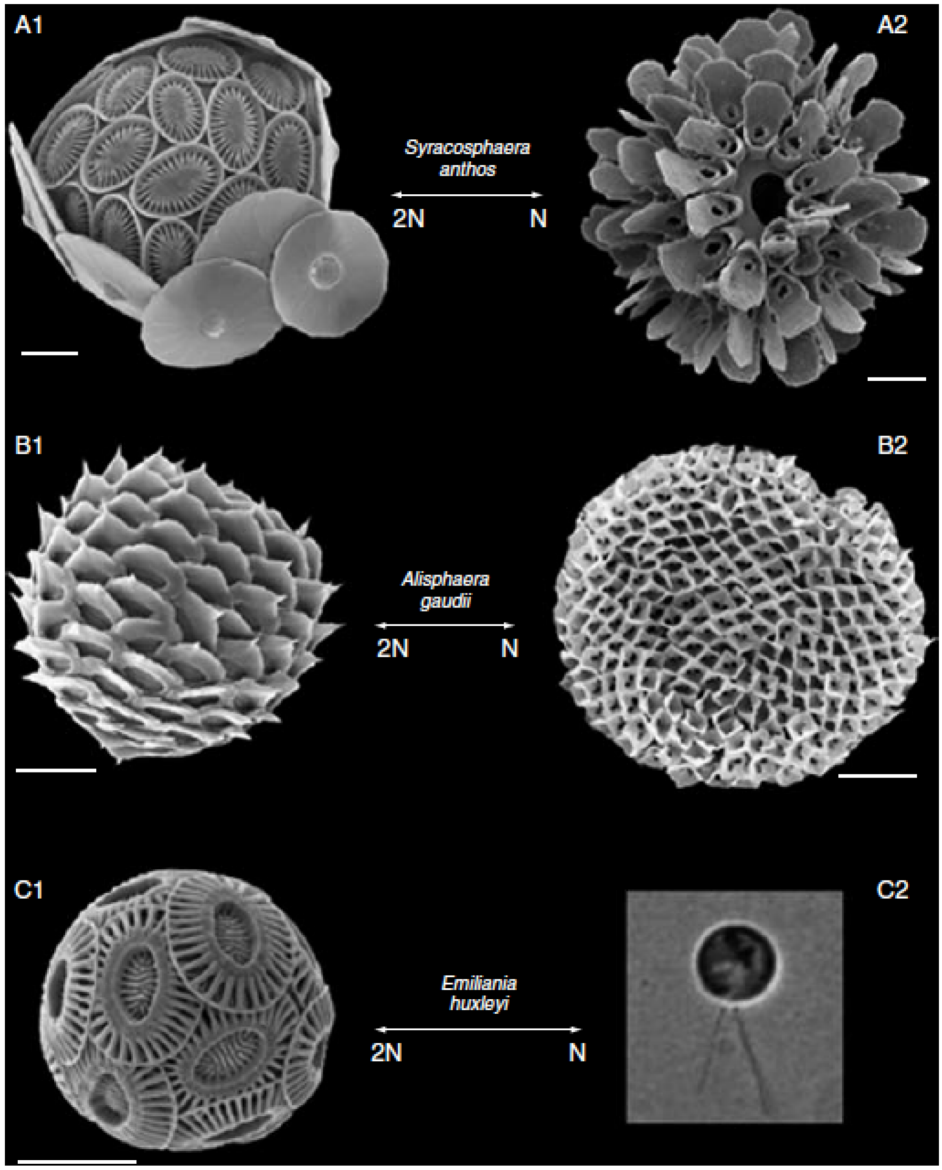

Fig. 4.3 Examples of haplo-diploid phases in a few Coccolithophorids. Diploid and haploid stages of a single species express radically different phenotypes and can be either calcifying or non-calcifying. Scale bars are 2 µm. [from De Vargas et al., 2007].

Coccolithophores developed two types of plates: heterococcoliths and holococcoliths. The two forms were previously regarded as belonging to independent species; however, it's still not entirely clear if holococcolithophores are not autonomous but stages in the life cycle of heterococcolith-covered oceanic species (Billard and Inouye, 2004a). Heteococcoliths consist of radial arrays of complex crystal units and holococcoliths are characterized by large numbers of tiny morphologically simple crystallites. Coccolithophores distinct feature is their haplo-diplontic life cycle: their typical life cycle consists of independent haploid and diploid phases, both of which are capable of indefinite asexual binary fissions (Billard, 1994). During both phases they produce coccoliths with this kind of alternation (Fig. 4.3): the diploid phase is characterized by heterococcoliths, whereas the haploid phase is characterized by holococcoliths. Within these basic categories, various terms are used to identify different kinds of coccoliths based on morphology: cricoliths, helicoliths, appoliths, etc. for heterococcoliths; calyproliths, liminoliths, etc. for holococcoliths (Young et al., 1997).

It should be mentioned that the function of coccoliths is unknown. Coccosphere is widely considered a protection against predation: the coccosphere could have the function to protect the cell from organism that can penetrate or ingest the algae. Penetrators can be considered both viruses and bacteria. The former needs to attach the cell surface and in that scenario, the coccosphere act as strong barrier against infections. In *E. huxleyi*, in fact, viral attack mostly happens during cell division (when the coccosphere is not completely closed, Mackinder et al., 2009). On the other hand bacteria, as is known, can both act as host and not only as infectious. There isn't any information available about the action of bacteria on coccolithophore algae. The most potent predator of coccolithophore is probably microzooplankton, which is a dominant group in today Ocean, and has a size that matches coccolithophores. Coccolith production and structure (e.g. spines that increase the coccosphere diameter) can be a strategy to become unappetizing.

It has been hypothesized that coccolith might act as light concentration regulators: phytoplankton in the upper ocean passively circulates up and down in the mixing layer, receiving fluctuating light levels. Biomass production is strictly related to sunlight: the coccosphere may act as a light gatherer (Gartner & Bukry 1969), as a protection to damages to the cell, or reflect the light inside the cell, allowing life at lower depth (Braarud et al., 1952). It is also plausible a connection between calcification and

photosynthesis: calcification might act as a source of carbon dioxide and the two reactions might be linked (Passche, 1962). Coccolithophore photosynthesis might benefit from calcification that produces CO_2, lowering the energy request from the cell to photosynthesize.

Experimental data are controversial: on one hand, it appears that when coccolithophores are grown in low calcium concentration, there's reduction in calcification but photosynthetic rates are not altered (Trimborn et al., 2007, Mackinder et al., 2011). At the same time there's evidence that the carbonate source that coccolithophorid algae need to photosynthesize is HCO^{3-} instead of CO_2 (Rost et al., 2002). On the other hand, coccolith production requires high energy-cost: there isn't any evidence of a reduction in the growth-rate of calcifying cell compared to naked one as we can expect. A possible function of the coccosphere might also be floating regulation (Young, 1994): accelerated or reduced sinking may help the cell to enter or to remain in suitable levels of the water column.

Besides their function, it's not completely understood how coccoliths are produced. Heterococcoliths production is better understood while fewer observations are available for holococcoliths. Coccoliths occur outside the cell forming a composite shell named coccosphere; coccoliths have a disc-shaped morphology with a more or less concave inner surface.

Heterococcoliths calcite precipitation and growth occurs in vesicles derived from the Golgi body (Young et al., 1999). The coccolith calcification process is, therefore, separated from the surrounding seawater by at least two membranes and can be considered a biological process (Fig., 4.4). Coccoliths are then transfer via exocytosis and become part of the coccosphere (Dixon, 1900). Calcification process starts with the formation of an organic scale named base plate (Van der Wal et al., 1983a) that normally has a microfibrillar structure. Some scales are exocytosed without any evolution while other scales undergo a nucleation process: nucleation of calcite occurs on the rim of the base plate, forming a closed ring (proto-coccolith ring), followed by an upward and outward crystal growth to form the complete coccoliths.

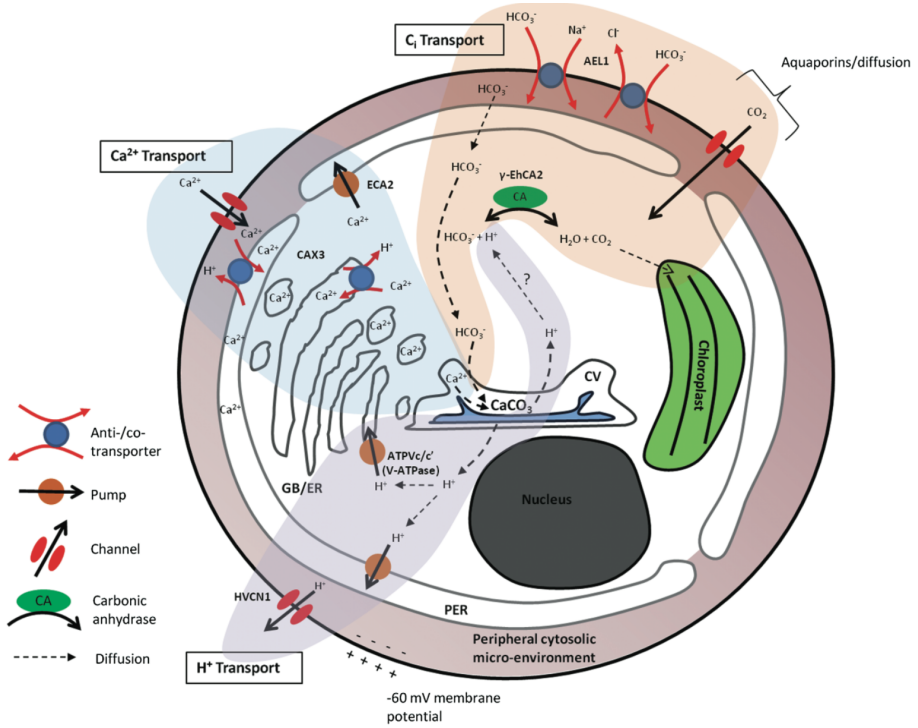

Fig. 4.4 A conceptual model of C_i, Ca^{2+} and H^+ transport related to calcification in coccolithophores [from Mackinder et al., 2011].

The coccolith ring is based on two crystals unit type with two different orientations that are alternated with one another: vertical oriented axes (V-unit) and radial oriented axes (R-unit). Nucleation controls total crystallographic orientation (Davis et al., 1995, Young et al, 1999). Coccoliths growth occurs inside vesicles that remain in close contact with it throughout the development; it is therefore plausible that the vesicle concur to the final coccolith shape (mechanical control), causing the crystal to grow in specific directions (Westbroek et al., 1984). Coccolith crystals seem to be also enveloped with a narrow coating of organic matter that cover coccoliths cover and extends between crystals. Even if in some species this coating material has not been detected, there are indirect evidences of its presence (e.g. obscured surface on SEM images; selectivity on dissolution of coccoliths…)

V/R nucleation process is a very common feature among heterococcoliths and has been identified in both fossils and modern coccoliths (Fig. 4.5, Young et al., 1999) and is supposed to have evolved only once and been conserved through the 230 Ma evolution of the group, suggesting a monophyletic origin for heterococcolithophores (Fig. 4.6).

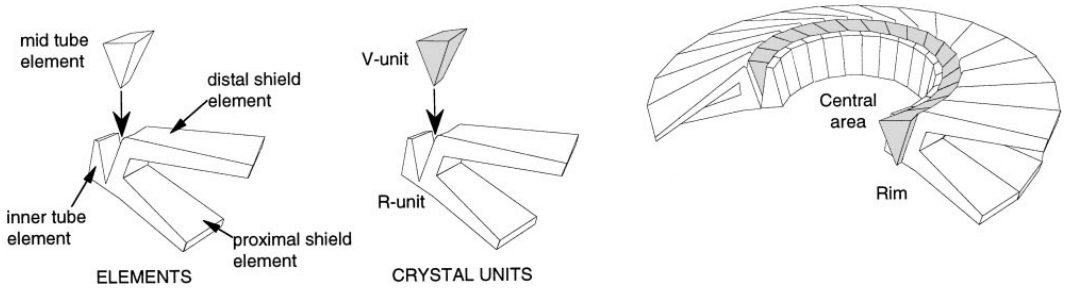

Fig.4.5 Heterococcolith structure and terminology (exemplified by Watznaueria). A single segment consists of two crystal units, V unit, and a R unit consisting of several superficially discrete elements. The concave surface is directed toward the cell and so is termed proximal, or lower [from Young et al.1999].

Less data are available for holococcoliths production. Holococcoliths are less common: they also have a disc-shaped structure but they are formed entirely of uniform-shaped crystallites. Even if, like heterococcoliths, they are surrounding by an organic coating, their calcification occurs outside the cell (Manton and Leedale, 1969) and it is hypothesized that the coccosphere grows progressively starting from the flagellar pole (Young et al., 1999). Holococcoliths calcification seems to involve less regulation of crystal growth and there are not clear indications of holococcolith-shape control mechanism.

Holococcoliths fossil record is much less complete, but is proven to be present in the Jurassic era (Young et al., 1999). It seems therefore plausible that both heterococcoliths and holococcoliths evolved near the evolution on the group and they both can be considered an alternative adaptation of a similar calcification mechanism.

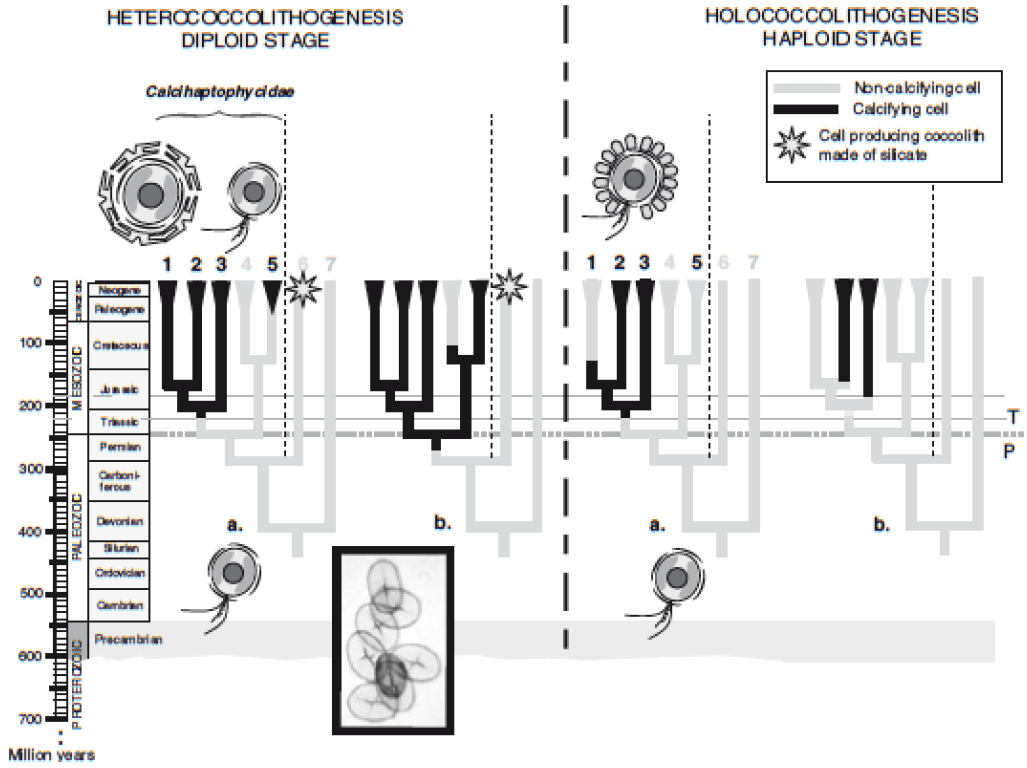

Fig. 4.6 The multiple origins of coccolithogenesis in the haploid and diploid stages of calcihaptophytes, based on DNA data. The horizontal dotted lines in the middle of the figure indicate, from bottom to top, the P/T boundary, the first fossil heterococcolith, and the first fossil holococcoliths [from De Vargas et al., 2007].

4.3 Cellular calcification to changing environmental conditions

In the face of global warming, coccolithophores are subjected to strong alterations of their environmental conditions. Dependency or interconnections on photosynthesis and calcification in coccolithophores are still under debate (Riebesell, 2004). Most of the available information originates from the massive works on *Emiliania huxleyi* that evolved only 270 kyrs ago and became the most dominant coccolithophore in the ocean. It seems plausible that calcification can be influenced by many environmental parameters that will be elucidated in the next paragraphs

4.3.1 Light

The general habitat for coccolithophores is the photic zone that provides the necessary sunlight necessary for photosynthesis. Coccolithophores have no photoinhibition: *E huxleyi* and *P. carterae* are known to photosynthesize and calcify even at very high irradiances up to 1700-2500 μmol photons m^{-2} s^{-1} (Nanniga & Tyrrell, 1996, Zordevan 2007) where other phytoplanktonic groups are inhibited (Nanniga & Tyrrell, 1996). As a comparison, the irradiance of the sun, that is controlled by the intensity of sun radiation, by the albedo and by the angle in between the sea surface and the sun, at noon and under clear skies is 2000 μmol photons m^{-2} s^{-1}. Even if lab experiments and midsummer bloom observations suggest that coccolithophores prefer growing at high irradiance (Baumann et al., 2000), although they are able to grow also at low irradiance but with lower growth rates (e.g. 0.5 day^{-1} at μmol photons m^{-2} s^{-1}, Zondervan et al., 2002). Cell volume and particulate organic matter concentrations are reported to increase with increasing light intensity (Muggli & Harrison, 1996) but, on the other hand, chlorophyll a concentration is reported to decrease relative to organic carbon with increasing light intensity (Harris et al., 2005). Coccolith production is less dependent to strong light compared to photosynthesis because up to 15% of the coccolithogenesis process happens in the dark (Paasche and Brubak, 1994).

4.3.2 Nitrogen and phosphorus

Nitrate and phosphate are distributed in the global ocean at a ratio 16:1 (Redfield, 1934) and they both increase with depth due to the consumption by phytoplankton in the euphotic zone and later recycling during sinking of organic matter particulates. Nitrogen is the most abundant element in the atmosphere and it dissolves in the sea-water, where the dominant bioavailable reservoir is represented by nitrate (NO_3). Phosphorous oceanic reservoir comes from continental weathering and the dominant bioavailable species is phosphate (PO_4^{3-}).

In coccolithophores it seems that reduced level of P increases the number of coccoliths in *E. huxleyi* (Paasche, 1998). Furthermore, *E huxleyi* displays an increase in size under P limitation situation. This is not observed in low N conditions. In general, coccoliths in N

limitation conditions appear to be undercalcified, while overcalcification is evident in P limitation condition (Paasche, 1998). Finally, *E huxleyi* in both lab and field observations show that malformations and size changes can be imposed by nutrient stress (Passche, 1998) with an inverse relationship: high nutrient stress induces smaller sizes and malformation.

4.3.3 Carbonate System

The dissolved inorganic carbon (DIC) is present in 3 forms:

$$DIC=[CO^{2}]+[HCO^{3-}]+[CO_3^{2-}]$$

bicarbonate (HCO_3) that is the most abundant carbonate species, carbonate (CO_3) and dissolved carbon dioxide (CO_2) that consists of less than 1%.

Coccolithophore algae mostly use bicarbonate to synthetize coccoliths (Paasche, 2002) but are very sensitive to carbonate ion concentrations. The on-going ocean acidification is altering the ocean carbonate chemistry with a reduction of $[CO_3^{2-}]$, seawater pH, increasing DIC, $[CO_2]$, and $[HCO_3^{-}]$ and keeping TA constant. The effect of ocean acidification and decrease in ocean calcium carbonate on living coccolithophores is difficult to measure because a combination of factors (nutrient, light, temperature…) can determine the response of coccolithophore algae to elevated CO_2 (Ridgwell et al., 2009). What we know so far it that there's a species-specific response of coccolithophores algae to increase CO_2 emission and low carbonate saturation state: experiments and observations on morphologically close species *E. huxleyi* and *G. oceanica* display reduced calcification per cell and a concomitant increase in photosynthesis rate (decreased PIC/POC ratio; although some strains of *E. huxleyi* show a less sensitive behaviour). *G. oceanica* furthermore appears to be more sensitive to changes in pH and pCO_2. At the same time there's also production of malformed coccoliths (Riebesell et al., 2000; Rost and Riebesell, 2004). On the other hand, other species like *C. pelagicus* and *C. leptoporus* seem to be less sensitive to increased $[CO_2]$. Particularly, *C. pelagicus* calcification is just a little bit affected by elevated CO_2 (Langer et al., 2006), while *C. leptoporus* display a CO_2/pH optimum interval (of both calcification and photosynthesis) with a maximum value at present CO_2 concentration (Krug et al., 2011).

4.3.4 Trace Metals

Coccolithphore algae need trace metals, such as iron, zinc, manganese, cobalt, selenium and cadmium for their metabolic processes. Trace metals play a critical role in a number of metabolic processes involving the utilization of essential algal resource like light, nutrients and CO_2. Macronutrients (like P, C, N, Si) and major ions (like Mg^{2+}, K^{+}, Ca^{2+}, Cl^{-}, Na^{+}, SO_4^{2-}) are fundamental for coccolithophore growth and are generally highly soluble and non-toxic. On the other hand, trace metal content might become toxic for coccolithophorid algae if threshold values are reached. The presence or absence of trace metals can play the role of limiting micronutrients. For example, iron is the most important of these micronutrients and can limit or increase phytoplanktonic growth in many regions of the ocean. Elevated concentrations of micronutrient metals, like copper or zinc, can have two effects: they can poison the cell entering into the cell via transport system of essential nutrients or can inhibit the nutrient uptake and interfere with the nutrient metabolism (Sunda et al., 2005). Not many studies have taken into account this subject and the effect of single trace metal on coccolithophorid metabolism and or calcification is not clear. Hoffmann et al. (2012) highlighted that in extreme local conditions (like desert dust or volcanic emissions), trace metal peak can both fertilize and have a toxic effect on coccolithophorid algae. So far Mg is supposed to play an important role in regulating antagonistic and synergistic effects on different trace metals.

4.3.5 Mg/Ca ratio

Calcium and magnesium concentrations varied over geological time scale. In the Mesozoic the shift from aragonitic to calcitic sea almost 200 Ma, coincides with the oldest record of relatively diversified nannofossils (Erba, 2006). It seems plausible therefore that increase Ca^{2+} concentration and consequently reduction in Mg/Ca ratio played a fundamental role in the appearance of calcified calcareous nannoplankton. Furthermore the maximum of Ca^{2+}recorded in the mid-Cretaceous define the beginning of expansion of coccolithophores: at a time when the very high CO_2 would have retarded the precipitation of calcium carbonate in the ocean, it can be hypothesize that both low Mg/Ca ratio and or increase in Ca^{2+} in the Cretaceous ocean, were responsible for the higher coccolithophorid growth rate and subsequent massive chalk deposits fin the Late

Cretaceous (Stanley & Hardie 1999, Erba, 2006).

On a short time scale, Mg/Ca variations influence coccolithophorid physiology and chemistry of biogenically produced coccoliths. Stanley et al. (2005) observed an increase in the population growth rates of three analysed species with decreasing Mg/Ca ratio and concomitant Ca increase. Furthermore, other studies (Herfort et al., 2004, Leonardos et al., 2009), revealed that increasing Ca concentration, have an effect on PIC_{prod} that increases till reaching a threshold value (50 mml L^{-1}), where it decreases again. Muller et al. (2011) suggested that only changes in $[Ca^{2+}]$ affect coccolithophorid physiology and that, on the contrary, coccolithophorid algae are insensitive to $[Mg^{2+}]$ changes. It seems however that coccolithophores respond in a specie-specific way to Mg/Ca ratio variations.

Chapter 5

Paleoecology of the Cenomanian-Turonian calcareous nannoplankton

Calcareous nannofossil assemblages have the potential to yield information about surface water conditions (e.g. temperature, productivity). During the Cenomanian - Turonian OAE 2, calcareous nannoplankton show anomalies that don't parallel the dramatic changes observed in other faunal groups such as ammonites, belemnites and foraminifera, in which major extinctions occurred. However, calcareous nannofossil experienced 8-9% turnover through the upper Cenomanian and lower Turonian. At least nine originations and four extinctions occurred between the second peak of the ^{13}C excursion and the base of the Turonian (Hardas and Mutterlose, 2006, 2007; Corbett and Watkins 2013). Therefore, calcareous nannoplankton experienced a very high rate of turnover in less than 20 kyrs (Corbett and Watkins, 2013), suggesting major paleoceogranographic changes during this interval and environmental stress for marine microplankton (Fig. 5.1).

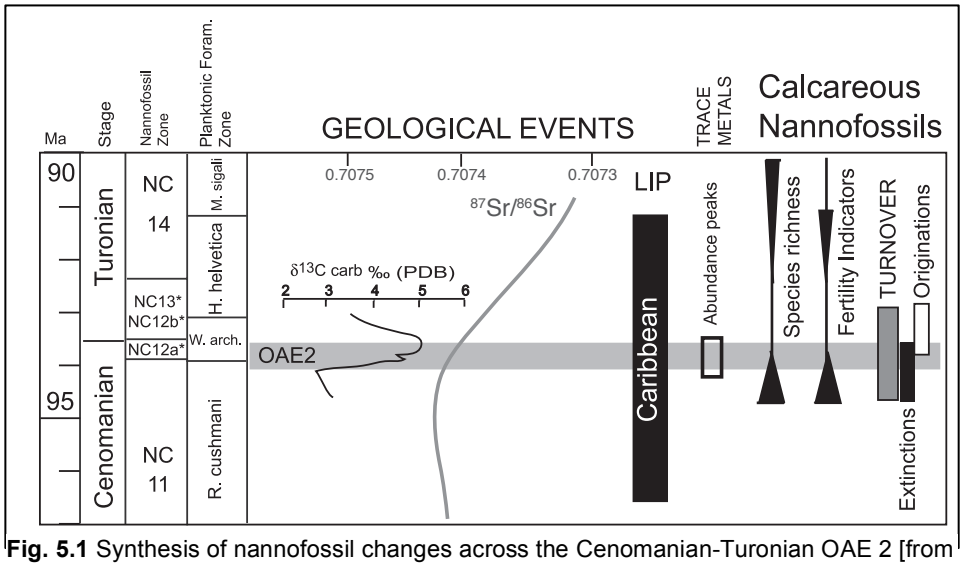

Fig. 5.1 Synthesis of nannofossil changes across the Cenomanian-Turonian OAE 2 [from Erba 2004].

The Cretaceous genera *Watznaueria, Biscutum* and *Zeugrhabdotus* are thought to indicate a range of trophic conditions (from oligotrophic to eutrophic fertility levels) depending on peaks in relative abundance between species (Corbett and Watkins, 2013). In the Cenomanian - Turonian boundary interval, *Watznaueria barnesiae* is known to dominate nannofossil assemblages. *W. barnesiae* is a cosmopolitan species, common in tropical and subtropical regions and dominant especially in oceanic gyres; it is described as an r-selected opportunistic species (Hardas and Mutterlose, 2007) and used as a low-productivity indicator (Erba, 2004). In the Cenomanian/Turonian boundary interval, *Watznaueria* spp., including *W. barnesiae,* show a decrease in abundance and nearly disappeared during some parts of the $\delta^{13}C$ excursion in tropical sections. This has been interpreted as an increase in primary productivity (Hardas and Mutterlose, 2007). On the other hand an increase of this low-fertility taxon is recorded at higher latitudes (Eastbourne section, Wunstorf core; Linnert et al., 2010; Linnert et al., 2011). *Biscutum constans* and *Zeugrabdothus erectus,* on the contrary, are described as high-nutrient indicators; *Z. erectus* is seen as an eutrophic species and shows a high increase in relative abundance during the $\delta^{13}C$ excursion in different sections: it is well represented in both Eastbourne and Tunisia sections (Paul et al., 1999; Tantawy, 2008; Linnert et al., 2011). *B. constans,* on the contrary, records a decrease in some area such as at Eastbourne, Gubbio, and Wunstorf (Paul et al., 1999; Erba, 2004; Linnert et al., 2010; 2011). However, *B. constans* show an increase in abundance in Tropical Atlantic (Demerara Rise ODP Site 1258) and Tethyan sections (Melinte-Dobrinescu & Bojar, 2008). *Discorhabdus rotatorius*, very rare in several sections (such as Eastbourne and Demerara rise) is also viewed as indicator of mesotrophic conditions (Erba, 1992; Hardas and Mutterlose, 2007). *Eprolithus floralis* has been observed at different high-and-low latitude successions. It is inferred to be adapted to cool surfaces waters (Roth and Krumbach, 1986). In Demerara Rise sections, two peaks are record at the top and above OAE 2, while in Eastbourne and Gubbio sections, two peaks are record in late phases of OAE 2 and immediately after it (Erba, 2004; Hardas and Mutterlose, 2006). Moreover, Demerara Rise sections show a decrease of *E. floralis* suggesting warmer conditions, in agreement with other isotopic data (Forster et al., 2007): this might indicate that the onset of OAE 2 coincided with a rapid warming of surface waters. All these information highlight very complicated picture suggesting higher trophic level in the tropical area and more oligotrophic conditions at higher latitudes. However, other parameters must be

taken into account: *B. constans* decline might also be explained with trophic conditions above threshold values or toxicity of specific metals or inability to thrive in very warm waters (Erba, 2004). Furthermore nannofossil decrease in total abundance and species richness might be determined by higher concentrations of biolimiting metals (e.g. Fe, Zn) and higher nutrient content that have favoured siliceous and organic walled groups (diatoms, dinoflagellates, cynobacteria; Erba, 2004).

Chapter 6

Studied Sections

For this thesis I investigated the Cenomanian- Turonian boundary interval recovered in 5 sedimentary successions (Fig. 6.1): Eastbourne section (Sussex, United Kingdom), Clot de Chevalier (France), Novara di Sicilia (Sicily, Italy) and two Western Interior sections (Pueblo, Colorado and Cuba, Kansas, USA). These five sections have been chosen based on availability of integrated stratigraphy. In fact, they all have a good time control, especially C isotopic stratigraphy and biostratigraphy, that offers the opportunity to correlate data from the different localities, discriminating between local, regional and global changes. Moreover, the selected sections represent short and long-distance location with respect to the Caribbean Plateau paleo-position.

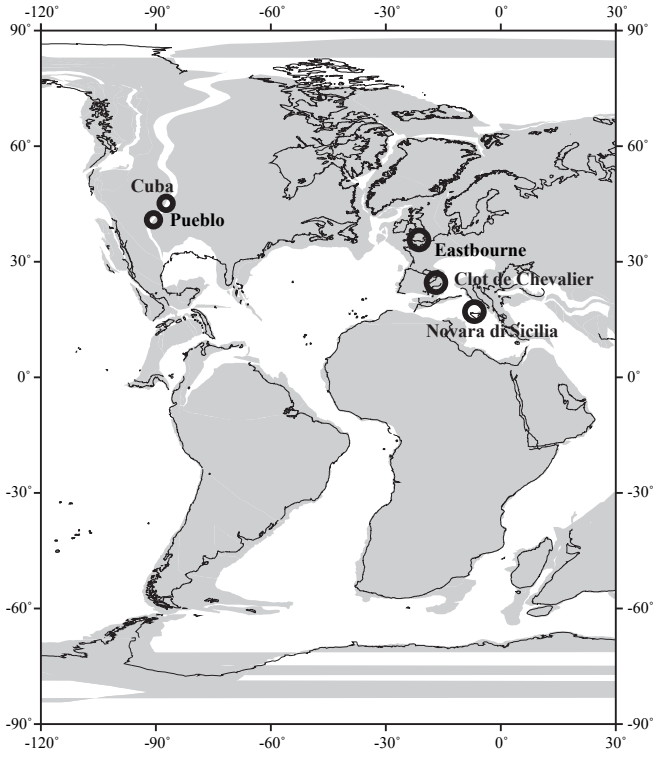

Fig. 6.1 Paleo-location of the studied sections: Eastbourne, Clot de Chevalier, Novara di Sicilia, Pueblo and Cuba [paleo-map from C/T-Net programm —Rapid global change during the Cenomanian/Turonian oceanic anoxic event: examination of a natural climatic experiment in earth history].

6.1 Eastbourne section

The sea-cliffs on the English Channel (Fig. 6.2) between the town of Eastbourne (Sussex) and the promontory of Beach Head, 4 Km southwest, display an expanded succession spanning the late Cenomanian and early Turonian. The outcrops at Gun Gardens, Beach Head and Holywell are the thickest and most complete successions of the Cenomanian-Turonian transition in the Anglo-Paris Basin (Gale et al., 1995; 1996; Gale et Hannock, 1999; Paul et al., 1999).

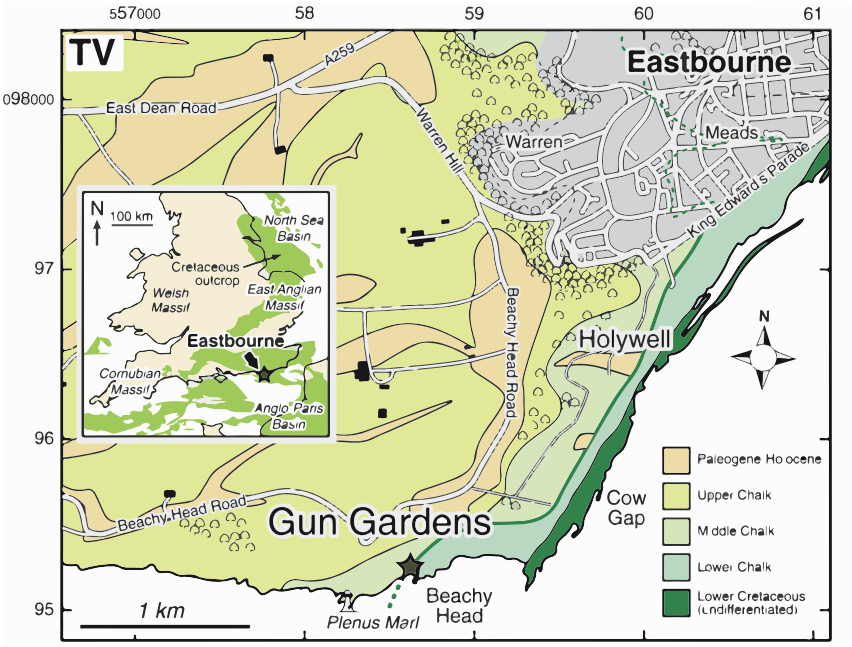

Fig. 6.2 Location of the Eastbourne section (Sussex, UK; from Pearce at al., 2009)

The succession I've focused on is almost 27 m thick and consists of an alternation of chalk, marly chalk and rhythmically bedded marlstones (Fig. 6.3). The chalk consists of clay-poor carbonate – rich in microfossils (calcispere-, coccolith-, and inoceramid – limestones); on the contrary, the marlstones consist of clay-rich carbonates (Fig., 6.4; Paul et al., 1999). Boundaries between chalk and marly chalk are variably bioturbated.

The lithological variations observed denote sea level changes: marls are associated with high detrital influx, increase erosion under arid and or cooler climatic conditions in

relationship with low sea level. In contrast, chalks are associated with a rise in the carbonate production, low detrital input under warm and humid conditions related to higher sea level period (Keller et al., 2001).

Following Gale et al. (2005), the Eastbourne section can be divided into two formations: Lower Chalk formation (from 0 m to almost 14 m) and the White Chalk formation (from 14 m to 27 m). Each of them has been divided into different members. The Lower Chalk formation is described as a variably rhythmically bedded bioturbated marly chalk containing 10-30% clay (Gale, 1995). It can be divided in four parts: Glauconite member, Chalk Marl member, Grey Chalk member and Plenus Marl member. At Eastbourne only the two uppermost members are outcropping. The Grey Chalk member (from 0 m to almost 6 m) is represented by well-developed, relatively pure chalks and marlstones.

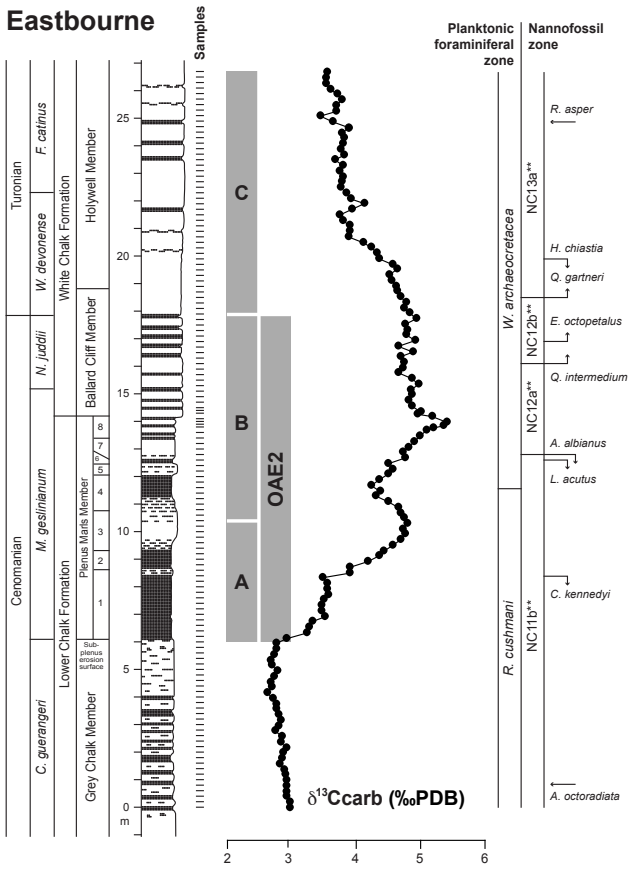

Fig. 6.3 Lithostratigraphy, biostratigraphy and C isotopic stratigraphy of the Eastbourne section studied within the CT-NET Project [after Tsikos et al, 2004 and Erba, unpublished data].

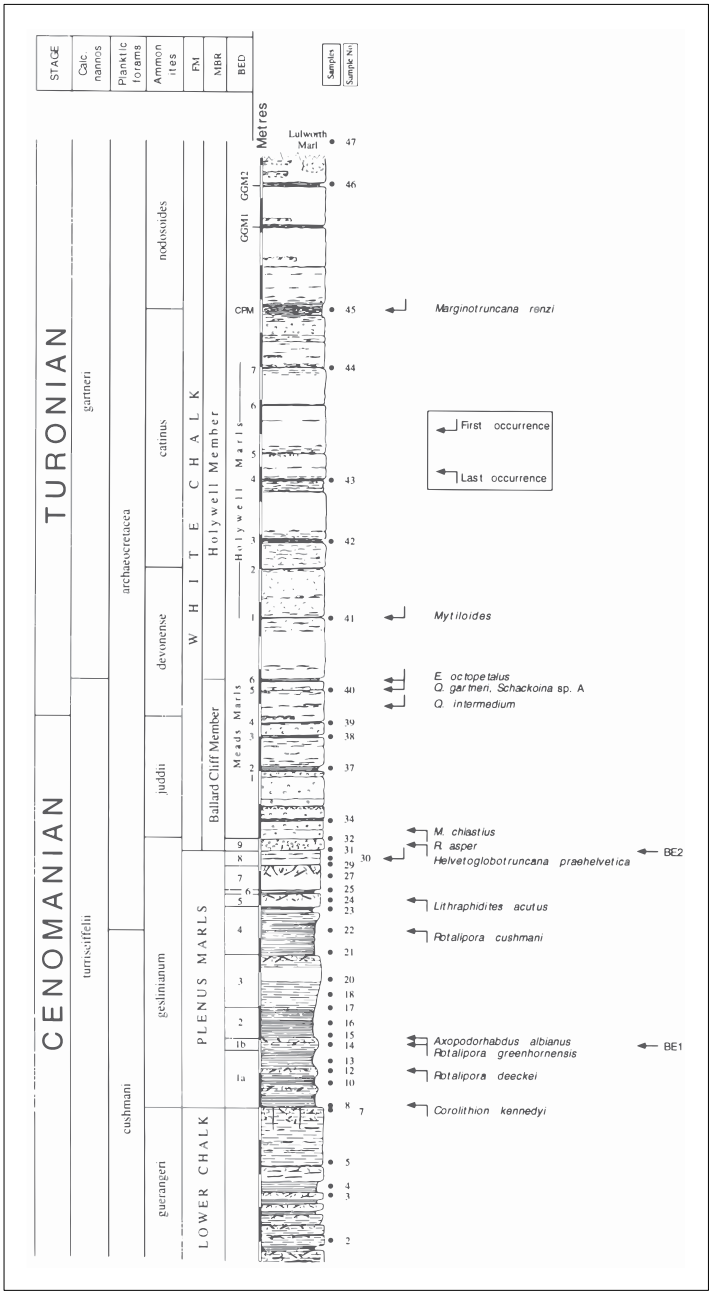

Fig. 6.4 Lithostratigraphy and nannofossil biostratigraphy of the Eastbourne section [from Paul et al., 1999]

The Plenus Marls member (from 6 m to 14 m) is a succession of marlstones and marly chalks which form a prominent marker in the upper Cenomanian throughout southern England, northern France and the North Sea basin (Gale et al., 2005). The term "Plenus Marls" was first used by Rowe, 1900, for the marly unit at the top of the Lower Chalk formation, for the presence of the belemnite *Actinonocamax plenus* (now *Preactinonocamax plenus*). The Plenus Marls is a relatively thin but highly distinctive

unit color: it has a greenish-grey coloration caused by a few percentage of chlorite (Gale et al., 2005). The outcrops in the west of Eastbourne are very thick (8 m at Gun Gardens) but lateral variations in the facies and thickness are recorded. The uppermost part of the Eastbourne section, shows, from a lithological point of view, the transition between the Plenus Marl member and the Ballard Cliff member: it is calcisphere-rich and has intermediate characteristics between the two underlying members (Gale et al., 2005). Mortimore (1986) introduced the first White Chalk lithological scheme; a newer scheme for the lower part was introduced by Gale (1996). He recognized three members: the Ballard Cliff member, the Hollywell member and the New Pit member. In the investigated section only the first two lower members are expressed (Ballard Cliff Member: from 14 to 19 m; Holywell member: from 19 m to the top). Gale et al. (2005) described the Ballard Cliff member and the Hollywell member as thinly bedded calcisphere-rich nodular and weakly nodular chalks, separated by wispy, flaser marlstones.

The Eastbourne section was investigated for integrated litho- bio- and chemostratigraphy (Jenkyns et al., 1994, Paul et al., 1999, Keller et al., 2001, Gale et al., 1993, 2005; Tsikos e al., 2004, Pearce et al. 2009, Linnert et al., 2011) and many geochemical and paleoenvironmental studies (e.g. Voigt et al., 2004, 2006, Kolonic et al., 2005, Pearce et al., 2009). The association of calcareous nannofossils allowed the recognition of two biozones (Paul et al., 1999): *Eifellithus turriseiffelii* Thierstein (1971) emend. Crux (1982) and *Quadrum gartneri* Cepek and Hay (1969) emend. Manivit et al., (1977).

Samples analyzed for my thesis were collected during the CTN Project. Nannofossil biostratigraphy was published in Tsikos et al (2004): that the OAE 2 is constrained by the last occurrence of *Corollithion kennedyi* and *Axopodorhabdus albianus* and the first occurrence of Quadrum *gartneri* at the onset and end, respectively. These events are consistent with more recent biostratigraphic data by Linnert et al. (2011).

6.2 Clot de Chevalier section

Clot de Chevalier section is located in the Vocontian Basin (France). The Vocontian Basin forms a part of the hemipelagic intrashelf basin of the European Tethyan passive margin (Wilpshaar et al., 1997). Major tectonic changes occurred in this basin at the beginning of the Late Cretaceous, with a transition from dominant extensional regime until the Albian, to dominant compressional or transgression starting in the Cenomanian (e.g. Fries and Parize, 2003). The study of this section is still on going, and no information about lithostratigraphy is available. Calcareous nannofossil biostratigraphic investigations of Clot de Chevalier section are part of an integrated litho-, chemo- and biostratigraphic study of this section. Samples were provided by Hugh Jenkyns (Dept. of Earth Sciences, Oxford University, UK) to E. Erba and M.R. Petrizzo (Univ. of Milan) to investigate nannofossil and planktonic foraminiferal biostratigraphy (Fig. 6.5). Specifically, nannofossil biostratigraphy was part of the pH thesis of Fabio Russo completed in 2014.

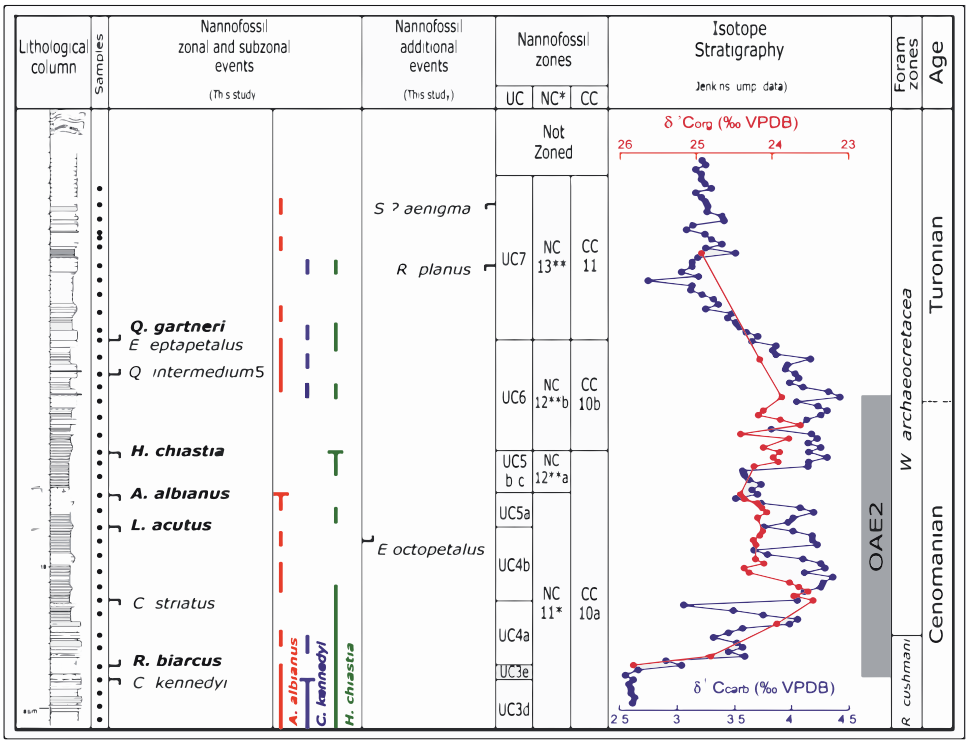

Fig. 6.5 Clot de Chevalier lithostratigraphy and isotope stratigraphy after Gale and Jenkyns (*unpublished data*); calcareous nannofossils after Erba, Russo, Bottini (*unpublished data*); planktonic foraminiferal zones after Falzoni and Petrizzo (*unpublished data*).

6.3 Novara di Sicilia section

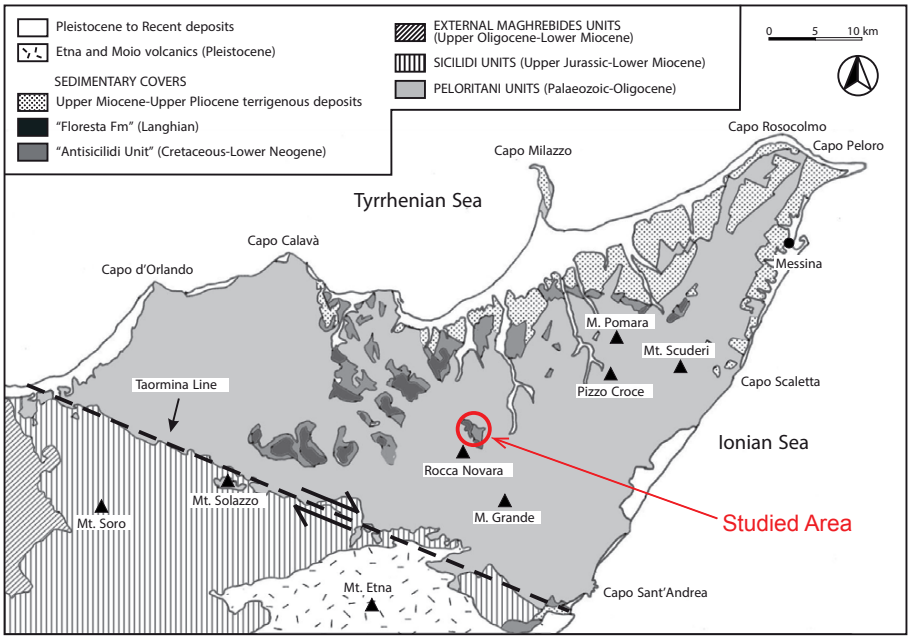

Fig. 6.6 Schematic structural map of northeastern Sicily and location of the Novara di Sicilia section (red open circle) [from Scopelliti et al., 2008]

This Upper Cenomanian to Turonian section is located east of Novara di Sicilia, in the North East of Sicily. The section exposes a 19 m stratigraphic interval and is contained in one of the several exotic blocks within the Argille Varicolori that is the informal name of a unit in the Peloritani Thrust Belt. The Peloritani Mountain belongs to the southern section of the Calabrian Arc that represents the conjunction between the North Alpine-Apennine system and the south Sicily-Maghrebide chain. The Peloritani Belt is formed by a set of south-verging tectonic units including crystalline basement and a sedimentary cover that over-thrusts the more external Sicilide Group along the Taormina Line (Amodio-Morelli et al., 1976; Giunta et al., 1989). Argille Varicolori is a pelitic unit that outcrops in Eastern Sicily and Southern Calabria and is tectonically located between the overlying Flysh Di Capo d'Orlando formation, a terrigenous deep - water succession dated as Aquitanian-Burdigalian and the overlying Calcareniti di Floresta formation, a shallow - water mixed deposit dated as Langhian. The contact between Argilli Varicolori and Flysh di Capo d'Orlando is interpreted as tectonic (Fig. 6.6).

Argille Varicolori is described as a lithosome characterized by a massive fine-grained

"matrix" that consists of a multi-colored chaotically textured clay-rich material, bearing huge exotic blocks, that lies on the underlying unit with stratigraphic contact (Cavazza e al., 1997). This complex unit represents a time interval of Cretaceous-Paleogene age: it includes the Aptian-Albian, the Cenomanian, the Eocene and the late Burdigian-Langhian.

The Novara di Sicilia section crops out in the form of an olistolith embedded within the melange of the Argille Varicolori (Scopelliti et al., 2008) and shows many similarities with coeval facies cropping out in Tunisia and Morocco (e.g. Nederbragt and Fiorentino, 1999). This section most probably has a southern provenance and might be derived from a depositional ramp located on the northern African continental shelf.

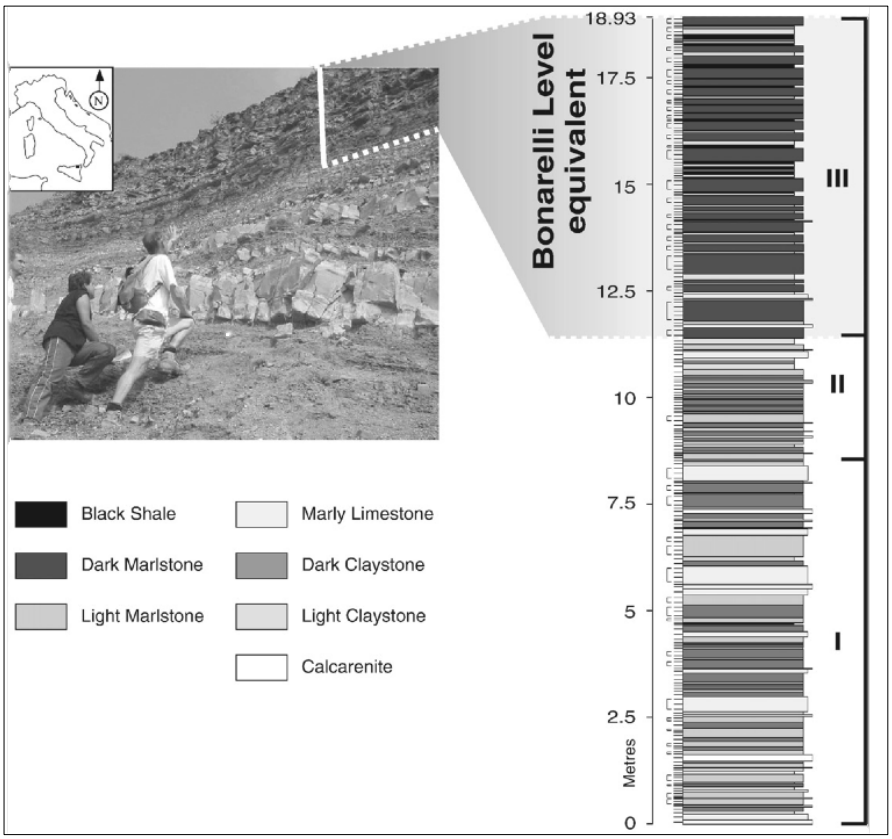

Fig. 6.7 Lithostratigraphy at Novara di Sicilia section [from Scopelliti et al., 2008]

The Novara di Sicilia section is 19 m thick; it has been dated as late Cenomanian using planktonic foraminifera and nannofossil biostratigraphy (Scopelliti et al., 2008) and represents an expanded record of the Cenomanian-Turonian ocean anoxic event. The section can be divided into three parts (Fig. 6.7):

1. Lower part from 0 to about 8.5 m; irregular alternations of thick marly limestone with light and dark marlstones and calcarenites; only one horizon of black shales (at 4.7 m);
2. Intermediate part from 8.5 to 11.5 m; thinner and light colored marlstones alternated with dark marlstones;
3. Upper part from 11.5 m to almost 19 m; black shales alternating with dark marlstones and claystones.

The boundary between intervals 2 and 3 marks the base of the Bonarelli Level equivalent.

Calcareous nannofossil biostratigraphy shows that the organic-rich interval (from 9.5 m upwards) represents only part of the late Cenomanian. In fact, n the Novara di Sicilia section the lower part of the section represent the upper NC11* zone; the transition between NC11* and NC12* at 13.54m, is defined by the last occurrence (LO) of *Axopodarhabdus albianus*. The Cenomanian/Turonian boundary, according to calcareous nannofossil biostratigraphy is not reached because the LOs of *Helenea chiastia* and *Rhagodiscus asper* were not detected and the first occurrence (FO) of *Quadrum gartneri* was not registered (Scopelliti et al., 2008). In the analyzed section there's a virtual absence of rotaliporidsdue to scarcity of this species before its disappearance (lower critical interval, Coccioni et al., 1991) or related to local oceanographic conditions (upwelling; fig. 6.8). The $d^{13}C_{org}$ stratigraphy shows a moderate fluctuations and an increasing trend: values vary from -26% at the bottom to -23% at the top. The first $\delta^{13}C_{org}$ peak at ~ 10 meters corresponds to the Bonarelli Level equivalent onset. Three other peaks occur but a well-defined positive plateau is not observed, thus confirming the biostratigraphic interpretation of absence of the upper part of the OAE 2 anomaly. Hence, from a stratigraphic point of view the Novara di Sicilia section contains only the lower part of the Bonarelli Level of the Umbria-Marche Basin (type area) and the underlying interval.

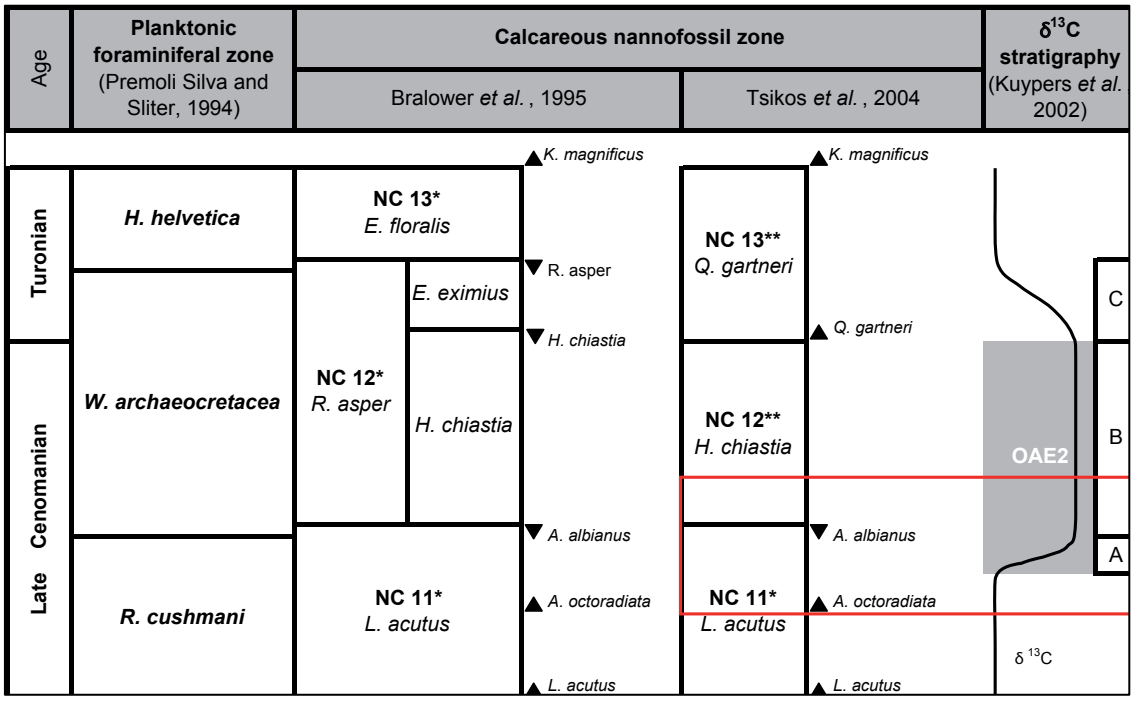

Fig. 6.8 Position of the Novara di Sicilia section (delimited with red rectangle) against revided C/T boundary nannofossil zonation ▲ : first occurrence (FO); ▼ : last occurrence (LO); [from Scopelliti et al., 2008].

6.4 Pueblo and Cuba sections (Western Interior Seaway)

During the Cenomanian, the Western Interior Basin of North America was inundated by an epicontinental seaway that connected the Gulf of Mexico with the Artic Ocean (Hancock and Kauffman, 1979, Kennedy et al., 2005, Bowman and Bralower 2005, Snow et al., 2005, Corbett and Watkins 2013, Corbett and Watkins, 2014). The Western Interior Seaway (WIS; fig. 6.9) extended for 6000 km and at the Cenomanian-Turonian boundary it was 2000 km wide and 500 m deep (Hay et al., 1993). The WIS was characterized by a range of different climatic regimes, because of its large latitudinal extent and oceanography was very variable too. Water column structure and circulation was affected by freshwater input from the Sevier Highlands (West), Mogollon Highlands (South West), influx of waters from the Artic sea (North, dense, cold and salty waters) and the Tethys sea (South, less dense, warm surface waters) that determined significant sea level fluctuations (Fisher et al., 1994, Watkins et al., 1998, Eleson and Bralower, 2005).

The Cenomanian-Turonian boundary interval in the WIS lies within the Bridge Creek Limestone Member above the Hartland Shale Member. They are both part of the Greenhorn Formation (Kennedy et al., 2005). Rhythmically bedded thin calcarenite or nodular calcarenite layers alternated with grey shale layers characterize the Hartland Shale Member. Bentonite layers are common and vary from 1-2 to 20 cm thick. The Bridge Creek Limestone Member in the Great Plain region on the United States is a widespread unit, generally 10-15 m thick, consisting of a striking alternation of limestone and dark grey marlstone (Eicher and Diner, 1989).

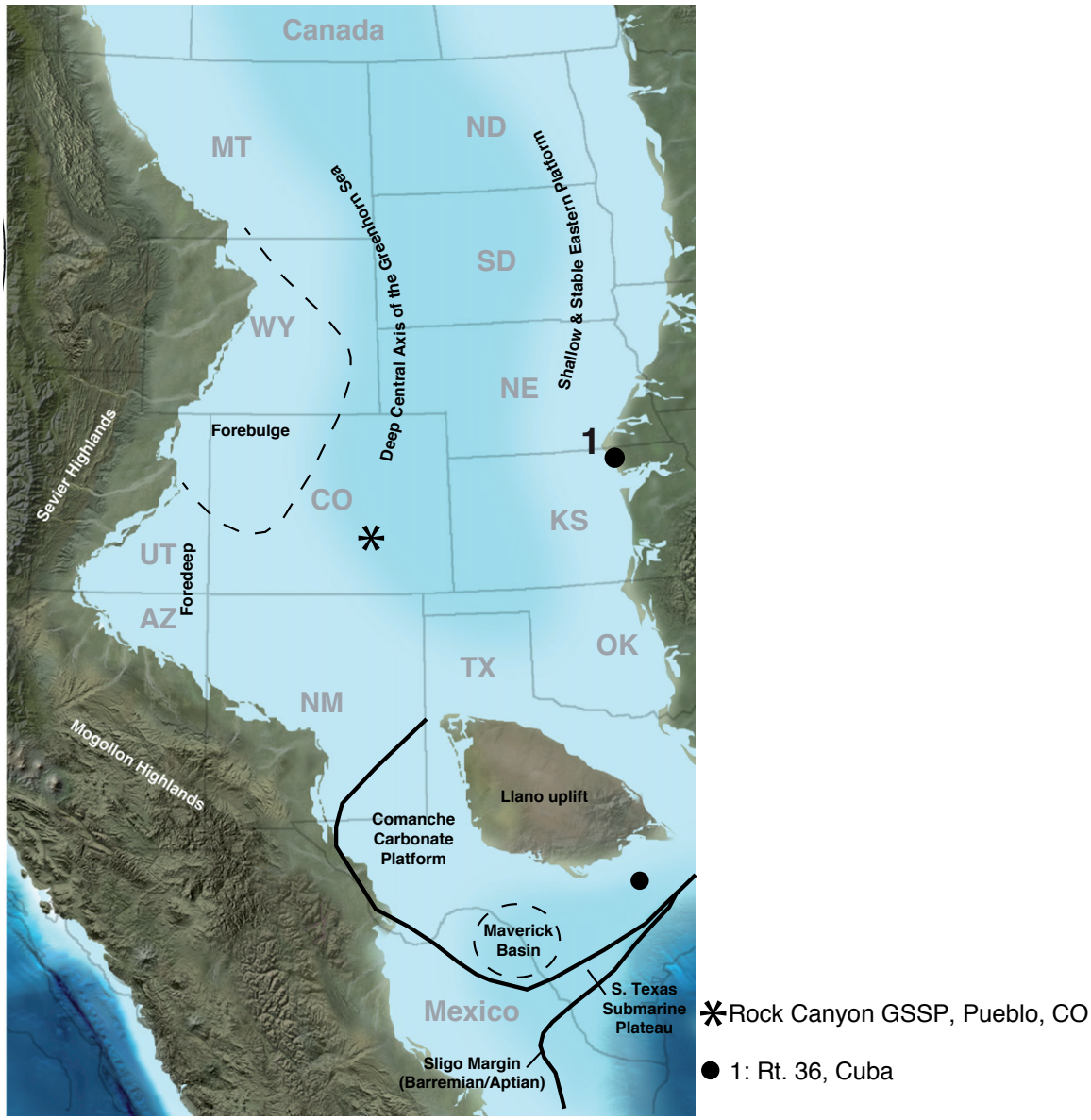

Fig. 6.9 Paleogeographic map of western North America approximately during peak transgression of the Western Interior Seaway in the Late Cenomanian–Early Turonian and localities of the two analyzed sections: Pueblo and Cuba [from Corbett and Watikins, 2013]

The Rock Canyon Anticline section is located in South central Colorado, near Pueblo. This section has been ratified in 2003 as the Global boundary Stratotype Section and Point (GSSP) for the base of the Turonian. The boundary coincides with the FO of the ammonite *Watinoceras devonense* that is at the top of the global positive $\delta^{13}C$ excursion and is bracketed by widespread bentonites that have yielded ages of 93-93.5 Ma (Kennedy et al., 2005). At the Cenomanian-Turonian boundary, Rock Canyon was located in the deepest part of the foreland basin at an estimated depth of 175-300m during peak transgression. The Bridge Limestone at Rock Canyon consists of a cyclically alternating pelagic carbonates (chalk and limestone) and more C_{org}-rich beds (marlstone and calcareous shale; Bowman and Bralower, 2005). Much of the section is bioturbated with laminated and sublaminated units. Petrographically limestones are fossiliferous biomicrites (Kennedy et al., 2005). The Rock Canyon section was sampled from the uppermost part of the Hartland Shale through the lower Bridge Creek Limestone spanning about 8m below and 6 m above the C/T boundary as defined by ammonites. I analyzed the upper 10m of the section that consists of the Bridge Limestone Member including the OAE 2 interval.

The Rock Canyon section was investigated for lito- bio- chemo- stratigraphy and for paleoecological and paleoenvironmental reconstructions (fig. 6.10; ammonite fauna: Stanton, 1894, Kennedy and Cobban 1991, Kennedy et al, 1999, 2000; inoceramid bivalves Kennedy & Cobban, 1991; planktonic foraminifera: Eicher and Diner, 1985, Leckie, 1985, Keller and Pardo, 2004; calcareous nannofossils: Watkins, 1985, Bralower, 1988, Russo, 2014; dinoflagellates: Dodsworth 2000, stable isotopes: Pratt, 1983, 1984, Pratt et al., 1993, Keller et al., 2004, Gale et al., 2005, Bowman and Bralower,2005; iridium anomalies: Orth et al., 1988; trace metal abundances: Snow et al., 2005).

At Rock Canyon well-defined lithological variations and a number of well-dated bentonite layers (Kauffmann et al., 1993) allow excellent time constraints and a good correlation with other WIS section. Furthermore the section shows a well expressed positive $\delta^{13}C$ shift (> 3‰) in both organic carbon and carbonate fractions (Pratt et al., 1993) that allows precise dating and correlations (Fig. 6.11)

For my thesis, I analyzed samples provided by Bob Duncan and taken from the same levels studied by Snow et al (2005). The same samples were also investigated for

nannofossil biostratigraphy by Russo (2014): the results are compared to previous data in figure 6.11.

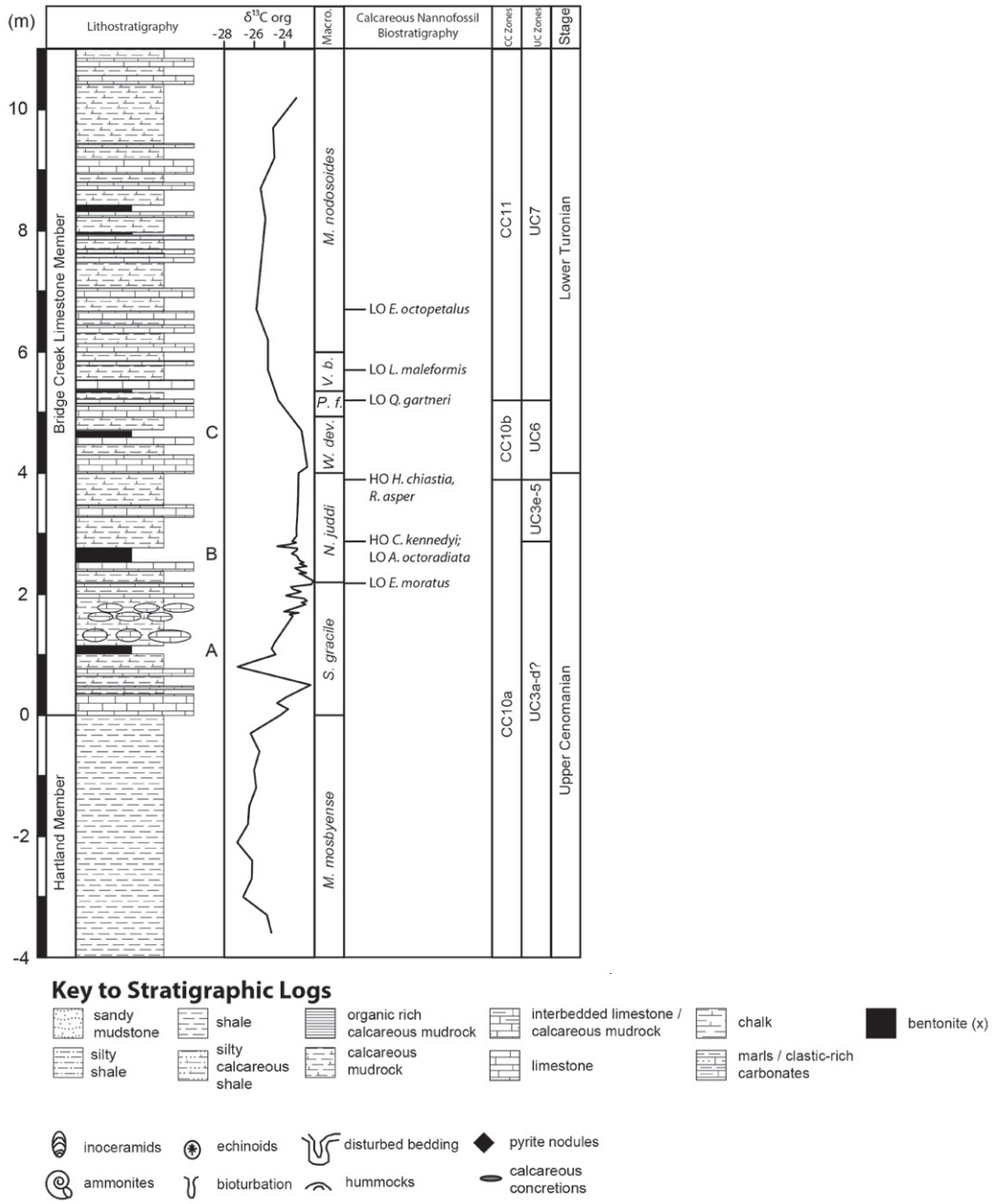

Fig. 6.10 Stratigraphic logs, calcareous nannofossil biostratigraphy, and carbon isotope values of Rock Canyon Anticline GSSP Pueblo section (CO) studied from the central Western Interior Basin. Letters A, B, and C indicate interpreted placement of bentonite marker beds of Elder (1985) [from Corbett and Watkins, 2014].

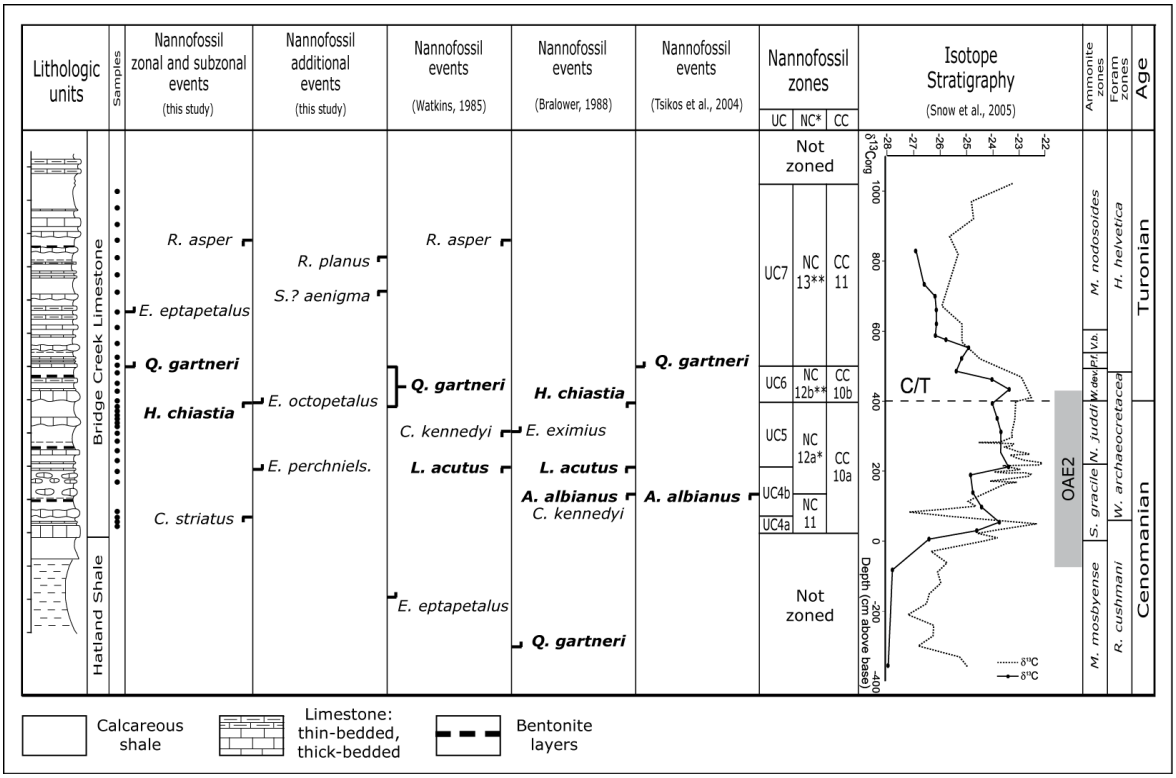

Fig. 6.11 Calcareous nannofossil bioevents and zones/subzones of the Rock Canyon section. Lithostratigraphy, ammonites and planktonic foraminiferal zones and ages after Kennedy et al. (2005); isotope stratigraphy after Snow et al. (2005) (from Russo, 2014).

The Cuba section in northen-central Kansas, is about 600 Km East of the Rock Canyon section. Equivalent strata around Cuba consist of more fine-grained calcareous to chalky shale within the Jetmore Chalk and Pfeifer Shale Members of the Greenhorn Formation. These two members are dominated by marlstone and calcareous shale (Bowman and Bralower, 2005).

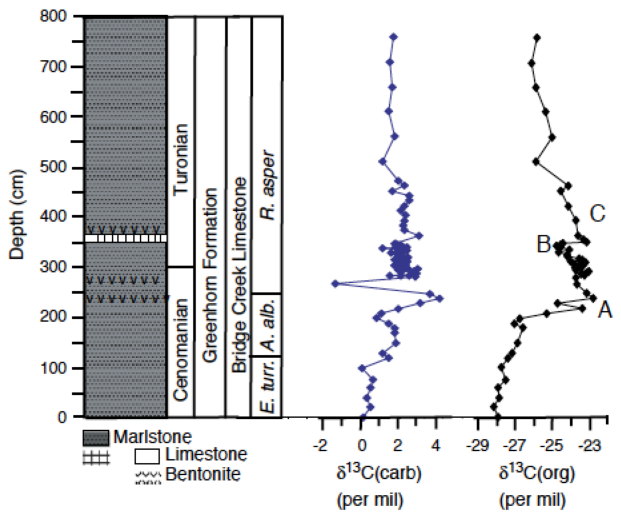

Fig. 6.12 C isotopic stratigrapgy and calcareous nannofossil biostratigraphy across the Cenomanian–Turonian boundary at Cuba. Points A–C refer to distinct segments in the $d^{13}C_{org}$curves of Pratt (1985) (Bowman and Bralower, 2005; Eleson and Bralower, 2005)

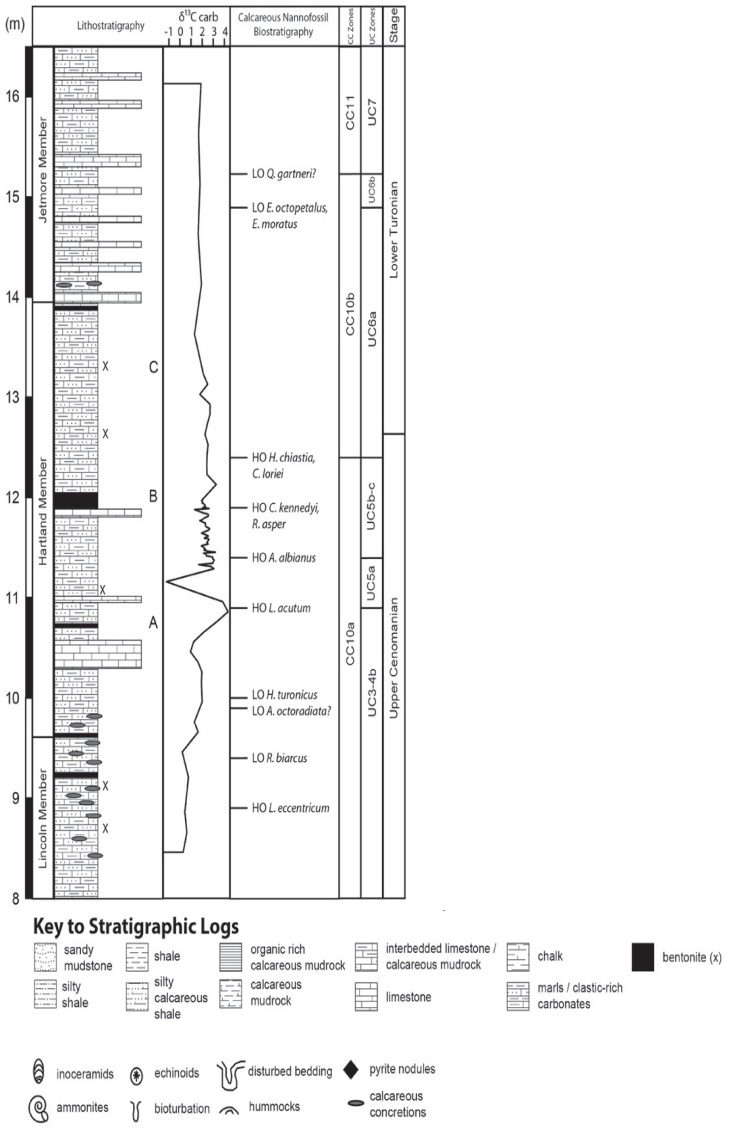

Fig. 6.13 Stratigraphic logs, calcareous nannofossil biostratigraphy, and carbon isotope values of Road 46 Road cuts, Cuba (KS) studied from the central Western Interior Basin. Letters A, B, and C indicate interpreted placement of bentonite marker beds of Elder (1985) [from Corbett and Watkins, 2014].

At the Cuba section the stratigraphic control is based on integrated lito- chemo- bio-stratigraphy (Fig. 6.13; Hattin, 1975, 1985; Desmares et al., 2007, Eleson and Bralower, 2005, Bowman and Bralower, 2005, Corbett and Watkins, 2013, Corbett et al., 20014). For my thesis I analyzed samples kindly provided by Tim Bralower and previously investigated by Eleson and Bralower (2005), Bowman and Bralower (2005) and Russo (2014).

Chapter 7
Material and Methods

7.1 Calcareous nannofossil biometric analyses

Samples from five sections (Fig.7.1) were analyzed through micropaleontolgical analysis. The investigated sections are Eastbourne, Clot de Chevalier, Novara di Sicilia, Pueblo and Cuba. In the Eastbourne section 53 samples were analyzed: samples have been collected every 40 cm across the Oceanic Anoxic Event 2 interval and every 80 cm before and after the event. The Clot de Chevalier section was sampled every 90 cm, resulting in 37 samples. In Novara di Sicilia, Pueblo and Cuba sections all the available samples have been analyzed, resulting respectively in 31, 19 and 18 samples investigated. The stratigraphic ranges of the studied sections are shown in Fig.7.2.

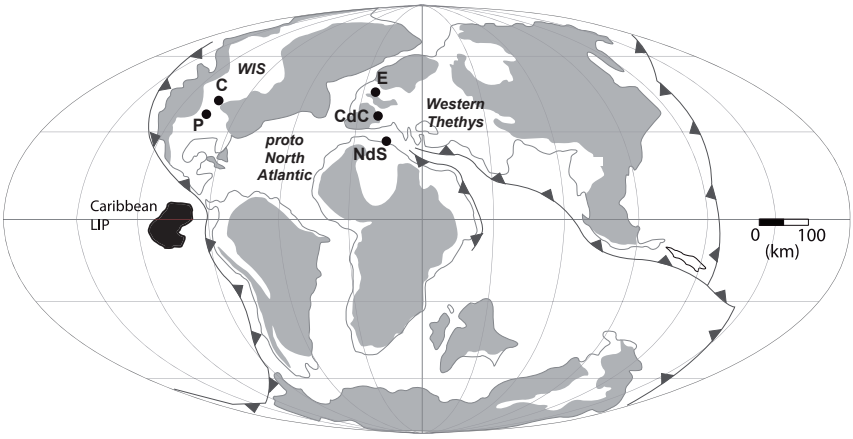

Fig. 7.1 Paleo-location of the studied sections (E Eastbourne, CdC Clot de Chevalier, NdS Novara di Sicilia, P Pueblo and C Cuba (paleo-map from Du Viver et al., 2014)

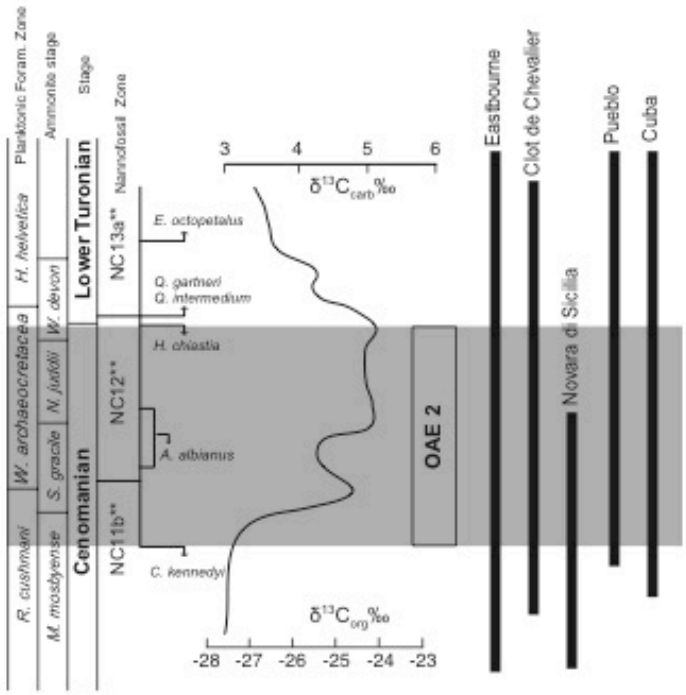

7.2 Summary of studied stratigraphic intervals

7.1.1 Calcareous nannofossil preparation and study techniques

Calcareous nannofossils were investigated in smear slides under light polarizing microscope at 1250X magnification.

7.1.2 Smear slides

For examination of calcareous nannofossils, smear slides were prepared using standard techniques without centrifuging and/or ultrasonic cleaning in order to retain the original

Fig. 7.3 Materials used for smear slides preparation

sediment composition. A few grams of rocks were powdered with bidistillate water in an agata mortar; some ml of suspension were extracted with a pipette and spread over a slide, leaving to dry on a hot plate. The dried suspension was sealed on a glass slide with Norland Optical adhesive under an UVA ray lamp (Fig.7.3).

7.1.3 Biometric Analyses

Morphometric analyses were performed with an image analysis system (Young et al., 1996). For each sample 30 specimens of *B.constans, D. rotatorius* and *Z. erectus* and 50 specimens of *W. barnesiae* were digitally photographed (Fig. 7.4; Tab. 7.1). In some sample, due to the paucity of calcareous nannofossils a smaller number of specimens were analyzed (Tab. 5.1). Specimens were chosen by scanning random traverses and all nannofossils were measured excluding those that were broken or heavily overgrowth. Specimens were photographed at 1250X magnification with a Q-imaging Micro publisher 5.0 RTV camera mounted on a Leitz Laborlux light microscope and a PC with Q-capture Pro suite software adapted for nannofossil analyses. Measurements were taken using ImageJ software. On each image length and width of distal shield of *B. constans, Z. erectus* and *W. barnesiae* were measured. Since *D. rotatorius* has a circular shape, the diameter had been measured. Statistical mean, median, maximum and minimum values, standard deviation (the error of measurements is ± 0.08 μm), 25 and 75 percentile have been calculated for each sample. Measurements of *W. barnesiae* and *B. constans* were also used to calculate ellipticity and surface area. Data have been statistically analysed using different software: Excel, R and Mathematica.

	W. barnesiae	***B. constans***	***Z. erectus***	***D. rotatorius***
Eastbourne	2,152	1,566	1,460	1,206
Clot de Chevalier	1,850	1,110	990	1,110
Novara di Sicilia	1,998	1,035	940	1,049
Pueblo	1050	600	533	570
Cuba	449	532	534	482

Tab. 7.1 Number of specimens analysed for each section.

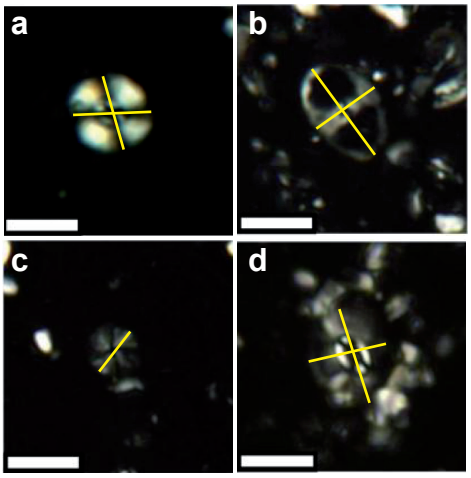

Fig. 7.4 Size parameters measured in the morphometric analyses **a)** *W. barnesiae* length and width; **b)** *Z. erectus* length and width; **c)** *D. rotatorius diameter* **d)** *B. constans* length and width

7.2 Coccolithophores culture methods

7.2.1 Stock culture and experimental culture

Experiments on living coccolithophores algae have been performed at the Geomar, Helmotz Centre for Ocean research Kiel under the supervision of Prof. Ulf Riebesell, Dr. Lennart Bach and Dr. Linn Hoffmann. During my internship, that last nearly a year, I performed five experiments on fours coccolithophores species.

The four different strains of coccolithophores used to test the response of coccolithophorid algae to environmental different conditions are:

1) *Emiliania huxley* RC1216
2) *Gephyrocapsa oceanica*
3) *Coccolithus pelagicus* ssp. *braarudii*
4) *Pleurochrysis carterae*

All experiments were conducted with dilute batch cultures (LaRoche et al., 2010) at 15° C in a 16/8 light/dark cycle and 150 µmol photons $m^{-2}s^{-1}$ incident photon flux density (except for the light experiment). The monospecific strains were grown in seawater-based K/2 medium after Kerster et al. (1967) but without addition of $NaHCO_3$. In the control treatments, the artificial seawater medium was enriched with 64 µmol kg^{-1} nitrate, 4 µmol kg^{-1} phosphate (that result in N:P ratio of 64:4) to avoid nutrient limitations, f/8

concentrations for trace metals and vitamins (Guillard and Ryther, 1962), 10 nmol kg^{-1} of SeO_2 and 10 nmol kg^{-1} of natural North Sea Water. In the controlled treatments the carbonate chemistry was adjusted by bubbling CO_2 –enriched air through the medium overnight, elevating [DIC] and decreasing pH. The medium was then sterile-filtered (0.2 μm) into sterile glass bottles. The culture medium was acclimated at 15°C overnight in order to avoid a thermal shock when transferring the cell from the pre-culture to the bottles where the experiments were performed. Cells were acclimated to the specific conditions of the main experiments for 7 generations prior inoculation.

All culture bottles where manually and carefully rotated three times a day, each time with 20 rotations in order to avoid cell precipitation.

Reaching the established number of cells, samples were processed after sampling and measured 3 times with the Coulter counter (Beckman coulter Multisizer). Afterwards, samples were acidified with 0.1 $mmoll^{-1}$ HCl to dissolve all free and attached coccoliths and subsequently measured again 3 times.

Finally 5-10 ml of sample were filtered by gravity on polycarbonate filters (0.2 μm pore size) and dried directly after filtration at 60°C for SEM analyses resulting in a total of 240 filters.

7.2.2 Coulter Counter

In the coulter principle method, particles suspended in an electrolyte solution flow through a small cylindrical opening (the aperture) that separates two electrodes between which an electric current flows (Fig., 7.5). This current has a small magnitude but the resistance created by the restriction separating the electrodes produces considerable current density within the aperture. Particles that pass through the aperture, with their own volume, increase the impedance of the aperture, creating a tiny but proportional current flow into an amplifier. The current fluctuation is then converted into a voltage pulse. The amplitude of this pulse is proportional to the volume of the particle that produced it. The height of the pulses are measured and scaled as volume units and a size spectrum can be obtained. Furthermore it is possible to obtain the concentration of particles per unit volume in the suspension.

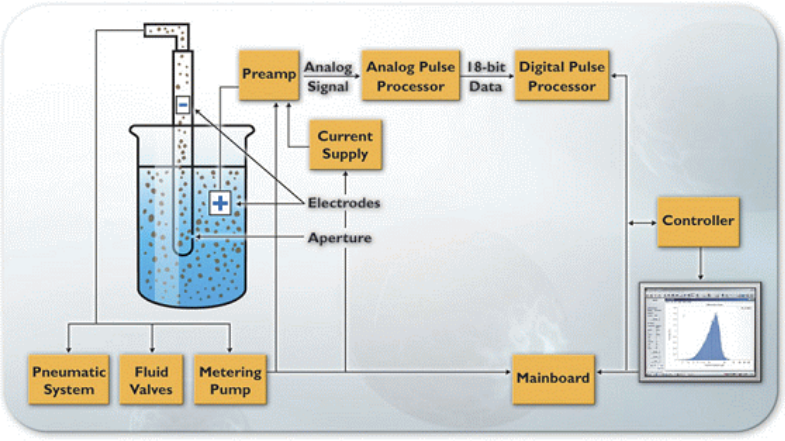

Fig. 7.5 Schematic image of the Coulter Counter principle. The aperture with an internal and an external electrode and filled with electrolyte solution is immerged into the sample. 500 µl of the sample is transported through aperture, particles displace a volume of the electrolyte and create voltage pulses, which are processed through an analog and a digital pulse processor to convert them into information on cell concentration, volume and diameter of the particles in the sample [from the Multisizer Brochure].

To simplify: the number of pulses can be transferred to the number of particles measured while the amplitude is transferred to the volume of the particle and finally the volume can be translated to the particle's diameter. After placing a sample in the Multisizer the instrument was set to carry out three replicate measurements of 500 µm subsample. Samples were acidified by addiction of HCl to remove coccoliths and measure cell volume (Buitenhuis et al., 2008).

Following Muller et al., 2012, and subtracting the acidified-sample spectrum from the non-acidified-spectrum, resulted in a spectrum to determine the average volume of the free coccoliths assuming normal distribution (Fig. 7.6).

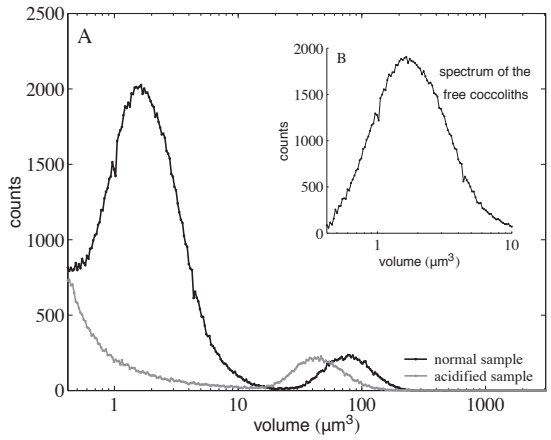

Fig. 7.6 Multisizer volume spectra. **(a)** Spectra of the *E. huxleyi* population (black line) and after treatment with HCl (grey line). **b)** Volume spectrum of the free coccoliths after subtracting the acidified sample from the normal sample [from Muller et al., 2012].

Coccolith measurements are expressed in volume (μm^3), while coccosphere/cell measurements are expressed in diameter (μm). This is due to the fact that measured volume can be translated to particle's diameter only if particle is of spherical appearance. This account for the coccosphere and for the cell but does not apply for coccoliths.

7.2.3 Growth rate

Cell density and size spectrum has been analyzed with the Multisizer Coulter counter: every sample was gently turned 10 times in order to obtain a homogenous suspension of the cells before sampling. Samples with densities above $150*10^3$ cell/ml were diluted prior to measurements (Coulter counter measures most accurate between 10-20 $*10^3$ cell/ml). Growth rate μ(d^{-1}) was determine taking into account the mean cell number as:

$$\mu = \frac{lnc1 - lnc0}{t1 - t0}$$

Where c0 and c1 are the cell concentrations respectively at the beginning (t0) and at the end of incubation period (t1), expressed in days.

7.2.4 Methodology adopted in Culture experiments

Five experiments were performed to test the reactions of coccolithophorid species (*C. pelagicus, E. huxleyi, G. oceanica* and *P. carterae*) to changes in light intensity, nutrients, carbonate chemistry, [Mg^{2+}] and [Ca^{2+}], and metal concentrations. Individual procedures are summarized below.

Experiment 1: Response of Coccolithophores to light intensities

The climate change is causing an increase in sea surface temperature in the oceans with the effect of a progressive reinforce of the temperature gradient between water masses and intensification of stratification. This might have an indirect effect on phytoplanktonic community: intense stratification is paralleled with a decrease of the mixed layer thickness establishing an increase in the light irradiance which phytoplankton in general and coccolithophorid algae in particular are exposed to.

Medium has been filtered in 60 ml polycarbonate bottles. The light was set at the highest and lowest possible intensity in the light chamber resulting in 12 different light levels for

each species. All the 4 species (*C. pelagicus* ssp. *brarudii, E. huxleyi, G. oceanica* and *P. carterae*) were investigated. The tested light intensities are:

45, 100, 130, 200, 250, 300, 350, 400, 450, 500, 560, 600 µmol photons $m^{-2}s^{-1}$.

This resulted in 48 polycarbonate bottles. From the stock culture, 50 specimens were inoculated for each species, starting the acclimation phase. After 7 generations, the same amount of cells was transferred in the bottles where the main experiment was performed. Cell volume was measured with the Beckman coulter Multisizer 3, after ~ 7 generations, reaching more or less:

1. 50000 cell/ml for *E. huxleyi,*
2. 20000 cell/ml for *G. oceanica*
3. 3000 cell/ml for *C. pelagicus* ssp. *brarudii* and *P. carterae*.

Samples were processed after sampling and measured 3 times with the Coulter counter. Afterwards, samples were acidified with 0.1 $mmoll^{-1}$ HCl to dissolved all free and attached coccoliths and subsequently measured again 3 times. Coccolith growth rate was then calculated. Finally, Filters for Scanning Electron Microscope (SEM) analyses were prepared.

Experiment 2: Response of Coccolithophores algae to carbonate chemistry

The chosen treatments only differed with respects to the carbonate chemistry manipulation of the culture medium. Four different treatments were chosen (see Table 7.2). In the first two treatments, cell was cultured at constant TA (2350 ± 22 µmol Kg^{-1}). In the control treatment the carbonate system was adjusted by bubbling with CO_2, increasing [CO_2], [HCO_3^-] and DIC, decreasing pH and [CO_3^{2-}]. This resulted in a pH of 8.1 and fCO_2 of 400 µatm. In the other three treatments, the carbonate parameters, TA or DIC, were added to the culture medium by calculated additions of hydrochloric acid (3.571 mol $l^{-1,}$ certified by Merck), and Na_2CO_3 (Merck, Suprapur quality dried for 5 hours at 400°C). In the second treatment this resulted in a DIC of 2264 µmol Kg^{-1} at constant TA (2350 µmol Kg^{-1}). In the third and fourth treatments, DIC and fCO_2 were adjusted to reach respectively 3500 (1000 µatm) and 5000 µmol Kg^{-1} (3000 µatm). For an overview of the carbonate chemistry conditions in all treatments see Table 7.1.

Carbonate chemistry parameters were tested on 4 different species in triplicates under dilute batch culture conditions in autoclaved and acid cleaned 600 ml glass bottles and this resulted in 16 treatments and 48 glass bottles. The headspace in the bottles was kept below 5 ml to avoid gas exchange. From the stock culture 50 µl have been inoculated for each species, starting the acclimation phase. Cells were acclimated to the carbonate chemistry conditions of the main experiment for at least 7 generations. In the main experiment, 50 specimens for each species were inoculated.

	Control	1st treatment Ocean Acidification (OA)	2nd treatment Cretaceous 1 (Creta1)	3rd treatment Cretaceaous 2 (Creta 2)
ta	2350.0	2350.0	3709.8	5052.2
DIC	2118.7	2264.8	3500.0	5000
fCO_2	400	1000	1000	3000
pHf	8.134	7.781	7.964	7.649
HCO_3^-	1939	2146	3275	4755
CO_3^{2-}	164	80	187	131

Tab. 7.2 Carbonate chemistry speciation; TA, DIC, HCO_3^-, CO_3^- are given in µm Kg^{-1}; fCO_2 in atm.

Cell volume was measured with the Beckman coulter Multisizer 3, after ~ 7 generations. For each bottle, filters for SEM analyses were prepared.

Samples for pH and Total Alkalinity (TA) analyses were taken at the beginning and at the end of the experiment. Samples were filtered (0.7 µm) and stored at 4°C until measurements (within 2 days for pH measurements and 14 days for TA). pH was measured spectrophotometrically with Varian Cary 100 in 10 cm cuvette at 25°C as described in Dickson (2010) and then recalculated to in-situ temperature (15°C). Every sample was measured 3 times. Samples for TA were measured in duplicate with Metrhom 862 Compact Tritino Sampler device, according to Dickson, 2003. TA data were corrected with certified reference material (A. Dickson, La Jolla, CA).

Experiment 3: Response of Coccolithophores to $[Mg^{2+}]$ and $[Ca^{2+}]$

Calcium and magnesium concentrations in seawater have varied over geological time scales. During the Cretaceous, and particularly during the so-called “Calcite II” seas (Lowenstein et al., 2001) coccolithophores were responsible for the massive and widespread deposition of the Late Cretaceous chalk. The success of these algae suggests that low Mg/Ca ratio of the Cretaceous seawater permitted coccolithophores to flourish, whereas the composition of modern seawater retards their productivity. To test this

hypothesis, four species of coccolithophore (*E. huxleyi, G.oceanica, C. pelagicus* ssp. *brarudii, P. carterae*) were cultured in seawater with different Mg/Ca ratio and [Sr].

This culturing setup was designed to test the physiological and morphological response of all the four chosen species (*E. huxleyi, G. oceanica, P. carterae* and *C. pelagicus* ssp. *brarudii*) to changing Ma/Ca ratio and [Sr]. The first experiment was the control one: Mg/Ca ratio was fixed at the modern ocean values (Mg/Ca = 5.2) with Ca^{2+} = 9.8 ± 0.1 mmol L^{-1} and Mg^{2+} = 50 mmol L^{-1}. In the second treatment the Mg/Ca ratio of the culturing fluid was modified keeping [Mg^{2+}] constant, adjusted [Ca^{2+}] reaching 50 mmol L^{-1}. This resulted in Mg/Ca ratio equal 1. In the third treatment, [Mg^{2+}] was kept constant and [Ca^{2+}] was increased reaching 25 mmol L^{-1}. This resulted in Mg/Ca ratio equal 2. In the last treatment Mg/Ca ratio was kept constant and the [Sr] was increased with double the amount (97.0 µmol L^{-1}). We obtained 16 different treatments tested in triplicates in autoclaved and acid cleaned glass bottles. The headspace in the 48, bottles was kept below 5 ml to avoid gas exchange. From the stock culture 50 µl have been inoculated for each species, starting the acclimation phase. Cells were acclimated to the salinity conditions of the main experiment for at least 7 generations, prior to inoculation (50 cells for each species). Cell volume was measured with the Beckman coulter Multisizer 3 after ~ 7 generations. For each bottle, filters for SEM analyses were prepared.

Experiment 4: Response of Coccolithophores to nutrient limitations

Studies on coccolithophores under nutrient-limited conditions are rare, even if micro- and macro-nutrient supplies in the upper ocean are the main factors controlling phytoplankton growth. The current progressive global warming, derived from an increase in greenhouse gasses, induces stratification of the water column. This can reduce the nutrient supply into the euphotic zone. Consequences of biogeographical nitrate and phosphate limitations in conjunction with ocean acidification seem to vary within species and strain of the same species. It is therefore a crucial theme that needs to be investigated.

This culturing setup was designed to test the physiological and morphological response of 4 species of coccolithophores to replete or limited nutrient conditions. All the other environmental parameters (salinity, temperature, light/dark cycle, carbonate chemistry) remained stable. In the acclimation phase the nutrient content was reduced by half of their concentration (32 µmol kg^{-1} nitrate and 2 µmol kg^{-1} phosphate, maintaining the same N:P

ratio, 64:4) except for the replete/control treatment. In the main experiment, the control treatment maintains the stable N:P concentration (64 μmol kg^{-1} nitrate and 2 μmol kg^{-1} phosphate). In the nitrate-limited experiments the N:P ratio was reduced to 2N:4P (resulting in 2 μmol kg^{-1} nitrate and maintaining the same concentration of phosphate). In the low phosphate experiment N:P ratio varies as low as 64N:0.1P (resulting in 0.1 μmol kg^{-1} phosphate and maintaining the stable concentration of nitrate). The experiments were performed in triplicates for every species in 600ml glass bottles. In the main experiment 10 cell/ml of *E. huxleyi, G. oceanica, P. carterae* and 20 cell/ml of *C. pelagicus* ssp. *brarudii* were transferred. Growth rate was checked every other day for *E. huxleyi* and every three days for the other three species. Reaching the stationary phase, samples were processed after sampling and measured 3 times with the coulter counter Beckman coulter Multisizer 3. Afterwards, samples were acidified with 0.10 $mmoll^{-1}$ HCl to dissolved all free and attached coccoliths and subsequently measured again 3 times and 5/10 ml of samples were filters by gravity on polycarbonate filters and dried after filtration, for SEM analyses. This procedure had been repeated again during the stationary phase, after four days.

Experiment 5: Response of Coccolithophores to trace metal enrichment

Phytoplankton growth is not only dependent on micro- and macro-nutrients (P, C, N, Si) and major ions (Mg^{2+}, K^{+}, Ca^{2+}, Cl^{-}, Na^{+}, SO_4^{2-}) but also a number of trace metals like Fe, Mn, Zn, Co, Cu, and Mo. Macronutrients and major ions are easily soluble (except for ammonium) and are normally present at high concentrations in surface waters. On the other hand, most trace metals become toxic beyond a threshold value. Furthermore, in lab simulations, trace metals are highly insoluble and create precipitates that are largely unavailable to aquatic algae. It is therefore fundamental to use a chelator (EDTA, ethylenediamine tetraacetic acid) as a buffering agent in seawater media. Nowadays antagonistic and synergistic effects of trace metals in coastal regions or open ocean are still very limited understood.

The chosen treatments only differ with respects to the metal manipulation of the culture medium; the control trace metal concentration from Kerster et al. (1967) was modified in all the treatments except for the control one. In the second, third, forth and fifth treatments Pb, V, Ni and Zn concentrations were progressively increased, maintaining the same concentrations of the other trace metals indicated in Kerster et al. (1967). Trace metal stocks were treated with EDTA chelators in order to let the non-chelated metals to be available for phytoplankton and to be readily replaced by dissociation of an equivalent concentration of the metal chelate, once they are removed by algal uptake in the exponentially growing batch cycle. For an otherview of the metals conditions in all treatments see Table 7.3.

Control treatment		**2nd treatment**		**3rd treatment**		**4th treatment**		**5th treatment**	
	µmol/l		µmol/l		µmol/l		µmol/l		µmol/l
$FeCl_3 \cdot 6H_2O$ $Na_2 \cdot 2H_2O$ $CuSO4 \cdot 5H_2O$ $Na_2MoO_4 \cdot 2H_2O$ **$ZnSO_4 \cdot 7H_2O$** $CoCl_2 \cdot 6H_2O$ $MnCl_2 \cdot 4H_2O$	11.65 11.71 0.039 0.026 **0.077** 0.042 0.91	$FeCl_3 \cdot 6H_2O$ $Na_2 \cdot 2H_2O$ $CuSO4 \cdot 5H_2O$ $Na_2MoO_4 \cdot 2H_2O$ $CoCl_2 \cdot 6H_2O$ $MnCl_2 \cdot 4H_2O$	11.65 11.71 0.039 0.026 0.042 0.91	$FeCl_3 \cdot 6H_2O$ $Na_2 \cdot 2H_2O$ $CuSO4 \cdot 5H_2O$ $Na_2MoO_4 \cdot 2H_2O$ $CoCl_2 \cdot 6H_2O$ $MnCl_2 \cdot 4H_2O$	11.65 11.71 0.039 0.026 0.042 0.91	$FeCl_3 \cdot 6H_2O$ $Na_2 \cdot 2H_2O$ $CuSO4 \cdot 5H_2O$ $Na_2MoO_4 \cdot 2H_2O$ $CoCl_2 \cdot 6H_2O$ $MnCl_2 \cdot 4H_2O$	11.65 11.71 0.039 0.026 0.042 0.91	$FeCl_3 \cdot 6H_2O$ $Na_2 \cdot 2H_2O$ $CuSO4 \cdot 5H_2O$ $Na_2MoO_4 \cdot 2H_2O$ $CoCl_2 \cdot 6H_2O$ $MnCl_2 \cdot 4H_2O$	11.65 11.71 0.039 0.026 0.042 0.91
			nmol/l		**nmol/l**		**nmol/l**		**nmol/l**
…… ….. ….. …..	….. ….. …..	**Pb** **$ZnSO_4 \cdot 7H_2O$** **$NiCl_2 \cdot 6H_2O$** **$VOSO_4$**	**10** **80** **80** **80**	**Pb** **$ZnSO_4 \cdot 7H_2O$** **$NiCl_2 \cdot 6H_2O$** **$VOSO_4$**	**80** **80** **80** **80**	**Pb** **$ZnSO_4 \cdot 7H_2O$** **$NiCl_2 \cdot 6H_2O$** **$VOSO_4$**	**800** **800** **800** **800**	**Pb** **$ZnSO_4 \cdot 7H_2O$** **$NiCl_2 \cdot 6H_2O$** **$VOSO_4$**	**8000** **8000** **8000** **8000**

Tab. 7.3 Trace metal concentrations in µmol/l or nmol/l of the growth medium

Twenty different treatments were obtained. The main experiment regarded the control treatment and the 2nd, 3rd and 4th treatments. Metal concentrations of the last treatment (5) was too high and none of the species where able to grow in the acclimation phase. In treatments 1 to 4, cells were acclimated to the metal conditions of the main experiment for at least 7 generations, prior to inoculation. Reaching the established concentration, 50 specimens were inoculated for each species, starting the main experiment. Every treatment was performed in triplicate and resulted in 48 glass bottles (300ml). Cell volume was measured with the Beckman coulter Multisizer 3, after ~ 7 generations. For each bottle filters for SEM analyses were prepared.

Scanning Electron Microscope analyses (SEM)

SEM analyses have been performed at the Università degli Studi di Milano, Earth Sciences Department with the Electron Microprobe under the supervision of Prof. S. Poli and A. Risplendente. Until now, SEM analyses have been performed for *E. huxleyi* first experiment (response of Coccolithophores to light intensities; e.g. Fig. 7.7).

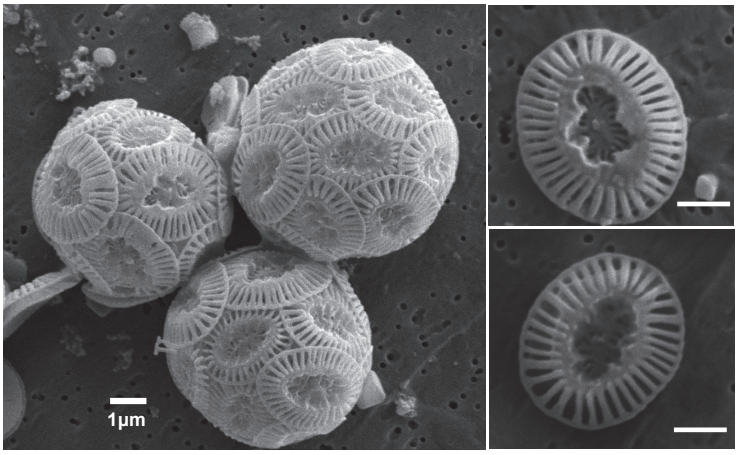

Fig. 7.7 *Emiliania huxleyi* coccospheres and coccoliths from the light intensity experiment. *E. huxleyi* cultured at 450 µmol photons $m^{-2}s^{-1}$

For every sample 50 specimens of *E. huxleyi* have been detected and photographed. I'm planning to performed SEM analyses for all the experiments and among experiments I have conducted and for every treatment among experiment. For every mono-specific sample, 50 specimens will be digitally taken. Subsequently morphometric analyses will be performed: length and width will be measured and obtained data will be statistical analyzed. Following Bach et al., (2012) calculation for the malformation index (an algorithm that quantify the degree al malformation) will be performed for *E. huxleyi* in order to record eventual irregular coccolith formation (e.g. reduced symmetry or altered shape of individual elements). Moreover, I will try to create a new malformation index for the remaining three species.

Chapter 8

Results

8.1 Calcareous nannofossil morphometric analyses

The nannofossil preservation was carefully assessed in order to avoid diagenetically altered material. In fact, partial dissolution or overgrowth have the potential to artificially decrease or enlarge the coccolith size, respectively. This is particularly relevant for the delicate *Biscutum* coccoliths that are diagenetic-prone (e.g. Theirstein, 1980). In the studied samples preservation is moderate to good and coccoliths show only very minor indications of etching and overgrowth. Accurate screening under light polarizing microscope ascertained that individual *B. constans, Z. erectus, D. rotatorius* and *W. barnesiae* coccoliths considered for morphometry were complete, with a continuous outline and without evidence of crimping due to etching or overgrowth. Further evaluation of diagenetic modifications was based on scanning electron microscope (SEM) analyses of selected samples from each section. I also tested the potential control – and its degree - of lithology on coccolith preservation, because it is well known that marlstones normally contain the best preserved nannofossil assemblages, while coccoliths in limestones are often affected by strong overgrowth and by etching in carbonate-poor lithotypes (Thierstein & Roth 1991). Samples analyzed from the five sections randomly consist of various lithologies with very similar degree of preservation and there is no correlation between coccolith size and carbonate content.

Four taxa were investigated through morphometric analyses in the five sections (Eastbourne, Clot de Chevalier, Novara di Sicilia, Pueblo and Cuba.) described in chapter 6. Tables 8.1 and 8.2 report all the obtained data and calculated parameters (mean length and mean width, maximum and minimum length and width, standard deviation, surface area, ellipticity). The results are here discussed per individual species.

8.1.1 *Biscutum constans*

Eastbourne section

Morphometric analyses were performed on 1,565 specimens. Coccolith length ranges from 6.62 to 1.67 μm (mean 3.79 μm, standard deviation sdt. dev. 0.70). Coccolith width ranges from 5.29 to 1.19 μm (mean 2.96 μm, standard deviation sdt. dev. 0.63; Tab. 8.1). Scatter plot in Fig 8.1 shows that the total coccolith length is linearly correlated with the total width with high Pearson correlation coefficient (r= 0.75). Table 8.2 illustrates mean sizes (length and width), maximum and minimum length and width, surface area and ellipticity in the different intervals (pre-event, during OAE 2 and after the event). *B. constans* displays smaller size during OAE 2, with a shift from mean length of 4.24 μm and mean width of 3.35 μm before the event, to 3.62 μm length and 2.83 μm width during OAE 2. Bigger sizes are recorded after the event (mean length of 3.83 μm and mean width of 2.95 μm).

Clot de Chevalier section

Morphometric analyses were performed on 1,110 specimens. Coccolith length ranges from 5.31 μm to 1.84 μm and width varies from 4.32 μm to 1.36 μm (mean length 3.31 μm, sdt.dev 0.57, mean width 2.56 μm sdt. dev. 0.50) Scatter plot in Fig. 8.1 displays a linear correlation of coccolith length and width (r=0.79). Table 8.2 illustrates mean length and width and other calculated parameters (e.g. surface area) in the three defined intervals (pre-event, OAE 2 and post-event). In the Clot de Chevalier section, *B. constans* shows bigger sizes (both length and width) before and after the event. During OAE 2 *B. constans* shows smaller mean size, with a shift from mean length of 3.77 μm and mean width of 2.97 μm, to respectively 3.24 μm and 2.50 μm during OAE 2. Partial increase in size (both length and width) is evident in the interval following the event.

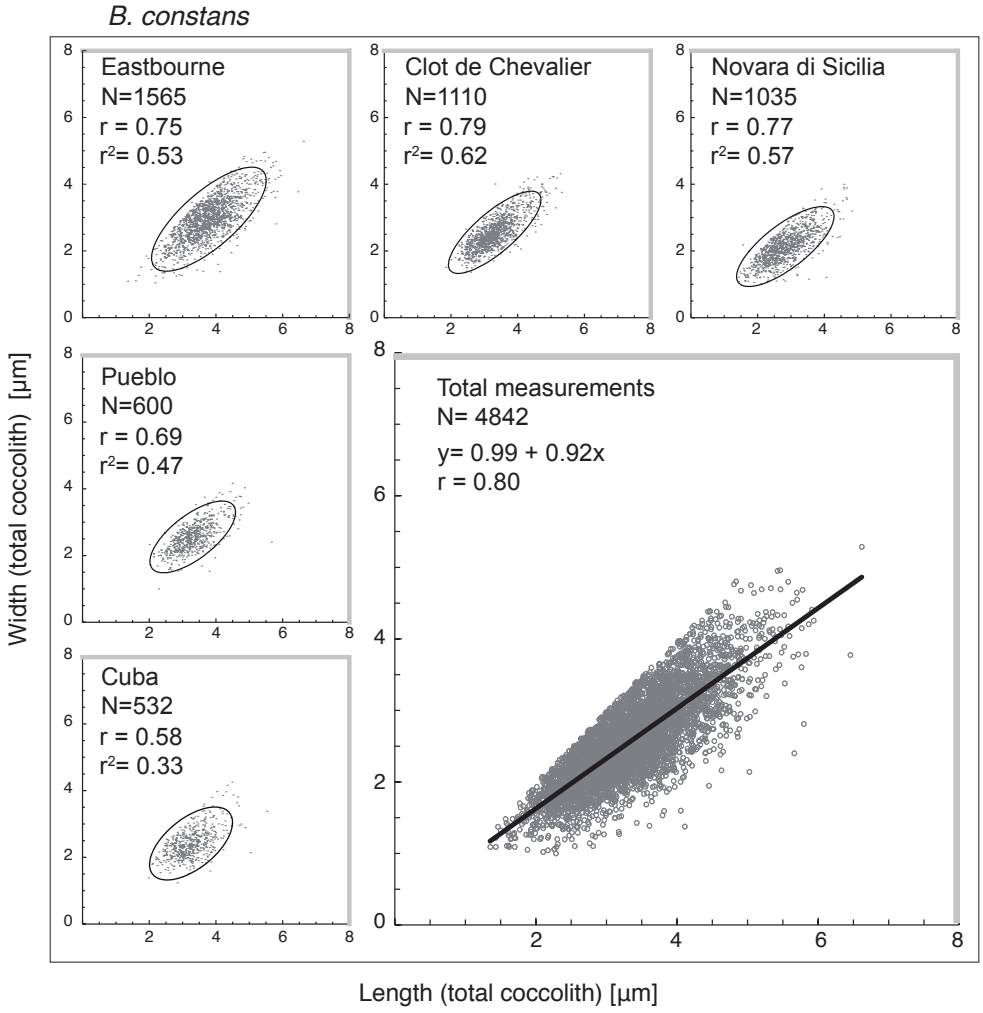

Fig. 8.1 Scatter plots of length and width of the total coccolith of *B. constans;* in addition the Pearson correlation coefficient (r), the number of measurements (N) and the linear regression function is given.

Novara di Sicilia section

Morphometric analyses on *B. constans* were performed on 1,035 specimens. Mean length is 2.82 µm (sdt. dev. 0.60) while mean width is 2.13 µm (sdt.dev. 0.48). Length ranges from 4.82 to 1.40 µm and width ranges from 4.00 to 1.05 µm. Throughout the investigated interval, specimens of *B. constans* are smaller in size compared to all the other analyzed sections. Scatter plot in Fig. 8.1 shows high Pearson correlation coefficient among length and width (r=0.77). Table 8.2 illustrates mean, maximum and minimum length and width and calculated sdt.dev, surface area and ellipticity in the two studied intervals: from the pre-event to the OAE interval, *B. constans* displays only a slight reduction in size (mean length shifts from 2.94 µm to 2.74, while mean width shifts from

2.24 to 2.05 μm). No data are available for the uppermost part of the event and post event interval that do not outcrop in the area.

Pueblo section

Morphometric analyses were performed on a total of 600 specimens. *B. constans* shows mean length and width of 3.31 μm (sdt. dev. 0.52) and 2.56 μm (sdt.dev 0.44), respectively. Length ranges from 5.66 to 2.03 μm while width ranges from 4.16 to 1.50 μm, Scatter plot in Fig 8.1 shows a high Pearson correlation coefficient among length and width (r=0.69) indicating that length and width are linearly correlated. There's any data available for the pre-event interval. Table 8.2 is a summary of obtained data and calculated parameters during OAE 2 and after the event. Mean length and width don't show significant variations. Maximum and minimum length and width shift respectively to bigger and smaller values from the OAE 2 interval to the overlying interval.

Cuba section

Morphometric analyses were performed on 534 specimens. Coccolith length ranges from 5.53 to 1.98 μm (mean length is 3.26 μm, sdt dev. 0.51) and width ranges from 4.25 to 1.24 μm (mean width 2.41 μm, sdt. dev. 0.45). Scatter plot Fig. 8.1 displays smaller values of the Pearson correlation coefficient (r=0.58), suggesting a less strong correlation among length and width in this section. Table 8.2 illustrates mean, maximum and minimum length and width and calculated parameters like ellipticity, surface area and std. dev. in the three defined intervals: pre-event, OAE 2 and after the event. Specimens of *B. constans* show a slight decrease in size in both length and width (length shifts from 3.41 to 3.23 μm, while width shifts from 2.55 to 2.40 μm) during OAE 2.

		B. constans				*W. barnesiae*				*Z. erectus*				*D. rotatorius*	
		length coccolith (µm)	width coccolith (µm)	area coccolith (µm2)	ellipticity coccolith	length coccolith (µm)	width coccolith (µm)	area coccolith (µm2)	ellipticity coccolith	length coccolith (µm)	width coccolith (µm)	area coccolith (µm2)	ellipticity coccolith	length coccolith (µm)	area coccolith (µm2)
Eastbourne	max.	6.62	5.29	27.48	2.60	9.22	8.67	4.55	1.89	4.34	3.14	10.41	2.23	4.80	72.35
	min.	1.67	1.19	1.66	1.01	2.67	2.17	60.50	1.01	1.94	1.17	2.11	1.01	1.20	4.52
	mean	3.79	2.96	9.06	1.31	5.76	5.03	23.50	1.15	3.11	2.12	5.25	1.48	3.05	29.82
	N	1564	1564	1564	1564	2152	2152	2152	2152	1460	1460	1460	1460	1576	1576
	sdt. dev.	0.70	0.63	3.35	0.21	1.08	1.00	8.65	0.11	0.42	0.31	1.37	0.16	0.45	8.85
Clot de Chevalier	max.	5.31	4.32	17.86	1.98	8.32	7.64	49.14	1.83	5.31	4.32	17.86	1.98	4.43	61.65
	min.	1.84	1.36	2.18	1.01	2.65	2.00	4.17	1.01	2.00	1.36	2.68	1.01	1.46	6.71
	mean	3.31	2.56	6.83	1.31	5.38	4.54	19.75	1.19	3.32	2.57	6.86	1.31	2.61	21.87
	N	1110	1110	1110	1110	1850	1850	1850	1850	1080	1080	1080	1080	1110	1110
	sdt. dev.	0.57	0.50	2.47	0.16	0.95	0.86	6.98	0.10	0.56	0.50	2.46	0.16	0.36	6.13
Novara di Sicilia	max.	4.82	4.00	12.56	3.05	9.35	8.47	60.47	1.95	5.08	3.86	15.30	2.57	4.61	66.77
	min.	1.40	1.05	3.31	1.01	2.35	2.15	4.08	1.02	1.40	1.09	1.32	0.90	1.19	4.44
	mean	2.82	2.13	6.68	1.35	5.49	4.66	20.80	1.19	3.04	2.08	5.06	1.47	2.66	22.76
	N	1035	1035	1035	1035	1998	1998	1998	1998	930	930	930	930	1019	1019
	sdt. dev.	0.60	0.48	1.52	0.22	1.04	0.94	7.74	0.12	0.47	0.34	1.55	0.18	0.42	7.18
WI Pueblo	max.	5.66	4.16	15.39	2.48	8.10	6.89	42.41	2.22	3.90	2.61	7.47	2.33	4.00	50.17
	min.	2.03	1.50	2.69	1.01	2.92	2.32	5.57	1.01	1.92	1.23	1.92	1.05	1.27	5.07
	mean	3.31	2.56	6.76	1.31	5.32	4.50	19.31	1.19	2.90	1.98	4.54	1.48	2.60	21.65
	N	600	600	600	600	1050	1050	1050	1050	532	532	532	532	570	570
	sdt. dev.	0.52	0.44	2.10	0.18	0.90	0.83	6.51	0.11	0.33	0.26	1.00	0.16	0.38	6.27
WI Cuba	max.	5.53	4.25	14.95	2.40	9.36	8.11	53.05	1.98	4.25	2.79	9.31	2.32	5.22	85.47
	min.	1.98	1.24	2.14	1.01	2.82	2.18	4.82	1.00	2.06	1.35	2.66	1.01	1.27	5.07
	mean	3.26	2.41	6.28	1.37	5.74	4.94	22.96	1.17	2.95	1.99	4.64	1.50	2.52	20.47
	N	532	532	532	532	449	449	449	449	482	482	482	482	482	482
	sdt. dev.	0.51	0.45	1.98	0.23	1.03	0.98	8.24	0.12	0.35	0.24	0.99	0.19	0.43	7.71

Table 8.1 Overview of the gained simple statistical parameters of the studied species and morphotypes. Abbreviation: max., maximum; min., minimum; N, number of measurements; sdt.dev., standard deviation.

8.1.2 *Zeugrhabdotus erectus*

Eastbourne section

Tab 8.1 and 8.2 summarize all the measured values and calculated parameters for *Z. erectus* (mean length and width, maximum and minimum length and width, surface area, ellipticity and sdt. dev.). *Z. erectus* length ranges from 4.34 to 1.94 µm (mean length 3.11 µm, sdt. dev. 0.42) while width ranges from 3.14 to 1.17 µm (mean width 2.12 µm, sdt. dev. 0.31). Total coccolith length is linearly correlated with the total width with high Pearson correlation coefficient (r= 0.72). *Z. erectus* consists of smaller coccoliths during the OAE 2 interval. Instead, bigger coccoliths are observed before and after the event.

Furthermore during OAE 2 an increase in ellipticity (increase in the length/width ratio) is detected, shifting from the pre-event interval to OAE, from 1.46 to 1.49.

Clot de Chevalier section

In the Clot de Chevalier section 1,080 specimens have been measured. *Z. erectus* length ranges from 5.31 to 2.00 μm (mean length 3.32 μm, sdt. dev. 0.56), while width ranges from 4.32 to 1.36 μm (mean width 2.57 μm, sdt. dev. 0.50). Total coccolith length is linearly correlated with the total width with very high Pearson correlation coefficient (r=0.79). In Table 2, *Z. erectus* size parameters are subdivided in the pre-event, OAE 2 and post-event intervals. During OAE 2 *Z. erectus* coccoliths show smaller width and length. In the OAE 2 interval there's an increase in coccolith ellipticity.

Novara di Sicilia section

In the Novara di Sicilia section, from the pre-OAE 2 event to OAE 2 a slight decrease in *Z. erectus* mean length and width is observed. Mean length is 3.04 μm and sdt. dev. 0.47 (length ranges from 5.08 to 1.40 μm), while mean width it 2.08 and sdt.dev. 0.34 (length ranges from 3.86 to 1.09 μm). Length and width appear to be linearly correlated and Pearson correlation coefficient is r=0.72. Shifting from the pre-OAE 2 interval to OAE 2, a small reduction in size of both length and width is observed, with a reduction of the mean surface coccolith area. Furthermore, during OAE 2 an increase in coccolith ellipticity is observed.

Pueblo section

A total of 532 specimens have been analyzed in the Pueblo section. *Z. erectus* length ranges from 3.90 to 1.92 μm (mean length 2.90 μm, sdt dev. 0.33) and width ranges from 2.61 to 1.23 μm (mean width 1.98 μm, sdt. dev. 0.26). Length and width have a lower Pearson correlation coefficient value compared to previous section (r=0.66). No data are available for the pre-OAE 2 interval. From OAE 2 interval to the post-event interval there's a minor increase in size and decrease in mean ellipticity.

Cuba section

The 482 analyzed specimens show a length range from 4.25 to 2.06 μm (mean length 2.95 μm, sdt. dev. 0.35), while width ranges from 2.79 to 1.35 μm (mean width 1.99 μm, sdt.

dev. 0.24 μm). The Pearson correlation coefficient (r=0.49) appears to be lower than in the other studied sections. Table 2 shows *Z. erectus* morphometric data, subdivided in the three intervals and highlights a little increase in size trend from the pre-OAE 2 event to the post-event interval. As size increases, a decrease in mean ellipticity is detected.

8.1.3 *Discorhabdus rotatorius*

Eastbourne section

In the Eastbourne section 1,576 *D. rotatorius* specimens were measured. Coccoliths of *D. rotatorius* show diameter ranging from 4.80 to 1.20 μm (mean diameter = 3.05 μm, sdt.dev. 0.45). Table 8.2 shows *D. rotatorius* variations in the three established intervals: from the pre-OAE 2 interval to OAE 2 there's a slight decrease in the diameter mean value. In the Eastbourne section *D. rotatorius* shows the largest mean diameter compared to the other investigated sections.

Clot de Chevalier section

D. rotatorius diameter ranges from 4.43 to 1.46 μm (mean diameter 2.61 μm, sdt. dev. 0.36). In the pre-OAE 2 interval the mean diameter is 2.99 μm while during OAE 2 it decreases to 2.54 μm. A slight increase in size is observed in the post-OAE 2 interval.

Pueblo section

In the Pueblo section 570 specimens were analyzed. Coccoliths of *D. rotatorius* display diameter ranging from 4.00 to 1.27 μm (mean diameter 2.60 μm, sdt.dev. 0.38). A very minor increase in diameter is observed passing from the OAE 2 interval to the overlying samples.

Cuba section

In the Cuba section a total of 482 specimens of *D. rotatorius* were measured. The diameter ranges from 5.22 to 1.27 μm (mean diameter 2.52 μm, sdt.dev. 0.43 μm). In the pre-OAE 2 interval, the mean diameter is 2.41 μm and slightly increases during OAE 2 to 2.57 μm. In the post-OAE 2 interval, mean diameter decrease once again to 2.49 μm.

8.1.4 *Watznaueria barnesiae*

Eastbourne section

Morphometric analyses were performed on 2,152 specimens. *W. barnesiae* length ranges from 9.22 to 2.67 µm (mean length 5.76 µm, std.dev. 1.08) while width ranges from 8.67 to 2.17 µm (mean width 5.03 µm, sdt.dev. 1.00). Scatter plot in Fig 8.2 displays that the coccolith length is linearly correlated with the total width with very high Pearson correlation coefficient (r= 0.81). In table 8.2 *W. barnesiae* displays very stable length, width and ellipticity through the three established intervals.

Clot de Chevalier section

A total of 1,850 specimens were analyzed in the Clot de Chevalier section. Length ranges from 8.32 to 2.65 µm (mean length 5.38 µm, sdt.dev. 0.95) and width ranges from 7.64 to 2.00 µm (mean length 4.54 µm, sdt. dev. 0.86). Length and width are linearly correlated with a high Pearson correlation coefficient (r=0.79).

Novara di Sicilia section

The 1,998 analyzed specimens show a size range of length from 9.35 to 2.35 µm (mean length 5.49 µm, sdt.dev. 1.04) and width from 8.47 to 2.15 µm (mean width 4.66 µm, sdt. dev. 0.94). Length and width are linearly correlated with a high Pearson correlation coefficient (r=0.79). Cocoliths of *W. barnesiae* display very stable values for length and width, and therefore ellipticity in the interval preceding OAE 2 and within the event.

Pueblo section

Size analyses of *W. barnesiae* coccoliths were performed on 1,050 specimens. The mean length is 5.32 µm (sdt. dev. 0.90) and it ranges from 8.10 to 2.92 µm. The mean width is 4.50 µm (sdt. dev. 0.83) and it ranges from 6.89 to 2.32. Length and width are linearly correlated with a high Pearson correlation coefficient (r=0.89). *W. barnesiae* displays very stable values for length and width and consequently ellipticity before, during and after OAE 2.

Cuba section

A total of 449 specimens were measured. *W. barnesiae* mean length is 5.74 μm (it ranges from 9.36 to 2.82 μm) and mean width is 4.94 (it ranges from 8.11 to 2.18 μm). Length and width are linearly correlated with a high Pearson correlation coefficient (r=0.86). *W. barnesiae* coccoliths display larger sizes during OAE 2.

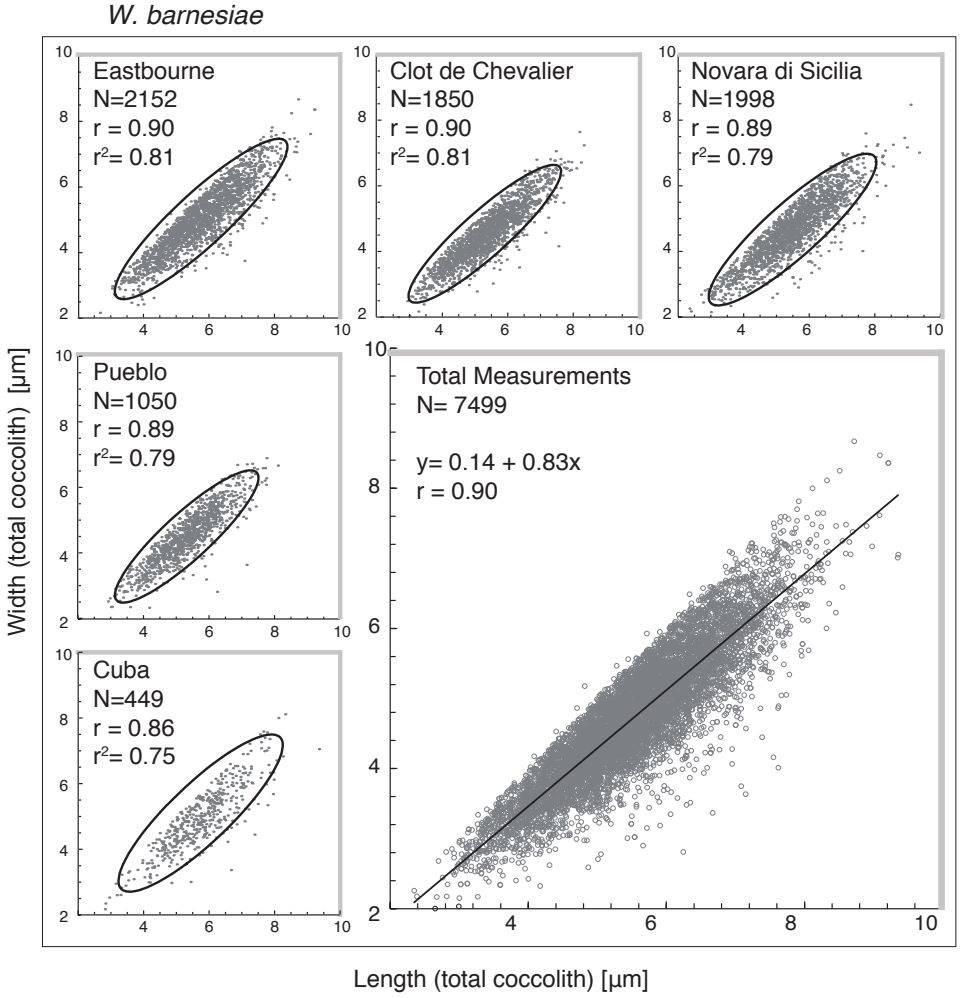

Fig. 8.2 Scatter plots of length and width of the total coccolith of *W. barnesiae;* in addition the Pearson correlation coefficient (r), the number of measurements (N) and the linear regression function is given.

8.2 Stratigraphic representations

8.2.1 Small coccolith: *B. constans, Z. erectus and D. rotatorius*

In the next paragraph the size variations through time are represented for every section. Morphometric mean length and width of each sample is represented in stratigraphic order, using the $d^{13}C$ curve as reference tool to correlate the investigated sections and compared the obtained results discriminating the interval before OAE 2, OAE 2 and the following interval. In order to identify possible trends, in each section, the coccolith size of individual species was compared to the total mean size of all analyzed specimens. Furthermore, the 25%, and 75% percentile values and standard deviation (sdt.dev.) of each sample are represented in the graphs.

Eastbourne section

B. constans, Z. erectus and *D. rotatorius* show the same size trends through the Eastbourne section. Six different size trends can be separated from the base to the top of the section. These trends are closely related to $\delta^{13}C$ variations (Fig. 8.3).

From base to the top of the section, in stratigraphic order, we observed:

a) Interval 1: mean sizes of all the three species appear bigger than the mean value.
b) Interval 2: at the OAE 2 onset the mean size of the three taxa decreases becoming slightly smaller than the mean values.
c) Interval 3: a slight increase in coccolith size is detected. During OAE 2, the bigger values are measured across the $\delta^{13}C$ peak A.
d) Interval 4: a decrease in size is observed in all the three species. Trend size displays a wavy pattern with frequent decreases and relative recoveries in size. The strongest reduction in size (dwarfism) is coeval with the $\delta^{13}C$ peak B.
e) Interval 5: a relative increase in size of all the three analyzed species. The increase in size of *D. rotatorius* coccoliths in more visible than in the other two species. The increase in size starts soon after the $\delta^{13}C$ peak B.
f) Interval 6: in the uppermost part of the section, approximately from the $\delta^{13}C$ peak D upwards, *B. constans, Z. erectus* and *D. rotatorius* show a progressive increase in size, that become slightly larger than the mean size (light blue line).

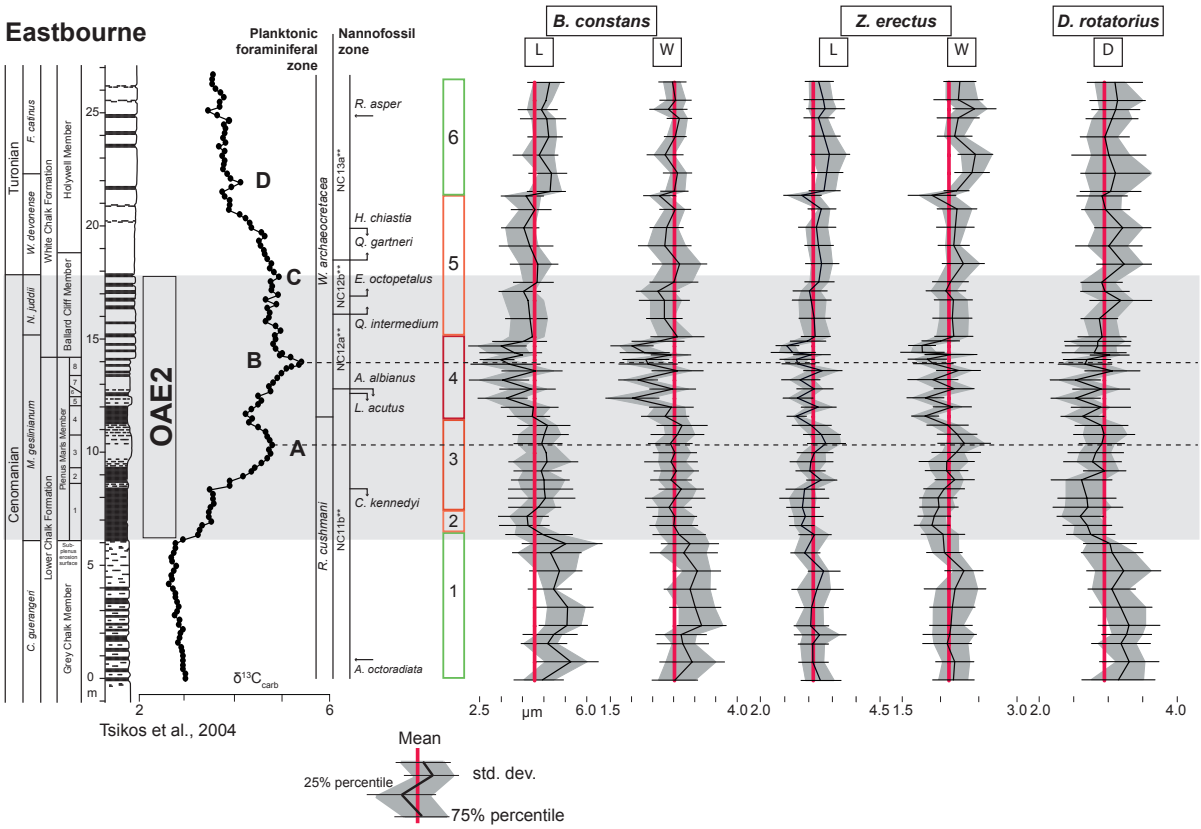

Fig. 8.3 Eastbourne section: size changes of *B. constans*, Z. erectus and D. rotatorius during OAE 2 against $\delta^{13}C$ curve. L total coccoith length, W total coccolith width and D total coccolith diameter.

Clot de Chevalier section

In the Clot de Chevalier section the interval preceding OAE 2 is rather thin and, therefore, just a few samples were available before the OAE onset. Furthermore, due to availability of samples, morphometric analyses were performed at lower resolution compared to the Eastbourne section. Not all the six intervals distinguished in the Eastbourne section are recognized at Clot de Chevalier. The mean values of length and width of *B. constans* is smaller than in the Eastbourne section, while *Z. erectus* and *D. rotatorius* display very similar values in both sections.

From the base to the top of the Clot de Chevalier section, five intervals are distinguished. These intervals are well expressed in *B. constans* while size fluctuations are less evident in the other two species. The four intervals are here described with the same numbers used for the Eastbourne section (Fig. 8.4).

a) Interval 1: from the base both *B. constans* and *D. rotatorius* show an increase in size compared to the total mean length and width or diameter.

b) Interval 2: only *D. rotatorius* evidences a reduction in size in one sample at the OAE 2 onset. There isn't any evidence of a reduction in size trend in *B. constans*. This however might be due to the low resolution analyses were performed or to possible presence of a hiatus at the beginning of OAE 2.

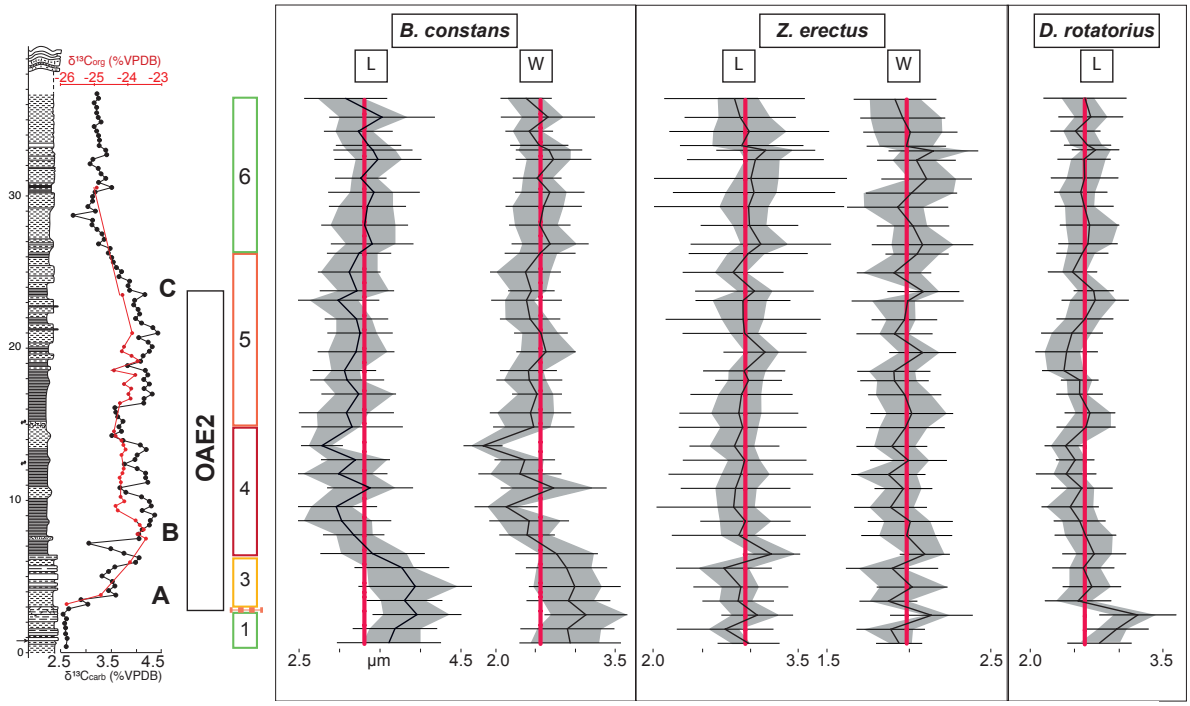

Fig. 8.4 Clot de Chevalier section: size changes of *B. constans*, Z. erectus and D. rotatorius during OAE2 against $\delta^{13}C$ curve. L, total coccolith length, W total coccolith width and D total coccolith diameter.

c) Interval 3: from OAE 2 onset an increase in size trend is observed. Major sizes are recorded around $\delta^{13}C$ peak A. In *Z. erectus* no specific trends are observed in the first part of the OAE 2.

d) Interval 4: a decrease in size trend is observed in all the three species. Particularly, this is well evident in *B. constans* that shows a marked reduction reaching the minimum size values (dwarfism) just after $\delta^{13}C$ peak B ^{13}C.

e) Interval 5: between $\delta^{13}C$ peak B and C, coccoliths of *B. constans* and *D. rotatorius* start to increase in size, although values remain smaller than the mean length, width or diameter. *Z. erectus* values are aligned to the mean value.

f) Interval 6: in the uppermost part of the section and particularly after $\delta^{13}C$ peak C, coccoliths of *B. constans*, *Z. erectus* and *D. rotatorius* show an increase in size. The diameter of *D. rotatorius* is very similar to the mean diameter value.

Novara di Sicilia section

In the Novara di Sicilia section only the pre-OAE 2 interval and the first part of the event are represented: as explained in Chapter 6, the outcrop physically ends just after the $\delta^{13}C$ peak B. At this location, the coccolith mean length and width of *B. constans* are smaller compared to all the other investigated sections. Indeed *B. constans* coccoliths are very tiny even before the OAE 2 onset. Similarities and differences of the previously described intervals are illustrated below (Fig. 8.5):

a) Interval 1: before OAE 2 onset all the three species show a wavy pattern with an increase, a subsequent decrease in size and another increase in size just below the base of the Bonarelli level equivalent. Moreover at the OAE 2 onset a barren interval has been detected.

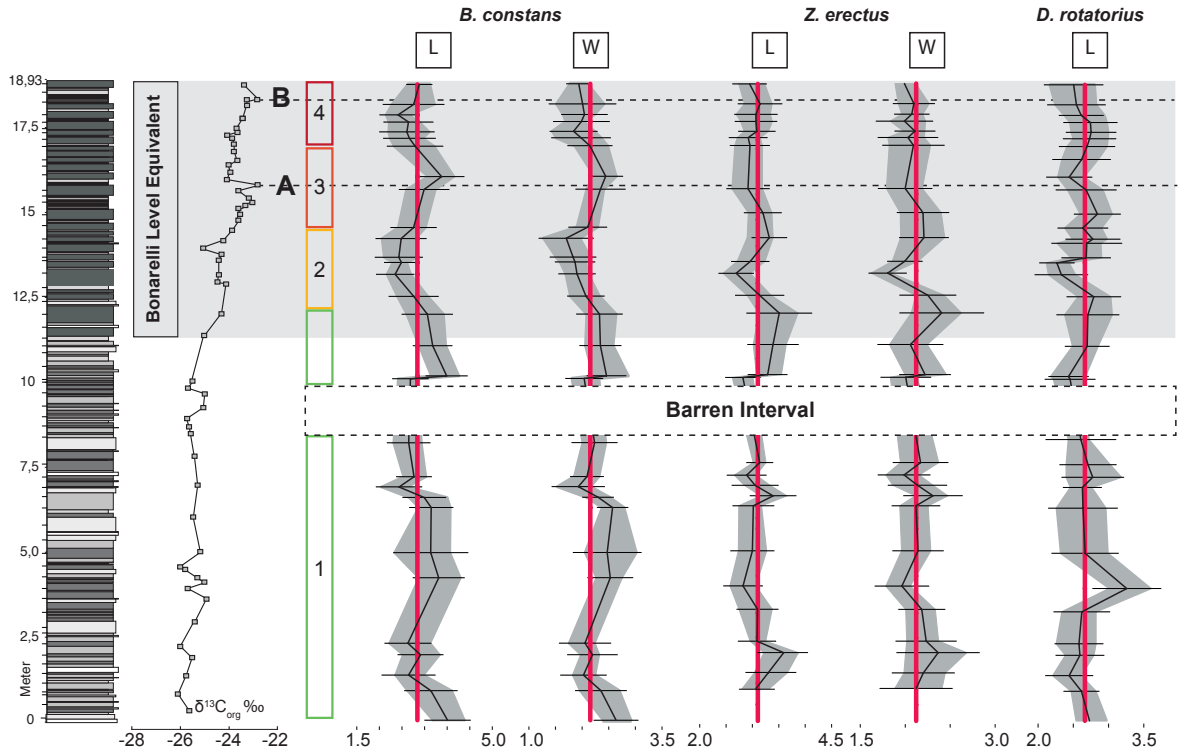

Fig. 8.5 Novara di Sicilia section size changes of *B. constans*, Z. erectus and D. rotatorius during OAE2 against $\delta^{13}C$ curve. L, total coccoith length, W total coccolith width and D total coccolith diameter.

b) Interval 2: at the base of the Bonarelli level equivalent, similarly to the results of the Eastbourne section, the three species show an approximately coeval decrease in size trend.

c) Interval 3: *B. constans, Z. erectus* and *D. rotatorius* show an increase in size trend and, in particular *B. constans* reaches maximum size values around $\delta^{13}C$ peak A.

d) Interval 4: below the $\delta^{13}C$ peak B, *B. constans* and *Z. erectus* show a reduction in size. Both species reach minimum values (dwarfism) at $\delta^{13}C$ peak B. Coccoliths of *D. rotatorius* do not show any size variation and values mean diameter value.

Pueblo section

In the Pueblo section no samples are available in the interval prior to the OAE 2 onset. Therefore, only four out of the six intervals identified at Eastbourne are observed (Fig.8.6).

a) Interval 3: an increase in size is observed in both *B. constans* and *D. rotatorius*; bigger sizes are coeval with $\delta^{13}C$ peak A. The size of *Z. erectus* coccoliths are similar to the mean length and width.

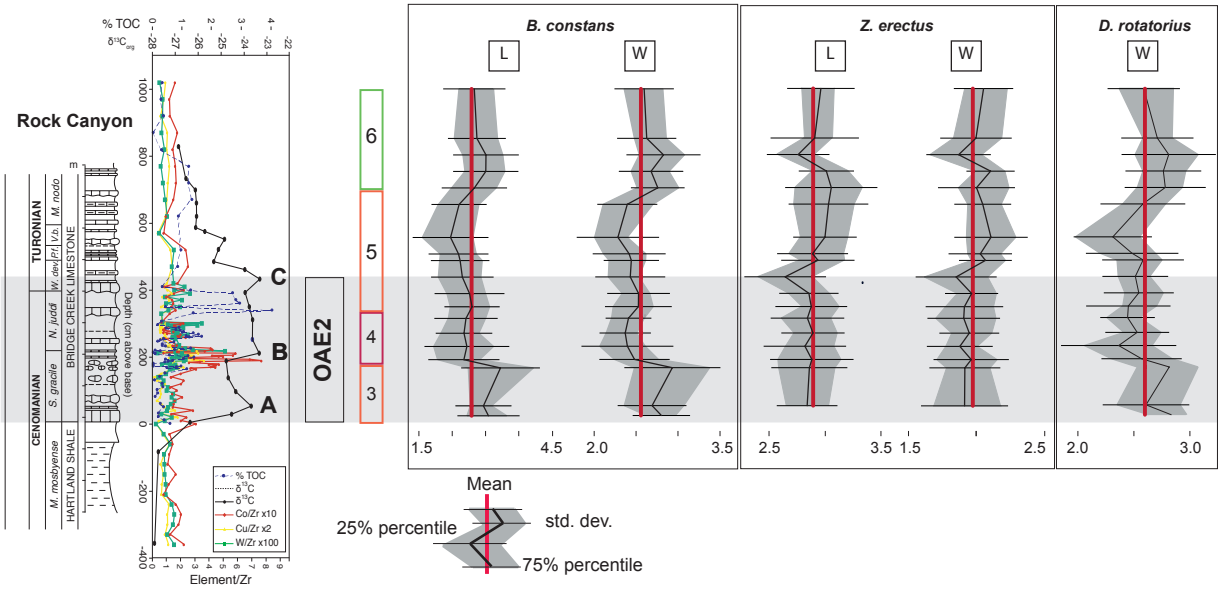

Fig. 8.6 Pueblo section size changes of *B. constans*, Z. erectus and D. rotatorius during OAE2 against $\delta^{13}C$ curve. L, total coccoith length, W total coccolith width and D total coccolith diameter.

b) Interval 4: *B. constans and D. rotatorius* display a decrease in size, reaching minimum values around $\delta^{13}C$ peak B. *Z. erectus* doesn't show any change, however at the top of this interval smaller coccoliths are detected.

c) Interval 5: a slightly increase in size is observed after $\delta^{13}C$ peak B. However a subsequent new decrease in size trend is displayed reaching minimum values around $\delta^{13}C$ peak C. Thereafter an increase in size trend is observed in all the

three species: size increase trend firstly occur in *Z. erectus* and subsequent in *B. constans and D. rotatorius*.

d) Interval 6: in the last part of the section *B. constans and D. rotatorius* show a increase in size trend with length, width or diameter bigger than the total mean values.

Cuba section

In the lowermost portion of this section, only a few samples were available to characterize the pre-OAE interval. The results are very similar to those obtained for the other sections. In particular, *B. constans, Z. erectus* and *D. rotatorius* show similar size trends although of different amplitude compared to the Eastbourne section (Fig. 8.7):

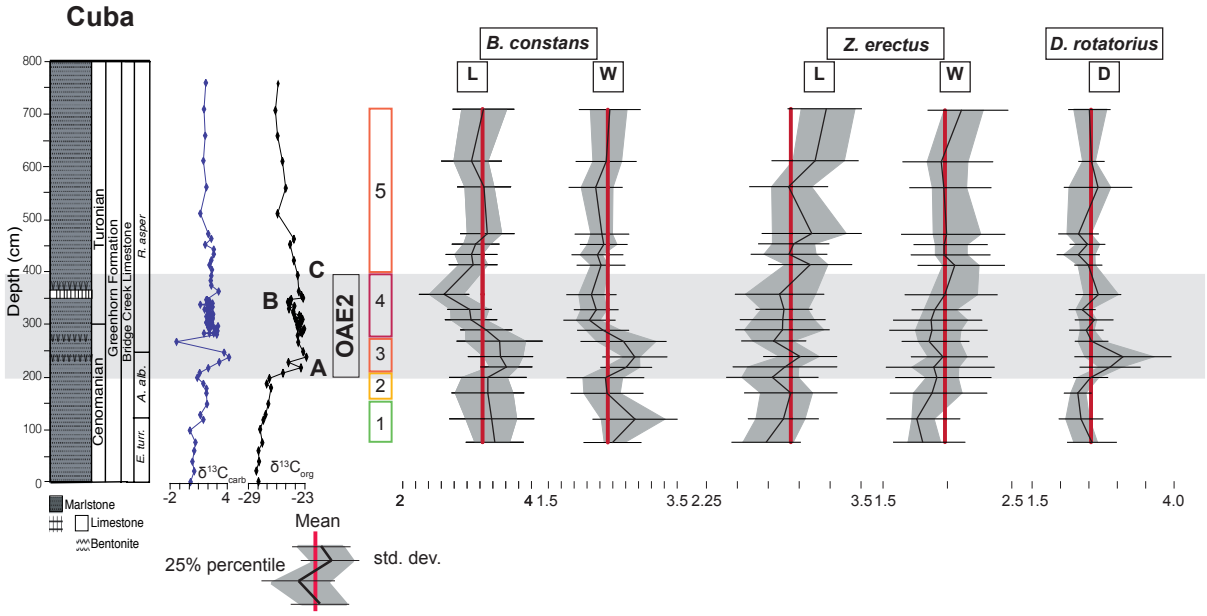

Fig. 8. 7 Cuba section size changes of *B. constans*, Z. erectus and D. rotatorius during OAE2 against $\delta^{13}C$ curve. L , total coccoith length, W total coccolith width and D total coccolith diameter.

a) Interval 1: only the bottom 2 samples contain coccoliths of *B. constans* larger than the mean size.

b) Interval 2: both *B. constans* and *D. rotatorius* are represented by coccoliths smaller than the mean size. *Z. erectus* has an erratic behavior.

c) Interval 3: *B. constans* and *D. rotatorius* show an increase in size reaching maximum values around $\delta^{13}C$ peak A.

d) Interval 4: *B. constans* displays a reduction in size reaching minimum size around $\delta^{13}C$ peak B. Coccoliths of *D. rotatorius* also show a decrease in although at a lesser extent.

e) Interval 5 (and 6): in the upper part of the section, above $\delta^{13}C$ peak C, the three species show an increase in size that return to values similar to the mean sizes.

8.2.2 *Watznaueria barnesiae*

Morphometric analyses of *W. barnesiae* through time were perfomerd in all the analysed sections. *W. barnesiae* doesn't show any specific trend through the OAE 2: the coccolith size remains rather stable and around the mean value (Fig. 8.8, Fig. 8.9). In the Clot de Chevalier and Pueblo sections a sligth reduction in size is observed during event.

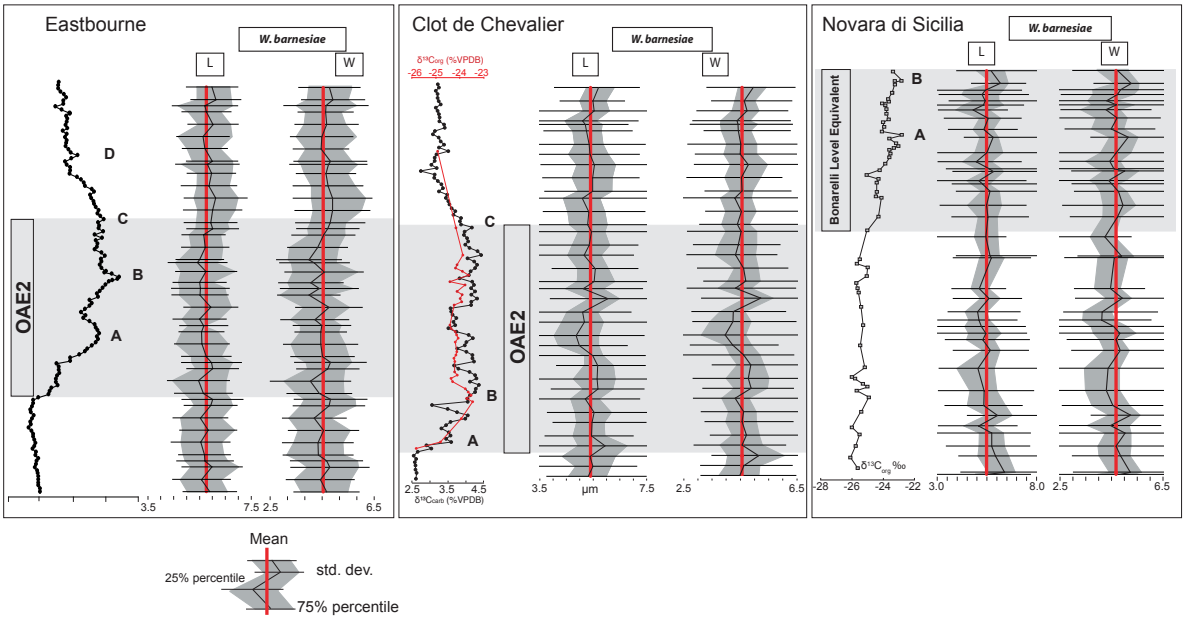

Fig. 8.8 Eastbourne, Clot de Chevalier and Novara di Sicilia sections: size changes of *W. barnesia* during OAE2 against $\delta^{13}C$ curve. L, total coccoith length, W total coccolith width.

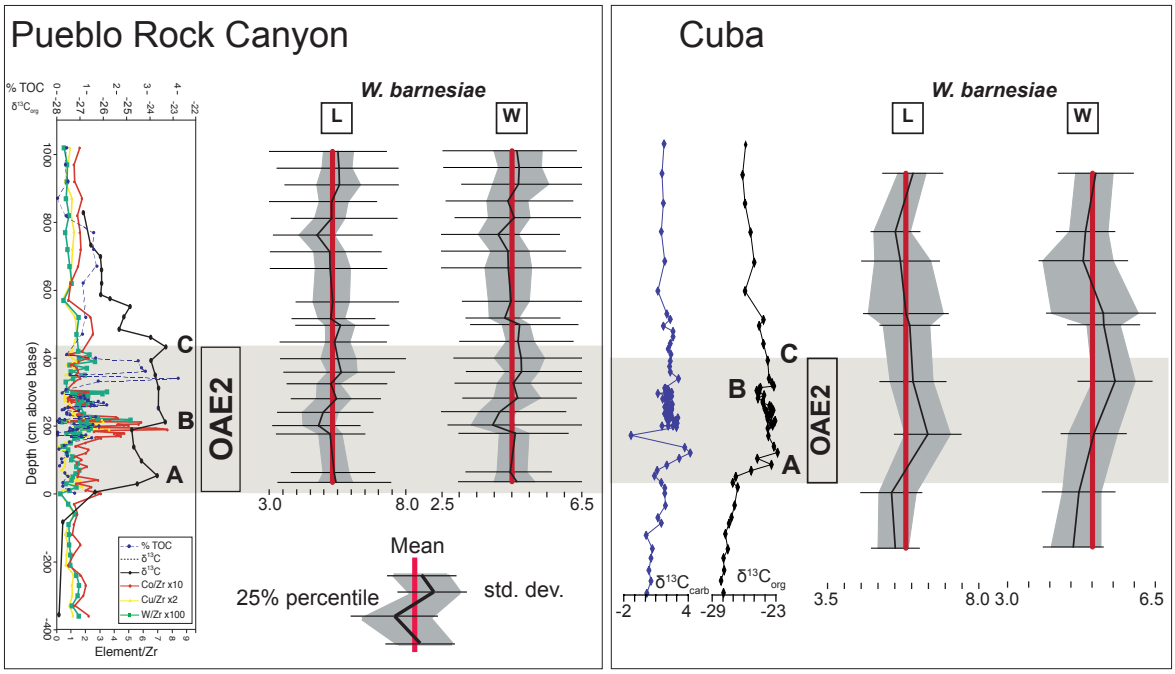

Fig. 8.9 Pueblo Rock Canyon and Cuba sections: size changes of *W. barnesia* during OAE2 against $\delta^{13}C$ curve. L, total coccoith length, W total coccolith width.

8.3 *Biscutum constans* morphometric analyzes

B. constans displays the greater variations in coccolith size throught the OAE 2 in all the analyzed sections. Furthermore, in all the studied sections, this taxon shows a major reduction in size in the same stratigraphic level (around the $\delta^{13}C$ peak B). Therefore further analyses on morphometric data were performed for *B. constans*.

Box Plot representation of *B. constans* length is represented in Fig. 8.10. In the pre-OAE 2 interval a reduction in size from the highest-latitudes section (Eastbourne) to the lowest one (Novara di Sicilia) is observed. At Clot de Chevalier, this taxon displays halfway values. During the OAE 2 the same latitudinal trend is observed. However, in the Eastbourne and Clot de Chevalier sections a strong reduction in size is observed. It is important to take into account that the Novara di Sicilia section physically ends just after the $\delta^{13}C$ peak B. Thus, most probably the major reduction in size interval observed in the other sections, is not recorded in this section. In the post-OAE 2 interval a partial recovery in size is observed especially in Eastbourne and Clot de Chevalier sections. To better understand the amplitude of the *B. constans* reduction in size, size ratios were calculated relative to the holotype values (length 5 µm, width 4.5 µm). Size ratio among OAE 2 data and holotype values are expressed as percentage. As indicated in table 8.3,

the Eastbourne and Clot de Chevalier sections record a stronger decrease in size from the pre-OAE 2 interval to OAE 2. Partial recovery is observed after the event. The Novara di Sicilia section shows a less expressed reduction in size during OAE 2, but coccolith size is very tiny even before OAE 2. In the Cuba section a small reduction in size is observed from the pre event interval to OAE 2.

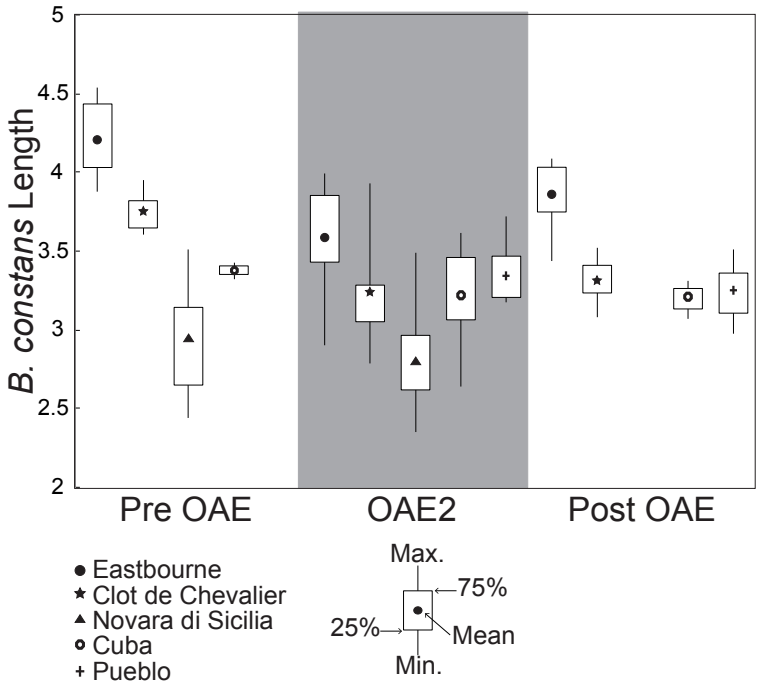

Fig. 8.10 Box plot of measured *B. constans* total coccolith length of the analyzed sections subdivided in the pre-event, OAE 2 and post-event intervals.

B. constans ellipticity (length/width ratio) was calculated for all the studied samples in order to point out possible malformation during OAE 2. In general an increased in ellipticity is observed when coccoliths reduce their size. This is less expressed in the Cuba section. In the Eastbourne section a wavy pattern is observed: size variation and ellipticity show the same fluctuating variation around the $\delta^{13}C$ peak B, with increased ellipticity when size values decrease (Fig. 8.11, 8.12). In the Novara di Sicilia section a trend towards more elliptical coccoliths is observed in the uppermost portion of the section, where a decrease in size is detected

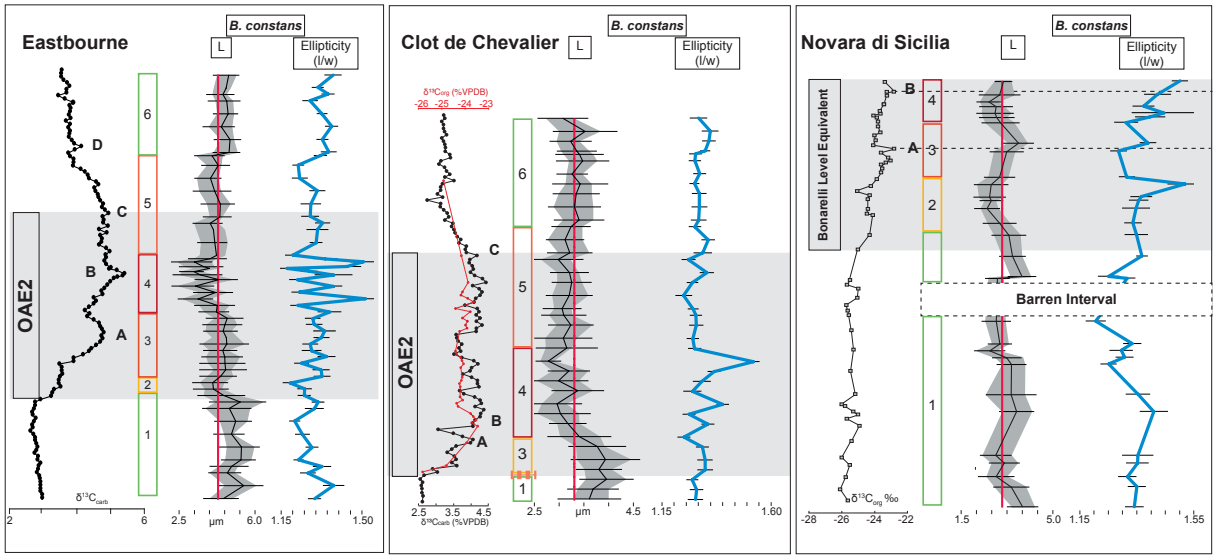

Fig. 8.11 *B. constans* length (L) versus *B. constans* ellipticity expressed as length/width (l/w) in Eastbourne, Clot de Chevalier and Novara di Sicilia sections. Morphometric and morphological data are expressed against $\delta^{13}C$ curve through OAE2.

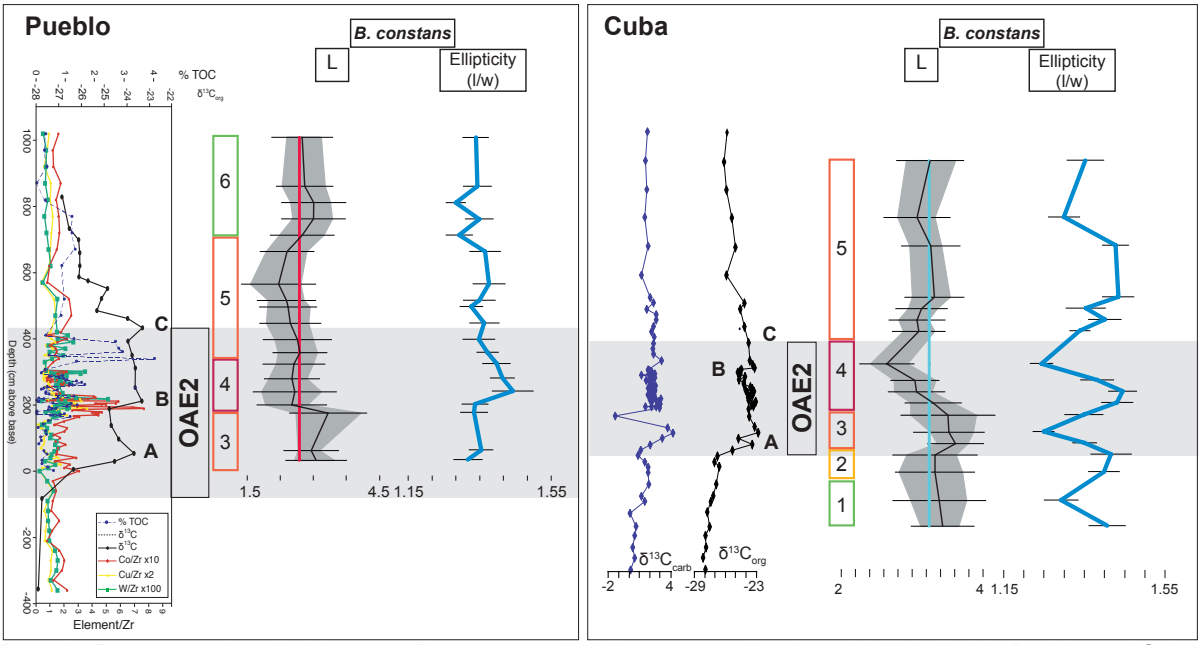

Fig. 8.12 *B. constans* length (L) versus *B. constans* ellipticity expressed as length/width (l/w) in Pueblo and Cuba sections. Morphometric and morphological data are expressed against $\delta^{13}C$ curve through OAE2.

In all studied sections, there is a difference in the mean ellipticity of *B. constans* between the pre-OAE 2, OAE 2 and post-OAE 2 intervals (Tab. 2): the pre-OAE 2 interval is characterized by less elliptical specimens (more circular) having a mean ellipticity ranging from 1.02 to 2.08. During OAE 2 the mean ellipticity is higher and it comprised between 1.31 and 1.36. The post-OAE 2 interval is characterized by mean ellipticity

ranging from 1.30 and 1.39. Smaller coccolith specimens are more elliptical (Fig., 8.13); specifically there is a negative correlation (r=-0.46) between width and ellipticity (smaller width corresponds to higher ellipticity), and between surface area and ellipticity (r=-0.23). The length does not show any correlation with the ellipticity, but more elliptical specimens are comprised between a length range of 2 - 4 μm

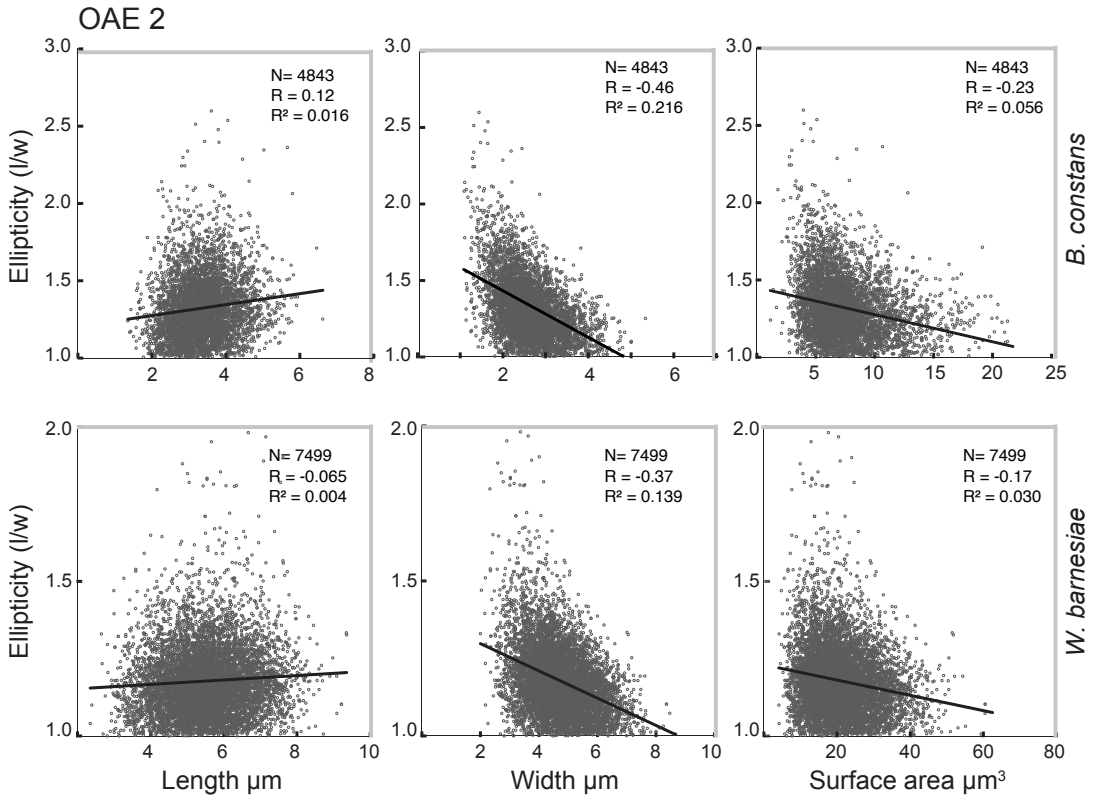

Fig 8.13 Scatter plots of ellipticity versus of length, width and surface area of *Biscutum constans* and *Watznaueria barnesia* species during the latest Cenomanian and across the OAE2

B. constans data were compared to results of morphometric analyses conducted across the OAE 1a interval (Erba et al., 2010; Bottini unpublished PhD thesis 2010, Fig. 8.14). The Cismon core and DSDP Site 463 morphometric data were compared with the two most complete sections for OAE 2, which are respectively the Eastbourne and Clot de Chevalier sections. Data are represented with box plots: OAE 1a sections were subdivided in three main intervals: pre-OAE 1a, OAE 1a and post-OAE 1a. Data for the Eastbourne and Clot de Chevalier sections are subdivided in four intervals: pre-OAE 2, OAE 2 and two post-event intervals before and after the $\delta^{13}C$ peak D, respectively.

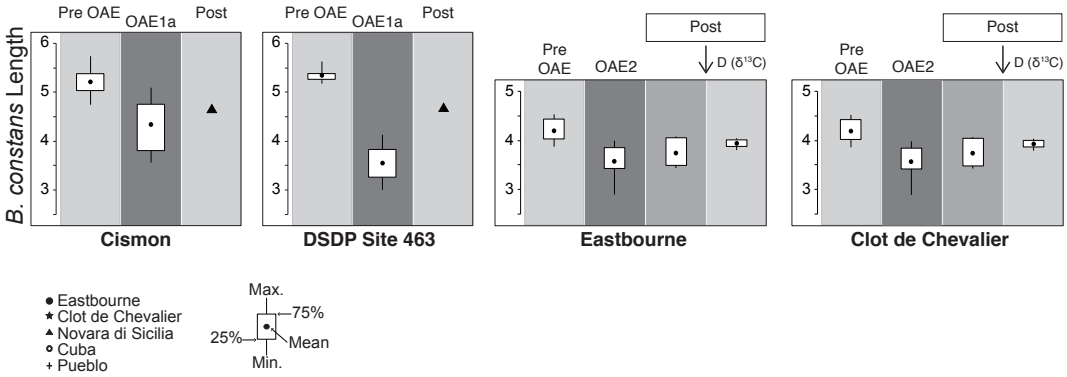

Fig. 8.14 Box plots of measured *B. constans* total coccolith length: comparison between OAE 1a data and OAE2. OAE 1a: Cismon core and DSDP Site 463; OAE2: Eastbourne section and Clot de Chevalier. Intervals (pre-OAE, OAE, post-OAE) have been chosen based on $\delta^{13}C$ isotope curve.

All the analyzed sections, both for OAE 1a and OAE 2, evidence e decrease in size from the pre-OAE to the OAE interval. At all sections, in the post event interval, *B. constans* coccoliths show an increase in size even if they remain smaller compared to the pre-event measurements. Coccolith sizes were compared to the holotype (length 5 μm, width 4.5 μm). In particular the coccolith length was used to calculate the percentage of dimension relative to the length of the holotype (Tab. 8.3). For both the OAE 1a and OAE 2 intervals (including pre- and post-OAE) the size reduction is evident during the perturbation. As far as OAE 1a is concerned, *B. constans* shows holotypic values before the event. A strong reduction in size is observed in both studied sections (Erba et al., 2010) but is more evident at DSDP Site 463. A recovery in size is observed after OAE 1a, although coccoliths remain slightly smaller than the holotype. During OAE 2 the same pattern is observed with smaller coccoliths during OAE 2 and a partial recovery after the event. I noticed that at all studied localities in the interval preceding OAE 2, *B. constans* coccoliths are already smaller than the holotype (mean length 72% of the holotype) and reach the smallest size (mean length 63% of the holotype) during OAE 2. This "dwarfism" is more accentuated than during OAE 1a, although the reduction *B. constans* size is larger for OAE 1a (- 21%) than for OAE 2 (- 9%).

	OAE 1a				OAE 2						
	Cismon	**463**	**Total**	Reduction	**Eastbourne**	**Clot de Chevalier**	**Novara di Sicilia**	**Pueblo**	**Cuba**	**Total**	Reduction
Post	93%	93%	**93%**	-7%	76%	66%	no data	66%	64%	**68%**	-32%
OAE	86%	71%	**79%**	-21%	72%	55%	54%	67%	65%	**63%**	-37%
Pre	104%	106%	**105%**	5%	85%	75%	59%	no data	68%	**72%**	-28%

Tab. 8.3 *B. constans* coccolith length vs holotype length ratio (percentage) in OAE 1a and OAE2.

8.4.4 *W. barnesiae* ellipticity analyzes

The ellipticity of *W. barnesiae* ranges from 1.01 to 2.22 (mean 1.18, 0.11 sdt. dev., Table 1). Any significant variation in the ellipticity is detected throughout the studied interval. However, I noticed that also for *W. barnesiae*, the smaller specimens are more elliptical (Fig. 8.13); specifically there is a negative correlation (r=-0.37) between width and ellipticity (smaller width corresponds to higher ellipticity), and between surface area and ellipticity (r=-0.17). The length does not show any correlation with the ellipticity, but I noticed that more elliptical specimens are comprised between a length range of 5 - 7 μm. Following Erba et al., 2010, I analysed *W. barnesiae* ellipticity of normal-sized specimens (length >5 μm) and small specimens (length <5 μm) in three intervals (Tab. 8.4):

1) Pre: consists of all analyzed specimens till interval 4.
2) Interval 4: all specimens measured around $\delta^{13}C$ peak B (maximum OAE 2 perturbation interval).
3) Post: consists of all specimens analyzed after interval 4.

	Pre-		Interval 4		Post	
	<5 μm	>5 μm	<5 μm	>5 μm	<5 μm	>5 μm
Eastbourne	1.15	1.16	1.15	1.17	1.14	1.15
Clot de Chevalier	1.18	1.19	1.20	1.20	1.18	1.20
Novara di Sicilia	1.18	1.20	1.14	1.16	No data	
Pueblo	1.15	1.19	1.20	1.20	1.18	1.20
Cuba	1.15	1.18	1.23	1.22	1.15	1.16
All measurements	1.17	1.18	1.18	1.18	1.17	1.18
	Pre		OAE2		Post	
	<5 μm	>5 μm	<5 μm	>5 μm	<5 μm	>5 μm
All measurements	1.18	1.19	1.17	1.18	1.16	1.18

Tab. 8.4 *W. barnesiae* ellipticity (l/w) of small-specimens (< 5 μm) and normal-specimens (> 5 μm) in established intervals.

Moreover ellipticity mean values of the pre-OAE 2, OAE 2 interval and post-OAE 2 are given. Very stable ellipticity values were detected for Eastbourne, Clot de Chevalier, in the three intervals in both normal-specimens and small-specimens. In Novara di Sicilia section both normal-specimens and small-specimens displayed a more circular shape (less elliptical) during OAE 2. In the two Western Interior sections, Pueblo and Cuba, small-specimens are more elliptical during interval 4. More circular shapes are detected in the pre and post interval. In cuba section more elliptical *W. barnesiae* are detected in normal-specimens too.

8.4 Coccolithophores algae response to environmental parameters

Only preliminary results of culture experiments on living coccolithophores are presented here. I intend to apply specific statistical analyses in the future and SEM analyses on already prepared filters will be performed in order to measure coccolith size and characterize the ultrastructure. These planned investigations aim at elucidating the environmental parameters (combination of individual) that influence coccolithophore calcification and more specifically coccolith size and morphology.

8.4.1 Light experiment

Emiliania huxleyi

E. huxleyi reached the established cell concentrations in all the light intensity treatments. *E. huxleyi* growth rate is lower with low light intensities, then starts to increase reaching faster growth rate at 450 μmol photons m^{-2} s^{-1} (Fig. 8. 14). From 500 μmol photons m^{-2} s^{-1} growth rate starts to decrease. Coccosphere diameter and cell size are very stable and similar among treatments. Low light intensities show smaller coccosphere and cell diameter. Under 200 μmol photons m^{-2} s^{-1} coccospheres display the bigger diameter and under 130 μmol photons m^{-2} s^{-1} the bigger cell size is detected. Following Muller et al. (2012), and subtracting the acidified-sample spectrum from the non-acidified-spectrum, I obtained the spectrum of the average volume of the free coccoliths. The resulted coccolith volume shows variable values: low light intensities correlate with higher coccolith volumes while middle-range light intensities have halfway coccolith values. Coccolith volume in the 300 μmol photons m^{-2} s^{-1} experiment displays the lowest coccolith volume.

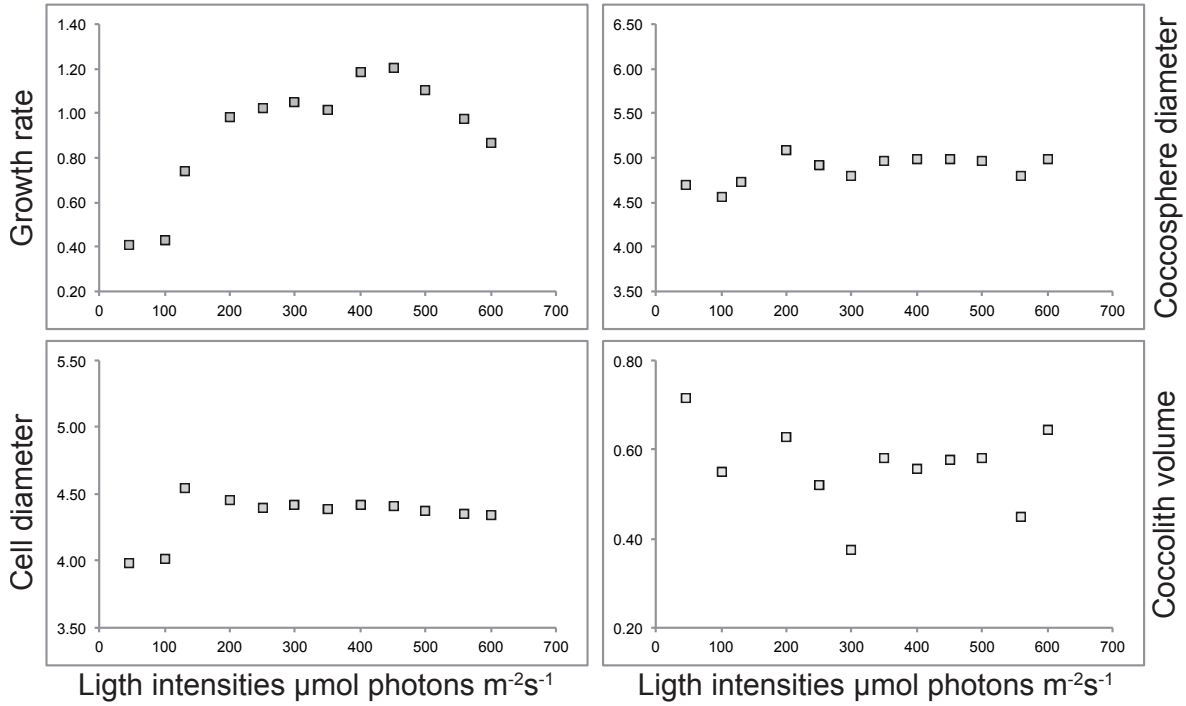

Fig. 8.14 *Emiliania huxleyi* growth rate, coccosphere diameter, cell diameter and coccolith volume over a range of light intensities. Points are data of individual coccolithophore cultures based on coulter counter measurements. Coccolith volume has been calculated following Muller et al. (2012) and subtracting the acidified-sample spectrum from the non-acidified-spectrum.

Gephyrocapsa oceanica

G. oceanica nicely grew in every light intensity treatment, reaching the established cell concentration. Growth rate is very similar among treatments (Fig. 8.15). Data for the 130 µmol photons m^{-2} s^{-1} treatment are not available due to a problem during cell counting measurements. Coccosphere diameters show variable values and low diameters are observed in the high light intensities treatments (500, 560 and 600 µmol photons m^{-2} s^{-1}). Bigger cell diameters are displayed in the 100 µmol photons m^{-2} s^{-1}; smaller cell diameters are observed in the lowest light intensities treatment (45 µmol photons m^{-2} s^{-1}) and in the higher light intensities treatments (from 300 µmol photons m^{-2} s^{-1}). The resulted coccolith volumes show higher values in the 100 and 200 µmol photons m^{-2} s^{-1} treatments. All the other treatments show similar coccolith volume values.

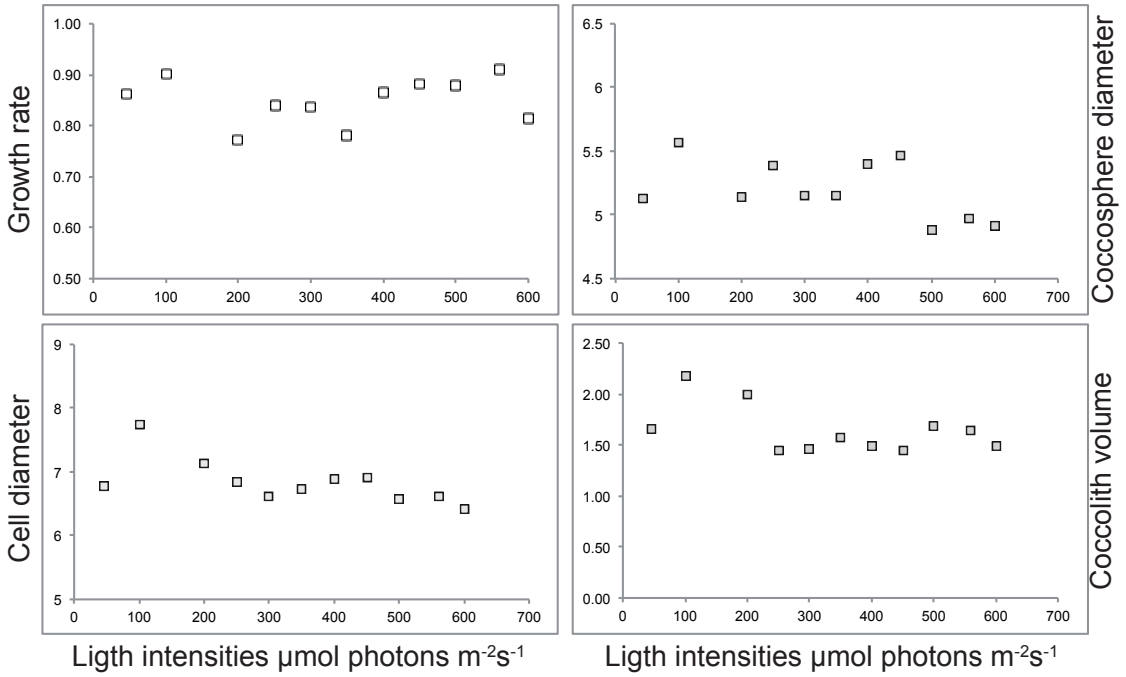

Fig. 8.15 *G.oceanica* growth rate, coccosphere diameter, cell diameter and coccolith volume over a range of light intensities. Points are data of individual coccolithophore cultures based on coulter counter measurements. Coccolith volume has been calculated following Muller et al., 2012 and subtracting the acidified-sample spectrum from the non-acidified-spectrum.

Pleurochrysis carterae

Data for the run at 200 µmol photons m^{-2} s^{-1} are not available due to a problem during cell counting. All treatments show very similar growth rate (Fig. 8.16). Slightly higher values are observed in the 130 and 250 µmol photons m^{-2} s^{-1} treatments. Coccosphere diameter show different values among treatments: the run at 45 µmol photons m^{-2} s^{-1} (lowest light intensities) shows the lowest coccosphere diameters. Halfway diameter values are observed in the runs at 100 and 130 µmol photons m^{-2} s^{-1} and in 450 and 500 µmol photons m^{-2} s^{-1}. The remaining treatments show higher coccosphere diameters. Cell diameter, on the contrary, shows small values in the low light treatments (45, 100, 130 µmol photons m^{-2} s^{-1}) and bigger cell size in the remaining treatments. Coccolith volume resulted in different and variable values.

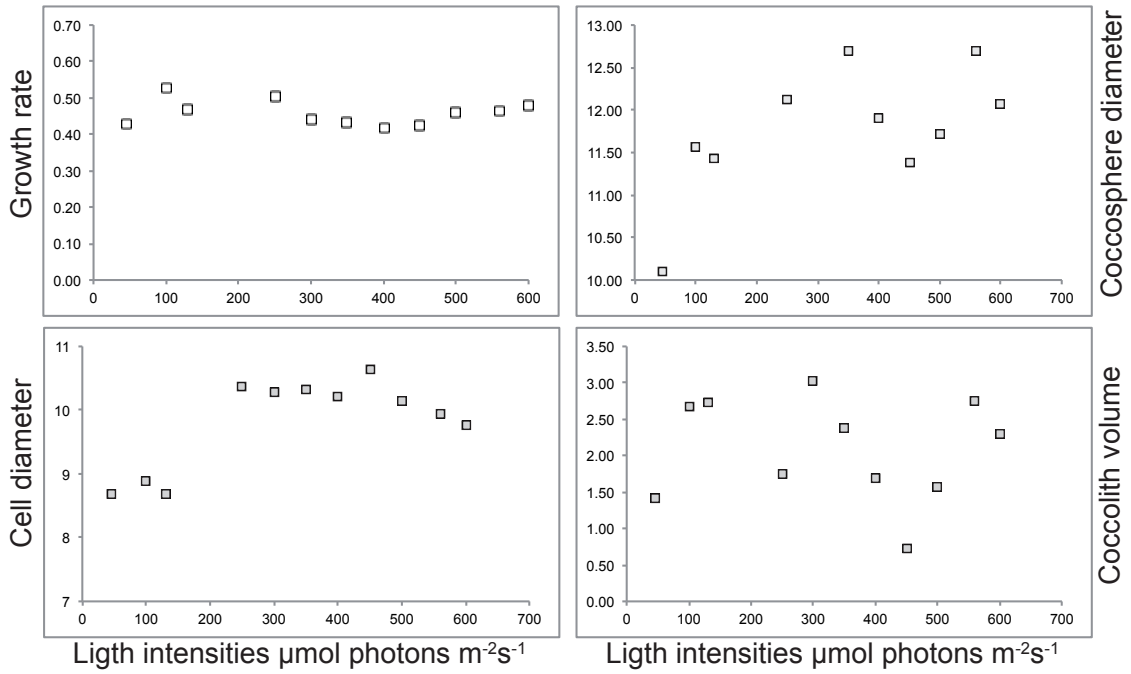

Fig. 8.16 Pleurochrysis *carterae* growth rate, coccosphere diameter, cell diameter and coccolith volume over a range of light intensities. Points are data of individual coccolithophore cultures based on coulter counter measurements. Coccolith volume has been calculated following Muller et al., 2012 and subtracting the acidified-sample spectrum from the non-acidified-spectrum.

Coccolithus pelagicus ssp. *braarudii*

C. pelagicus ssp. *braarudii* grew in every light intensity treatments. Low growth rates are detected in low light intensity conditions, while higher values are recorded in the halfway light intensities (Fig. 8.17). Coccosphere diameters are very stable but three peaks, respectively in the runs with 45, 200 and 450 µmol photons m^{-2} s^{-1}, are obtained. Cell diameters are very similar among light treatments. The coccolith values show a progressive increase in volume from the lowest light intensities (45 µmol photons m^{-2} s^{-1}) reaching maximum values in the 200 µmol photons m^{-2} s^{-1}.

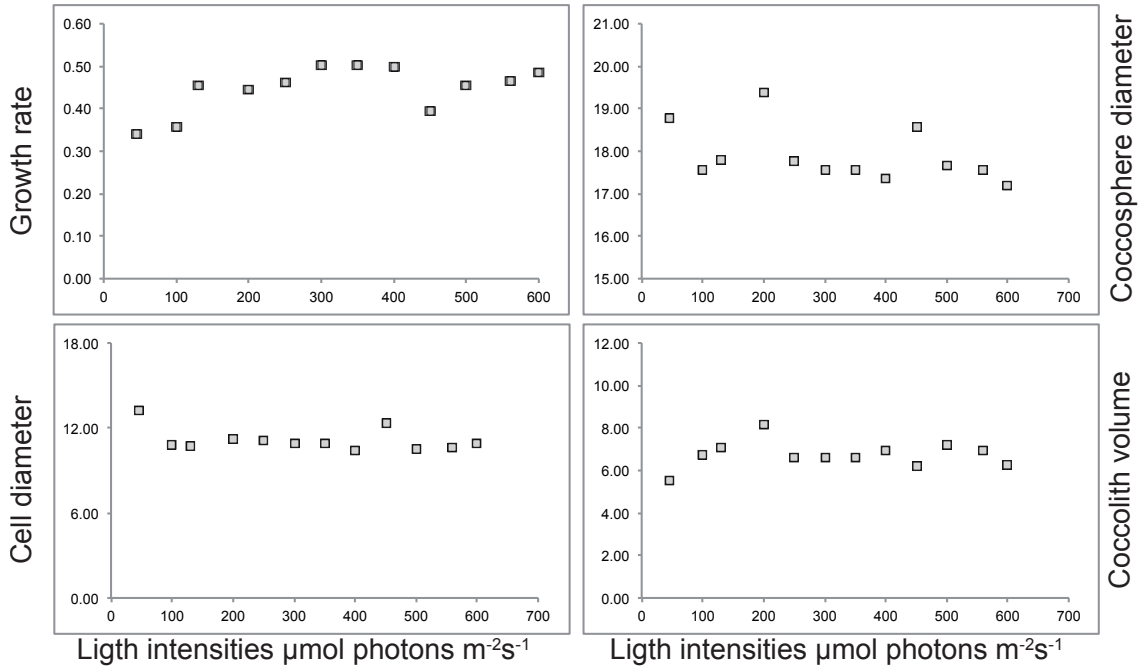

Fig. 8.16 *C. pelagicus* ssp. *braarudii* growth rate, coccosphere diameter, cell diameter and coccolith volume over a range of light intensities. Points are data of individual coccolithophore cultures based on coulter counter measurements. Coccolith volume has been calculated following Muller et al., 2012 and subtracting the acidified-sample spectrum from the non-acidified-spectrum.

8.4.2 Nutrients, carbonate chemistry, [Mg^{2+}] and [Ca^{2+}] and trace metals

Emiliania huxleyi

Cultures in nutrients limited conditions, altered salinity, trace metal enrichments and altered carbonate chemistry reached significant levels of cell concentration (Fig. 8.17 and 8.18), demonstrating the ability of *E. huxleyi* to live under "stressed" environment.

Response of of *E. huxleyi* to carbonate chemistry

In the carbonate experiment, *E. huxleyi* shows different growth rates among treatments even if it reaches a significant cell concentration; the control experiment shows the highest growth rate compare to the other treatments (Fig. 8.17). The "Creta 2" treatment (highest TA and DIC and lowest pH) shows the lowest growth rate values. In second place, the "Creta1" treatment (intermediate TA and DIC) shows high growth rate, while the "OA" (stable DIC, increased DIC and low pH) shows intermediate values. The coccosphere diameter shows a parabolic pattern with higher diameter in the OA treatment

followed by "Creta 1" and subsequently by the control experiment, while the "Creta 2" run shows the lowest diameter values. Cell diameter obtained after HCl acidification shows very similar values with the exception of the OA treatment that evidences higher cell diameter values. This results in coccolith volume with erratic patterns: in the control, "OA" and "Creta1" treatments coccolith volume is very similar even if some differences among replicates are observed within individual treatment. However, the "Creta 2" treatment shows very low coccolith volume in all the replicates.

Response of *E. huxleyi* to [Mg^{2+}] and [Ca^{2+}]

E. huxleyi shows very similar growth rate (cell/d^{-1}) in all the treatments. In the control treatment the growth rate is slightly higher than in the third (Mg/Ca=2) and fourth treatment (Sr x 2). The second treatment that has the highest calcium content (Mg/Ca=1), the growth rate is lower compared to the other experiments (Fig. 8.17). On the contrary *E. huxleyi* coccospheres show bigger diameters in the Mg/Ca=1 experiment. Coccosphere diameter is progressively smaller in Mg/Ca=2 and in Srx2 treatments, while the control treatment shows the smaller diameter. The same pattern is observed for the cell diameter after HCl acidification: the highest values are observed in the Mg/Ca=1 treatment and the lowest in the control treatment. Subtracting the acidified-sample spectrum from the non-acidified-spectrum, the average volume of the free coccolith shows very similar values among all the analyzed treatments.

Response of *E. huxleyi* nutrient limitations

E. huxleyi shows higher growth rates (cell/d^{-1}) in the control treatment compared to the other two runs (Fig. 8.18). In the second (low nitrogen) and third (low phosphate) treatments *E. huxleyi* shows lower concentrations and that results in a lower growth rate. On the other hand, *E. huxleyi* coccosphere is smaller compared to low nitrogen and low phosphate treatments and, specifically, in the "64N:0.1P" treatment *E. huxleyi* reaches the biggest size in all the analyzed replicates. After HCl acidification, cell diameter shows the same pattern with bigger cell in the low phosphate treatment followed by low nitrate treatments. The control treatment shows the smallest cell diameter. Following Muller et al. (2012) and subtracting the acidified-sample spectrum from the non-acidified-spectrum, I obtained the spectrum of the average volume of the free coccoliths. Once again the low-

phosphate treatment shows higher coccolith volume. However, coccolith volume of the control and low-nitrogen treatments appear to be very similar.

Response of *E. huxleyi* to trace metal enrichment

No control treatment was performed in the metal experiment *E. huxleyi* reached significant levels of cell concentration and high growth rates. Specific trends among the three toxic treatments aren't observed (Fig. 8.18). Furthermore coccosphere diameter and cell diameter show very similar and stable values. Therefore the average volume of free coccoliths, obtained after subtracting the acidified-sample spectrum from the non-acidified-spectrum, show very similar values among treatments. It is important to emphasize that in the fourth treatment with highest metal concentration (8000 nmol/l of Pb, $ZnSO_4 \cdot 7H_2O$, $NiCl_2 \cdot 6H_2O$, $VOSO_4$) cells weren't able to survive in the acclimation phase and, therefore, no data are available.

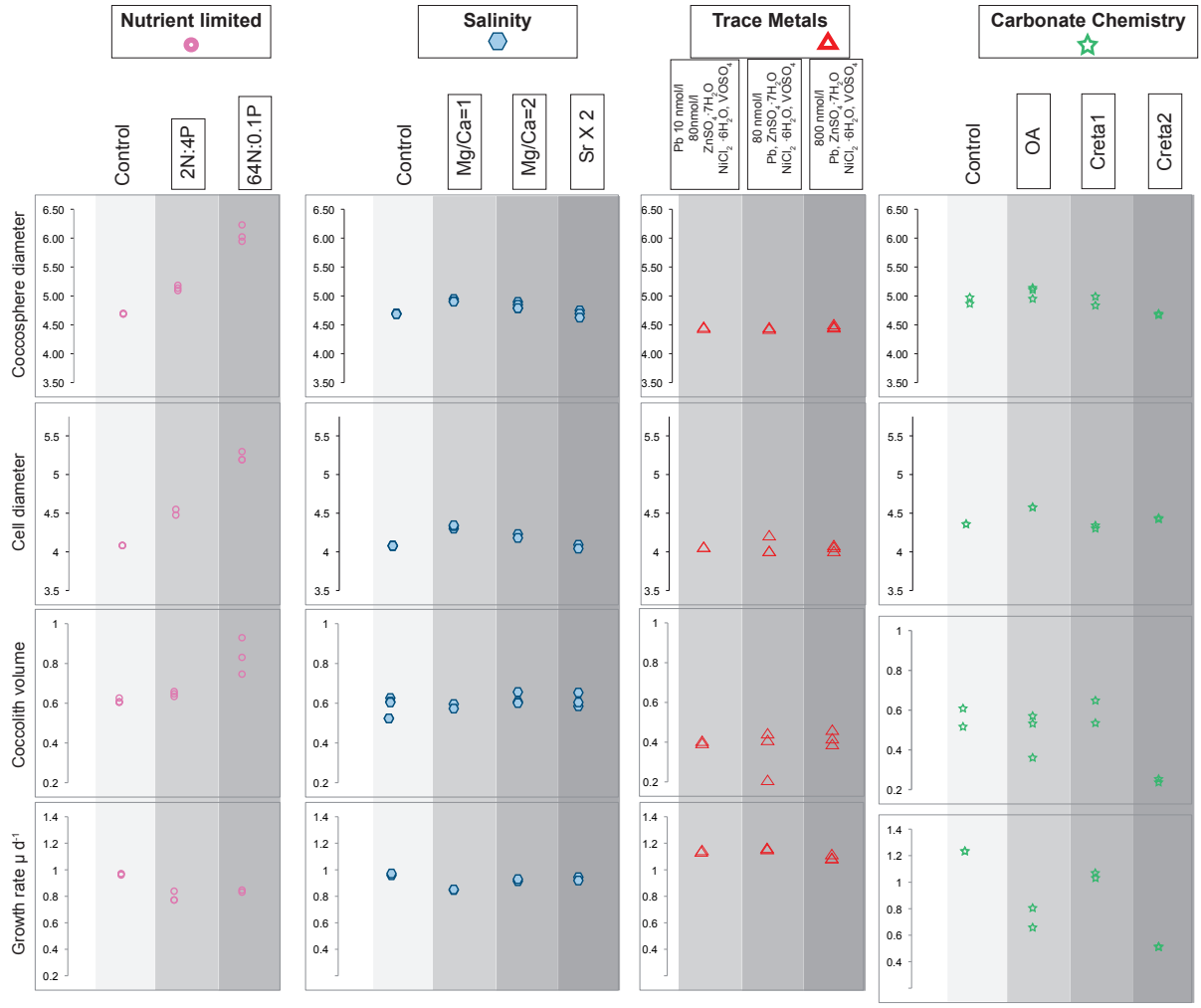

Fig. 8.17 *E. huxleyi* growth rate, coccosphere diameter, cell diameter and coccolith volume in the different experiments. Points are data of individual coccolithophore cultures: every treatment has been performed in replicates. Measurements are based on coulter counter analyses. Coccolith volume has been calculated following Muller et al. (2012) and subtracting the acidified-sample spectrum from the non-acidified-spectrum.

E. huxleyi size response to environmental parameters

E. huxleyi data shows different values among experiments (Fig. 8.18) as summarized below. The growth rate of the control treatments shows different values in different experiments. This might be due to the different time (months) when the experiments were performed (winter time vs summer time). Growth rate of the control data therefore should be compared only among every single experiment. However, for the metal concentration experiment, the comparison could be made with the nutrient data because the runs were performed simultaneously.

1. Growth rate

E. huxleyi shows very high growth rate in the all the treatments of the metal experiment. The "Creta1" (carbonate chemistry) experiment shows high growth rates, while the "Creta 2" experiment shows the lowest values of all treatments. All the other treatments show halfway values.

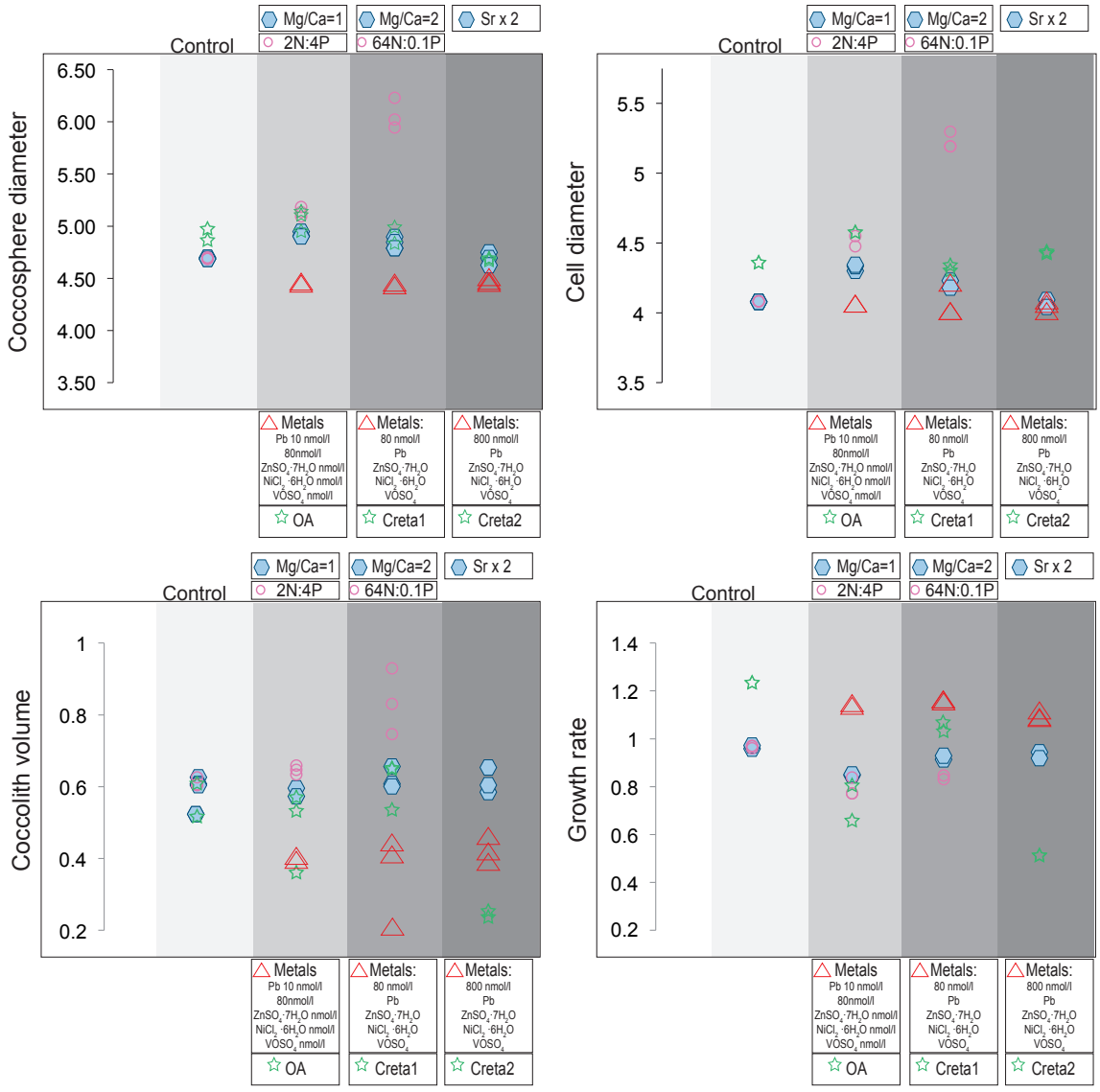

Fig. 8.18 *E. huxleyi* data comparison among different experiments and treatments: coccosphere diameter, cell diameter. coccolith volume and growth rate in the different experiments. Points are data of individual coccolithophore cultures: every treatment has been performed in replicates. Measurements are based on coulter counter analyses. Coccolith volume has been calculated following Muller et al., 2012 and subtracting the acidified-sample spectrum from the non-acidified-spectrum.

2. Coccosphere and cell diameters

The diameter of *E. huxleyi* coccospheres displays lowest values in all the three metal treatments compared to the other experiments. The low-phosphate treatment shows, on the contrary, the highest values in both coccosphere and cell diameters. Cell diameter is very similar for the metal experiment and the control treatment.

3. Coccolith volume

E. huxleyi coccolith volume shows very high values in the low-phosphate treatment. On the contrary, lower values are observed in the metal experiment. The smallest values are recorded in the "Creta 2" (carbonate chemistry) treatment.

Gephyrocapsa oceanica

Cultures in nutrient-limited conditions, altered salinity, trace metal enrichments and altered carbonate chemistry reached significant levels of cell concentrations (Fig. 8.19, Fig. 8.20), demonstrating the ability of *G. oceanica* to adapt to stressed conditions.

Response of *G. oceanica* to carbonate chemistry

G.oceanica in the carbonate experiment shows different growth rates among treatments (Fig. 8.19). Furthermore, in the "OA" and "Creta 2" treatments the experiment was stopped before reaching the established cell concentration (~ 20,000 cell/ml). In this respect it is noted that the growth rate is very low in the "Creta 2" treatment and in "OA" treatment. On the other hand, the control and "Creta"1 treatments show higher and very similar values. The coccosphere diameter shows bigger size in the control treatment and the smallest sizes are recorded in the "Creta 2" treatment. Results of the "OA" and "Creta1" treatments show halfway values. Cell diameter shows very similar values for the control, "OA" and "Creta 1" treatments, while the "Creta 2" run shows a reduction in cell size. Subtracting the acidified-sample-spectrum from the non-acidified-spectrum, coccolith volume has the biggest values in the control treatment compared to all the other experiments. Furthermore, the "Creta 1" treatment shows the highest values followed by "OA" treatment while the "Creta 2" run evidences the smallest coccolith volume.

Response of *G. oceanica* to $[Mg^{2+}]$ and $[Ca^{2+}]$

In the salinity experiment the growth rate is higher in the control treatment compared to all the other experiments. The "Mg/Ca=1" treatment has the lowest growth rate. The

"Mg/Ca=2" and "Sr x 2" experiments resulted in similar growth rates. The coccosphere and cell diameters don't show any specific trend and similar values are observed among

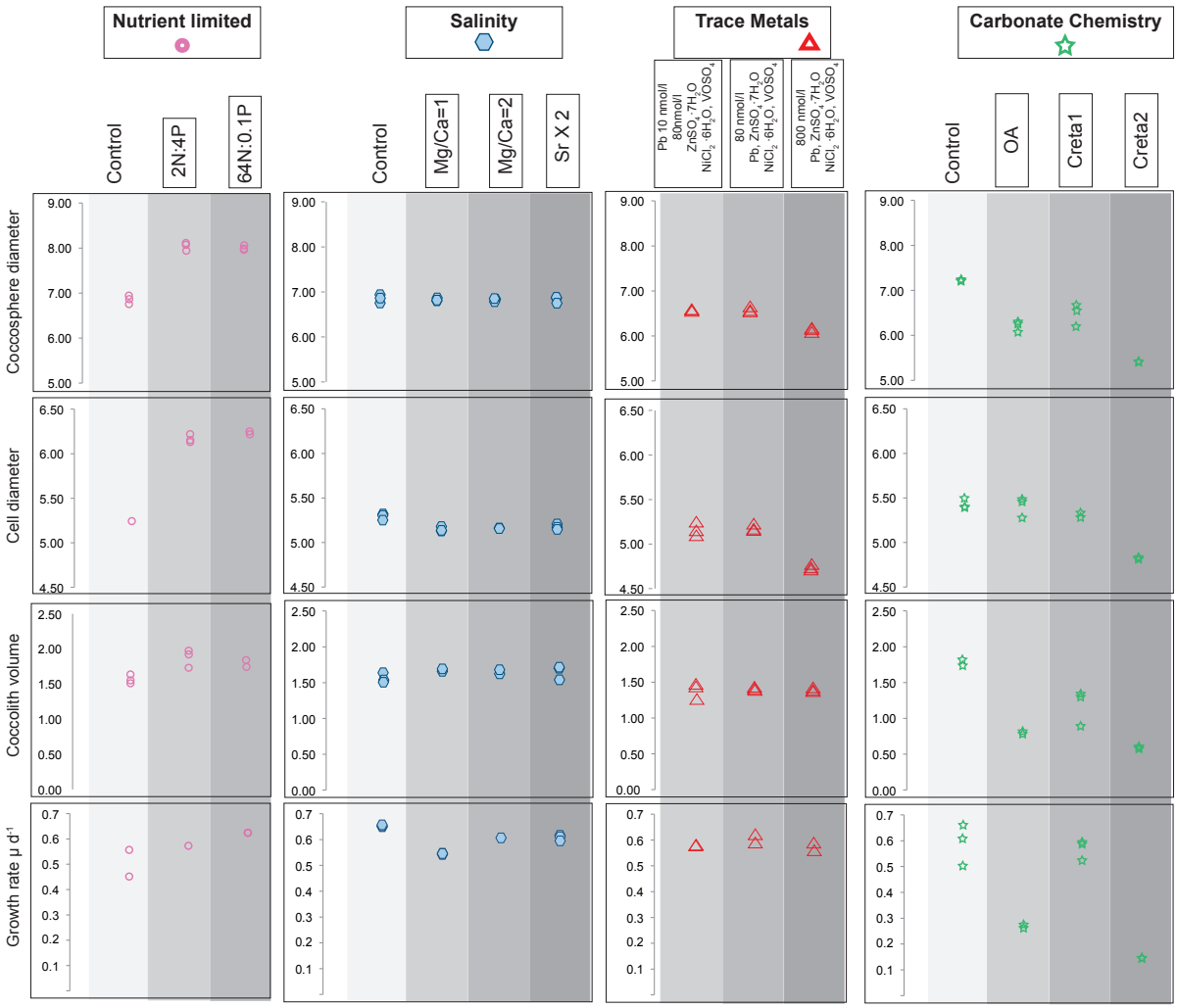

Fig. 8.19 *G. oceanica* growth rate, coccosphere diameter, cell diameter and coccolith volume in the different experiments. Points are data of individual coccolithophore cultures: every treatment has been performed in replicates. Measurements are based on coulter counter analyses. Coccolith volume has been calculated following Muller et al., 2012 and subtracting the acidified-sample spectrum from the non-acidified-spectrum.

treatments. This results in similar values for the coccolith volume for all the experiments (Fig. 8.19).

Response of *G.oceanica* to nutrient limitations

G.oceanica easily adapted to live with reduced nitrate or phosphate levels. This species shows a slightly increase in growth rate (μ) in low-nitrate and low-phosphate treatments compared to the control treatment. Specifically, the higher μ is observed in the low-phosphate treatment. *G.oceanica* coccospheres evidence an increase in size from the control to the low-nitrate and the low-phosphate treatments reaching very similar values.

The same pattern is observed for cell size. Following Muller et al. (2012) and subtracting the acidified-sample spectrum from the non-acidified-spectrum, I obtained the average volumes of the free coccoliths. Coccolith volumes of the low-nitrogen and low – phosphate treatments appear to be very similar with slightly higher values in the former treatment. Coccolith volume shows smaller values in the control treatment (Fig. 8.19).

Response of *G. oceanica* to trace metal enrichment

In the metal experiment any control treatment has been performed. The growth rate is very similar in all the three treatments (Fig. 8.19). The diameter of *G.oceanica* coccospheres is smaller in the last treatment (800 nmol/l of Pb, $ZnSO_4 \cdot 7H_2O$, $NiCl_2 \cdot 6H_2O$, $VOSO_4$). The same pattern is observed for the cell diameter with bigger diameters in the first two treatments (10 nmol/l of Pb and 80 nmol/l of $ZnSO_4 \cdot 7H_2O$, $NiCl_2 \cdot 6H_2O$, VOSO4, and 80 nmol/l of Pb, $ZnSO_4 \cdot 7H_2O$, $NiCl_2 \cdot 6H_2O$, $VOSO_4$). The coccolith volume, on the other hand, doesn't show any variation among treatments. In the fourth treatment with highest metal concentrations (8000 nmol/l of Pb, $ZnSO_4 \cdot 7H_2O$, $NiCl_2 \cdot 6H_2O$, $VOSO_4$) the cells weren't able to survive the acclimation phase and therefore no data are available.

G. oceanica size response to environmental parameters

The control treatment wasn't performed for the metal experiments on *G. oceanica*; comparisons were made with the nutrient data because the experiments were performed simultaneously.

1. Growth rate

   G. oceanica shows similar growth rates in the all the experiments. The "OA" and "Creta 2" treatments evidence the lowest growth rates.

2. Coccosphere and cell diameters

   G. oceanica shows the bigger coccosphere diameter and cell diameter in the low-phosphate and low-nitrate treatments. The carbonate chemistry treatments (OA, Creta1 and Creta 2) show the smallest coccosphere diameter. However, the cell diameter shows very similar values in the salinity, metals and carbonate chemistry treatments, with the exception of the "Creta 2" run that displays the smallest cell size (Fig. 8.20).

3. Coccolith volume

Coccolith volume is bigger in the nitrogen-limited experiment, while the smallest volumes are recorded in the carbonate chemistry experiments (OA, Creta 1, Creta 2) reaching the smallest coccolith volume in the "Creta 2" treatment.

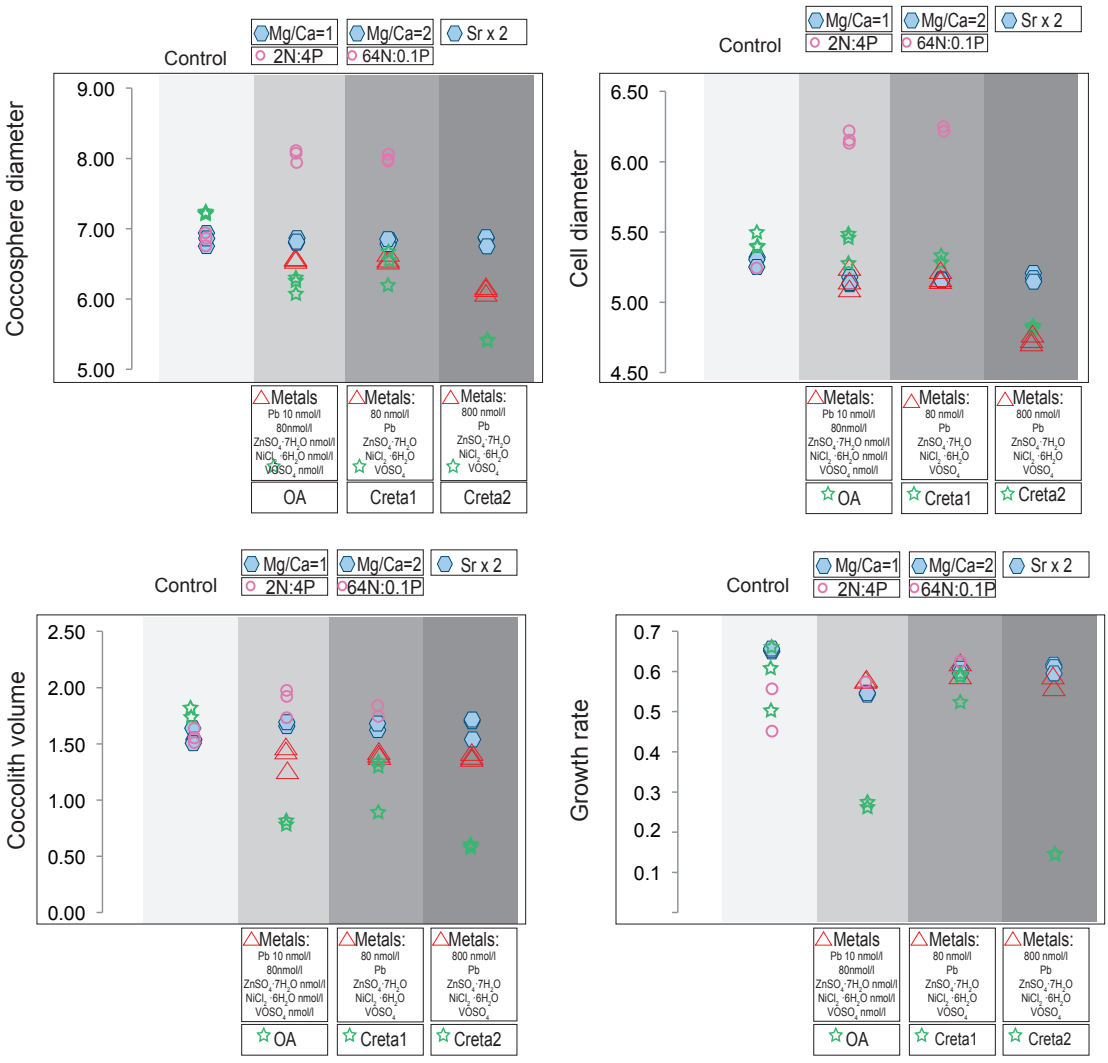

Fig. 8.20 *G. oceanica* data comparison among different experiments and treatments: coccosphere diameter, cell diameter. coccolith volume and growth rate in the different experiments. Points are data of individual coccolithophore cultures: every treatment has been performed in replicates. Measurements are based on coulter counter analyses. Coccolith volume has been calculated following Muller et al. (2012) and subtracting the acidified-sample spectrum from the non-acidified-spectrum.

Pleurochrysis carterae

Cultures in nutrient-limited conditions, altered salinity, trace metal enrichments and altered carbonate chemistry reached significant levels of cell concentrations (Fig. 8.21, Fig. 8.22), demonstrating the ability of *P. carterae* to live under stressful conditions.

Response of *P. carterae* to carbonate chemistry

P. carterae shows very similar growth rates among treatments. Coccosphere diameters, on the contrary, show some differences: the control treatment has the bigger coccosphere diameter, followed by the "Creta 1" treatment. On the contrary, the "OA" and "Creta 2" treatments resulted in the smallest diameters. Cell diameter shows very erratic values among replicates among treatments. Subtracting the acidified-sample-spectrum from the non-acidified-spectrum, the calculated coccolith volumes show bigger values in the "OA" treatment followed by the control treatment. The "Creta 2" treatment exhibits the most reduced coccolith volume.

Response of *P. carterae* to $[Mg^{2+}]$ and $[Ca^{2+}]$

P. carterae has very similar growth rates in all the salinity experiment treatments. However, the "Srx2" treatment growth rate is more erratic and in the three replicates, values are slightly different. The coccosphere diameter exhibits the highest values in the "Mg/Ca=1" treatment followed by the control treatment and subsequently by the "Mg/Ca=2" treatment. The "Srx2" treatment shows the smallest diameter size. However, replicates number 3 has bigger coccosphere diameters compared to the other two replicates. After HCl acidification, cell diameters show a progressive decrease from the control treatment to the "Mg/Ca=1", to "Mg/Ca=2" and "Srx2" treatments. The resulted coccolith volumes show smaller values in the control treatment compared to the other three experiments. However, the "Srx2" run shows very erratic values; the "Mg/Ca=1" and "Mg/Ca=2" evidence very similar values.

Response of *P. carterae* to nutrient limitations

P. carterae was able to adapt and live in nutrient-limited conditions. The growth rate is very similar among all three treatments: control, N-limited and P-limited. Replicate 2 of the control treatment and replicate 1 of the P-limited experiment show lower growth rate

values. The diameter of *P. carterae* coccospheres shows similar values in the control and nitrogen-limited treatments. In the phosphate-limited experiment coccosphere diameter is bigger than in the other experiments. The cell diameter doesn't follow the same pattern: bigger cell diameter is observed in the control treatment. Nitrogen-limited experiment shows smaller size even if replicate 1 shows bigger diameters. The P-limited experiment gave halfway values. Following Muller et al. (2012) and subtracting the acidified-sample spectrum from the non-acidified-spectrum, I obtained the average volumes of the free coccolith. Coccolith volumes of the nitrogen-limited and phosphate-limited treatments are similar and bigger than in the control treatment.

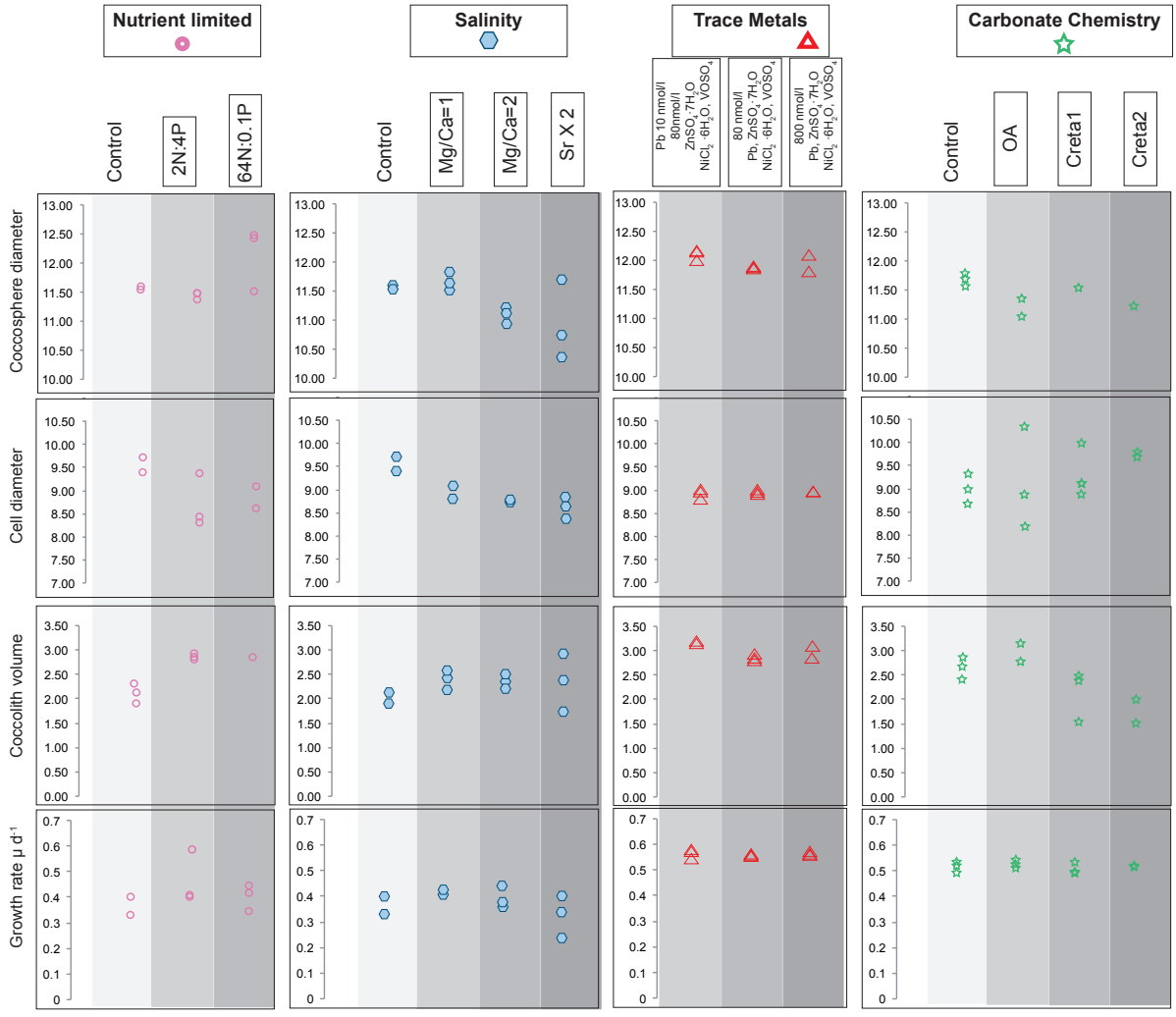

Fig. 8.21 *P. carterae* growth rate, coccosphere diameter, cell diameter and coccolith volume in the different experiments. Points are data of individual coccolithophore cultures: every treatment has been performed in replicates. Measurements are based on coulter counter analyses. Coccolith volume has been calculated following Muller et al. (2012) and subtracting the acidified-sample spectrum from the non-acidified-spectrum.

Response of *P. carterae* to trace metal enrichment

In the metal experiment any control treatment was performed. In the fourth treatment, with highest metal concentrations (8000 nmol/l of Pb, $ZnSO_4 \cdot 7H_2O$, $NiCl_2 \cdot 6H_2O$, $VOSO_4$), *P. carterae* cells weren't able to survive the acclimation phase and, therefore, no data are available. However, *P. carterae* easily adapt to live in the other three treatments (10 nmol/l of Pb and 80 $ZnSO_4 \cdot 7H_2O$, $NiCl_2 \cdot 6H_2O$, $VOSO_4$, 80 $ZnSO_4 \cdot 7H_2O$, $NiCl_2 \cdot 6H_2O$, $VOSO_4$ and 800 $ZnSO_4 \cdot 7H_2O$, $NiCl_2 \cdot 6H_2O$, $VOSO_4$). *P. carterae* showed very similar growth rates in all three treatments reaching the established cell concentration. The coccosphere diameter is very similar among the three treatments, although a slightly decrease in size is observed in second and third treatments. The cell diameter is similar in the three treatments. The obtained coccolith volumes show very similar values among treatments even if a small reduction in size in the second (80 $ZnSO_4 \cdot 7H_2O$, $NiCl_2 \cdot 6H_2O$, $VOSO_4$) and third (800 $ZnSO_4 \cdot 7H_2O$, $NiCl_2 \cdot 6H_2O$, $VOSO_4$) treatments was observed.

P. carterae size response to environmental parameters

The control treatment wasn't performed for the metal experiments on *P. carterae*; comparisons were made with the nutrient data because the experiments were performed simultaneously.

1. Growth rate

   Metal and carbonate chemistry experiments show the higher growth rates Nutrient and salinity treatments have very similar and slower growth rates. The "Sr x 2" treatment of the salinity experiment has the slowest growth rate even if values among treatments are erratic.

2. Coccosphere and cell diameter

   The bigger coccosphere diameter is recorded in the phosphate-limited treatment of the nutrient experiment. Metal treatments, however, show relatively high diameter values. The salinity "SrX2" treatment shows the smallest coccosphere diameters. However, in the "Mg/Ca=2" treatment *P. carterae* has small sizes, too. The cell diameter doesn't show the same patterns: cell diameter mostly lies in the same size range. The "Creta 1" and "Creta 2" treatments of the carbonate chemistry experiment resulted in bigger cell sizes. Replicates 2 and 3 of the nitrogen-limited

treatment of the nutrient experiment and replicate 3 of the OA treatment of the carbonate chemistry experiment show the smaller cell diameters (Fig. 8.22).

3. Coccolith volume The smaller coccolith volume is recorded in the "Srx2" treatment of the salinity experiment. However, replicate 1 of the "Creta 1" treatment and replicate 1 of the "Creta 2" treatment (carbonate chemistry experiment) show reduced coccolith volumes, too.

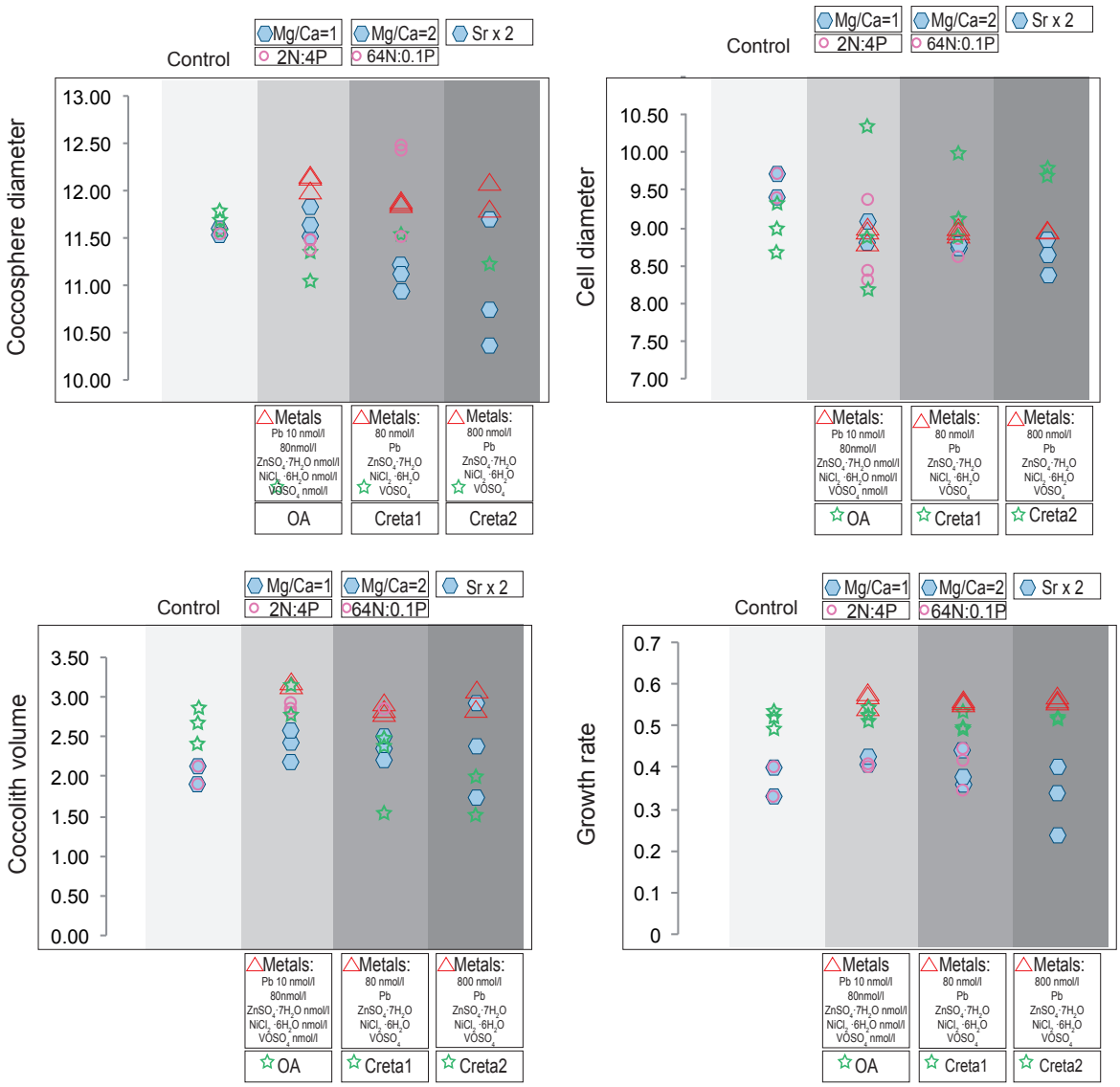

Fig. 8.23 *P. carterae* data comparison among different experiments and treatments: coccosphere diameter, cell diameter. coccolith volume and growth rate in the different experiments. Points are data of individual coccolithophore cultures: every treatment has been performed in replicates. Measurements are based on coulter counter analyses. Coccolith volume has been calculated following Muller et al. (2012) and subtracting the acidified-sample spectrum from the non-acidified-spectrum.

Coccolithus pelagicus ssp. *braarudii*

Cultures in nutrient-limited conditions, altered salinity, trace metal enrichments and altered carbonate chemistry reached significant levels of cell concentration (Fig. 8.23, fig. 8.24), demonstrating that *C. pelagicus* ssp. *braarudii* can live under stressful conditions.

Response of *Coccolithus pelagicus* ssp. *braarudii* to carbonate chemistry

C. pelagicus ssp. *braarudii* shows very different response in the various treatments. The control treatment shows the highest growth rate. The "OA" and "Creta 1" treatments display similar growth rates, while the "Creta 2" treatment has the smallest growth rate. However, every treatment has reached the established cell concentration. The control treatment shows the highest coccosphere diameter. The smaller size is observed in the "Creta 2" treatment even if replicates have different mean values. The "OA" and "Creta 1" treatments gave similar values. The cell diameter shows bigger values in the control treatment while the "OA", "Creta 1" and "Creta 2" treatments show a progressive increase in size trends. Coccolith volume shows different mean values among replicates and among treatments. However, higher values are observed in the "OA" treatment followed by the "Creta 1" treatment. Both the "Creta 2" and the control treatments show the smallest volume values.

Response of *Coccolithus pelagicus* ssp. *braarudii* to [Mg^{2+}] and [Ca^{2+}]

C. pelagicus ssp. *braarudii* shows a progressive decrease in growth rates from the control treatment to the "Mg/Ca=1" and "Mg/Ca=2" reaching minimum values in the "Srx2" treatment. The mean coccosphere diameter is similar in the control, "Mg/Ca=2" and "Srx2" treatments, while the "Mg/Ca=1" treatment resulted in smaller values. The cell diameter shows the biggest size in the control treatment, while the "Mg/Ca=1" treatment evidences the smallest sizes. The coccolith volumes are smaller in the control treatment compared to the other 3 experiments. After the "Mg/Ca=1", "Mg/Ca=2" and "Srx2" treatments the coccolith volumes are very similar values.

Response of *Coccolithus pelagicus* ssp. *braarudii* to nutrient limitations

C. pelagicus growth rate is higher in the control treatment compared to the nitrogen-limited and phosphate-limited conditions. N-limited and P-limited treatments show

similar growth rate values. The coccosphere diameter is higher in the control treatment compared to the other two treatments. The P-limited resulted in slightly larger coccosphere diameters compared to the N-limited conditions. On the other hand, cell diameter is much bigger in the control treatment compared to nutrient-limited treatments: P-limited treatment shows the smallest cell diameters. Following Muller et al. (2012) and subtracting the acidified-sample spectrum from the non-acidified-spectrum, I obtained the average volumes of the free coccoliths. Contrarily to the coccosphere and cell diameters, the coccolith volume shows the highest values in the P-limited treatment followed by the N-limited treatment. The control treatment shows smallest values for coccolith volumes.

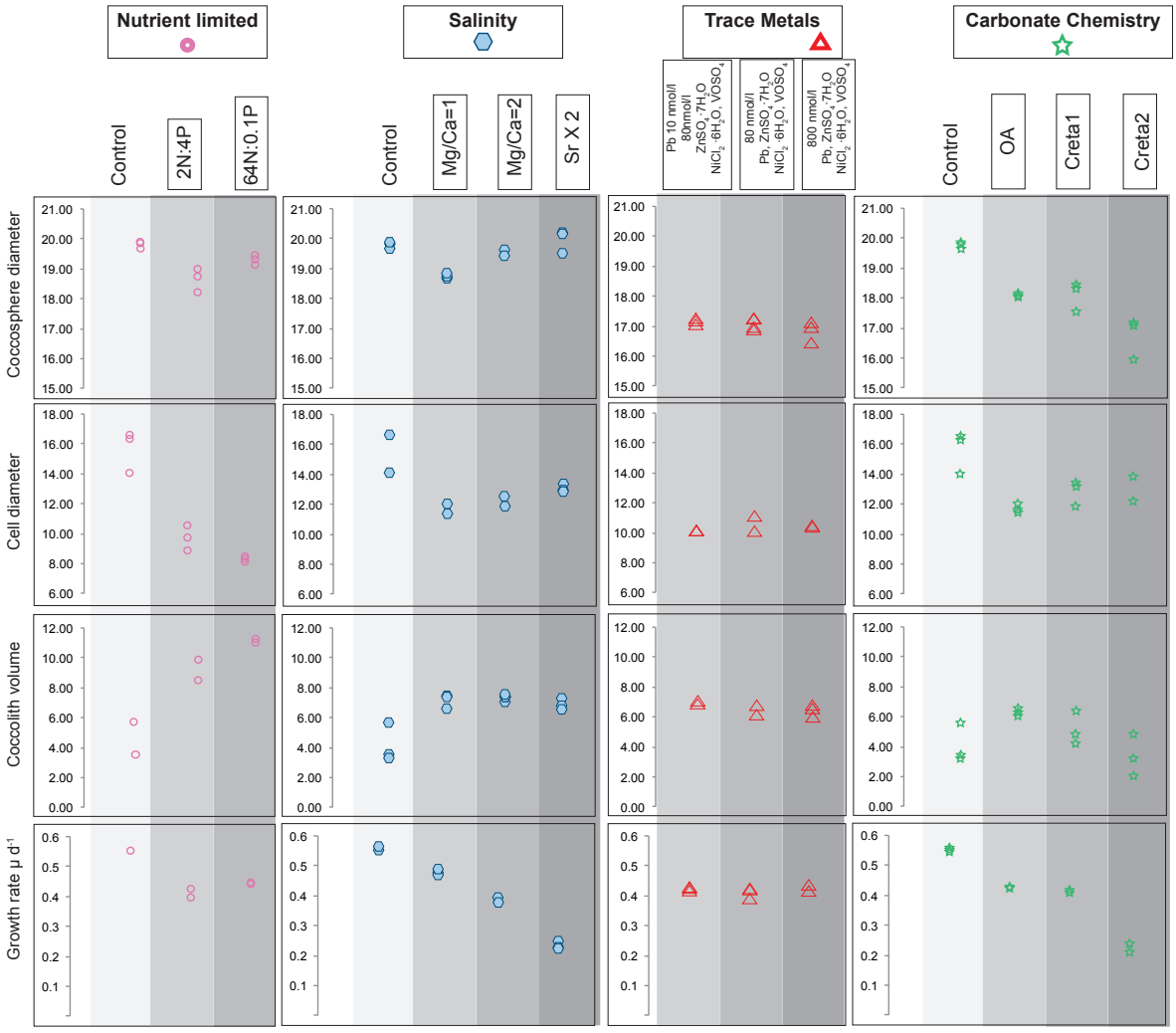

Fig. 8.23 *C. pelagicus* ssp. *braarudii* growth rate, coccosphere diameter, cell diameter and coccolith volume in the different experiments. Points are data of individual coccolithophore cultures: every treatment has been performed in replicates. Measurements are based on coulter counter analyses. Coccolith volume has been calculated following Muller et al. (2012) and subtracting the acidified-sample spectrum from the non-acidified-spectrum.

Response of *Coccolithus pelagicus* ssp. *braarudii* to trace metal enrichment

In the metal experiment no control treatment was performed. In the fourth treatment, with highest metal concentrations (8000 nmol/l of Pb, $ZnSO_4 \cdot 7H_2O$, $NiCl_2 \cdot 6H_2O$, $VOSO_4$), *C. pelagicus* ssp. *braarudii* cells weren't able to survive the acclimation phase and therefore no data are available. The growth rate is very similar among the three treatments. Furthermore, the coccosphere and cell diameters are very stable and similar among the three treatments (10 nmol/l of Pb and 80 $ZnSO_4 \cdot 7H_2O$, $NiCl_2 \cdot 6H_2O$, $VOSO_4$, 80 $ZnSO_4 \cdot 7H_2O$, $NiCl_2 \cdot 6H_2O$, $VOSO_4$ and 800 $ZnSO_4 \cdot 7H_2O$, $NiCl_2 \cdot 6H_2O$, $VOSO_4$). This resulted in very similar coccolith volumes among the three treatments.

Coccolithus pelagicus ssp. *braarudii* size response to environmental parameters

The control treatment wasn't performed for the metal experiment on *C. pelagicus* ssp. *braarudii*; comparisons were made with the nutrient data because the experiments were performed simultaneously.

1. Growth rate

   The control treatments show the highest growth rates. The "Creta 2" treatment of the carbonate chemistry experiment and "Srx2" of the salinity experiment show the slowest growth rates.

2. Coccosphere and cell size

   Metal treatments show the smallest diameters compared to the other experiments. The "Creta 2" treatment (carbonate chemistry experiment) shows smaller sizes, too. Bigger sizes are reached in the "Srx2" treatment of the salinity experiment. Cell size, however, shows different size amplitude: bigger sizes are reached in the control treatment, while smallest diameters are observed in the phosphate-limited treatment of the nutrient experiment.

3. Coccolith volume

Most treatments appear to be beneficial to coccolith volumes: in fact smaller coccolith volume is reached in the control experiment. The lowest values, however, are reached in the "Creta 2" treatment of the carbonate chemistry experiment. Bigger volumes are observed in the nutrient-limited treatment and in the P-limited treatment the highest coccolith volume values were reached.

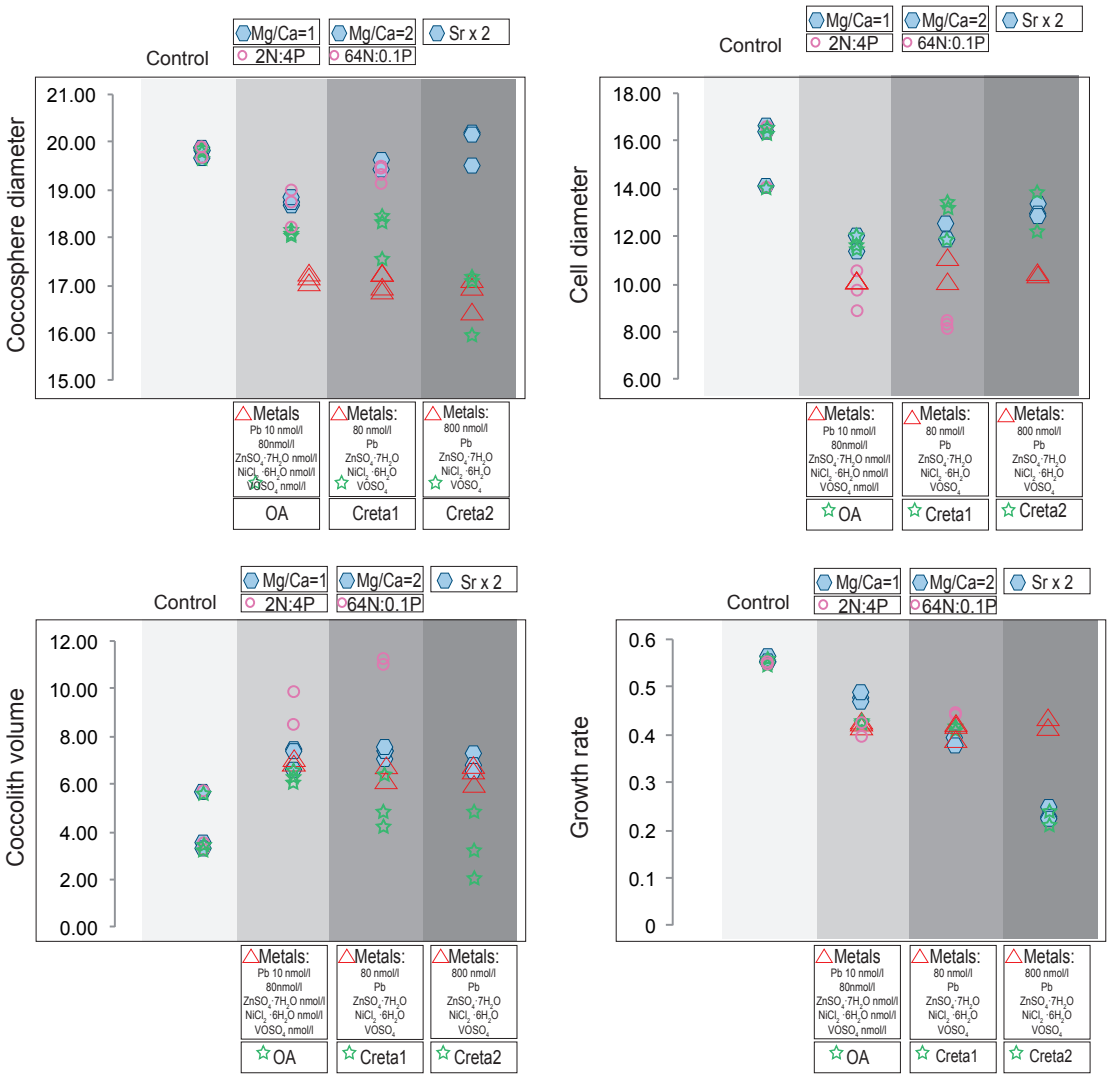

Fig. 8.24 *C. pelagicus* ssp. *braarudii* data comparison among different experiments and treatments: coccosphere diameter, cell diameter. coccolith volume and growth rate in the different experiments. Points are data of individual coccolithophore cultures: every treatment has been performed in replicates. Measurements are based on coulter counter analyses. Coccolith volume has been calculated following Muller et al. (2012) and subtracting the acidified-sample spectrum from the non-acidified-spectrum.

Chapter 9

Discussion

9.1 Size analyses of the coccolith species *B. constans* during OAE 2

B. constans shows a consistent decrease in size during OAE 2. *B. constans* size variations during OAE 2 have been compared to OAE 1a data (Erba et al., 2010; Bottini, unpublished PhD thesis). Furthermore previously published data from Bornemann and Mutterlose (2006) who analyzed *B. constans* size variations during OAE 1d have been taken in account. Ranges of length of *B. constans* coccoliths in OAE 1a, OAE 1d and OAE2 are:

1. in OAE 1a length ranges from: 7.30 to 2.07 μm; mean length 4.63 μm;
2. in OAE 1d length ranges from: 5.85 to 1.58 μm; mean length 3.43 μm;
3. in OAE 2 length range from 6.62 to 1.40 μm; mean length 3.27 μm.

The analyses obtained in this thesis are therefore consistent with literature data. The holotype of *Biscutum testudinarium*, considered to be synonymous to both *B. constans* (Perch-Nielsen, 1968; Bukry, 1969) and *B. ellipticum* (Grün and Allemann, 1975), has a length of 3.7 μ m according to Black in Black and Barnes (1959). Bukry (1969) documented a maximum length of 6.6 μ m for *B. testudinarium*. For *B. ellipticum*, Górka (1957) documented a maximum dimension of 7 μ m, and Grün and Allemann(1975) observed length measurements between 2 and 10 μ m. Subsequent revisions subdivided the two species depending on the number of distal elements. Separation of different morphotypes based on morphometric analyses is rather problematic and permits a wide range of interpretations depending upon authorship. Therefore, in this study I preferred to maintain one species attribution and consider size variations as related to intraspecific variability of ephemeral morphotypes influenced by paleoenvironmental stress or stability.

During OAE 1a and OAE 2 *B. constans* shows a strong decrease in size. In OAE 1a, in the pre-event interval, coccoliths have holotypic values and their dimensions decrease of about 20% in the event. The available data for the post-event interval suggest a recovery in size although without reaching the pre-event values. I notice that the strongest decrease in size is measured at DSDP Site 463 where coccoliths, during OAE 1a, are even smaller than in the Cismon section. This suggests that the same paleoenvironmental factors control coccolith size during OAE 1a, however the response to the paleoenvironmental perturbation was expressed with different amplitude in the Pacific Ocean and in the Thethys. Bornemann and Mutterlose (2006) highlight a reduction in size in "Niveau Breistroffer" black shales representing the late Albian OAE 1d. In the analyzed France section smaller sizes are observed during the event and specifically after the second black shale. Also, the Authors evidence short-term size fluctuations, which however don't parallel any lithological variation. During OAE 2 a decrease in size of *B. constans* coccoliths is observed followed by a partial recovery in size at the end of the event. Size reduction is less expressed in OAE 2 compared to OAE 1a: coccoliths show a general reduction of about 10% from the pre-event values, but *B. constans* size in the pre-event interval is already smaller than the holotype.

A latitudinal decrease in size is evident in our dataset for the pre-OAE 2 and OAE 2 interval (in the post-OAE2, no data are available for Novara di Sicilia): with larger *B. constans* coccoliths at Eastbourne and Clot de Chevalier and smaller specimens at Novara di Sicilia The two sections located at intermediate paleolatitudes in the WIS display in-between values. This suggests that coccoliths size variations are controlled by regional/local conditions.

Studies on modern and culture coccolithophores assemblages highlight the impact of trophic and temperature of surface waters (Zondervan, 2007; Muller et al., 2013; Sett et al., 2014) on coccolith morphology. Coccolith calcification might be therefore controlled by paleoenvironmental factors. Mattioli et al. (2004) suggest that coccolith size of different Biscutaceae species during the Pliensbachian-Toarcian was related to higher trophic and/or very high surface-water paleotemperature. Bornemann and Mutterlose (2006) observe a parallel long-term trend of *B. constans* size and surface water temperature suggesting that forms consisting of a large central unit were formed during intervals with warmer surface water, as indicated by the nannofossil temperature index

(TI) and oxygen isotopes. They suggest that the trend towards smaller coccoliths is related to a cooler interval. Contrarily, a correlation between coccolith size and water trophic conditions is excluded.

OAEs are characterized by extreme environmental conditions and specifically very high CO_2 concentration and an abrupt increase in SST that set in train an accelerated hydrological cycle.

B. constans size might have been influenced by the nutrient content: in tropical oceanic settings (e.g. ODP Site 1258, Demerara Rise) increase in TOC up to 20-35 % (Kolonic et al., 2005), evidence an intense surface productivity in the area that resulted in anoxia and carbon sequestration. On the other hand, the more boreal sites, like mid-latitude shallow shelf, epicontinental settings in WIS or Europe where characterized by an interval of more oligotrophic and probably less anoxic conditions during OAE 2, returning to more mesotrophic conditions in the early Turonian. Particularly, in the WIS, Tethyan influx of saline and dense water from the south, and contemporary incursion of lighter and freshened Boreal water mass due to a rise in sea level, might have resulted in strong ocean stratification (Corbett and Watkins, 2013). This might have prevented mixing of nutrient with surface waters and subsequently established oligotrophic conditions. However, the Cuba section appears to be an exception because nannofossil abundances and dinoflagellates cysts data, suggest periodic mixing through the event that may have sustained continued eutrophic conditions along the shallower western margins of the seaway through OAE 2 (Corbett and Watkins, 2013). Linnert and Mutterlose (2012), highlight a reduction in size of *Biscutum* specimens that is positively correlated with the nannofossil nutrient index in the Eastbourne section and hypothesized therefore, that large *Biscutum* coccoliths may have favored higher nutrient availability. This is not consistent with size variations observed in this thesis. Particularly, in Eastbourne, Clot de Chevalier and Pueblo sections characterized by intervals of oligotrophic conditions, *B. constans* coccoliths are generally larger than at Novara di Sicilia where mesotrophic conditions marked the latest Cenomanian interval. In the Cuba section, where constant eutrophic conditions continue through the event (Corbett and Watkins, 2013), coccoliths show already smaller size in the pre-OAE2 interval but a minor reduction in size is observed within OAE 2. Similarly, Novara di Sicilia black shales have a southern provenance and is considered to be derived from a depositional ramp located on the North of African

continental shelf. This succession was probably characterized by an upwelling regime and high surface productivity under meso/eutrophic conditions. Here, *B. constans* shows the minimum size compared to the other analyzed sections and a less intense size reduction is recorded. I hypothesize that the smaller mean size of *B. constans* specimens observed in the Cuba and Novara di Sicilia sections, are the result of an accelerated life cycle due to high nutrient availability with secretion of smaller coccoliths.

The shift in temperature during OAEs may have affected the size of *B. constans*; OAE 2 onset coincided with a rapid shift towards a very warm regime at both high and low latitudes. It is plausible therefore, that species with cooler-water preferences might have reacted with a reduction of their mean size. However, during OAE 2, SST fluctuations are recorded at different latitudes: intermitted cooling events are seen in the latest Cenomanian in tropical records (cooling of about 4°C) (Forster et al., 2007) and a coeval southward migration of boreal faunal elements to mid latitudes is registered (Gale and Christensen, 1996; Jarvis et al., 2011). *B. constans* was globally common in the latest Cenomanian, from high to middle and tropical latitudes (Erba, 2004; Hardas and Mutterlose, 2006, 2007; Linnert et al., 2010, 2011). The low abundance interval of *B. constans* (Linnert et al., 2010; Linnert et al., 2011) detected in the Boreal realm during OAE 2, postdates the "Plenus Cold Event" and is coeval with a trend towards higher SST. It doesn't seem, therefore, that *B. constans* size was affected by surface-water temperature.

During OAE 1a proxy data suggest that large quantities of CO_2 was emitted in subsequent volcanic pulses, reaching a concentration of about 1000/2000 ppm. During OAE2 an increase up to 600 ppm CO_2 has been stated, reaching values of about 900-1000 ppm (Barclay et al., 2010). It is plausible therefore that the occurrence of dwarf coccoliths is the response to a pressure of CO_2 (pCO_2) above threshold values: decrease in size correlate with high CO_2 concentration hence if calcification is a strategy to reduce the energy cost of photosynthesis, living in a high-concentration world, made calcification less necessary.

Submarine volcanism possibly introduced high concentrations of biolimiting metals (Erba, 2004): trace metals peak have been detected in the Pueblo section (Snow et al., 2005) and Novara di Sicilia (Duncan et al., 2013). Some living nannoplankton species

appear to be sensitive to high trace metal concentration (Brand, 1994; Hoffmann et al., 2012). Therefore it can't be ruled out that *B. constans* suffered the introduction of large quantities of toxic metals via hydrothermal plumes during OAEs and reacted with a reduction in size and/or reduction in calcification rate. For further details, the reader should consider Appendix II.

9.2 Calcareous nannofossil response to extreme environmental condition during OAE 2

Morphometric analyses of calcareous nannofossil reconstructed in the five analyzed sections, Eastbourne, Clot del Chevalier, Novara di Sicilia, Pueblo and Cuba, show similar variations and patterns. The major change in calcareous nannofossil size corresponds to the time interval around the second $\delta^{13}C$ isotopic peak, named peak B, when dwarf coccoliths of the analyzed species are dominant.

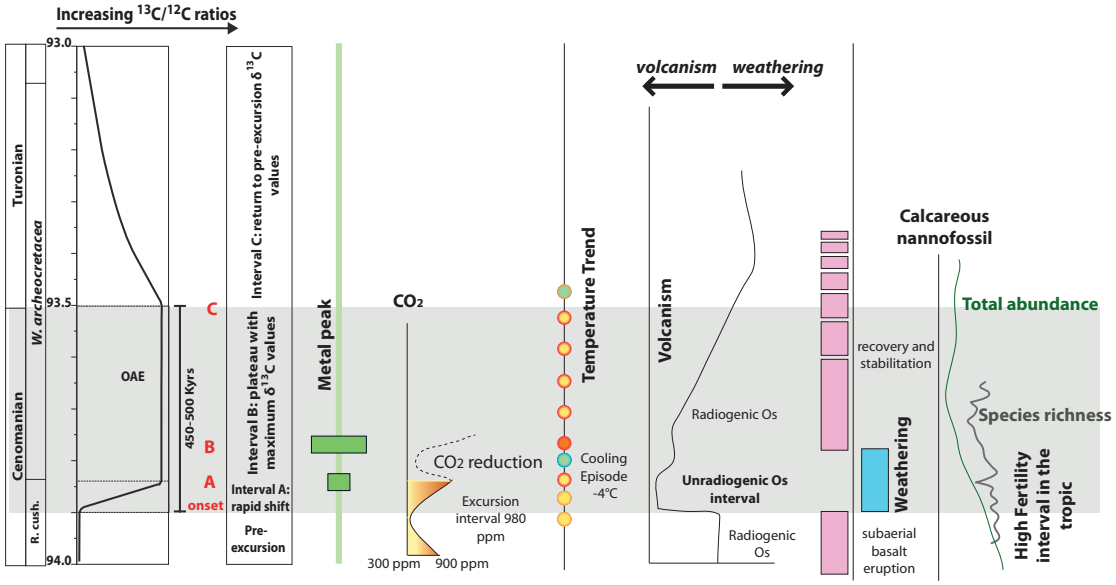

Fig. 9.1 Synthesis of major biotic and geological events in the Late Cenomanian– Turonian interval. $^{13}C/^{12}C$ from Kuypers et al., 1999; Metal peaks from Snow et al., 2005; CO_2 from Barclay et al., 2010; Temperature trend from Forster et al., 2007; Osmium data from Turgeon and Creaser 2008 and Du Vivier et al., 2014; Ca data from Blättler et al., 2011; Li data from Pogge Von Strandmann et al., 2013; calcareous nannofossil data from Erba et al., 2004.

OAE 2 was characterized by extreme environmental conditions that lasted around 450-500 kyrs. It is hypothesized that OAE 2 is related to the formation of large igneous provinces (LIPs) and specifically to the formation of the Caribbean plateau traps. Intense submarine volcanic activity would have increased oceanic and atmospheric CO_2 and set in train a numbers of consequences (e.g. increase SST, accelerated hydrological cycle...). As summarized in figure 9.1, volcanic activity was influencing atmospheric pCO_2 levels before the OAE 2 onset (Barclay et al., 2010): an increase in atmospheric CO_2 from about 60 ppm to 300 ppm has been reconstructed and suggests that a massive magmatic episode occur up to 500 kyrs in advance of the positive C-isotopic excursion that described and defined OAE 2. Furthermore lithium and osmium isotopic signature move towards less radiogenic values around 23-30 kyrs before OAE 2 onset and are interpreted as a switch towards a mantle source of these elements before OAE. This major magmatic pulse released up to 7-12 x 10^4 Gt of CO_2 (Kuroda et al., 2007) and triggered an increase in SST globally recorded. An intensification of the hydrological cycle is also expected (Blättler et al. 2011; Pogge von Stradmann et al., 2013) with a consequent increased in the basaltic weathering rate and intensities in both subaerial and marine real. Pogge von Stradmann et al. 2013, reconstructed that almost a third of the CO_2 emitted was balanced by silicate weathering by the end of OAE2 and highlight that a weathering peak occur ~ 200/300 kyrs after the volcanism onset. This well fixed with the temperature fluctuations: a cooling trend is observed between the first $\delta^{13}C$ isotopic peak, named peak A, and the second $\delta^{13}C$ isotopic peak, named peak B (Forster et al., 2007; Pearce et al., 2009). However Turonian temperature reconstructions suggest peak warmth and indicate that the cooling trend, owing to CO_2 decrease, was only transient. A new and more intense increase in SST temperature indeed nicely correlate with the $\delta^{13}C$ isotopic peak B that occur slightly after (Forster et al.2007): no direct CO_2 reconstruction are available but major, minor and trace metal analyses highlight a strong peak suggesting an increase of the submarine volcanic activity (Snow et al., 2005). A progressive reduction of the volcanic activity and at the same time a decline of the strength of continental weathering suggest a gradual recovery of the oceanic-atmospheric system reaching pre-eruption levels is ~ 100 kyrs after $\delta^{13}C$ isotopic peak B.

Calcareous nannofossil data were compared with C isotope data (Tsikos et al., 2004; Bowman and Bralower, 2005, Snow et al., 2005; Scopelliti et al., 2008; Gale et al., in prep). Morphometric analyses performed on *B. constans, Z. erectus* and *D. rotatorius* revealed the existence of "dwarf" coccoliths with evident reduced sizes with respect to the holotype value. In all the five analyzed sections *B. constans* shows the most expressed size fluctuations through the event. *D. rotatorius* shows a well express reduction in size while *Z. erectus* displays the less express size fluctuations. In Eastbourne section size fluctuations through the event are better expressed compared to the other sections, however in all the other sections similar size trends are observed. Specifically from the OAE 2 onset an increase in size trend leads to the maximum size increase around the first $\delta^{13}C$ isotopic peak (peak A). Subsequently *B. constans, Z. erectus* and *D. rotatorius* show a progressive decrease in the mean size, reaching the maximum size reduction at $\delta^{13}C$ isotopic peak B. Smaller specimens are still present till the end of the event and only after $\delta^{13}C$ isotopic peak C and in the upper part of the analyzed sections a partial recovery in size is observed. *W. barnesiae* doesn't show significant changes in mean size furthermore any morphological variation (e.g. ellipticity) has been observed.

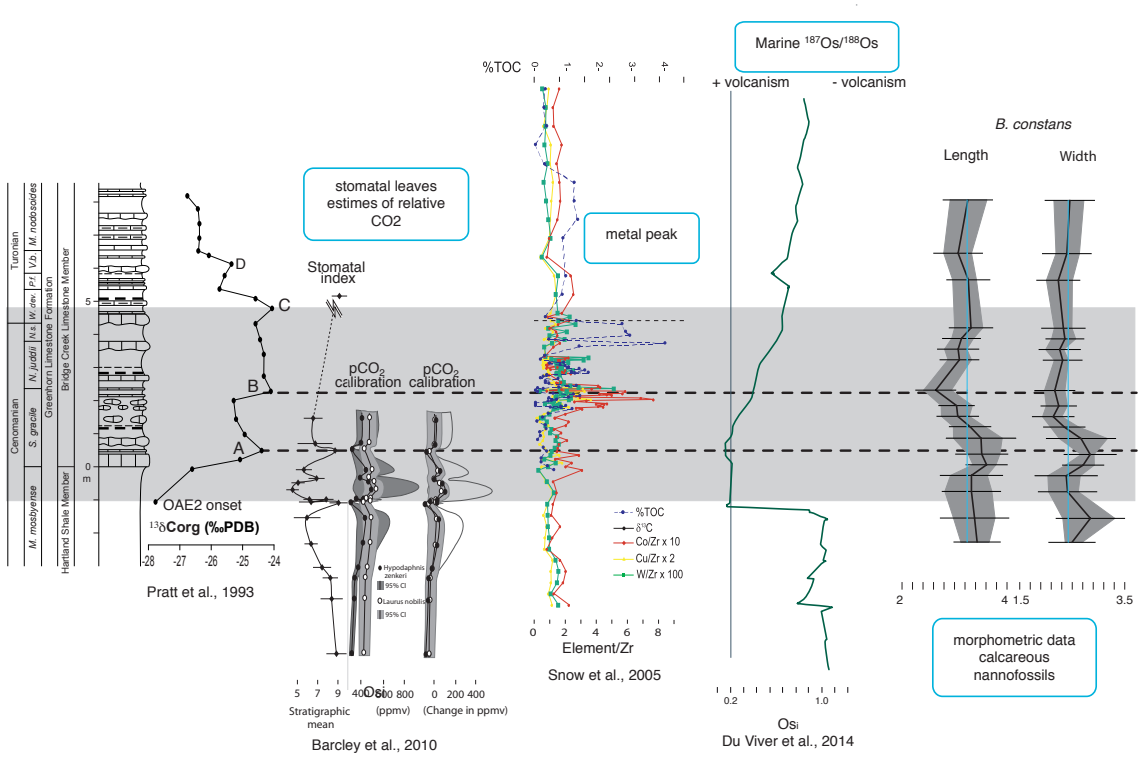

Fig. 9.2 Western Interior δ ^{13}C curve (Pratt et al., 1993), pCO_2 reconstruction (Barclay et al., 2010), Trace metals (Snow et al., 2005) and Osmium signature (Du Vivier et al., 2014) against calcareous nannofossil morphometric data (this study).

Changes in size are similar and synchronous in all the analyzed sections therefore at distant sites, different ocean contests, yielding identical preservation state: for this reason diagenesis can be excluded as the cause of the detected dwarfism. Thence dwarfism is observed in complete specimen with no corrosion in the outline. In Fig. 9.2 all the available data for the western interior area has been used in order to reconstruct the paleoceanic and paleoenvironmental characteristic of the WIS seaway during the Cenomanian - Turonian OAE2 and compared it with the obtained morphometric data of this area. During the first phase of OAE 2, the Osmium isotopic curve from Du Viver et al., 2014, suggests an intense submarine volcanism. Furthermore, the stomatal leave index shows an increase in the atmospheric pCO_2 concentration: two pulses are reconstructed and separated from a slightly CO_2 drawdown.

The correlation of pCO_2 intervals with the $\delta^{13}C$ isotopic curve suggests that OAE 2 was characterized by enhanced marine primary productivity that induced a global increase in rates of organic carbon burial (Barclay et al., 2010). The marine system therefore was able to remove the pCO_2 emitted in the atmosphere within 0-100 kyrs and specifically it seems plausible that the CO_2 removed was proportional to the associated pCO_2 pulse. Similarly in the first phase of OAE, calcareous nannofossils and especially *B. constans*, displays a decrease in size trend during the pCO_2 pulse. A subsequent increase in size trend, reaching maximum values at $\delta^{13}C$ isotopic peak A, is well correlated with the pCO_2 drawdown event described by Barclay et al., 2010. There's any further pCO_2 reconstruction for the upper part of OAE2, however the subsequent calcareous nannofossil decrease in size trend and the most expressed dwarfism is nicely correlated with $\delta^{13}C$ isotopic peak B where a strong minor, major and trace metal peaks occur. The presence of these concentration anomalies needs an explanation other than influx of terrigenous sediment and the most reliable explanation is the release of magmatic fluids in event plumes (Snow et al., 2005). Furthermore the metal-rich intervals are more abundant in the less volatile and more reactive elements (such as Sc, Co, Mn and Fe) and this is in good agreement with the position of the Caribbean plateau, which was reasonably proximal to the WIS area. Cuba and Pueblo area are therefore expected to be rich in a wide range of near-field and far-field elements.

For the Eastbourne section all the available data for paleoceanographic and paleoecological reconstruction has been used and compared to the morphometric obtained

results (Fig. 9.3). Lithium, calcium and strontium isotopic signature (δ^7L, δ^{44} Ca, $\delta^{87/86}$ Sr) are used to reconstruct the intensity of continental weathering. Data and models suggest that just before the OAE2 onset increase submarine volcanism increased the CO_2 concentration. This triggered global warming as suggested by δ^{18}O isotope and SST reconstruction. An intensification of the hydrological cycle might have promoted basaltic weathering intensification and could explain the negative trend of δ^7Li and δ^{44}Ca. Coccolith size follow this trend: starting from bigger specimens at the OAE 2 onset, a progressive decrease in size trend go hand in hand with the decrease of the δ^7Li and δ^{44}Ca isotopic signature. A consequent increase in size trend, that reached maximum size at the δ^{13}C isotope peak A, is coeval with a slightly increase of the δ^7 Li signature that suggest a less intense basaltic weathering as a direct consequence of a reduced intensity of the hydrological cycle. This furthermore is in good agreement with δ^{18}O and SST temperature reconstruction: a short term decrease of about 4°C (named Plenus Cold Event) corresponds exactly to a trough of the carbon-isotope curve (δ^{13}C peak A) and is associated with a temporary spread southwards of North Boreal biota (including the index belmnite *Praectinocamax plenus*). This support the idea of a sea-level fall, oxidation of organic matter and release of light ^{12} C back to the ocean-atmosphere system that result in transient drawdown of atmospheric CO_2 levels. Eastbourne data suggest a subsequent increase in SST and unstable δ^7Li fluctuations with a first decrease trend, subsequent higher value and a new gradual reduction trend. It can be therefore hypothesized a new intense volcanic pulse as furthermore suggested from the trace metal peak that is coeval, or slightly preceded, the δ^{13}C peak B. From δ^{13}C peak A, calcareous nannofossils show size fluctuation and a progressive reduction in size trend. The maximum dwarfism occurs at δ^{13}C peak B and goes along with a strong reduction of the nannofossil productivity index (Linnert et al., 2011*). W. barnesiae, B. constans* and *Z. erectus,* in fact, are used as proxies for surface water fertility: a decrease of *B. constans* and *Z. erectus* suggests lower nannofossil productivity. The end of OAE 2 at Eastbourne, evidence a reduced silicate weathering and a more weathering limited regime after δ^{13}C peak B, allowing a gradual ocean recovery. Similarly calcareous nannofossil displays a progressive recovery in size after δ^{13}C peak C and a gradual increase of the productivity index.

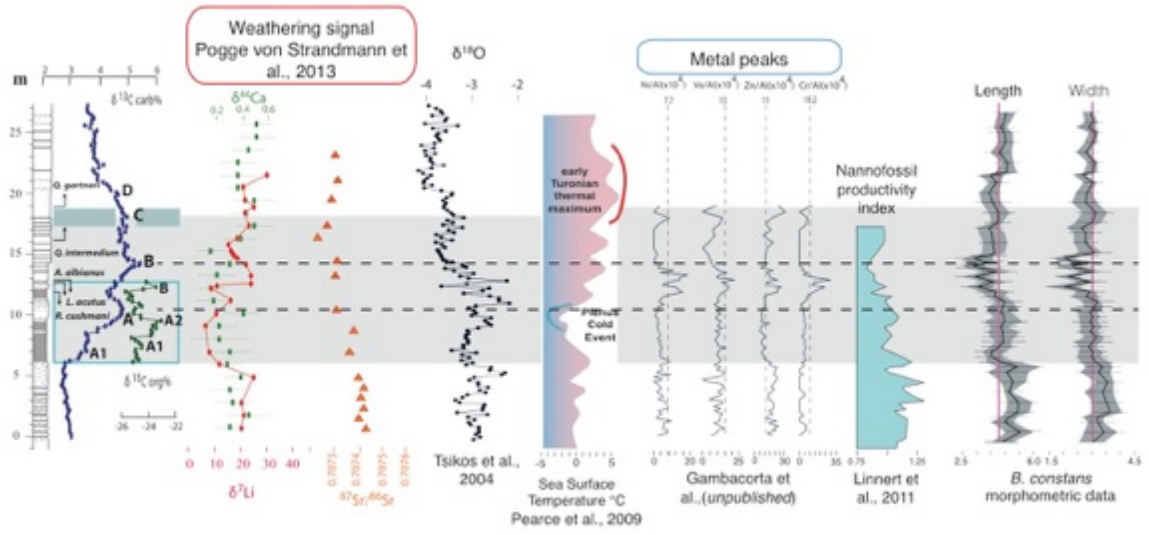

Fig. 9.3 Eastbourne δ ^{13}C curve and δ ^{18}O (Tsikos et al., 2004), δ ^{44}Ca, δ ^{7}Li, ^{87}Sr/^{86}Sr from Pogge von Strandmann et al., 2013; Sea Surface Temperature from Pearce et al., 2009; Metals peak from Gambacorta et al., (*in prep.):* nannofossil productivity index from Linnert et al., 2011; against calcareous nannofossil morphometric data (this study).

All the gathered information suggests a direct influence of the oceanic abiotic conditions on coccolith morphologies and/or abundances. The main paleoenvironmental factors influencing calcareous nannofossil size will be summarized here under:

1) **Nutrients**

Linnert and Mutterlose, (2012) evidence a decrease in size of *Biscutum* specimens during OAE 2 in sections from northwestern Europe. They underline that the detected decrease in mean coccolith size is accompanied by a decrease of *Biscutum* abundance: the positive correlation between Lmax *Biscutum*/relative abundance *Biscutum* spp, and Lmax *Biscutum*/Nutrient index, is therefore interpreted as evidence of a nutrient-affinity for *Biscutum*. This is in good agreement with the data from Eastbourne and Pueblo sections where oligotrophic conditions (Linnert et al., 2011; Corbett and Watkins, 2013) have been reconstructed around δ^{13}C peak B where dwarfer coccoliths are observed. Specifically in the WIS seaway, Tethyan influx of saline and dense water from the south and contemporary incursion of lighter and freshened Boreal water mass due to a rise in sea level might have resulted in ocean stratification (Corbett and Watkins, 2013). This might have prevented mixing of nutrient with surface water

and established sea surface oligotrophic conditions. However, the WIS Cuba section is an exception because nannofossil abundance and dinoflagellates cyst data, suggest periodic mixing through the event: along the shallower western margin of the seaway eutrophic conditions might have been persistent through OAE 2. Furthermore Novara di Sicilia was located in an area of permanent upwelling regime and was therefore characterized by high surface productivity under meso-eutrophic conditions. In both Cuba and Novara di Sicilia sections the same decrease in size trend around $\delta^{13}C$ peak B has been observed. In addition, coccolith size shows the smallest mean values in Cuba and even more in Novara di Sicilia section. It can be speculated, therefore, that in these localities high nutrient availability induced accelerated life cycle: smaller cells might have resulted in secretion of smaller coccoliths.

2) **Sea surface temperature**

Calcareous nannofossil morphometric data evidence an increase in size around $\delta^{13}C$ peak A, where a cooling has been recognized at global scale, while the smallest specimens occur in both *B. constans, Z. erectus* and *D. rotatorius* at $\delta^{13}C$ peak B where an increase in SST has been reconstructed. A cool-water preference has not been ascertained for these three species. Contrarily to the Boreal sections, *B. constans* is abundant through OAE 2 in the tropical Atlantic (Hardas and Mutterlose, 2007) that was characterized by SST up to 35°C. Also, high SST are recorded in the earliest Turonian where an increase of about 3°C has been reconstructed (Forster et al., 2007). During the early Turonian, *B. constans* is present with high abundances in the Boreal area and all the three species display a gradual recovery in size.

3) **Carbonate Chemistry and ocean acidification**

Proxy-based detailed reconstruction of pCO_2 is available only for the lower part of OAE 2 (Barclay et al., 2010). The stomatal index suggests an increase of about 600 ppm in the first part of the event. Pogge von Strandmann et al. (2013) furthermore calculated the amount of CO_2 sequestered via continental weathering (~4-8 x 10^4 Gt CO_2) and the estimated CO_2 drawdown is in agreement with previous calculation of the amount of CO_2 emitted in the first phase of the volcanic activity (7-12 x 10^4 Gt CO_2; Kuroda et al., 2007). It is therefore plausible that calcareous nannofossils were subjected to a progressive acidification of

seawaters in the early phase of OAE 2. As a matter of fact in the studied sections, coccolith size fluctuations mimic CO_2 reconstructions: a decreasing trend is observed in the interval with high CO_2 concentration and, conversely, bigger coccoliths occur at $\delta^{13}C$ peak A, where a reduction in CO_2 has been reconstructed. Then, the reduction of coccolith dimensions correlates with a further increase of pCO_2. I noticed that small *B. constans* coccoliths are characterized by more elliptical shape interpreted as malformation: both characters (dwarfism and malformation) might be linked to chemically stressed surface water conditions and hint towards an ocean acidification episode. Linnert and Mutterlose (2012) argued that the more massive *Eprolithus* nannoliths should have declined during a potential OAE 2 acidification event. But these groups of polycyclolthaceae are generally quite abundant with the exception of the tropical Atlantic area (Linnert and Mutterlose, 2012), thus arguing against an ocean acidification scenario. However, genus *Eprolithus* typically occurs in discrete abundance peaks in the OAE 2 interval (e.g. Erba 2004) and might represent intermitted alkalinity recovery similarly to *Assipetra-Rucinolithus* peaks during OAE 1a (Erba et al., 2010)

4) **Toxic trace metals**

Submarine volcanism introduced high concentrations of biolimiting metals during OAE 2 (Snow et al., 2005) that might results in ocean fertilization and/or toxification (Leckie et al., 2002; Erba, 2004) and possibly influence coccolith calcification. This is in agreement with morphometric data here presented: the metal peak detected at Pueblo (Snow et al., 2005), Eastbourne (Gambacorta et al., in prep), Novara di Sicilia (Duncan et al., 2013) is coeval with $\delta^{13}C$ peak B interval where dwarf coccoliths are observed.

9.3 Calcareous nannoplankton response to OAEs: comparison between OAE 1a and OAE 2

Calcareous nannofossil morphometric and morphological data of the latest Cenomanian OAE 2 have been compared with the early Aptian OAE 1a data in order to derive similarities and differences.

OAE 1a was an extreme oceanic event triggered from the emplacement of the Ontong Java Plateau (Larson, 1991; Larson & Erba 1999; Kuroda et al., 2011; Erba et al., 2015) that altered the structure, composition and dynamics of the ocean-atmosphere system. OAE 1a was associated with major climate change, ocean fertilization and acidification. The marine biota responded to these extreme conditions in different ways. Specifically, calcareous nannoplankton was able to survive extreme climatic, trophic and chemical conditions without extinctions. In fact, during OAE 1a the nannofossil calcification failure best expressed by the nannoconid crisis is interpreted as a false extinction assimilable to a case of "Lazarus effect" (Erba and Tremolada, 2004; Erba et al., 2010). Moreover before, during and after OAE 1a a major origination episode has been documented (Erba, 2004). However, calcareous nannofossils display morphological response to OAE 1a perturbation similar to those observed across OAE 2.

Before the OAE1a onset a progressive failure of heavily calcified nannofossils has been interpreted as related to increased surface-water fertility and incipient acidification: excess nutrients and trace metals combined with increasing CO_2 concentrations might have affected the oligotrophic and heavily calcified nannoconids (Erba 1994, 2004; Erba and Tremolada, 2004; Weissert and Tremolada, 2004; Erba et al., 2010, 2015; Bottini et al., 2014, 2015). In the early phase of OAE 1a a final crash of nannoconids was accompanied with a progressive coccolith size reduction of the mesotrophic species such as *B. constans, Z. erectus* and *D. rotatorius*. During the most negative carbon isotopic anomaly of OAE 1a (segment C3/A3 *sensu* Bottini et al., 2015), a brief cooling pulse followed a warming maximum. During this cooling interval that might be related to a temporary CO_2 drawdown subsequent to a weathering spike (Bottini et al., 2012, 2015), a partial nannofossil recovery has been observed. However, a following further CO_2 pulse caused an increased in temperature and shoaling of the CCD up to 1200m: in this interval

B. constans, Z. erectus and *D. rotatorius* are characterized by dwarf coccoliths while *W. barnesiae* specimens are affected by some deformation/malformation (Erba et al., 2010). At the end of the negative carbon isotope excursion nannofossil total abundance recovery is paralleled by a decrease in paleotemperature and metal concentration that are inferred to represent a significant CO_2 decrease (Bottini et al., 2015; Erba et al., 2015). Mesotrophic taxa are still abundant, suggesting high nutrient availability, but they are no longer affected by dwarfism.

Similarly to OAE 2, during OAE 1a there's a species-specific response to the ocean-atmosphere perturbation: *B. constans* turns out to be the most sensitive species displaying the maximum reduction in size; *D. rotatorius* shows a significant reduction in size while *Z. erectus* diminishes to a lesser extent. Moreover, in both OAE 1a and OAE 2, seawater fertility combined with temperature, trace metal enrichment and CO_2 concentration played a fundamental role on calcareous nannoplankton calcification. During OAE 1a nutrient content was very high during the first part of the event when dwarfism is observed. Since during Cretaceous episodes of enhanced fertility other than OAEs, no evidence of coccolith size reduction has been documented, it is unlikely that the trophic level was crucial for calcification changes. On the contrary a direct link among coccolith size and malformation with CO_2 concentration appears to be the most plausible explanation: from the early phase of OAE 1a perfect match between CO_2 reconstructions and coccolith dwarfism has been observed. Data suggest that increase and/or decrease in pCO_2 could favor a decrease or increase in biocalcification and that dwarfism and production of "malformed" coccoliths possibly represents species-specific adjustment to survive lower pH.

The results of coccolith morphometry for both OAE 1a and OAE 2 point to a potential control of metal enrichment on coccolithophores calcification. Indeed, in both episodes, species-specific dwarfism and some malformation occur in the intervals with metal spikes and it might be that toxic metals disturbed the functioning of some intolerant coccolithophore species affecting the calcification of their coccoliths (Fig. 9.4).

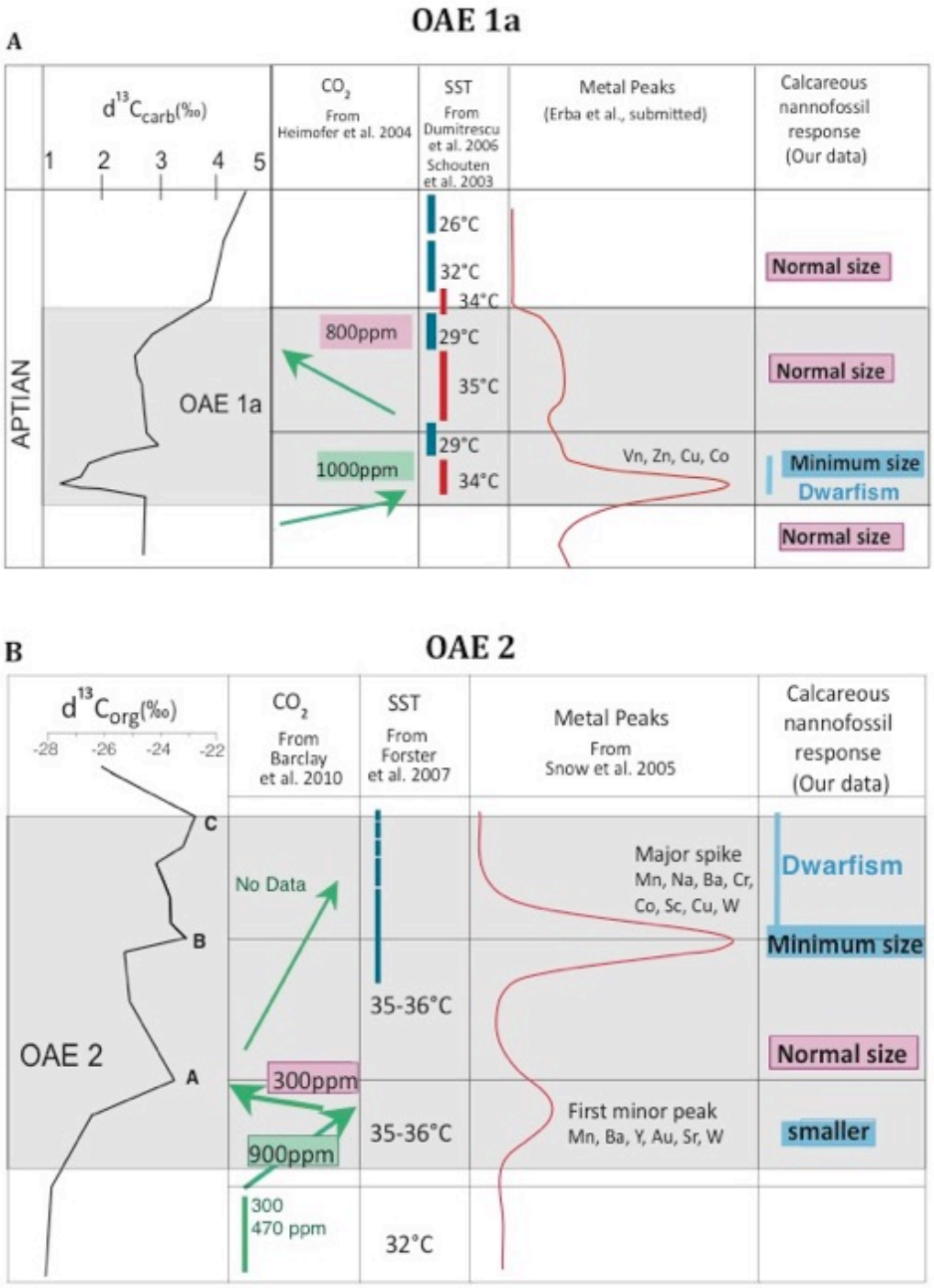

Fig. 9.4 Summary diagram for (A) OAE 1a and for OAE 2 (B) reporting estimated CO_2 concentrations, sea surface temperatures (SST), peaks in trace metals abundance and calcareous nannofossil response (size variations

9.2 Coccolithophores responses to environmental parameters

Coccolithophores calcification is not exclusively related to carbonate chemistry conditions but also to other environmental parameters such as light availability, temperatures and nutrient concentrations. The main goal of the experiments I've performed is to recognize if environmental parameters affect coccolith growth and/or which environmental parameter is crucial for coccolithophore calcification. Aside from laboratory results, that are discussed here, I intend to perform in the near future statistical analyses on the obtained data and perform detailed SEM analyses. In this respect, the planned SEM investigations of individual treatments are aimed at quantification of coccolith size and ultrastructure, including the malformation index designed by Bach et al. (2011) for *E. huxleyi*. Also I'll try to derive analogous (new) malformation indices for the other three species I've investigated. Only preliminary results and an overview of the main experiment results available from literature, will be discuss here; the discussions will be mainly focussed on coccolith volume and cell size.

The 4 analyzed species, respectively *E. huxleyi, G. oceanica, P. carterae* and *C. pelagicus* ssp. *braarudii,* have been chosen based on Liu et al. (2010): the Isochrysudales group (*G.oceanica and E. huxleyi*) diverged from Coccolithales *(C. pelagicus* ssp. *braarudii and P. carterae)* 220 million years ago (Fig. 9.5). *P. carterae,* furthermore, produces frequent blooms in coastal area. *E. huxleyi* forms large bloom over wide areas in the ocean but, because of it's small coccoliths and cell volumes, is not dominant in term of production and vertical flux of calcite to the deep sea. In contrast, *C. pelagicus* ssp. *braarudii* is a heaviest calcifying living coccolithophore and probably the most important in term of calcite export to the sediments.

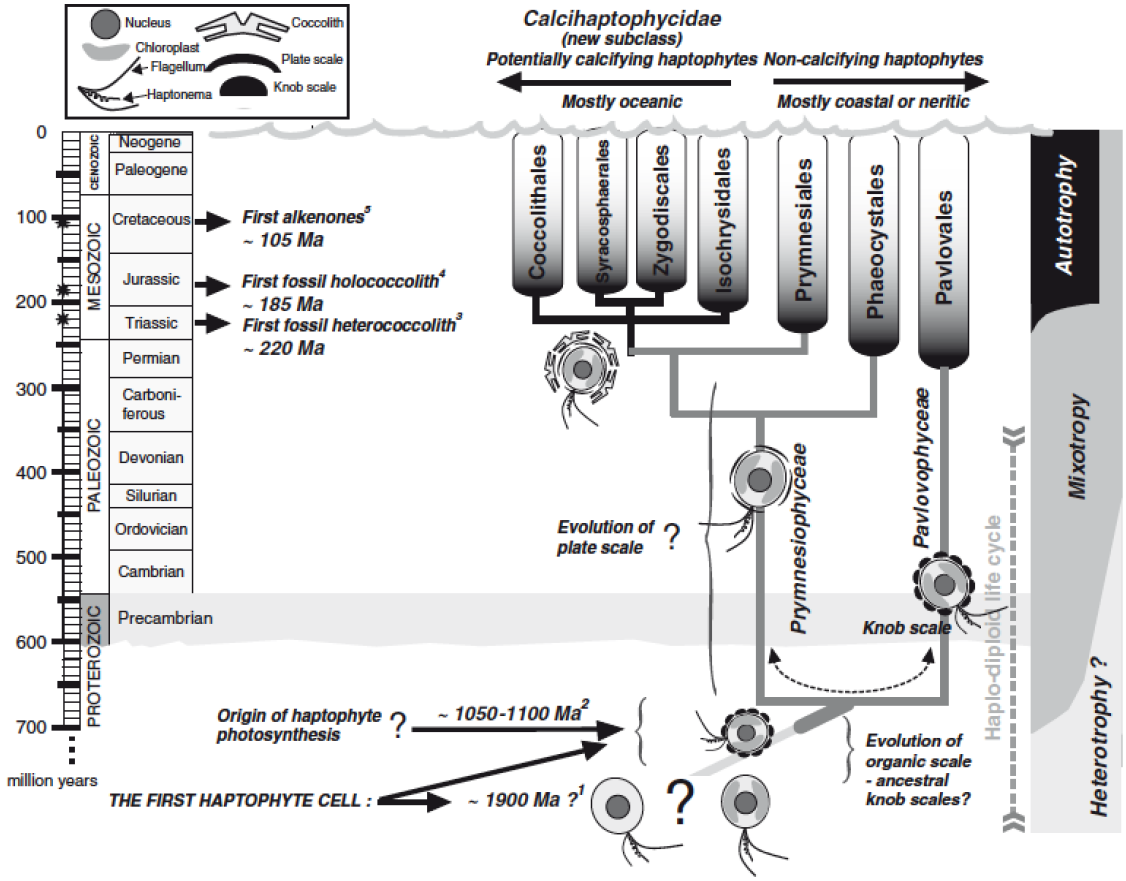

Fig. 9.5 Benchmarks in the evolutionary history of the Haptophytes and Calcihaptophytes. Major innovations are shown along a geological time scale on the left side of the figure [from De Vargas et al., 2007].

Response of Coccolithophores to light intensities

The progressive increase in temperature related to the global warming will have an indirect effect on light for phytoplankton: the reinforcement of the temperature gradient among surface water and deep water will result in stratification. The vertical mixing of the upper layer of the ocean modifies the light intensity; however, the phytoplankton have a specific affinity to light or the ability to deal with light irradiance variability: photosynthetic rates versus irradiances curve (Fig. 9.6) highlight three steps:

1) Light limitation conditions where photosynthesis increases rapidly
2) Light optimum conditions: threshold levels by which photosynthesis is light saturated and reaches maximal rate
3) High light conditions where photoinhibition occurs.

Sarmiento and Gruber (2006) documented a species-specific response to varying light irradiances and, specifically, evidenced that different taxa has different light affinity. For

example green algae, has the highest light affinity compared to diatoms and dinoflagellate, becoming light-saturated at lower light irradiances.

The data I've obtained are only partially in agreement with previous studies. *E. huxleyi* displays a progressive increase in growth rates with increasing light intensities. The coccosphere diameters and cell diameters show smaller values in low light intensities and higher and very stable values in all the other treatments. The obtained coccolith volumes show erratic values and not specific pattern was observed. *G. oceanica* has similar growth rate among treatments, with higher values with low and high light intensities. The resulted coccolith volumes show bigger sizes with low light irradiances (up to 200 μmol photons m^{-2} s^{-1}) and smaller volumes in all the other treatments with higher light intensities. *P. carterae* shows very erratic values for coccolith volumes and no specific trends were observed. However, *P. carterae* growth rate appears to be very stable among treatments. Finally, *C. pelagicus* ssp. *braarudii* has bigger coccolith volumes in treatments among 100 and 200 μmol photons m^{-2} s^{-1}, while lower values are observed in higher light intensities treatments.

E. huxleyi blooms with a shallow mixed layer (between 10 and 20 m) where high light intensities (light exceed 500 μmol photons m^{-2} s^{-1}) occurs. Indeed, light might be a requisite for *E. huxleyi* bloom formation (Tyrrell and Taylor, 1996). This is further supported by lab experiments where growth rate is saturate with light intensities among 200 and 300 μmol photons m^{-2} s^{-1} but doesn't decrease up to the 800 μmol photons m^{-2} s^{-1} (Harris et al., 2005), while at low irradiances (15 μmol photons m^{-2} s^{-1}) *E. huxleyi* is still able to grow (Zondervan et al., 2002). Photosynthesis is not inhibited even at the highest tested light intensities of 1700 and 2500 μmol photons m^{-2} s^{-1} (Paasche, 2002) that are equal to the higher light intensity by full sunshine. Different saturation irradiances has been detected for different species: Brand & Guillard (1981) highlighted that *G. oceanica* and *P. carterae* saturate at 1000 μmol photons m^{-2} s^{-1}; while *Calcidiscus leptoporus* saturate already at 200 μmol photons m^{-2} s^{-1}. Calcification is a light-depended process, too: increased calcification has been observed with increased light intensity (Zondervan, 2002). However, calcification is less affected than photosynthesis andsaturate at lower light intensities (Paasche, 1998 and Zondervan (2002). It is important, therefore, to compare results coming from other experiments, using the same light intensities, to avoid any irradiances influx on coccolithophore calcification.

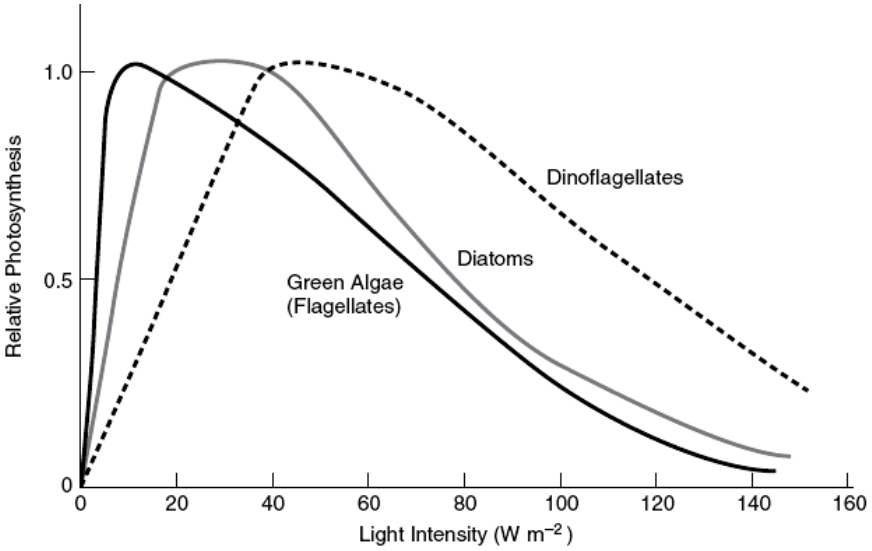

Fig. 9.6 Photosynthesis response at different light intensities for different phytoplanktonic groups; from Sarmiento and Gruber, 2006.

Response of Coccolithophores to nutrient limitations

The performed nutrient experiments display an increase in coccolith volume in all investigated species. Specifically, *E. huxleyi* shows a considerable increase in coccolith volume in the phosphate-limited (P-limited) treatment while nitrogen-limited (N-limited) treatment displays a slight increase in coccolith volume compared to the control treatment. *G. oceanica* shows similar coccolith volumes under N and P deficiency with a minor increase in coccolith volume compared to the control treatment. *P. carterae* shows a similar behavior with bigger and similar coccolith volume under N and P deficiency conditions, compared to the control treatment. Finally, *C. pelagicus* ssp. *braarudii* shows higher coccolith volumes in the P-limited treatment, and N-limited conditions induce bigger coccolith volumes too compared to the control treatment. Most experiment data available in the literature are based on *E. huxleyi*, whose blooms almost always occur in areas with low nitrate and/or phosphate concentrations (Balch et al., 1991). It was therefore argued that *E. huxleyi* produces massive blooms by outcompeting other phytoplankton species sensitive to low P and N concentrations (Riegman et al., 1992 and 2000). However, in culture experiments *E. huxleyi* appears to grow well under both high and low nutrient concentrations. Paasche (1998) suggests that phosphate and nitrate have

a pronounced effect on the regulation of cellular calcification. Specifically, Paasche (1998) evidences and increase in the number of coccoliths per cell in both N- and P-limited conditions: from 36 coccoliths per cell in nutrient replete conditions, the number rises to 70-120 coccolith/cell in strongly limited N or P conditions (Paasche, 1998). Moreover, Paasche & Brubak, (1994) evidence an increase in the proportion of cells with two or more coccolith layers in nutrient-limited conditions. Analyzing both *E. huxleyi* and *G. oceanica*, Berry et al. (2002) and Shiraiwa et al. (2003) document increased calcification to photosynthesis ratio in cultures starved by N or P and highlight that this is mainly due to an absolute increase in the rates of calcification and not inhibition of photosynthesis or cell division. Finally, Paasche et al. (1998) evidence morphological changes in single coccoliths N- and P- starved cultures: P deficiency leads in some cases to coccolith overcalcification even if not drastic variations for coccolith morphology has been observed. N deficiency, on the contrary, reduces calcification of individual coccolith: this might be related to a delay in the crystal growth and or premature release of coccoliths. Future SEM analyses on all the four species, will give a better understanding of calcification response to limited nutrient concentrations.

Response of Coccolithophores to [Mg^{2+}] and [Ca^{2+}]

The salinity experiment shows very stable and similar coccolith volume and growth rate in *E. huxleyi, G. oceanica* and *P. carterae*. On the contrary, *C. pelagicus* ssp. *braarudii,* displays larger coccolith volumes in the treatments with altered salinity compared to the control treatment. Growth rates, however, are higher in the control treatment while a progressive decrease in observed for the “Mg/Ca=1”, “Mg/Ca=2” and “Srx2” treatments.

The composition of seawater has changed significantly during the Phanerozoic: major constituents of seawater Mg^{2+} and Ca^{2+} have varied between 1.0 and 5.2 (Stanley and Hardie, 1998; Lowenstein et al., 2001, 2003; Erba, 2006). Based on these fluctuations two different types of oceans are distinguished: the “Calcite” seas and the “Aragonitic sea”. Calcareous nannoplankton evolution seems to be strictly connected to Mg/Ca and Ca^{2+} fluctuations: the shift from the “Aragonitic” sea to the “Calcitic sea” around 200 Ma, correlates with the oldest nannofossil record and it is plausible that seawater composition played a key-role in the appearance of coccolithophores biocalcification (Erba, 2006). In the same way, maximum Ca^{2+} concentration correlates with the maximum expansion of

coccolithophores in the Late Cretaceous, while the progressive decline in coccolithophore diversity of the past 30 Ma correlates with an increase in Mg/Ca ratio due to a rise in Mg^{2+} concentrations. Experiments on living coccolithophores highlight a general increase in growth rate with low Mg/Ca ratio culture water. Conversely, high Mg/Ca ratio and low Ca^{2+} concentrations are observed to be limiting factors: *Ochrosphaera neopolitana* for example displayed a low growth rate that quadrupled once transferred to seawater with lower Mg/Ca ratio (Stanley et al., 2005). Morphological variations have been detected, too: *Ochrosphaera neopolitana* appeared to be more heavily calcified in "Cretaceous seawater medium" compared to modern seawater (Ries et al., 2010). Moreover, there is apparently a species-specific sensitivity to low Mg/Ca ratios (Ries et al., 2010; Muller et al., 2011) that results in a major or minor decrease in growth rate, PIC content and calcification.

Response of Coccolithophores algae to carbonate chemistry

Coccolithophores have been tested under different CO_2 concentration ranging from 400 µatm to 3000 µatm. The "OA" and "Creta 1" treatments differed for the TA and DIC. The most sensitive species to carbonate chemistry variations appears to be *G. oceanica*: in all treatments there's a reduction in coccolith volume relative to the control. *E. huxleyi*, on the other hand, shows very similar coccolith volumes in all treatments with the exception of "Creta 2" treatment. This is also observed in *P. carterae* while *C. pelagicus* ssp. *braarudii* seems to be insensitive to carbonate chemistry variations and in some cases, increases in CO_2 appear to be beneficial.

The absorption of anthropogenic CO_2 into the ocean has been changing the marine carbonate chemistry by increasing carbon dioxide [CO_2] and [H^+], decreasing carbonate ion [CO_3^{2-}] and slightly increasing [HCO_3^-]. During the last 15 years coccolithophores have gained considerable attention due to the sensitivities of calcification to changing pCO_2. Coccolithophores are significant pelagic calcifiers that contribute about half of the calcium carbonates in open ocean sediments. They are the best-examined organisms because of their double response to ocean acidification and carbonification (e.g. Riebesell et al., 2000; Langer et al., 2006; Langer et al., 2009; Iglesias Rodrigues et al., 2008). Therefore it's a big challenge to discuss and take into consideration all the results

available from other studies. However, most works mainly focus on one species, namely *E. huxleyi*.

The species analyzed so far show different response to changing carbonate chemistry: *E. huxleyi* and *G. oceanica* usually decrease calcification rates with increased pCO_2 (Riebesell et al., 2000). Furthermore, *G. oceanica* appears to be even more sensitive to carbonate chemistry conditions than *E. huxleyi* (Riebesell et al. 2000). However, different strains highlighted partial different behaviour even if this might be due to different experiment procedures (e.g. Iglesias Rodriguez et al., 2008). *Calcidiscus quadriperforatus* showed an optimum cure response with maximum calcification rates at present CO_2 concentration. *Coccolithus braruudii* on the other hand didn't show any significant variation in calcification with increasing pCO_2 from 180 to 800 µatm (Langer et al., 2006). However, Krug et al. (2011) highlighted that when extending the pCO_2 range towards higher values, *C. brarudii* displayed the same changes observed in *E. huxleyi* and *G. oceanica* and, specifically, a decreased calcification rate with increasing pCO_2 (Fig. 9.7).

Indeed, it seems that both calcification and photosynthesis in all coccolithophore species follow an optimum curve suggesting the same cellular mechanism, but different sensitivities among different species and strains to carbonate chemistry. However, it still not completely understood how changing calcification rates are reflected in coccolith size, shapes and weight. Bach et al. (2011) stated that malformations in *E. huxleyi* are most likely induced by high concentrations of $[H^+]$ this might be due to coccolith formation, because H^+ is known to easily enter into the cytosol of *E. huxleyi* where a change in $[H^+]$ could disturb the correct functioning of cytoskeleton elements or enzymes associated, resulting in an altered expansion of the coccolith vesicles where coccolith formation takes place. Langer and Bode (2011) analyzed malformations in *Calcidiscus leptoporus* and identified CO_2 as the parameter causing distortion in coccoliths. Malformations in different species (or strains) might be caused by different carbonate parameters and, thus, different species and strains might have different sensitivities to carbonate chemistry changes.

The planned SEM analyses will give a better understanding on the influence of altered carbonate chemistry on coccolith size and shapes on a wide number of coccolithophores.

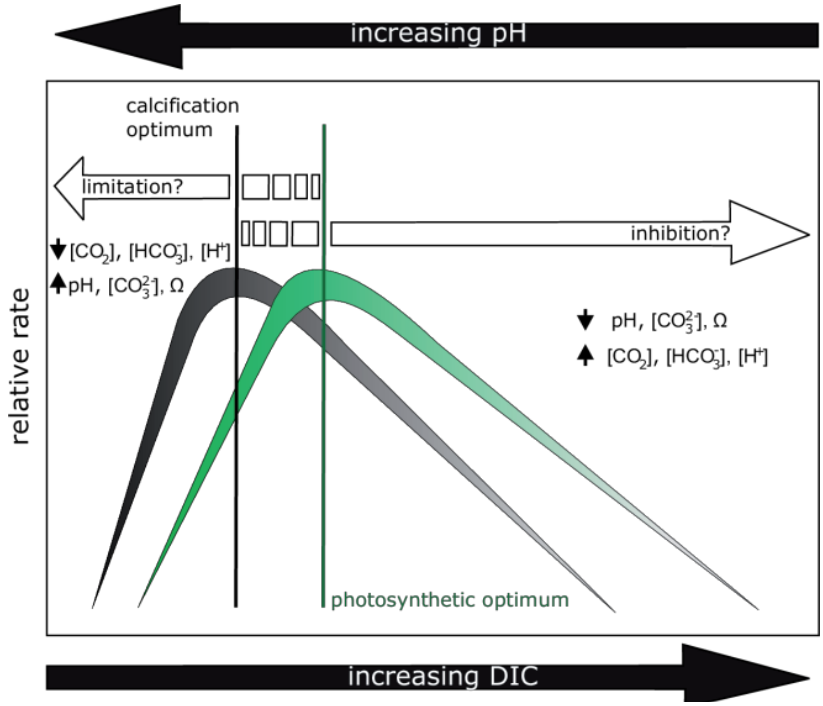

Fig. 9. 7 Conceptual model of coccolithophorid photosynthesis an calcification in response to changes in carbonate chemistry speciation due to increasing DIC and decreasing pH; [from Krug et al., 2011].

Response of Coccolithophores to trace metal enrichment

Three treatments with progressive increases in metal contents were tested on the four analyzed species. Different responses were observed, compared to the other experiments. They show similar response in the three treatments: increased metal content doesn't seem to affect growth rates. *E. huxleyi* shows substantially high growth rate but small coccolith volumes compared to the other experiments. *G. oceanica* shows similar changes in the various treatments as far as growth rate and coccolith volume are concerned, with comparable values with the other experiments. Likely, *C. pelagicus* ssp. *braarudii* shows similar coccolith volumes compared to the other experiments while growth rate is smaller than the control treatments; this suggests some limits/difficulties in *C. pelagicus* ssp. *braarudii* growth under higher metal contents. On the other hand, *P. carterae* shows comparable values among treatments in both growth rate and coccolith volume. Furthermore, coccolith volume is relatively high and might be related to *P. carterae*'s

preference to coastal environment that is expected to be enriched in nutrients and trace metals. Moreover, all species weren't able to survive the acclimation phase in the 5th treatment with the highest trace metal concentrations (8000 nmol/l of Pb, $ZnSO_4 \cdot 7H_2O$, $NiCl_2 \cdot 6H_2O$, $VOSO_4$): this suggests that there's a threshold value over which trace metals have a toxic effect on coccolithophores. Very few studies focused on coccolithophore response to trace metal concentrations. Some works have demonstrated that *E. huxleyi* needs metals for its metabolism such as iron, zinc, cobalt, selenium, cadmium and manganese (Brand et al., 1983; Sunda et Huntsman 2000). Schulz et al. (2004) investigated the influence of the essential trace metals iron and zinc on $CaCO_3$ production of *E. huxleyi*, showing that this species experiences a reduction in both growth rate and calcification under iron-limited conditions. On the other hand, a decrease in zinc content induces a growth rate reduction while $CaCO_3$ production rates per cell remains unaffected with highly calcified cells. It seems, therefore, that trace metal limitation can affect biogenic calcification.

Hoffmann et al. (2012) studied the response of phytoplanktonic organisms to increased metal contents: trace metals released in different volcanic ashes have been tested in order to verify their fertilizing or toxic effects. The experiment focused on *E. huxleyi* among coccolithophores and took into account only cell concentrations and growth rate. *E. huxleyi* displayed no growth variations during treatments (Hoffmann et al., 2012).

The experiments that I performed are pioneristic and it will be fundamental to analyze coccolith sizes and shapes on SEM pictures in order to evidence potential malformations and or errors in crystal growth due to high trace metal contents.

Chapter 10
Conclusion

The study performed for this thesis, aimed at combining geological and biological approaches, and can be regarded as a first step to identify whether specific (paleo)ecological factors or a combination of stressing environmental conditions can affect calcareous nannoplankton calcification in the geological record and in living coccolithophores and if positive and negative feedbacks are similar in the geological archive and in laboratory cultures. The geological case-study selected for morphometric analyses of a few nannoplankton taxa, is the latest Cenomanian OAE 2. The quantitative characterization of coccolith size and morphology in the intervals preceding, coeval and postdating OAE 2 was aimed at assessing the relationship between nannoplankton and paleoenvironamental changes. My results were compared with available nannofossil data for other Cretaceous OAEs in order to evaluate similarities and/or differences in nannoplankton response to chemical and physical extreme conditions in subsequent episodes of paleoenvironmental perturbation.

The results obtained for nannofossils across OAE 2 integrated with paleoceanographic and paleoclimatic reconstructions led to the following conclusions:

- During OAE 2 *B. constans*, *Z. erectus* and *D. rotatorius* coccoliths show a decrease in mean size and area followed by a partial recovery at the end of the event, but dimensions remained smaller than in the interval preceding the paleoenvironmental perturbation. *B. constans* results to be the most sensitive species to environmental changes compared to the other analyzed taxa. Indeed, dwarf *B. constans* specimens are affected by some malformation marked by increased ellipticity during OAE 2. Conversely, specimens of *W. barnesiae* display very constant sizes, with very minor changes and negligible variation of ellipticity across OAE 2. I underline that *B. constans, Z. erectus* and *D. rotatorius* dwarfism is observed in complete specimens with no corrosion in their outline and therefore cannot be explained as an artifact of diagenesis.

- The size reduction of *B. constans* is less expressed in OAE 2 compared to OAE 1a. Although during OAE 2 their mean length is only 63% of the holotype while during OAE 1a the average size is 72% of the holotype, the reduction relative to the preceding interval is of ~10% for OAE 2 and ~ 20% for OAE 1a. Indeed, *B. constans* coccoliths are already smaller than the holotype in the pre-OAE 2 interval whereas in the pre-OAE 1a interval average size of *B. constans* is close to holotipic values.
- *B. constans* evidences a latitudinal decrease in size in the dataset for the pre-OAE 2 and OAE 2 interval (in the post-OAE 2, no data are available for Novara di Sicilia), with larger *B. constans* coccoliths at Eastbourne and Clot de Chevalier and smaller specimens at Novara di Sicilia. The two sections located at intermediate paleolatitudes in the Western Interior display in-between values. This suggests that coccolith size variations are somehow controlled by regional/local conditions.
- I observed a progressive decrease in the mean length and area of *B. constans* coccoliths from the early Aptian OAE 1a to the late Albian OAE 1d and to the latest Cenomanian OAE 2 - when the lowest average size is reached. I speculate that size variation are somehow affected by the degree of paleoenvironmental global changes: the early Aptian OAE 1a marks the onset of the mid-Cretaceous supergreenhouse (Larson and Erba, 1999), OAE 1d correlates with a marked warming in the late Albian and OAE 2 is linked to most extreme paleoceanographic conditions and warmth culminating in the early Turonian thermal maximum.
- The comparison of these morphometric data (this study) with those available for the early Aptian and latest Albian OAEs indicates that *B. constans* repeatedly underwent size reduction and some malformation (increase in ellipticity). This presumably suggests that the same paleoenvironmental factors controlled calcification of *B. constans* coccoliths during OAE 1a, OAE 1d and OAE 2. *Z. erecuts* and *D. rotatorius* evidence a less-expressed decrease in size in both OAE 1a and OAE 2 and show dwarfism only in the interval of strongest perturbation during these events. The very little variability measured in *W. barnesiae* specimens indicate that this taxon was most adaptable and was only marginally affected by the paleoenvironmental perturbations characterizing Cretaceous OAEs.
- The reconstructed paleoclimatic and paleoceanographic changes across OAE 1a, OAE 1d and OAE 2 allow the evaluation of the factor or combination of factors inducing coccolith dwarfism and malformation. Temperature and nutrient availability in

surface waters do not seem to be crucial for *B. constans* size, although warmer and more fertile oceans preconditioned the specific environmental perturbation associated to OAEs. Available data, instead, suggest that ocean chemistry related to the amount of CO_2 concentrations, played a central role in coccolith secretion with a repetitive reduction in size during OAE 1a, OAE 1d and OAE 2.

- Experiments on living coccolithophore algae highlight, similarly to fossil data, a species-specific response to different environmental parameters. In particular, *E. huxleyi* shows a decrease in coccolith volume with the highest CO_2 concentration tested (3000 ppm) while nutrient-depleted conditions appear to be beneficial to coccolith growth. *G. oceanica* appears to be the most sensitive species to carbonate chemistry variations. *P. carterae* on the other hand shows very erratic patterns to tested parameters, suggesting very little sensitivity to specific environmental conditions. Calcification of *C. pelagicus* ssp. *braarudii* appears to be advantaged under low nutrient content, while increased CO_2 concentration seems to impart a negative feedback on coccolith volume with decreasing values that go hand in hand with increasing CO_2 concentration. As mentioned, these data are only preliminary and further analyses are planned in the near future and particularly SEM investigation of coccolith morphology and morphometry to quantify changes in coccolith size and malformation.

In conclusion the observed variations in both culturing and fossils data reflect the biomineralization response to changes in surface waters conditions and ocean carbonate chemistry. My data suggest that changes in environmental factors like temperature, nutrient content and carbonate chemistry have the potential to significantly influence the pelagic carbonate production. Parallel changes among fossils data and living coccolithophores suggest that biomineralization "failure" and "success" during past extreme events were likely to be just as significant as today.

Geological evidence of Cretaceous OAEs indicates that past oceanic perturbations were quite severe and that the species-specific production of dwarf and malformed coccoliths possibly represents adjustment of individual taxa to survive lower pH. It seems, therefore, that calcareous nannoplankton has been resilient to pH changes (and other extreme conditions), but it is certainly possible that the rate of change have been decisive for

coccolithophores adaptation. The geological record indicates that at wide spatial scale calcareous nannoplankton can generally adjust to high pCO_2, but past changes occurred over tens of thousands of years, giving enough time to adjust or even take advantage.

Laboratory experiments on modern coccolithophore species (evolutionary-linked to Cretaceous taxa) remain the only means to quantitatively assess if and which role environmental parameters have on quantity, type and amount of coccolith secretion. Although conscious of the very different time scales of processes and achievable resolution, the double biological and geological approach to coccolithophore calcification is aimed at critically integrating the daily-decadal datasets (biology) with medium- to long-term (thousands to millions of years in duration) data (paleontology = paleobiology). The ultimate goal of this challenging approach is an improved understanding of coccolith biomineralization mechanisms to derive some guidance as to the response of biota to abrupt massive CO_2 releases and how and at what rate pre-perturbation conditions are eventually restored.

References

AMODIO-MORELLI L., BONARDI G., COLONNA V., DIETRICH D., GIUNTA G., IPPOLITO F., ... & ZUPPETTA A., 1976. *L'arco calabro-peloritano nell'orogene appenninico-maghrebide*. Memorie della Società Geologica Italiana, 17, pp. 1-60.

ANDO A., KAIHO K., KAWAHATA H., & KAKEGAWA T., 2008. *Timing and magnitude of early Aptian extreme warming: Unraveling primary< i> δ</i>< sup> 18</sup> O variation in indurated pelagic carbonates at Deep Sea Drilling Project Site 463, central Pacific Ocean.* Palaeogeography, Palaeoclimatology, Palaeoecology, 260(3), pp. 463-476.

ARMSTRONG R.A., LEE C., HEDGES J.I. , HONJO S., AND WAKEHAM S.G., 2002. *A new, mechanistic model for organic carbon fluxes in the ocean based on the quantitative association of POC with ballast minerals*. Deep-Sea Research II 49, pp. 219-236.

ARTHUR M. A., JENKYNS H. C., BRUMSACK H.-J. AND SCHLANGER S. O., 1990. *Stratigraphy, geochemistry, and paleoceanographyof organic-carbon-rich Cretaceous sequences.* In Cretaceous Resources, Events and Rhythms, NATO ASISer., vol. 304, Ed by R. N. Ginsburg and B. Beaudoin, pp. 75–119, Kluwer Acad., Dordrecht, Netherlands.

BACH L. T., BAUKE C., MEIER K. J. S., RIEBESELL U., & SCHULZ K. G., 2012. *Influence of changing carbonate chemistry on morphology and weight of coccoliths formed by Emiliania huxleyi*. Biogeosciences Discussions, 9(5), 5849-5885.

BALCH, W. M., HOLLIGAN, P. M., ACKLESON, S. G., & VOSS, K. J., 1991. *Biological and optical properties of mesoscale coccolithophore blooms in the Gulf of Maine*. Limnology and Oceanography, 36(4), pp. 629-643.

BARCLAY R. S., MCELWAIN J. C., & SAGEMAN B. B., 2010. *Carbon sequestration activated by a volcanic CO2 pulse during Ocean Anoxic Event 2*. Nature Geoscience, 3(3), pp. 205-208.

BAUMANN K. H., ANDRULEIT H., & SAMTLEBEN C.,2000. *Coccolithophores in the Nordic Seas: comparison of living communities with surface sediment assemblages.* Deep Sea Research Part II: Topical Studies in Oceanography, 47(9), pp. 1743-1772.

BAUMANN K. H., BÖCKEL B., DONNER B., GERHARDT S., HENRICH R., VINK A., ... & ZONNEVELD K. A. F., 2004. *Contribution of calcareous plankton groups to the carbonate budget of South Atlantic surface sediments.* In The South Atlantic in the Late Quaternary pp. 81-99 Springer Berlin Heidelberg.

BEAUFORT L., PROBERT I., DE GARIDEL-THORON T., BENDIF E. M., RUIZ-PIN D., METZL, N., ... & DE VARGAS C., 2011. *Sensitivity of coccolithophores to carbonate chemistry and ocean acidification*. Nature, 476(7358), pp. 80-83.

BICE K. L., BIRGEL D., MEYERS P. A., DAHL K. A., HINRICHS K. U., & NORRIS R. D., 2006. *A multiple proxy and model study of Cretaceous upper ocean temperatures and atmospheric CO2 concentrations*. Paleoceanography, 21(2).

BILLARD C., 1994. *Life cycles.* Systematics Association Special Volume, 51, pp. 167-167.

BILLARD C., & INOUYE I., 2004. *What is new in coccolithophore biology?* In Coccolithophores, Springer Berlin Heidelberg, pp. 1-29.

BLACK M., BARNES B., 1959. *The structure of coccoliths from the English Chalk.* Geological Magazine 96, 321–328.

BLÄTTLER C. L., JENKYNS H. C., REYNARD L. M., & HENDERSON G. M., 2011. *Significant increases in global weathering during Oceanic Anoxic Events 1a and 2 indicated by calcium isotopes.* Earth and Planetary Science Letters, 309(1), 77-88.

BOLLMANN J., & HERRLE J. O., 2007. *Morphological variation of< i> Emiliania huxleyi</i> and sea surface salinity.* Earth and Planetary Science Letters, 255(3), 273-288.

BORNEMANN A., & MUTTERLOSE J. (2006). *Size analyses of the coccolith species< i> Biscutum constans</i> and< i> Watznaueria barnesiae</i> from the Late Albian "Niveau Breistroffer"(SE France): taxonomic and palaeoecological implications.* Geobios, 39(5), pp. 599-615.

BOTTINI, C. 2011. *pCO_2 effects on the production of pelagic biogenic carbonate and ocean chemistry: a case history from the Cretaceous*. Università degli Studi di Milano, PhD thesis.

BOTTINI C., COHEN A. S., ERBA E., JENKYNS H. C., & COE A. L., 2012. *Osmium-isotope evidence for volcanism, weathering, and ocean mixing during the early Aptian OAE 1a.* Geology, 40(7), pp. 583-586.

BOTTINI C., ERBA E., TIRABOSCHI D., JENKYNS H. C., SCHOUTEN S., SINNINGHE DAMSTE' J. S., 2014. *Climate variability and relationship with ocean fertility during the Aptian Stage*. Clim. Past Discuss., v. 10, pp. 689-738.

BOTTINI C., ERBA E., TIRABOSCHI D., JENKYNS, H.C., SCHOUTEN, S., SINNINGHE DAMSTÉ, J.S., 2015: *Climate variability and ocean fertility during the Aptian Stage*. **Clim. Past.** In press**.**

BOWMAN A. R., & BRALOWER T. J., 2005. *Paleoceanographic significance of high-resolution carbon isotope records across the Cenomanian–Turonian boundary in the Western Interior and New Jersey coastal plain, USA*. Marine Geology, 217(3), pp. 305-321.

BOWN P., 1998. *Calcareous nannofossil biostratigraphy.* Chapman & Hall; Kluwer Academic pp. 1-31.

BOWN P.R., YOUNG J. R. 1998. *Introduction, In: Bown P.R. (Ed) Calcareous nannofossil biostratigraphy.* British Micropalentol. Soc. Publ. Series, Kluver Academic Publ., University press Cambridge, UK, pp. 1-15

BRAARUD T., GAARDER K. R., MARKALI J., & NORDLI E., 1952. *Coccolithophorids studied in the electron microscope. Observations on Coccolithus huxleyi and Syracosphaera carterae.* Nytt Magasin for Botanik, 1, pp. 129-134.

BRALOWER T. J.,1988. *Calcareous nannofossil biostratigraphy and assemblages of the Cenomanian–Turonian boundary interval: Implications for the origin and timing of oceanic anoxia.* Paleoceanography, 3(3), pp. 275-316.

BRAND L. E., & GUILLARD R. R. L. (1981). *The effects of continuous light and light intensity on the reproduction rates of twenty-two species of marine phytoplankton*. Journal of Experimental Marine Biology and Ecology, 50(2), pp.119-132.

BRAND, L.E. 1994. *Physiological ecology of marine coccolithophores.* In: Winter, A., Siesser, W. (Eds.), Coccolithophores. Cambridge University Press, Cambridge, pp. 39 – 49.
BROECKER W. S., & TAKAHASHI T.,1966. *Calcium carbonate precipitation on the Bahama Banks.* Journal of Geophysical Research, 71(6), pp. 1575-1602.

BUKRY, D. 1969. *Upper Cretaceous coccoliths from Texas and Europe.* University of Kansas Paleontological Contribution Papers 33, pp. 1–79.

CAVAZZA, W., BLENKINSOP, J., DE CELLES, P. G., PATTERSON, R. T., & REINHARDT, E. G. 1997. *Stratigrafia e sedimentologia della sequenza sedimentaria oligocenica-quaternaria del bacino calabro-ionico.* Bollettino della Società Geologica Italiana, 116(1), pp.51-77.

GALE A. S., AND CHRISTENSEN W. K., 1996. *Occurrence of the belemnite Actinocamax plenus in the Cenomanian of SE France and its significance.* Bulletin of the Geological Society of Denmark, 43, pp. 68-77.

COHEN, A. S., COE, A. L., HARDING, S. M., & SCHWARK, L. 2004. *Osmium isotope evidence for the regulation of atmospheric CO2 by continental weathering.* Geology, 32(2), pp. 157-160.

CORBETT M. J., & WATKINS D. K., 2013. *Calcareous nannofossil paleoecology of the mid-Cretaceous Western Interior Seaway and evidence of oligotrophic surface waters during OAE2.* Palaeogeography, Palaeoclimatology, Palaeoecology, 392, pp. 510-523.

CORBETT M. J., WATKINS D. K., & POSPICHAL J. J., 2014. *A quantitative analysis of calcareous nannofossil bioevents of the Late Cretaceous (Late Cenomanian–Coniacian) Western Interior Seaway and their reliability in established zonation schemes.* Marine Micropaleontology, 109, pp. 30-45.

DAMSTÉ J. S. S., KUYPERS M. M., PANCOST R. D., & SCHOUTEN S., 2008. *The carbon isotopic response of algae,(cyano) bacteria, archaea and higher plants to the late Cenomanian perturbation of the global carbon cycle: Insights from biomarkers in black shales from the Cape Verde Basin (DSDP Site 367).* Organic Geochemistry, 39(12), pp. 1703-1718.

DAVIS S. A., YOUNG J. R., & MANN, S., 1995. *Electron microscopy studies of shield elements of Emiliania huxleyi coccoliths*. Botanica marina, 38(1-6), pp.493-498.

DE VARGAS C., AUBRY, M. P., PROBERT, I., & YOUNG, J., 2007.*Origin and evolution of coccolithophores: From coastal hunters to oceanic farmers.* Evolution of primary producers in the sea, pp. 251-285.

DEFLANDRE G., 1970. *Presence de nannofossiles calcaires (coccolithes et Incertae sedis) dans le Siluro-Devonien d'Afrique du Nord.* Acad Sci Compt Rend Ser D.

DESMARES D., GROSHENY D., BEAUDOIN B., GARDIN S., & GAUTHIER-LAFAYE F., 2007. *High resolution stratigraphic record constrained by volcanic ash beds at the Cenomanian–Turonian boundary in the Western Interior Basin, USA*. *Cretaceous Research*, *28*(4), pp. 561-582.

DICKSON A. G., 1981. *An exact definition of total alkalinity and a procedure for the estimation of alkalinity and total inorganic carbon from titration data*. Deep Sea Research Part A. Oceanographic Research Papers v. 28.6 pp. 609-623.

DICSKON A. G., SABINE C. L., CHRISTIAN J. R., 2007. *Guide to best practices for CO2 measurements.* PICES Special Publication, pp 3- 191.

DIXON H. H., 1899. *On the structure of coccospheres and the origin of coccoliths.* Proceedings of the Royal Society of London, 66(424-433), pp.305-315.

DODSWORTH P., 2000. *Trans-Atlantic dinoflagellate cyst stratigraphy across the Cenomanian–Turonian (Cretaceous) Stage boundary*. Journal of Micropalaeontology, 19(1), pp. 69-84.

DONEY S. C., FABRY V. J., FEELY R. A., & KLEYPAS J. A., 2009. *Ocean acidification: the other CO2 problem.* Marine Science, 1.

DUNCAN R., SNOW L., SCOPELLITI G., 2013. The Caribbean Plateau and OAE2: Resolution of Timing and Trace Metal Release. Mineralogical Magazine 77, 5, 1018.

DU VIVIER A. D., SELBY D., SAGEMAN B. B., JARVIS I., GROECKE D. R., & VOIGT S., 2014. *Marine< sup> 187</sup> Os/< sup> 188</sup> Os isotope stratigraphy reveals the interaction of volcanism and ocean circulation during Oceanic Anoxic Event 2.* Earth and Planetary Science Letters, 389, pp. 23-33.

EICHER D. L., & DINER R., 1989. *Origin of the Cretaceous Bridge Creek cycles in the western interior, United States.* Palaeogeography, Palaeoclimatology, Palaeoecology, 74(1), pp. 127-146.

ELESON J. W., & BRALOWER T. J., 2005. *Evidence of changes in surface water temperature and productivity at the Cenomanian/Turonian Boundary.* Micropaleontology, 51(4), pp. 319-332.

ENGEL A., ZONDERVAN I., AERTS K., BEAUFORT L., BENTHIEN A., CHOU L., ... & RIEBESELL U., 2005. *Testing the direct effect of CO2 concentration on a bloom of the coccolithophorid Emiliania huxleyi in mesocosm experiments.* Limnology and Oceanography, *50*(2), pp. 493-507.

ERBA E., 1992. *Middle Cretaceous calcareous nannofossils from the western Pacific (Leg 129): evidence for paleoequatorial crossings*. In Proceedings of the Ocean Drilling Program, Scientific Results. Vol. 129, pp. 189-201.

ERBA E., 1993. *The Early Aptian "nannoconid crisis": a paleobiologic response to global change.* Paleopelagos, 3, pp. 59-73.

ERBA E., 2004. *Calcareous nannofossils and Mesozoic oceanic anoxic events*. Marine Micropaleontology, 52(1), pp. 85-106.

ERBA, E., 2006. *The first 150 million years history of calcareous nannoplankton: biosphere–geosphere interactions. Palaeogeography, Palaeoclimatology, Palaeoecology*, v. *232*(2), pp. 237-250.

ERBA E., & TREMOLADA, F. 2004. *Nannofossil carbonate fluxes during the Early Cretaceous: Phytoplankton response to nutrification episodes, atmospheric CO2, and anoxia.* Paleoceanography, 19(1).

ERBA E., CHANNELL J. E., CLAPS M., JONES C., LARSON R., OPDYKE, B., ... & TORRICELLI S. (1999). *Integrated stratigraphy of the Cismon Apticore (southern Alps, Italy); a" reference section" for the Barremian-Aptian interval at low latitudes.* The Journal of Foraminiferal Research, 29(4), pp. 371-391.

ERBA E., BOTTINI C., WEISSERT H. J., & KELLER C. E., 2010. *Calcareous nannoplankton response to surface-water acidification around Oceanic Anoxic Event 1a.* Science, 329(5990), pp. 428-432.

ERBA E., DUNCAN R.A., BOTTINI C., TIRABOSCHI D., WEISSERT H., JENKYNS H.C., MALINVERNO, A., 2015. *Environmental Consequences of Ontong Java Plateau and Kerguelen Plateau Volcanism.* GSA Special Paper 511, doi:10.1130/2015.2511(15).

FABRY V. J., MCCLINTOCK J. B., MATHIS J. T., & GREBMEIER J. M., 2009. *Ocean acidification at high latitudes: the bellweather.* Oceanography, v22 (4), pp.160.

FALKOWSKI P. G., KATZ M. E., KNOLL A. H., QUIGG A., RAVEN, J. A., SCHOFIELD O., & TAYLOR F. J. R., 2004. *The evolution of modern eukaryotic phytoplankton*. Science, 305(5682), pp. 354-360.

FIELDING S. R., HERRLE J. O., BOLLMANN J., WORDEN R. H., & MONTAGNES D. J., 2009. *Assessing the applicability of Emiliania huxleyi coccolith morphology as a sea-surface salinity proxy.* Limnology and Oceanography, 54(5), p. 1475.

FISHER, C. G., HAY, W. W., & EICHER, D. L., 1994. *Oceanic front in the Greenhorn Sea (late middle through late Cenomanian).* Paleoceanography,9(6), pp. 879-892.

FORSTER A., SCHOUTEN S., BAAS M., & DAMSTÉ J. S. S., 2007. *Mid-Cretaceous (Albian–Santonian) sea surface temperature record of the tropical Atlantic Ocean.* Geology, 35(10), pp. 919-922.

FRIES G., & PARIZE O., 2003. *Anatomy of ancient passive margin slope systems: Aptian gravity-driven deposition on the Vocontian palaeomargin, western Alps, south-east France.* Sedimentology, 50(6), pp. 1231-1270.

GALE, A. S., 1995. *Cyclostratigraphy and correlation of the Cenomanian stage in Western Europe. Geological Society*, London, Special Publications, 85(1), pp.177-197.

GALE A. S., 1996. *Turonian correlation and sequence stratigraphy of the Chalk in southern England.* Geological Society, London, Special Publications, 103(1), pp.177-195.

GALE A., HANCOCK J.,1999. *Lithostratigraphy for mapping the Chalk of southern England' by Bristow et al., 1997: discussion*. Proceedings of the Geologists' Association, 110(1), pp.65-72.

GALE A. S., JENKYNS H. C., KENNEDY W. J., & CORFIELD R. M., 1993. *Chemostratigraphy versus biostratigraphy: data from around the Cenomanian–Turonian boundary.* Journal of the Geological Society, 150(1), pp. 29-32.

GALE A. S., KENNEDY W. J., VOIGT S., & WALASZCZYK I., 2005. *Stratigraphy of the Upper Cenomanian–Lower Turonian Chalk succession at Eastbourne, Sussex, UK: ammonites, inoceramid bivalves and stable carbon isotopes*. Cretaceous Research, 26(3), pp. 460-487.

GAMBACORTA G., JENKYNS, H.C., RUSSO, F., TSIKOS H., WILSON P.A. , FAUCHER, G., ERBA, E. *High-resolution carbon- and oxygen-isotope records of mid-*

Cretaceous Tethyan pelagic sequences from the Umbria–Marche and Belluno Basins (Italy). Newsletter on Stratigraphy, in review.

GARTNER JR, S., & BUKRY D., 1969. *Tertiary holococcoliths.* Journal of Paleontology, pp. 1213-1221.
GATTUSO J. P., **HANSSON L.,** *Ocean acidification*. Oxford University Press, 2011.

GIUNTA G., BELLOMO D., CARNEMOLLA S., PISANO A., PROFETA R., & RUNFOLA P., 1989. *La "Linea di Taormina": residuo epidermico di una paleostruttura crostale del fronte cinematico maghrebide.* Atti, 8, pp. 1197-1213.

GREEN J. C., HEIMDAL B. R., PAASCHE E., & MOATE R., 1998. *Changes in calcification and the dimensions of coccoliths of Emiliania huxleyi (Haptophyta) grown at reduced salinities.* Phycologia, 37(2), pp.121-131.

GRÜN W., ALLEMANN F., 1975. T*he Lower Cretaceous of Caravaca (Spain). Berriasian calcareous nannoplankton of the Miravetes Section (Subbetic Zone, Prov. of Murcia).* Eclogae Geologicae Helvetiae 68, 147–211.

HALLORAN P. R., HALL I. R., COLMENERO-HIDALGO E., & RICKABY R. E. M., 2008. *Evidence for a multi-species coccolith volume change over the past two centuries: understanding a potential ocean acidification response*. Biogeosciences, *5*(6), pp. 1651-1655.

HANCOCK J. M., & KAUFFMAN E. G., 1979. *The great transgressions of the Late Cretaceous*. Journal of the Geological Society, 136(2), pp.175-186.

HAQ, B. U., & LOHMANN, G. P., 1976. *Early Cenozoic calcareous nannoplankton biogeography of the Atlantic Ocean*. Marine Micropaleontology, 1, pp.119-194.

HARDAS P., & MUTTERLOSE J., 2006. *Calcareous nannofossil biostratigraphy of the Cenomanian/Turonian boundary interval of ODP Leg 207 at the Demerara Rise.* Revue de micropaléontologie, 49(3), pp.165-179.

HARDAS P., & MUTTERLOSE J.. 2007. *Calcareous nannofossil assemblages of Oceanic Anoxic Event 2 in the equatorial Atlantic: Evidence of an eutrophication event.* Marine Micropaleontology, 66(1), pp. 52-69.

HARRIS G. N., SCANLAN D. J., & GEIDER R. J., 2005. *Acclimation of emiliania huxleyi (prymnesiophyceae) to photon flux density1.* Journal of phycology, 41(4), 851-862.

HATTIN D. E., 1975. *Petrology and origin of fecal pellets in Upper Cretaceous strata of Kansas and Saskatchewan.* Journal of Sedimentary Research, 45(3).

HATTIN D. E., 1985. *Distribution and significance of widespread, time-parallel pelagic limestone beds in Greenhorn Limestone (Upper Cretaceous) of the central Great Plains and southern Rocky Mountains.* Limestone (Upper Cretaceous) of the Central Great Plains and Southern Rocky Mountains. In: Pratt, L.M., Kauffman, E.G., Zelt, F.B. (Eds.), Fine-Grained Deposits and Biofacies of the Cretaceous Western Interior Seaway: Evidence of Cyclic Sedimentary Processes. SEPMField Trip Guidebook No. 4, pp. 28–37.

HAY W. W., EICHER D. L., & DINER R.,1993. *Physical oceanography and water masses in the Cretaceous Western Interior Seaway. Evolution of the Western Interior Basin. Edited by WGE Caldwell and EG Kauffman.* Geological Association of Canada, Special Paper, 39, 297-318.

HARRIS G. N., SCANLAN D. J., & GEIDER R. J., 2005. *Acclimation Of Emiliania Huxleyi (Prymnesiophyceae) to photon flux density*. Journal of phycology, *41*(4), 851-862.

HERFORT L., LOSTE E., MELDRUM F., & THAKE B., 2004. *Structural and physiological effects of calcium and magnesium in< i> Emiliania huxleyi</i>(Lohmann) Hay and Mohler.* Journal of structural biology, 148(3), pp. 307-314.

HERRLE, J. O., KÖßLER, P., FRIEDRICH, O., ERLENKEUSER, H., & HEMLEBEN, C. (2004). *High-resolution carbon isotope records of the Aptian to Lower Albian from SE France and the Mazagan Plateau (DSDP Site 545): a stratigraphic tool for paleoceanographic and paleobiologic reconstruction.* Earth and Planetary Science Letters, 218(1), pp. 149-161.

HESSELBO S. P., GRÖCKE D. R., JENKYNS H. C., BJERRUM C. J., FARRIMOND P., BELL H. S. M. & GREEN O. R. , 2000. *Massive dissociation of gas hydrate during a Jurassic oceanic anoxic event.* Nature, *406*(6794), pp. 392-395.

HERFORT L., LOSTE E., MELDRUM F., & THAKE B., 2004. *Structural and physiological effects of calcium and magnesium in< i> Emiliania huxleyi</i>(Lohmann) Hay and Mohler.* Journal of structural biology, 148(3), pp. 307-314.

HOFFMANN L. J., BREITBARTH E., ARDELAN M. V., DUGGEN S., OLGUN N., HASSELLÖV M., & WÄNGBERG S. Å., 2012. *Influence of trace metal release from volcanic ash on growth of< i> Thalassiosira pseudonana</i> and< i> Emiliania huxleyi</i>*. Marine Chemistry, 132, pp. 28-33.

HÖNISCH B., HEMMING N. G., ARCHER D., SIDDALL M., & MCMANUS J. F., 2009. *Atmospheric carbon dioxide concentration across the mid-Pleistocene transition.* Science, v. 324(5934), pp. 1551-1554.

IGLESIAS-RODRIGUEZ M. D., HALLORAN P. R., RICKABY R. E., HALL I. R., COLMENERO-HIDALGO E., GITTINS J. R., ... & BOESSENKOOL K. P. 2008. *Phytoplankton calcification in a high-CO2 world*. Science, v. 320 (5874), pp. 336-340.

INOUYE I., 1995, *An Illustrated Guide to Microorganisms (translated from Japanese) (in Japanese).* Kojima S., Sudo S. and Chihara M (eds), Kodansha Scientific Co. Ltd, pp. 299-308.

INOUYE I., 1997. *Systematics of haptophyte algae in Asia-Pacific waters*. Algae, 12, pp. 247-261.

IPCC, 2013; *Climate Change 2013: The Physical Science Basis. Contribution of Working Group I to the Fifth Assessment Report of the Intergovernmental Panel on Climate Change* [Stocker, T.F., D. Qin, G.-K. Plattner, M. Tignor, S.K. Allen, J. Boschung, A. Nauels, Y. Xia, V. Bex and P.M. Midgley (eds.)]. Cambridge University Press, Cambridge, United Kingdom and New York, NY, USA, 1535 pp. doi:10.1017/CBO9781107415324.

JAHREN A. H., ARENS N. C., SARMIENTO G., GUERRERO J., & AMUNDSON R., 2001. Terrestrial record of methane hydrate dissociation in the Early Cretaceous. Geology, 29(2), pp. 159-162.

JARVIS I., LIGNUM J. S., GRÖCKE D. R., JENKYNS H. C., & PEARCE M. A., 2011. *Black shale deposition, atmospheric CO2 drawdown, and cooling during the Cenomanian-Turonian Oceanic Anoxic Event.* Paleoceanography, 26(3).

JENKYNS H. C., 1999. *Mesozoic anoxic events and palaeoclimate.* Zentralblatt für Geologie und Paläontologie, v. 1997, pp. 943-9.

JENKYNS, H. C. (2003). *Evidence for rapid climate change in the Mesozoic–Palaeogene greenhouse world.* Philosophical Transactions of the Royal Society of London. Series A: Mathematical, Physical and Engineering Sciences, 361(1810), 1885-1916.

JENKYNS, H. C. 2010. *Geochemistry of oceanic anoxic events.* Geochemistry, Geophysics, Geosystems, 11(3).

JENKYNS H. C., GALE A. S., & CORFIELD R. M., 1994. *Carbon-and oxygen-isotope stratigraphy of the English Chalk and Italian Scaglia and its palaeoclimatic significance*. Geological Magazine, 131(01), pp. 1-34.

JENKYNS H. C., FORSTER A., SCHOUTE S., & DAMSTÉ J. S. S., 2004. *High temperatures in the late Cretaceous Arctic Ocean*. Nature, 432(7019), pp. 888-892.

JONES C. E., & JENKYNS H. C., 2001. *Seawater strontium isotopes, oceanic anoxic events, and seafloor hydrothermal activity in the Jurassic and Cretaceous.* American Journal of Science, 301(2), pp.112-149.

JOO Y. J., & SAGEMAN B. B., 2014. *Cenomanian To Campanian Carbon Isotope Chemostratigraphy from the Western Interior Basin, USA*. Journal of Sedimentary Research, 84(7), pp. 529-542.

JORDAN R. W., & CHAMBERLAIN A. H. L., 1997. *Biodiversity among haptophyte algae.* Biodiversity & Conservation, 6(1), pp. 131-152.

KAUFFMAN E. G., & CALDWELL W. G. E., 1993. *The Western Interior Basin in space and time.* Evolution of the Western Interior Basin: Geological Association of Canada, Special Paper, 39, pp. 1-30.

KEELING C. D., & WHORF T. P., 2004. *Atmospheric CO2 concentrations derived from flask air samples at sites in the SIO network.* Trends: A Compendium of Data on Global Change. Carbon Dioxide Information Analysis Center, Oak Ridge National Laboratory, US Department of Energy, Oak Ridge, Tennessee, USA.

KELLER G., HAN Q., ADATTE T., & BURNS S. J., 2001. *Palaeoenvironment of the Cenomanian–Turonian transition at Eastbourne, England.* Cretaceous Research, 22(4), pp. 391-422.

KELLER G., & PARDO, A., 2004. *Age and paleoenvironment of the Cenomanian–Turonian global stratotype section and point at Pueblo, Colorado*. Marine Micropaleontology, 51(1), pp. 95-128.

KELLER G., BERNER Z., ADATTE T., & STUEBEN D., 2004. *Cenomanian–Turonian and< i> δ</i>< sup> 13</sup> C, and< i> δ</i>< sup> 18</sup> O, sea level and salinity variations at Pueblo, Colorado*. Palaeogeography, Palaeoclimatology, Palaeoecology, 211(1), pp. 19-43.

KEMP D. B., COE A. L., COHEN A. S., & SCHWARK L., 2005. *Astronomical pacing of methane release in the Early Jurassic period.* Nature, 437(7057), pp. 396-399.

KENNEDY W. J., & COBBAN W. A., 1991. *Stratigraphy and interregional correlation of the Cenomanian-Turonian transition in the Western Interior of the United States near Pueblo, Colorado, a potential boundary stratotype for the base of the Turonian stage*. Newsletters on Stratigraphy, 24(1-2), pp. 1-33.

KENNEDY W. J., COBBAN W. A., ELDER W. P., & KIRKLAND J. I., 1999. *Lower Turonian (Upper Cretaceous)< i> Watinoceras devonense</i> Zone ammonite fauna in Colorado, USA*. Cretaceous Research, 20(5), pp. 629-639.

KENNEDY W., WALASZCZYK I., & COBBAN W., 2000. *Pueblo, Colorado, USA, candidate Global Boundary Stratotype Section and Point for the base of the Turonian Stage of the Cretaceous and for the base of the middle Turonian Substage, with a revision of the Inoceramidae (Bivalvia)*. Acta Geologica Polonica, 50, 295-334.

KENNEDY W. J., WALASZCZYK I., & COBBAN W. A., 2005. *The global boundary stratotype section and point for the base of the Turonian stage of the Cretaceous: Pueblo, Colorado, USA*. Episodes-Newsmagazine of the International Union of Geological Sciences, 28(2), 93-104.

KOLONIC S., WAGNER T., FORSTER A., SINNINGHE DAMSTÉ J. S., WALSWORTH-BELL B., ERBA E., ... & KUYPERS M. M., 2005. *Black shale deposition on the northwest African Shelf during the Cenomanian/Turonian oceanic anoxic event: Climate coupling and global organic carbon burial*. Paleoceanography, 20(1).

KRUG S., SCHULZ K., & RIEBESELL U., 2011. *Effects of changes in carbonate chemistry speciation on Coccolithus braarudii: a discussion of coccolithophorid sensitivities*. Biogeosciences (BG), 8, pp. 771-777.

KUMP L. R., BRALOWER T. J, RIDGWELL A., 2009. *Ocean acidification in deep time.* Oceanography, 22(4) pp. 94-107, http://dx.doi.org/10.5670/oceanog.2009.100.

KURODA J., OGAWA N. O., TANIMIZU M., COFFIN M. F., TOKUYAMA H., KITAZATO H., & OHKOUCHI N., 2007. Contemporaneous massive subaerial volcanism and late cretaceous Oceanic Anoxic Event 2. Earth and Planetary Science Letters,256(1), pp. 211-223.

KURODA, J., TANIMIZU, M., HORI, R. S., SUZUKI, K., OGAWA, N. O., TEJADA, M. L., ... & OHKOUCHI, N., 2011. *Lead isotopic record of Barremian–Aptian marine sediments: Implications for large igneous provinces and the Aptian climatic crisis*. Earth and Planetary Science Letters, 307(1), 126-134.

KUYPERS M. M., PANCOST R. D., & DAMSTE J. S. S., 1999. *A large and abrupt fall in atmospheric CO2 concentration during Cretaceous times*. Nature, 399(6734), pp.342-345.

KUYPERS M. M., PANCOST R. D., NIJENHUIS I. A., & SINNINGHE DAMSTÉ J. S., 2002. *Enhanced productivity led to increased organic carbon burial in the euxinic North Atlantic basin during the late Cenomanian oceanic anoxic event.* Paleoceanography, 17(4), pp. 3-1.

LANGER G., GEISEN M., BAUMANN K. H., KLÄS J., RIEBESELL U., THOMS S., & YOUNG J. R., 2006. *Species‐specific responses of calcifying algae to changing seawater carbonate chemistry.* Geochemistry, Geophysics, Geosystems, 7(9).

LARSON, R. L., 1991. *Geological consequences of superplumes.* Geology,19(10), 963-966.

LARSON, R. L., & ERBA, E., 1999. *Onset of the Mid-Cretaceous greenhouse in the Barremian-Aptian: Igneous events and the biological, sedimentary, and geochemical responses.* Paleoceanography, 14(6), pp. 663-678.

LECKIE R. M., 1985. *Foraminifera of the Cenomanian-Turonian Boundary Interval, Greenhorn Formation, Rock Canyon Anticline, Pueblo, Colorado.* Society of Economic Paleontologists and Mineralogists Field Trip Guidebook 4, Midyear Meeting, Golden, Colorado, pp. 139-155.

LECKIE R. M., BRALOWER T. J., & CASHMAN R., 2002. *Oceanic anoxic events and plankton evolution: Biotic response to tectonic forcing during the mid-Cretaceous.* Paleoceanography, 17(3), 13-1.

LEONARDOS N., READ B., THAKE B., & YOUNG J. R., 2009. *No mechanistic dependence of photosynthesis on calcification in the Coccolithophorid Emiliania Huxleyi (Haptophyta) 1*. Journal of Phycology, 45(5), pp. 1046-1051.

LINNERT C., MUTTERLOSE J., & ERBACHER J., 2010. *Calcareous nannofossils of the Cenomanian/Turonian boundary interval from the Boreal Realm (Wunstorf, northwest Germany).* Marine Micropaleontology, 74(1), pp. 38-58.

LINNERT C., MUTTERLOSE J., & MORTIMORE, R., 2011. *Calcareous nannofossils from Eastbourne (southeastern England) and the paleoceanography of the Cenomanian–Turonian Boundary interval.* Palaios, 26(5), pp. 298-313.

LINNERT C., & MUTTERLOSE J., 2012. *Biometry of Cenomanian–Turonian placoliths: a proxy for changes of fertility and surface-water temperature?* Lethaia, 46(1), pp. 82-97.

LIU H., ARIS-BROSOU S., PROBERT I., & DE VARGAS, C., 2010. *A time line of the environmental genetics of the haptophytes.* Molecular biology and evolution,*27*(1), 161-176.

LOWENSTEIN T. K., TIMOFEEFF M. N., BRENNAN S. T., HARDIE L. A., & DEMICCO R. V., 2001. *Oscillations in Phanerozoic seawater chemistry: evidence from fluid inclusions.* Science, 294(5544), pp. 1086-1088.

LOWENSTEIN T. K., HARDIE L. A., TIMOFEEFF M. N., & DEMICCO R. V., 2003. *Secular variation in seawater chemistry and the origin of calcium chloride basinal brines.* Geology, *31*(10), pp. 857-860.

MALINVERNO A., ERBA E., & HERBERT T. D., 2010. *Orbital tuning as an inverse problem: Chronology of the early Aptian oceanic anoxic event 1a (Selli Level) in the Cismon APTICORE.* Paleoceanography, *25*(2).

MACKINDER L. C., WORTHY C. A., BIGGI G., HALL M., RYAN K. P., VARSANI A., ... & SCHROEDER D. C., 2009. *A unicellular algal virus, Emiliania huxleyi virus 86, exploits an animal-like infection strategy.* Journal of General Virology, 90(9), pp. 2306-2316.

MACKINDER L., WHEELER G., SCHROEDER D., VON DASSOW P., RIEBESELL U., & BROWNLEE, C., 2011. *Expression of biomineralization-related ion transport genes in Emiliania huxleyi.* Environmental microbiology, 13(12), pp. 3250-3265.

MANTON I., & LEEDALE G. F., 1969.*Observations on the microanatomy of Coccolithus pelagicus and Cricosphaera carterae, with special reference to the origin and nature of*

coccoliths and scales. Journal of the Marine Biological Association of the United Kingdom, 49(01), pp. 1-16.

McARTHUR J. M., DONOVAN D. T., THIRLWALL M. F., FOUKE B. W., & MATTEY D., 2000. *Strontium isotope profile of the early Toarcian (Jurassic) oceanic anoxic event, the duration of ammonite biozones, and belemnite palaeotemperatures.* Earth and Planetary Science Letters, 179(2), pp. 269-285.

McELWAIN J. C., WADE-MURPHY J., & HESSELBO S. P., 2005. *Changes in carbon dioxide during an oceanic anoxic event linked to intrusion into Gondwana coals.* Nature, 435(7041), pp. 479-482.

MEDLIN, L. K., DOUCETTE, G. J., & VILLAC, M. C., 2008. *Phytoplankton evolution, taxonomy and ecology.*(No. 133). J. Cramer.

MÉHAY S., KELLER C. E., BERNASCONI S. M., WEISSERT H., ERBA E., BOTTINI C., & HOCHULI P. A., 2009. *A volcanic CO2 pulse triggered the Cretaceous Oceanic Anoxic Event 1a and a biocalcification crisis.* Geology, 37(9), pp. 819-822.

MEYERS S. R., 2007. *Production and preservation of organic matter: The significance of iron.* Paleoceanography, 22(4).

MENEGATTI, A. P., WEISSERT, H., BROWN, R. S., TYSON, R. V., FARRIMOND, P., STRASSER, A., & CARON, M., 1998. *High‐resolution δ13C stratigraphy through the Early Aptian "Livello selli" of the Alpine tethys.* Paleoceanography, 13(5), pp. 530-545.

MELINTE-DOBRINESCU M. C., & BOJAR A. V., 2008. *Biostratigraphic and isotopic record of the Cenomanian–Turonian deposits in the Ohaba-Ponor section (SW Haţeg, Romania)*. Cretaceous Research, 29(5), pp. 1024-1034.

MORTIMORE R. N., 1986. *Stratigraphy of the Upper Cretaceous White Chalk of Sussex.* Proceedings of the Geologists' Association, 97(2), pp. 97-139.

MUGGLI D. L., & HARRISON P. J., 1996. *Effects of nitrogen source on the physiology and metal nutrition of Emiliania huxleyi grown under different iron and light conditions*. Marine ecology progress series. Oldendorf, 130(1), pp. 255-267.

MÜLLER, M. N., KISAKÜREK, B., BUHL, D., GUTPERLET, R., KOLEVICA, A., RIEBESELL, U., ... & EISENHAUER, A. (2011). *Response of the coccolithophores< i> Emiliania huxleyi</i> and< i> Coccolithus braarudii</i> to changing seawater Mg< sup> 2+</sup> and Ca< sup> 2+</sup> concentrations: Mg/Ca, Sr/Ca ratios and δ< sup> 44/40</sup> Ca, δ< sup> 26/24</sup> Mg of coccolith calcite.* Geochimica et Cosmochimica Acta, 75(8), pp. 2088-2102.

NANNINGA H. J. & TYRRELL, T., 1996. *Importance of light for the formation of algal blooms by Emiliania huxleyi.* Marine ecology progress series. Oldendorf,136(1), pp. 195-203.

NEDERBRAGT A. J., & FIORENTINO A., 1999. *Stratigraphy and palaeoceanography of the Cenomanian-Turonian boundary event in Oued Mellegue, north-western Tunisia*. Cretaceous Research, 20(1), pp. 47-62.

NOËL D., 1971. *Contribution à la Révision des Coccolithes secondaires: Essai d'établissement d'une hiérarchie des caractères génériques.* In Proceedings of the II Planktonic Conference, Roma, 1970 (Vol. 2, p. 879). Edizioni Tecnoscienza.

ORTH C. J., ATTREP M., MAO X. Y., KAUFFMAN E. G., DINER R., & ELDER W. P., 1988. *Iridium abundance maxima in the Upper Cenomanian extinction interval.* Geophysical Research Letters, 15(4), pp. 346-349.

PAASCHE E., 1962. *Coccolith formation*. Nature, 193, pp.1094-1095.

PAASCHE E., 1998. *Roles of nitrogen and phosphorus in coccolith formation in Emiliania huxleyi (Prymnesiophyceae).* European Journal of Phycology, 33(1), pp. 33-42.

PAASCHE, E., 2002. *A review of the coccolithophorid Emiliania huxleyi (Prymnesiophyceae), with particular reference to growth, coccolith formation, and calcification-photosynthesis interactions*. Phycologia, 40(6), pp. 503-529.

PAASCHE E., & BRUBAK S., 1994. *Enhanced calcification in the coccolithophorid Emiliania huxleyi (Haptophyceae) under phosphorus limitation.* Phycologia, 33(5), pp. 324-330.

PAUL C. R. C., LAMOLDA M. A., MITCHELL S. F., VAZIRI M. R., GOROSTIDI A., & MARSHALL J. D., 1999. The Cenomanian–Turonian boundary at Eastbourne (Sussex, UK): a proposed European reference section. Palaeogeography, Palaeoclimatology, Palaeoecology, 150(1), pp. 83-121.

PEARCE M. A., JARVIS I., & TOCHER B. A., 2009. *The Cenomanian–Turonian boundary event, OAE2 and palaeoenvironmental change in epicontinental seas: New insights from the dinocyst and geochemical records.* Palaeogeography, Palaeoclimatology, Palaeoecology, 280(1), pp. 207-234.

PERCH-NIELSEN K., 1968. *Feinbau und die Klassifikation der Coccolithen aus dem Maastrichtien von Danemark.* Biologiske Skrifter. Kongelige Danske Videnskabernes Selskab 16, 5–96.

PIENAAR R. N., 1994. *Ultrastructure and calcification of coccolithophores.Coccolithophores.* Cambridge University Press, Cambridge, pp. 13-37.

PIRINI-RADRIZZANI C., 1970. *Coccoliths from Permian deposits of eastern Turkey.* In Proceedings II Plankton Conference, pp. 993-1001.

POGGE VON STRANDMANN P. A. P., JENKYNS H. C., & WOODFINE R. G., 2013. *Lithium isotope evidence for enhanced weathering during Oceanic Anoxic Event 2.* Nature Geoscience, 6(8), pp. 668-672.

PRATT, L. M., 1983. *Isotopic studies on organic matter and carbonates in mid-Cretaceous strata near Pueblo, Colorado.* In Penrose Conference on Paleoclimates, Florissant, Colorado, Excursion Guidebook, pp. 77-98.

PRATT L. M.,1984. *Influence of paleoenvironmental factors on preservation of organic matter in Middle Cretaceous Greenhorn Formation, Pueblo, Colorado.* AAPG Bulletin, 68(9), pp.1146-1159.

PRATT L. M., ARTHUR M. A., DEAN W. E., & SCHOLLE P. A., 1993. *Paleo-oceanographic cycles and events during the Late Cretaceous in the Western Interior Seaway of North America.* Evolution of the Western Interior Basin, *39*, 333.

REDFIELD A. C., 1934. *On the proportions of organic derivatives in sea water and their relation to the composition of plankton.* (pp. 176-192). University Press of Liverpool.

REVELLE R., & SUESS H. E., 1957. *Carbon dioxide exchange between atmosphere and ocean and the question of an increase of atmospheric CO_2 during the past decades.* Tellus, 9(1), pp.18-27.

RIEGMAN R., NOORDELOOS A. A., & CADÉE G. C., 1992. *Phaeocystis blooms and eutrophication of the continental coastal zones of the North Sea.* Marine Biology, 112(3), pp. 479-484.

RIDGWELL, A., SCHMIDT, D. N., TURLEY, C., BROWNLEE, C., MALDONADO, M. T., TORTELL, P., & YOUNG, J. R., 2009. *From laboratory manipulations to Earth system models: scaling calcification impacts of ocean acidification.* Biogeosciences. 6(11), 2611-2623.

RIEBESELL, U., 2004. *Effects of CO2 enrichment on marine phytoplankton.* Journal of Oceanography, 60(4), pp. 719-729.

RIEBESELL U., ZONDERVAN I., ROST B., TORTELL P. D., ZEEBE, R. E., & MOREL, F. M. (2000). *Reduced calcification of marine plankton in response to increased atmospheric CO_2.* Nature, v 407(6802), pp. 364-367.

RIEBESELL, U., SCHULZ K. G., BELLERBY R. G. J., BOTROS M., FRITSCHE P., MEYERHÖFER M., NEILL C., NODAL G., OSCHILIES A., WOHLERS J., & ZÖLLNER E. (2007). *Enhanced biological carbon consumption in a high CO_2 ocean.* Nature, v 450 (7169), pp. 545-548.

RIEBESELL U., BELLERBY R. G., ENGEL A., FABRY V. J., HUTCHINS D. A., REUSCH T. B., ... & MOREL F. M., 2008. *Comment on" Phytoplankton Calcification in a High-CO2 World".* Science, v. 322(5907), pp. 1466-1466.

RIEBESELL U., KÖRTZINGER A., & OSCHLIES A., 2009. *Sensitivities of marine carbon fluxes to ocean change.* Proceedings of the National Academy of Sciences, v. 106 (49), pp. 20602-20609.

RIEBESELL U., & TORTELL P. D. (2011). *Effects of ocean acidification on pelagic organisms and ecosystems.* Gattuso, JP and Hanson, L., Oxford University Press, Oxford, pp. 99-121.

RIEBESELL U., KÖRTZINGER A., OSCHLIES A., 2009. *Sensitivities of marine carbon fluxes to ocean change.* Proceedings of the National Academy of Sciences 106.49, pp. 20602-20609.

RIES, J. B., 2010. *Review: geological and experimental evidence for secular variation in seawater Mg/Ca(calcite-aragonite seas) and its effects on marine biological calcification*. Biogeosciences, *7*(9), pp. 2795-2849.

ROST B., ZONDERVAN I., & RIEBESELL U., 2002. *Light-dependent carbon isotope fractionation in the coccolithophorid Emiliania huxleyi.* Limnology and Oceanography, 47, pp. 120-128.

ROST B., & RIEBESELL U., 2004. *Coccolithophores and the biological pump: responses to environmental changes.* In Coccolithophores, Springer Berlin Heidelberg, pp. 99-125.

ROTH P. H., 1987. *Mesozoic calcareous nannofossil evolution: relation to paleoceanographic events.* Paleoceanography, 2(6), pp. 601-611.

ROTH P. H., & KRUMBACH K. R., 1986. *Middle Cretaceous calcareous nannofossil biogeography and preservation in the Atlantic and Indian Oceans: implications for paleoceanography.* Marine Micropaleontology, 10(1), pp. 235-266.

RUSSO F., 2014. Calcareous nannofossil revised biostratigraphy of the latest Albian-earliest Campanian time interval (late Cretaceous). Università degli Studi di Milano, PhD thesis.

SABINE, C. L., FEELY, R. A., GRUBER, N., KEY, R. M., LEE, K., BULLISTER, J. L., ... & RIOS, A. F., 2004. *The oceanic sink for anthropogenic CO2.* Science, 305(5682), pp. 367-371.

SETT, S., BACH, L. T., SCHULZ, K. G., KOCH-KLAVSEN, S., LEBRATO, M., & RIEBESELL, U., 2014. *Temperature Modulates Coccolithophorid Sensitivity of Growth, Photosynthesis and Calcification to Increasing Seawater pCO_2.* PloS one, 9(2), e88308.

SAGEMAN B. B., MEYERS S. R., & ARTHUR M. A., 2006. *Orbital time scale and new C-isotope record for Cenomanian-Turonian boundary stratotype.* Geology,34(2), 125-128.

SCHLANGER S. O., & JENKYNS H. C., 1976. *Cretaceous oceanic anoxic events: causes and consequences.* Geologie en mijnbouw, v. 55 (3-4), pp. 179-184.

SCHOUTEN S., H. M. E. VAN KAAM PETERS W. I. C. RIJPSTRA M. SCHOELL AND J. S. SINNINGHE DAMSTÉ, 2000. *Effects of an oceanic anoxic event on the stable carbon isotopic composition of Early Toarcian carbon.* Am. J. Sci., 300, pp. 1–22, doi: 10.2475/ajs.300.1.1.

MÜLLER, M. N., LEBRATO, M., RIEBESELL, U., BARCELOS E RAMOS, J., SCHULZ, K. G., BLANCO-AMEIJEIRAS, S., ... & STOLL, H. M., 2013. *Influence of temperature and CO2 on the strontium and magnesium composition of coccolithophore calcite*. Biogeosciences Discussions, 10(10), 15559-15586.

SHIRAIWA, Y., 2003. *Physiological regulation of carbon fixation in the photosynthesis and calcification of coccolithophorids*. Comparative Biochemistry and Physiology Part B: Biochemistry and Molecular Biology, 136(4), pp. 775-783.

SCOPELLITI G., BELLANCA A., NERI R., BAUDIN F., & COCCIONI R., 2006. *Comparative high-resolution chemostratigraphy of the Bonarelli Level from the reference Bottaccione section (Umbria–Marche Apennines) and from an equivalent section in NW Sicily: Consistent and contrasting responses to the OAE2.* Chemical Geology, 228(4), pp. 266-285.

SCOPELLITI, G., BELLANCA, A. ERBA, E., JENKYNS, H. C., NERI, R., TAMAGNINI, P., ... & MASETTI, D., 2008. *Cenomanian–Turonian carbonate and organic-carbon isotope records, biostratigraphy and provenance of a key section in NE Sicily, Italy: Palaeoceanographic and palaeogeographic implications.* Palaeogeography, Palaeoclimatology, Palaeoecology, 265(1), pp. 59-77.

SINTON C. W., & DUNCAN R. A., 1997. *Potential links between ocean plateau volcanism and global ocean anoxia at the Cenomanian-Turonian boundary.* Economic Geology, 92(7-8), pp. 836-842.

SNOW L. J., DUNCAN R. A., & BRALOWER T. J., 2005. *Trace element abundances in the Rock Canyon Anticline, Pueblo, Colorado, marine sedimentary section and their relationship to Caribbean plateau construction and oxygen anoxic event 2.* Paleoceanography, 20(3).

STANLEY S. M., RIES J. B., & HARDIE L. A., 2005. *Seawater chemistry, coccolithophore population growth, and the origin of Cretaceous chalk.* Geology, 33(7), pp. 593-596.

STANLEY S. M., & HARDIE L. A., 1999. Hypercalcification: paleontology links plate tectonics and geochemistry to sedimentology. GSA Today, 9(2), pp. 1-7.

STANTON T.W., 1894. *The Colorado Formation and its invertebrate fauna*. Bulletin of the United States Geological Survey 106, 288.

SUNDA W. G., PRICE N. M., & MOREL F. M., 2005. *Trace metal ion buffers and their use in culture studies*. Algal culturing techniques, pp. 35-63.

TANTAWY, A. A., 2008. *Calcareous nannofossil biostratigraphy and paleoecology of the Cenomanian–Turonian transition in the Tarfaya Basin, southern Morocco.* Cretaceous Research, *29*(5), pp. 995-1007.

TEJADA M. L. G., SUZUKI K., KURODA J., COCCIONI R., MAHONEY J. J., OHKOUCHI N., ... & TATSUMI Y., 2009. *Ontong Java Plateau eruption as a trigger for the early Aptian oceanic anoxic event.* Geology, 37(9), pp. 855-858.

THIERSTEIN H. R., 1980. *Selective dissolution of Late Cretaceous and earliest Tertiary calcareous nannofossils: experimental evidence*. Cretaceous Research, *1*(2), pp. 165-176.

THIERSTEIN H. R., & ROTH P. H., 1991. *Stable isotopic and carbonate cyclicity in Lower Cretaceous deep-sea sediments: dominance of diagenetic effects*. Marine Geology, 97,1, pp. 1-34.

TSIKOS H., JENKYNS H. C., WALSWORTH-BELL B., PETRIZZO M. R., FORSTER A., KOLONIC S., ... & DAMSTÉ J. S., 2004. *Carbon-isotope stratigraphy recorded by the Cenomanian–Turonian Oceanic Anoxic Event: correlation and implications based on three key localities.* Journal of the Geological Society, 161(4), pp. 711-719.

TRIANTAPHYLLOU M. V., KOULI K., TSOUROU T., KOUKOUSIOURA O., PAVLOPOULOS K., & DERMITZAKIS M. D., 2010. *Paleoenvironmental changes since 3000 BC in the coastal marsh of Vravron (Attica, SE Greece).* Quaternary International, 216(1), 14-22.

TRIMBORN S., LANGER G., & ROST B., 2007. *Effect of varying calcium concentrations and light intensities on calcification and photosynthesis in Emiliania huxleyi.* Limnology and Oceanography:, 52(5), pp. 2285-2293.

TYRRELL T., & TAYLOR A. H., 1996. *A modelling study of< i> Emiliania huxleyi</i> in the NE atlantic.* Journal of Marine Systems, 9(1), pp. 83-112.

TURGEON S. C., & CREASER R. A., 2008. *Cretaceous oceanic anoxic event 2 triggered by a massive magmatic episode.* Nature, 454(7202), pp. 323-326.

VAN DER WAL P., DE JONG E. W., WESTBROEK P., DE BRUIJN W. C., & MULDER-STAPEL A. A., 1983. *Ultrastructural polysaccharide localization in calcifying and naked cells of the coccolithophorid Emiliania huxleyi*. Protoplasma, 118(2), pp. 157-168.

VOIGT S., GALE A. S., & FLÖGEL S., 2004. *Midlatitude shelf seas in the Cenomanian–Turonian greenhouse world: Temperature evolution and North Atlantic circulation.* Paleoceanography, 19(4).

VOIGT S., GALE A. S., & VOIGT T., 2006. *Sea-level change, carbon cycling and palaeoclimate during the Late Cenomanian of northwest Europe; an integrated palaeoenvironmental analysis.* Cretaceous Research, 27(6), pp. 836-858.

WAGNER T., SINNINGHE DAMSTÉ J. S., HOFMANN P., & BECKMANN B. 2004. *Euxinia and primary production in Late Cretaceous eastern equatorial Atlantic surface waters fostered orbitally driven formation of marine black shales.* Paleoceanography, *19*(3).

WATABE N., WILBURN K.M., 1966. *Effects of temperature ongrowth, calcification, and coccolith form in Coccolithus huxleyi (Coccolithineae).* Limnol Oceanogr 11 pp. 567–575.

WATKINS D. K.,1985. *Biostratigraphy and paleoecology of calcareous nannofossils in the Greenhorn marine cycle*. Biostratigraphy and paleoecology of calcareous nannofossils in the Greenhorn marine cycle. In: Pratt, L.M., Kauffman, E.G., Zelt, F.B. (Eds.), Fine-grained Deposits and Biofacies of the CretaceousWestern Interior Seaway: Evidence of Cyclic Sedimentary Processes: SEPM Field Trip Guidebook No. 4, pp. 151–156.

WATKINS D. K., 1986. *Calcareous nannofossil paleoceanography of the Cretaceous Greenhorn Sea.* Geological Society of America Bulletin, 97(10), pp. 1239-1249.

WATKINS D. K., SHAFIK, S., & SHIN I. C.,1998. *Calcareous nannofossils from the Cretaceous of the Deep Ivorian Basin.* In: Watkins, D. K., Shafik, S., & Shin, I. C. (1998). Calcareous nannofossils from the Cretaceous of the Deep Ivorian Basin. In Lohmann, M. J., Moullade, M. (Eds) Proceedings of the Ocean Drilling Program, Scientific Results, 159, pp. 319-333.

WEISS R. F., 1974. *Carbon dioxide in water and seawater: the solubility of a non-ideal gas.* Marine chemistry, v. 2, issue 3 pp. 203-2015, doi:10.1016/0304-4203(74)90015-2.

WEISSERT H., 1989. *C-isotope stratigraphy, a monitor of paleoenvironmental change: a case study from the Early Cretaceous.* Surveys in Geophysics, 10(1), pp. 1-61.

WEISSERT H., 2000. *Global change: Deciphering methane's fingerprint.* Nature,406(6794), pp. 356-357.

WEISSERT H., & ERBA E., 2004. *Volcanism, CO2 and palaeoclimate: a Late Jurassic–Early Cretaceous carbon and oxygen isotope record.* Journal of the Geological Society, 161(4), pp. 695-702.

WESTBROEK P., DE JONG E. W., VAN DER WAL, P., BORMAN A. H., DE VRIND J. P. M., KOK D., ... & PARKER,S. B., 1984. *Mechanism of Calcification in the Marine Alga Emiliania huxleyi [and Discussion*]. Philosophical Transactions of the Royal Society of London. B, Biological Sciences, 304(1121), pp. 435-444.

WILPSHAAR M., LEEREVELD H., & VISSCHER H., 1997. *Early Cretaceous sedimentary and tectonic development of the Dauphinois Basin (SE France).* Cretaceous Research, 18(3), pp. 457-468.

YOUNG J. R., 1994. *Functions of coccoliths*. Coccolithophores. Cambridge University Press, Cambridge, pp. 63-82.

YOUNG J. R., & WESTBROEK P., 1991. *Genotypic variation in the coccolithophorid species< i> Emiliania huxleyi</i>*. Marine Micropaleontology,18(1), pp. 5-23.

YOUNG J. R., BERGEN J. A., BOWN P. R., BURNETT J. A., FIORENTINO A., JORDAN R. W., ... & VON SALTS K., 1997. *Guidelines for coccolith and calcareous nannofossil terminology.* Palaeontology, 40(4), pp. 875-912.

YOUNG J. R., DAVIS S. A., BOWN P. R., & MANN S., 1999. *Coccolith ultrastructure and biomineralisation. Journal of structural biology*, *126*(3), pp. 195-215.

ZEEBE R. E , 2012. *History of seawater carbonate chemistry, atmospheric CO_2, and ocean acidification*. Annual Review of Earth and Planetary Sciences v. 40 pp. 141-165.

ZONDERVAN I., 2007. *The effects of light, macronutrients, trace metals and CO< sub> 2</sub> on the production of calcium carbonate and organic carbon in coccolithophores*—A review. Deep Sea Research Part II: Topical Studies in Oceanography, 54(5), pp. 521-537.

ZONDERVAN I., ROST B., & RIEBESELL U., 2002. *Effect of CO< sub> 2</sub> concentration on the PIC/POC ratio in the coccolithophore< i> Emiliania huxleyi</i> grown under light-limiting conditions and different day lengths*. Journal of Experimental Marine Biology and Ecology, 272(1), pp. 55-70.

APPENDIX I

Gambacorta et al., *submitted*

January 2015
Newsletter on Stratigraphy
ID 244

Title:

High-resolution carbon- and oxygen-isotope records of mid-Cretaceous Tethyan pelagic sequences from the Umbria–Marche and Belluno Basins (Italy)

Author names and affiliations

Gambacorta, G. [1], Jenkyns, H.C. [2], Russo, F. [1], Tsikos, H. [3], Wilson, P.A. [4], Faucher, G.[1], Erba, E.[1]

[1] Dipartimento di Scienze della Terra ''A. Desio'', Università di Milano, Via Mangiagalli 34, Milan 20133, Italy

[2] Department of Earth Sciences, University of Oxford, South Parks Road, Oxford OX1 3AN, UK

[3] Geology Department, Rhodes University, Grahamstown 6140, South Africa

[4] Southampton Oceanography Centre, School of Ocean & Earth Sciences, European Way, Southampton SO14 3ZH, UK

Corresponding author

Gabriele Gambacorta. E-mail address: gambacorta.gabriele@libero.it
Telephone number: +39 02503 15530
Fax number: +39 0250315494

Abstract

The late Albian–early Turonian time interval was marked by major environmental changes at regional to global scales. Oceanic Anoxic Event (OAE) 1d and OAE 2 and the mid-Cenomanian Event (MCE) are both associated with δ13C anomalies that indicate perturbations of the global carbon cycle. In this study, new high-resolution carbon- and oxygen-isotope records are presented from four Italian Tethyan sections: Cismon (Belluno Basin), and Furlo, Le Brecce and Monte Petrano (Umbria-Marche Basin) deposited in pelagic settings characterized by the alternation of nannofossil-planktonic foraminiferal oozes, radiolarian-rich intervals and shales. The δ13C records exhibit a ~1‰ positive excursion in δ13Ccarb corresponding with OAE 1d and a much larger positive anomaly (~2–3‰) in δ13Corg corresponding with OAE 2. Between these two events. a double-spiked minor (~0.7‰) excursion in the δ13Ccarb marks the MCE. Locally, between deposition of the MCE and the Bonarelli Level, sedimentation shifted to alternate dysoxic/anoxic and well-oxygenated conditions as represented by lithological rhythms of black shales/black chert bands and whitish limestones. δ18O data indicate a common pattern throughout the studied sections: values progressively decrease from the upper Albian up to the Bonarelli Level (uppermost Cenomanian), indicating an overall warming trend. Low δ18O values are recorded across the OAE 1d suggesting relatively warm conditions. The interval above the Bonarelli Level presents very low δ18O values, indicating the persistence of warm conditions in the early Turonian followed by a relative cooling trend.

Detailed carbon-isotope stratigraphy, calibrated with biostratigraphy, provides high-resolution dating and correlation, allowing identification of hiatuses in the studied sections. The high-resolution δ13C profiles across the OAE 2 interval highlight the presence of hiatuses of variable extent that affect the middle to upper part of the characteristic carbon-isotope excursion and part of the following interval in all of the studied sections. Locally, a hiatus may also be present at the base of the Bonarelli Level. Correlations with carbon-isotope records from widespread other localities, allows the duration of missing intervals to be estimated (between 400 and 700kyrs in the middle to late part of the OAE 2 and succeeding interval). The origin of these stratigraphic gaps can be attributed to physical and/or chemical processes operating at the sea floor. Complete recovery from the peculiar physico-chemical conditions that characterized the deeper parts of the Tethys Ocean during OAE 2 took a long time (at least 1 million years).

Keywords

Cretaceous, carbon and oxygen isotopes, MCE, OAE1d, OAE2, chemostratigraphy

APPENDIX II

Faucher et al., *submitted*

January 2015

Coccolith size variations during the latest Cenomanian Oceanic Anoxic Event 2

Giulia Faucher[1], Cinzia Bottini[1], Elisabetta Erba[1]

[1]*Department of Earth Sciences, Università degli Studi di Milano, 20133 Milan, Italy*

Contact author: giulia.faucher@unimi.it

Key words: Morphometry, coccoliths, Oceanic Anoxic Event 2, Cretaceous, paleoceanography

Abstract

Morphometric analyses were performed on *Biscutum constans* and *Watznaueria barnesiae* specimens from five sections spanning the Cenomanian-Turonian boundary interval including Oceanic Anoxic Event (OAE)2 (~ 94 Ma). The study provided evidence for tiny specimens of *B. constans*, smaller than the holotype, throughout the entire studied interval with further marked reduction, interpreted as dwarfism, in size during OAE 2, followed by a partial recovery at the end of the event. The decrease in size has also resulted to be accompanied by an increase in the mean ellipticity of the coccoliths. Preservation is moderate to good in all studied sample and dwarfism is observed in complete specimens with no corrosion in their outline and, therefore, cannot be explained as an artifact of diagenesis. Specimens of *W. barnesiae* display rather constant sizes, with very minor changes and negligible variation of ellipticity across OAE2. A latitudinal decrease in *B. constans* size has been noticed in our dataset for the pre-OAE 2 and OAE 2 intervals, with the larger coccoliths found at middle-higher latitudes. The comparison of our morphometric data with those available for the early Aptian OAE 1a and latest Albian OAE 1d, indicates that *B. constans* repeatedly underwent size reduction and malformation possibly suggesting that the same paleoenvironmental factors controlled calcification of *B. constans* during OAEs. The analyses also pointed out a progressive reduction of the mean size of *B. constans* through time, with generally larger specimens in the early Aptian, intermediate in the late Albian and smaller in the Cenomanian-Turonian boundary interval, here potentially ascribed to different degrees of paleoenvironmental changes. The

data available for OAE 1a, OAE 1d and OAE 2 suggest that ocean chemistry related to the amount of CO_2 concentrations, played a central role in coccolith secretion by *B. constans* with a repetitive reduction in size during the three OAEs, while temperature and nutrient availability in surface waters do not seem to have been crucial for *B. constans* size.

Acknowledgments

This PhD thesis is the result of a challenging journey, for which many people have contributed and given their support.

I would like to extend my upmost gratitude to my thesis advisor and mentor, Prof. Elisabetta Erba, for her interminable knowledge, support, guidance, patience, and perseverance. Her expertise was matched only by her enthusiasm, and her willingness to share her time, energy, and experience has been truly inspirational, and a gift.

A great thank goes to Dr. Cinzia Bottini (Unimi): without your support, ideas, direction, time and endless passion for science I would have been lost in many situations.

My appreciation goes to Prof. Isabella Premoli Silva and Dr. Maria Rose Petrizzo for their personal support and for every good advice.

I want to extend my gratitude to Dr. Gabriele Gambacorta for his help in metal data analyses and for his endless enthusiasm for science. And to Cristina for her support and every nice scientific chats.

Spending one year of my PhD between an Italian and German institution has given me the opportunity to meet many exciting and enthusiastic people and form fruitful collaborations.

I gratefully acknowledge Prof. Ulf Riebesell for hosting me at the GEOMAR institute providing the opportunity of working in the laboratories of the Biological Oceanography group.

A great thanks goes to Dr. Lennart Bach (GEOMAR) for having introduce me to the culturing world and for his crucial help in my personal process from “culturing-for-dummies” to “culturing-like-a-pro”.

My thanks go to Dr. Linn Hoffmann (GEOMAR) for helpful discussions and for introducing me into the magic world of trace metals.

Special thanks go to my “guardian-angel” Lothar Schlüter, (GEOMAR) who guided me from the beginning and helped me in every possible way till the end of my experiments.

I want to thank my office mate Mathias Haunost (GEOMAR) for all small scientific chats in between running experiments and for all the weekend spent together in the lab.

I thank Dr. Sonja Endres for access to laboratory facilities for my algae measurements.

Many thanks to all the techinician staffs that helped at the University of Milan and at the Geomar: Andrea Risplendente and Agostino Rizzi for SEM pictures; Renate, Tania, Kerstin and Diana for their technical support in the labyrinthine laboratories of the GEOMAR.

I would like to thank Silvana Gagliardi (GEOMAR) for her friendly and open-hearted support in the administrative planning of my research period in Kiel.

I extend my gratitude to Allanah Paul, Scarlet Sett, Magda Gutowska who made my stay at the GEOMAR institute a really enjoyable experience**.**

Now for the people I've probably spent most of my professional time with, by which I mean my office mates. I want to thank the "Ufficio 70" girls: without you all, Alessia, Gaia and Irene, these years wouldn't have been so special.

I extend my thanks to Claudio, Andrea, Andrea Z., Dario, Francesca, Silvia, Michele, Kirti, Sasha and Dr. Miguel Soares for all the cheerful conversations and laughs shared between us and I must say it has been an absolute pleasure.

My mind also goes to my housemates in Kiel, Lara and Tessina, to Fede and to Giulia and Gloria: thanks for your friendship and all your support, for the great time spent together outside science, for every dinners and chat after a long day at work.

A special thank goes to Rosy and Ennio for their kind and affectionate help.

I heartily thank my dad and mum and my sister for always supporting me whatever I have done or wherever I have decided to go. Thanks for your presence and good advises.

And finally, I am in debt to my boyfriend, Giorgio, who has been an endless source of support and always with a smile on his face after a long day or a long time apart. My biggest thank goes to you, and *ladidà*…